Vol. 50 ■ No. 2 ■ June 2022

JNMT

Journal of Nuclear Medicine Technology

FEATURED IMAGE

Amino Acid PET Imaging with ^{18}F-DOPA in the Evaluation of Pediatric Brain Tumors. Mehdi Djekidel et al. See page 137.

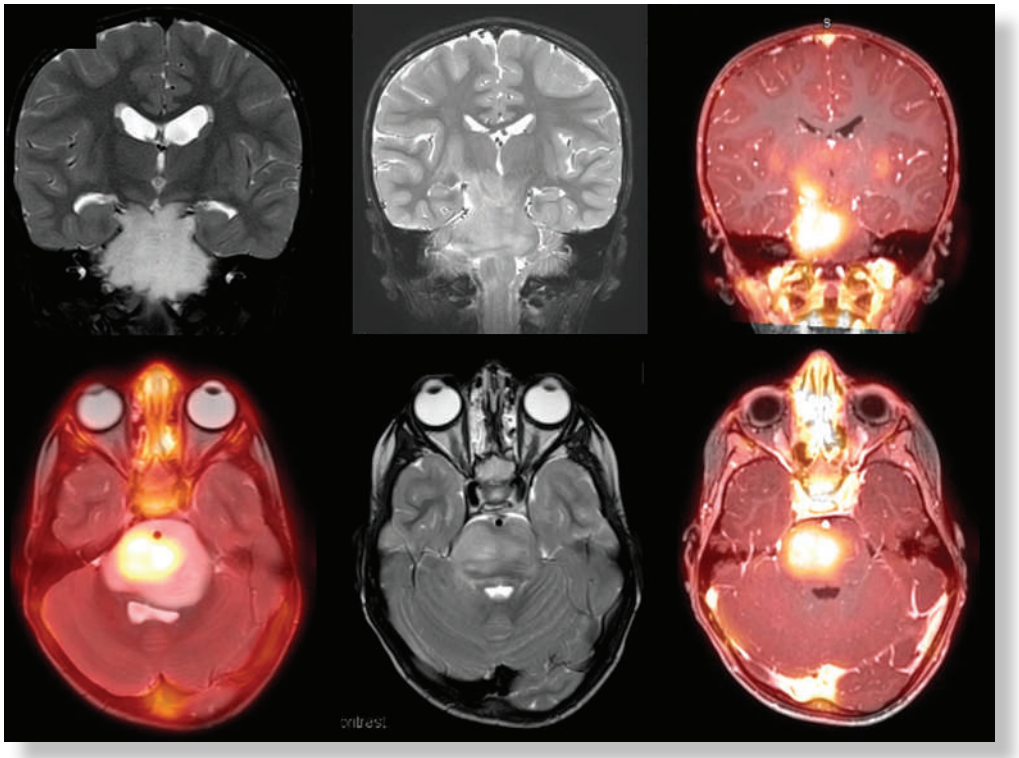

RADQUAL

Global Sources

Accuracy counts!

Avoid patient administration errors! THE FIRST EVER simulated I-131 source using NIST traceable Ba-133.

♦ Ensure that your I-131measurements are accurate to within + or -5% utilizing RadQual's new Simulated I-131 Sources. Available in two different geometries.

♦ RadQual's Patent Pending source designs are intended to mimic a 5 cc syringe or a capsule contained in a 15ml vial.

♦ New Patent Pending Simulated I-131 Capsule design allows calibration of individual doses.

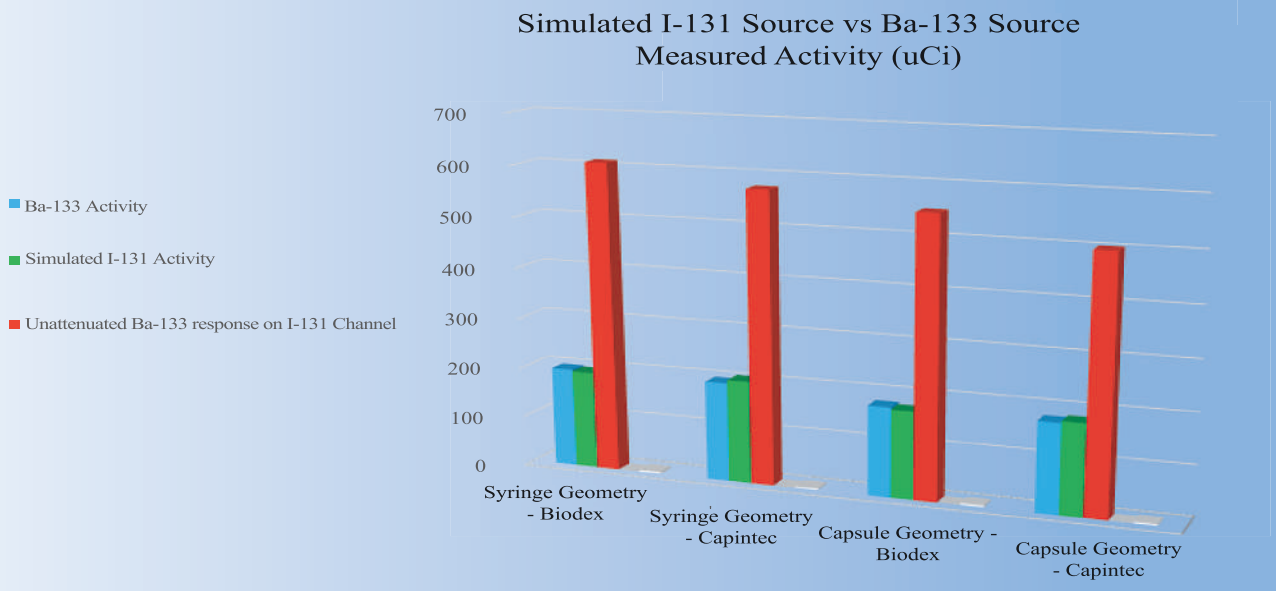

	Syringe Geometry - Biodex	Syringe Geometry - Capintec	Capsule Geometry - Biodex	Capsule Geometry - Capintec
Simulated I-131 Error	-1.57%	3.62%	-2.35%	2.02%
Ba-133 Overestimate on I-131 Channel	310%	293%	309%	282%

The design of RadQual's patent pending Simulated I-131 Source geometries better aligns the photon energy spectrum and yield, giving results within 5% of the NIST traceable Ba-133 activity, when measured on the I-131 dial setting of the dose calibrator.

www.radqual.com **(208) 524-5300** **Email: info@radqual.com**

Pass the NMTCB CT Exam. We *GUARANTEE* It!

Because **MIC** is all about ***outcomes***.

Over 30 Years!

We guarantee you'll pass the NMTCB CT Exam or *your money back!*

- Technologists must complete 35 hours of didactic education related to CT during the 3 year period prior to applying for the CT Exam.
- NMTCB has approved MIC's **CT Registry Review Program** along with **Sectional Anatomy & Imaging Strategies** to ***completely satisfy that 35-hour CT didactic requirement!***
- Excellent companion for technologists in hybrid imaging.

There's no better time to participate in

MIC's Self-Study CE

- Prepare for **CT certification**
- Satisfy NMTCB's **prerequisite**
- Ensure the **highest standards**

Ask for the CNMT discount when you enroll in both courses!

Technologists and their managers agree:
"MIC's courses really work!"

Sectional Anatomy & Imaging Strategies™

Learn the essentials of sectional imaging in a convenient self-study format!

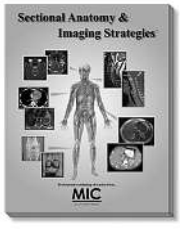

- Patient positioning, artifact reduction, image orientation, slice thickness, etc., for each clinical area.
- Explains sectional imaging with over 1,000 images and figures. The perfect companion to **The CT Registry Review Program**.
- 18 Credits
- 6 StudyModules

The CT Registry Review Program™

Pass the CT Exam after completing this course or we will refund your entire tuition!

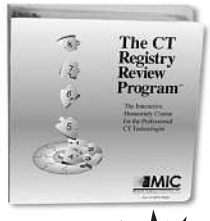

5th Ed!

- Learn **essential** and **advanced** topics on the NMTCB and ARRT CT Exam.
- Prior training in CT is recommended.
- Pass the NMTCB or ARRT Exam in CT or your money back!
- 22 Credits
- 8 StudyModules

A Proud Member of...
SNMMI

Call today for your
Free Info Kit
800-589-5685
or visit www.MIC*info*.com

MIC®
Medical Imaging Consultants, Inc.
1037 US Highway 46, Suite G2 • Clifton, NJ 07013 • 800-589-5685
...for *your* perfect image.

JNMT06/22

SPECTRUM
DYNAMICS MEDICAL

VERITON-CT®

DIGITAL SPECT/CT

Optimization of Every Step

Spectrum Dynamics has integrated its ground-breaking BroadView Technology design into the VERITON-CT system, providing a digital platform enabling routine 3D imaging in Nuclear Medicine. The result is optimization of every step, from image acquisition to interpretation.

VERITON-CT digital SPECT/CT combines the best-in-class CZT detectors, novel system design, high resolution CT, and advanced software technology to elevate the performance of 360° digital SPECT/CT.

BroadView Technology
Proprietary swiveling detector design provides increased sensitivity for faster scans

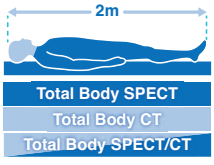

Total Body 3D Imaging
200cm continuous coverage vertex to feet
SPECT | CT | SPECT/CT

80cm NM and CT bore
Wide Bore SPECT/CT
80cm NM and CT bore

Choice of 16/64 slice
Choice of high-resolution CT for diagnostic applications and low dose total body CTAC

TruView Console
One platform, one location for clinical care decision-making:

1. Acquisition
2. Advanced quantitative reconstruction
3. Both 3D and 4D data analysis and review

VERITON-CT Feature Application: 3D Dynamic Imaging

TruFlow for VERITON-CT offers real-time 3D in-vivo fast dynamic imaging to capture the radiopharmaceutical distribution, uptake, or clearance over time in 3D SPECT/CT parametric imaging.

TruFlow

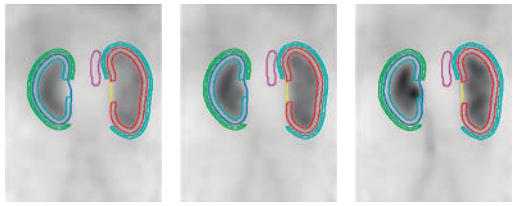

spectrum-dynamics.com

JNMT

Volume 50, Number 2 • June 2022

JNMT Journal of NUCLEAR MEDICINE TECHNOLOGY

The Official Publication of **SNMMI-TS**

The *JOURNAL OF NUCLEAR MEDICINE TECHNOLOGY* (ISSN 0091-4916 [print]; ISSN 1535-5675 [online]) is published quarterly by the SNMMI, 1850 Samuel Morse Dr., Reston, VA 20190-5316; phone: (703) 708-9000; fax: (703) 708-9018. Periodicals postage paid at Reston, VA, and at additional mailing offi ces.

POSTMASTER: Send address changes to the *Journal of Nuclear Medicine Technology*, 1850 Samuel Morse Dr., Reston, VA 20190-5316.

EDITORIAL COMMUNICATIONS should be sent to the editor, Kathy S. Thomas, MHA, CNMT, PET, FSNMMI-TS, JNMT Office, SNMMI, 1850 Samuel Morse Dr., Reston, VA 20190-5316; phone: (703) 326-1185; fax: (703) 708-9018. To submit a manuscript, go to http://submit-tech.snmjournals.org.

BUSINESS COMMUNICATIONS concerning permission requests should be sent to the publisher, SNMMI, 1850 Samuel Morse Dr., Reston, VA 20190-5316; phone: (703) 708-9000; home page address: http://tech.snmjournals.org. Subscription requests, address changes, and missed issue claims should be sent to Membership Department, SNMMI, at the address above. Notify the Society of change of address and telephone number at least 30 days before date of issue by sending both the old and new addresses. Claims for copies lost in the mail are allowed within 90 days of the date of issue. Claims are not allowed for issues lost as a result of insufficient notice of change of address. For information on advertising, contact Team SNMMI (Kevin Dunn, Rich Devanna, and Charlie Meitner; (201) 767-4170; fax: (201) 767-8065; TeamSNMMI@cunnasso.com). Advertisements are subject to editorial approval and are restricted to products or services pertinent to nuclear medicine. Closing date is the 25th of the second month preceding the date of issue.

INDIVIDUAL SUBSCRIPTION RATES for the 2022 calendar year are $249 within the United States and Canada; $265 elsewhere. CPC IPM Sales Agreement No. 1415131. Sales of individual back copies are available for $58 at http://www.snmmi.org/subscribe (subscriptions@snmmi.org; fax: (703) 667-5134). Individual articles are available for sale online at http://tech.snmjournals.org.

MISSION: SNMMI-TS is dedicated to the advancement of molecular and nuclear medicine technologists by providing education, advocating for the profession, and supporting research to achieve clinical excellence and optimal patient outcomes. **VISION:** To be recognized as the leader in molecular imaging and therapy. To be dedicated to the advancement of the profession through adoption of emerging technologies.

JNMT Journal of NUCLEAR MEDICINE TECHNOLOGY

A Productive Year Sets Up SNMMI-TS for Future Success

Dusty M. York, CNMT, PET, RT(N)(CT)

As I write this column, the last column of my presidency, I can confidently say that SNMMI is truly a one-of-a-kind organization. This past weekend I had the opportunity to take part in the SNMMI Strategic Planning Board of Directors meeting. This was the first time the SNMMI Board of Directors has met in-person since the 2020 Mid-Winter Meeting—more than two years ago! The discussion over the weekend and the collegial family atmosphere among board members and invited guests left me feeling excited and hopeful for all the Society and the field have to offer in the future.

As president, you are often exposed to the detailed workings of the SNMMI—and this year, although mostly virtual, has been no exception. We have seen several local state wins at the legislative level thanks to the outstanding efforts of the State TAGs across the United States. Our curriculum is under revision with changes that will help to shape future nuclear medicine technologists and programs, an effort that the Educators Curriculum Task Force led with excitement and critical strategy. The SNMMI-TS is months away from releasing a molecular therapy–focused issue of the *Journal of Nuclear Medicine Technology,* with therapy education following closely behind. We have reconnected with our international partners after a long 3 years and are collaborating to provide important nuclear medicine sessions to technologists during the World Federation of Nuclear Medicine and Biology (WFNMB) meeting later this year. The SNMMI-TS Publications Committee published the 2-part *PET/CT in Oncology* "mini-book," which has been widely distributed and utilized since the release of Part 2 just a few months ago.

I am so proud of all the work that the SNMMI-TS committees, National Council of Representatives, and Executive Board have accomplished this year. I want to recognize the amazing leadership team and each of the talented committee chairs I have had the pleasure to work with over the last year. The commitment and passion within the committees throughout this past year has led to unparalleled success and paved the way for an amazing year. Thank you to each of the following chairs for their dedication:

Dusty M. York, CNMT, PET, RT(N)(CT)

- Advocacy Committee – Dmitry Beyder and Tricia Peters
- Awards Committee – Mark Crosthwaite
- Bylaws Committee – Kelli Schlarbaum
- Continuing Education Committee – Kathy Thomas (Chair) and Roberta Alvarez (Vice-Chair)
- Educators Committee – Lauren Shanbrun
- Finance Committee Report – Jay Smith
- History Committee – Leo Nalivaika
- International – David Gilmore
- Membership Committee – Sarah Gibbons
- Molecular Therapy Task Force – Wendy Territo
- Nominating Committee – Tina Buehner
- Nuclear Medicine Week Task Force – Leesa Ann Ross
- PET/MRI Task Force Update – Peter Kamvosoulis
- Professional Development & Education Fund (PDEF) – Dori Nelson
- Professional Development Committee – Matthew McMahon
- Program Committee – Kathleen Krisak
- Publications Committee – Jessica Williams
- Quality Committee – April Mann (Chair) and Paul Riley (Vice-Chair)
- Scope of Practice Task Force – Jeremy Iman
- State TAG – Cheryl Rickley
- Student and Graduate Task Force – Thalia Zolis
- Women in Nuclear Medicine Working Group – Sarah Frye

I hope to see many of you in Vancouver, BC, Canada, in June as we celebrate our first live SNMMI Annual Meeting since 2019. Thank you for letting me serve as your president—it has truly been a pleasure!

It's Time to Gather and Share

Kathy S. Thomas, MHA, CNMT, PET, FSNMMI-TS

Editor, *JNMT*

June marks an extraordinary time of year for the nuclear medicine community. It's a time when physicians, scientists, pharmacists, lab professionals, technologists, and commercial representatives gather together to share the latest research and development and their clinical applications at the Society of Nuclear Medicine and Molecular Imaging (SNMMI) Annual Meeting. This year, the SNMMI's Annual Meeting will be held in beautiful Vancouver, British Columbia. This four-day event will allow participants to attend state-of-the-art educational programs, network with peers and industry partners, and enjoy the special programs and interactive gatherings that we've missed for the last two years.

Whether you're attending the meeting in person or choosing to attend virtually, be sure to participate in the SNMMI Technologist Section's (SNMMI-TS) Business Meeting on Monday, June 13, 2022 (4:45-6:00 pm PDT), where we will celebrate the Section's many accomplishments, announce the winners of the 2022–2023 elections, and present multiple awards including the *JNMT* Best Paper Awards. Each year, published manuscripts written by technologists as the first author are judged in the following categories: Scientific Papers (1st, 2nd, and 3rd place), Continuing Education, Teaching Case Studies, and Educators' Forum. You can find a complete list of the *JNMT* 2021 Best Paper Awardees on the SNMMI website (in the About SNMMI section, Grants, Awards, and Scholarships [https://www.snmmi.org/AboutSNMMI/Content.aspx?ItemNumber=38829]) — and don't miss the September issue of *JNMT*, where the best paper awards and photos of the authors will be included. So, once again, my question to you is, "Is your name on that list?" If not, why not consider sharing your expertise by summarizing a clinical research study, writing a continuing education article, highlighting an unusual finding as a teaching case study, or sharing a technique that has resulted in a successful outcome in the classroom … and maybe next year we'll see your name on *JNMT*'s 2022 Best Paper awards! Don't know where to start? Need some assistance with an idea for a publication in *JNMT*? Help is available! General publication information can be found on the *JNMT* website at https://tech.snmjournals.org/authors. For individual help, please contact me at ksthomas0412@msn.com.

Kathy S. Thomas, MHA, CNMT, PET, FSNMMI-TS

You will find a diverse selection of continuing education articles in this issue, including an interesting discussion on the biology of cancer and PET imaging (*1*); the final article in the PET/MRI series (*2*); part II in the SNMMI Clinical Trials Network research series for technologists (*3*); and the latest procedure guideline on molecular breast imaging (*4*).

The Practical Protocol Tip (PPT), *Small Bowel and Colon Transit,* summarizes small bowel and colon transit study using single-isotope liquid gastric emptying with small bowel and colon follow-through (*5*). As always, the PPT is designed to be clipped from the *JNMT* to update your Policy and Procedure Manual.

In the Educators' Forum, a survey of educators summarizes the trends and changes in nuclear medicine technology (NMT) programs resulting from the COVID-19 pandemic (*6*). On the basis of approval of new diagnostic and therapeutic radiopharmaceuticals, the group concluded that the field of NMT looks bright but entry-level practice will require a revision of curriculum content and the need for increased use of virtual interaction formats.

Another innovative educational technique for NMT programs created during the COVID-19 pandemic and practiced at the University of Newcastle, Australia, demonstrates the use of videos as an "alternative clinical portfolio" to assist NMT students in developing the required skills necessary in the clinical setting (*7*).

Artificial intelligence (AI) in imaging technology continues to gain momentum and acceptance. A fascinating discussion is included regarding using AI in thyroid scintigraphy as a second reader to minimize errors and increase confidence (*8*).

When reading time is available, explore the many interesting scientific manuscripts, radiation safety discussions, and teaching case studies included, or perhaps earn a few more of those much-needed continuing education credits.

REFERENCES

1. Sarikaya I. Biology of cancer and PET imaging: pictorial review. *J Nucl Med Technol.* 2022;50:81–89.

2. Currie GM, Leon J, Nevo E, Kamvosoulis P. PET/MRI, part 4: clinical applications. *J Nucl Med Technol.* 2022;50:90–96.
3. Jeffers CD, Hoffman JM. SNMMI Clinical Trials Network research series for technologists: clinical research primer—regulatory process, part II: the role of the institutional review board in Food and Drug Administration–regulated radiopharmaceutical research. *J Nucl Med Technol*. 50:97–102.
4. Hruska CB, Corion C, Geus-Oei LF, et. al. SNMMI procedure standard/EANM practice guideline for molecular breast imaging with dedicated γ-cameras. *J Nucl Med Technol.* 2022;50:103–110.
5. Farrell, MB. Small-bowel and colon transit. *J Nucl Med Technol.* 2022;50:111–114.
6. Frye S, Prekeges JL. Interview with nuclear medicine technology educators on the impact of COVID-19 on programs, outcomes, and employers. *J Nucl Med Technol.* 2022;50:174–178.
7. Shields M, Warren-Forward HM. The impact of COVID-19 on first-year undergraduate nuclear medicine students' practical skills training. *J Nucl Med Technol.* 2022; 50:166–173.
8. Currie GM, Iqbal BM. Remodeling ^{99m}Tc-pertechnetate thyroid uptake: statistical, machine learning and deep learning approaches. *J Nucl Med Technol.* 2022;50:143–152.

Biology of Cancer and PET Imaging: Pictorial Review

Ismet Sarikaya

Kuwait University Faculty of Medicine and Mubarak Al-Kabeer Hospital Department of Nuclear Medicine, Kuwait City, Kuwait

CE credit: For CE credit, you can access the test for this article, as well as additional *JNMT* CE tests, online at https://www.snmmilearningcenter.org. Complete the test online no later than June 2025. Your online test will be scored immediately. You may make 3 attempts to pass the test and must answer 75% of the questions correctly to receive Continuing Education Hour (CEH) credit. Credit amounts can be found in the SNMMI Learning Center Activity. SNMMI members will have their CEH credit added to their VOICE transcript automatically; nonmembers will be able to print out a CE certificate upon successfully completing the test. The online test is free to SNMMI members; nonmembers must pay $15.00 by credit card when logging onto the website to take the test.

Development and spread of cancer is a multistep and complex process that involves a number of alterations, interactions, and molecular networks. PET imaging is closely related to cancer biology and pathology, as it uses various radiotracers targeting biologic and pathologic changes in cancer cells and the tumor microenvironment. In this review article, the biology of the development and spread of cancer and the role of PET imaging in oncology are summarized and supported by various PET images demonstrating patterns of cancer spread.

Key Words: cancer; spread; invasion; metastasis; PET

J Nucl Med Technol 2022; 50:81–89
DOI: 10.2967/jnmt.121.263534

Approximately 17 million new cancer cases were diagnosed and 10 million people died because of cancer in 2018 (*1*). The 3 most common sites of new cancers were the lung (1,368,500), prostate (1,276,100), and colorectal region (1,026,200) in men and the breast (2,088,800), colorectal region (823,300), and lung (725,400) in women in 2018 (*1*). Each year, approximately 400,000 children (0–19 y old) are diagnosed with cancer (*2*).

The development and spread of cancer is a multistep and complex process that involves a number of alterations in the cell, interactions between cancer cells and multiple cell types in the local and distant environments, and multiple molecular networks. Carcinogenesis is a multistep process with initiation, promotion, and progression phases and requires multiple mutations over a lifetime. PET/CT has been widely used for cancer imaging in the last 20 years. In this review article, the biology of cancer (development of cancer, modes and mechanisms of cancer spread) and current role of PET imaging in oncology are summarized and supported by PET images of various patterns of cancer spread.

Received Nov. 16, 2021; revision accepted Jan. 10, 2022.
For correspondence or reprints, contact Ismet Sarikaya (isarikaya99@yahoo.com).
Published online Apr. 19, 2022.

BIOLOGY OF DEVELOPMENT, INVASION, AND METASTASIS OF CANCER

Carcinogenesis is the development of cancer cells from a normal cell. In normal cells, the cell cycle is regulated by positive and negative feedback signals. The cell cycle has multiple phases, which include a quiescent or resting phase (G0), an interphase (G1, S, and G2), a mitotic phase (M), and a programmed cell death phase with checkpoints in interphase and mitosis (*3*,*4*). p53 is one of the main control proteins that suppress cell cycle progression in DNA-damaged cells and also aid DNA repair. Several genetic alterations occur in cancer cells to overcome the regulated cell growth. In most malignancies, the G1/S checkpoint is involved (*3*).

Acquired mutations are the most common cause of cancer, which can occur because of various factors such as tobacco use, radiation, viruses, chemicals, chronic inflammation, aging, and the environment. Germline mutations are the cause in about 5%–20% of malignancies (*5*). The carcinogenic process involves alteration or mutation in cancer genes, such as activation of oncogenes (e.g., HER2, RAS family, and RAF), inactivation of tumor suppressors (e.g., BRCA1, BRCA2, and p53), evasion of apoptosis genes, and defects in DNA repair genes. In up to 60% of cancers, there is mutation in the p53 gene, and in 30% of the cancers, there is mutation in the RAS/RAF/MEK/ERK pathway (*4*).

Neoplasms are derived from a single clone of cells that grow in an uncoordinated manner. The biologic characteristics and hallmarks of cancer cells include ability to generate mitogenic signals, evasion or resistance of immune killing, resistance of growth suppression, genetic instability, evasion of apoptosis, acquisition of unregulated sustained proliferation (immortality), angiogenesis, altered metabolism, inflammation, tumor heterogeneity, tissue invasion, and metastasis (*6*–*8*). Cancer cells within the tumor are morphologically, biochemically, and genetically heterogeneous. The most definite hallmark of cancer is the subset of neoplastic cells that escape through the basement membrane and penetrate the stroma (*6*).

Remodeling in cellular junctions, interaction between the cells and the extracellular matrix through cell adhesion molecules (e.g., integrins, selectins, cadherins, immunoglobulin

superfamily, and CD44), focal adhesions, and other substances (e.g., matrix metalloproteinases and EPLIN [epithelial protein lost in neoplasm]) are involved in various steps of cancer progression, cell motility, and migration (*9*). After cancer cells escape the basement membrane, tumor invades or penetrates the surrounding tissues and metastasizes to distant organs. Various promoter genes are implicated in invasion and metastasis. Detachment and escape of cells from the primary tumor mimics the developmental process known as epithelial mesenchymal transition (*9*,*10*). Degradative enzymes produced by the tumor or tumor-associated cells remodel the extracellular matrices and facilitate tumor cell invasion and progression. The tumor microenvironment consists of tumor cells and various tumor-associated host cells, which make up about half the total number of cells in malignant tumors and play a critical role in cancer initiation, progression, and metastasis (particularly cancer-associated fibroblasts expressing fibroblast activation protein-α and immune cells) (*6*,*11*). Tumor cells can disseminate as individual cells or move as collective groups (plasticity of tumor cell movement) (*12*,*13*). Tumor cells eventually migrate toward transportation compartments such as blood vessels, lymphatic channels, or celomic cavities with interconnectivity between transit compartments. Most of the distant metastases are hematogenous. Initially, the tumor receives a blood supply from the vessels in the new soil or form tubes to anastomose with the existing capillaries, but later, angiogenesis is induced for further growth of the tumor.

Growth of new blood vessels and lymphatic vessels occurs in the primary and metastatic tumor. Angiogenesis occurs via various mechanisms such as formation and outgrowth of sprouts, formation of new vasculature from existing vessels, recruitment of circulating endothelial progenitor cells, vascular mimicry, and transdifferentiation of cancer stem cells (*14*). Lymphatic enlargement and lymphangiogenesis via growth factors produced by tumor and tumor microenvironment cells occur in the primary tumor and sentinel lymph nodes (*15*).

SUMMARY OF PET IMAGING IN ONCOLOGY

PET imaging is closely related to cancer biology and pathology, because PET imaging uses various radiotracers for cancer detection based on biologic and pathologic changes in cancer cells and the tumor microenvironment. PET/CT has been widely used for cancer imaging since early 2000. PET/MRI has also become available in the last 10 years. The recent introduction of total-body PET/CT cameras allow imaging of the entire body simultaneously within a few minutes (*16*).

PET is used for initial staging, assessing response to various treatments, detecting recurrences, differentiating benign from malignant lesions, guiding biopsies, planning radiotherapy, selecting patients for treatments, searching for the primary tumor in cases with primary-unknown metastases and paraneoplastic syndromes, and predicting tumor grade, aggressiveness, heterogeneity, prognosis, and survival. There are various PET radiotracers that can detect cancer cells on the basis of increased metabolism (e.g., glucose, fatty acids, and lactate); synthesis of proteins, DNA, and cell membranes as markers of cellular proliferation; and expression of various receptors, enzymes, and tumor-associated or -specific antigens. Table 1 shows the common and uncommon PET radiotracers for cancer imaging.

^{18}F-FDG is the most commonly used PET radiotracer to image cancer. Cancer cells mainly use glucose for their energy needs (aerobic glycolysis, Warburg effect), with accelerated glucose metabolism, increased rate of glucose transport and glycolysis, overexpression of glucose transporters, and increased level of hexokinase enzyme. The tumor microenvironment also affects the glucose metabolism of cancer cells. Breast cancer, particularly invasive and inflammatory, is among the most common indications of ^{18}F-FDG PET imaging, mainly for staging (particularly stages 3 and 4), assessing response to treatments, and detecting recurrences (*17*,*18*). ^{18}F-FDG PET is indicated for initial staging of all cases of non–small cell lung cancer and initial staging of pure and combined small cell lung cancer (*17*). ^{18}F-FDG PET is used for differential diagnosis of solid solitary pulmonary nodules that are larger than 8 mm (*19*). In multiple myeloma, ^{18}F-FDG PET helps to distinguish inactive from active disease, to detect extramedullary disease, to monitor the effect of treatments, and to determine progression from smouldering myeloma. ^{18}F-FDG PET is standard for lymphoma staging (Hodgkin and various non-Hodgkin lymphomas such as diffuse large B-cell, follicular, mucosa-associated lymphoid tissue, and mantle cell subtypes) and end-of-treatment response assessment. In head and neck cancer, ^{18}F-FDG PET is indicated for detecting an occult primary tumor and is recommended for initial staging and assessing response to treatment. ^{18}F-FDG PET is recommended in anaplastic thyroid cancer and in papillary, follicular, and Hürthle cell carcinomas if stimulated thyroglobulin is more than 2–5 ng/mL and ^{131}I imaging results are negative (*17*). High-grade gliomas, particularly glioblastoma multiforme, are usually ^{18}F-FDG–avid. ^{18}F-FDG PET helps to differentiate high- from low-grade gliomas, determine the extent of tumor for treatment planning, detect recurrences, and guide biopsies. Most soft-tissue and bone sarcomas are highly ^{18}F-FDG–avid. ^{18}F-FDG PET helps in staging and assessing the response to treatment with thyrosine kinase inhibitors in gastrointestinal stromal tumors. Most paragangliomas are ^{18}F-FDG–avid, particularly cases with succinate dehydrogenase-B mutation (*20*). Malignant melanoma is highly ^{18}F-FDG–avid. ^{18}F-FDG PET is recommended for initial staging of stage 3 and 4 melanoma and can be used in earlier stages if patients have clinical signs and symptoms (*17*). ^{18}F-FDG PET can also demonstrate cancer-related complications such as tumor thrombus and emboli, fracture, and inflammatory changes.

Radiolabeled ligands of prostate-specific membrane antigen (PSMA), most notably ^{68}Ga-PSMA-11, are used for initial staging of high-risk prostate cancer and detecting recurrences with higher efficiency than ^{11}C-choline PET and ^{18}F-fluciclovine PET at low PSA levels (*21*,*22*). PSMA PET is also used

TABLE 1
Oncologic PET Radiotracers and Their Mechanisms of Uptake in Cancer

Radiotracer	Measures or targets	Uptake mechanism	Main indications studied	Availability
^{18}F-FDG	Glucose metabolism (indirect)	Is taken up via GLUT1 and phosphorylation by hexokinase	Various cancers	Widely, routine
SSTA	Somatostatin receptors	Binds mainly to subtype 2 and in lesser degree to subtypes 3 and 5	Well- and moderately differentiated NETs	Increasing
^{68}Ga-PSMA	Cellular PSMA	Binds to cellular PSMA and internalizes	Prostate cancer	Increasing
^{18}F-NaF	Osteoblastic activity	Exchanges ^{18}F ions with hydroxyl ions on surface of hydroxyapatite to form fluoroapatite	Bone metastases from various cancers	Increasing
^{18}F-FLT	Cellular proliferation (indirect)	Is phosphorylated by thymidine kinase (not incorporated into DNA)	Various cancers; NSCLC, lymphomas	Limited
^{18}F-FET	AA uptake by transporters	Enters cells by LAT1	Brain tumors, particularly gliomas	Limited
^{11}C-MET	AA uptake and protein synthesis	Enters cells by LAT1 and is involved in synthesis of proteins and phospholipids	Brain tumors, particularly gliomas	Limited
^{18}F-FLUC	AA uptake by transporters	Enter cells by AA transporter ASCT2 and LAT1	Prostate cancer	Limited
^{18}F-DOPA	^{18}F-DOPA transport, storage, and metabolism	Enters neuroendocrine cells by LAT1, is converted to dopamine by AA decarboxylase, and is trapped in vesicles via VMAT	NETs, pheo, neuroblastoma, PG, gliomas	Limited
^{11}C-choline and ^{18}F-fluorocholine	Cell membrane synthesis or cellular proliferation	Is phosphorylated by choline kinase to phosphocholine and converted to phosphatidylcholine	Prostate cancer	Limited
^{11}C-acetate	Cellular proliferation	Incorporates into cellular membrane	HCC (well-differentiated), renal cancers	Limited
^{68}Ga-FAPI	Cancer-associated fibroblasts	Binds to fibroblast activation protein on cancer-associated fibroblasts	Various cancers	Limited
^{18}F-FES	Estrogen receptor	Binds to estrogen receptor	Breast cancer, ovarian cancer	Limited
^{89}Zr-trastuzumab	Human epidermal growth factor	Binds to human epidermal growth factor	Breast cancer	Limited
^{18}F-FDHT	Androgen receptor	Binds to androgen receptor	Prostate cancer	Limited
^{124}I	Iodine metabolism	Is taken up by thyroid follicular cells via Na+/I− symporter, is oxidized by thyroid peroxidase, stays in colloid, or leaves as thyroid hormones	Well-differentiated thyroid cancer	Limited
^{124}I-MIBG	Norepinephrine transporter	Is taken up by sympathicomedullary tissue via norepinephrine transporter (uptake-1 system) and stored in neurosecretory granules	Pheo, neuroblastoma, PG	Limited
^{18}F-FMISO	Hypoxia	Nitro-group undergoes reduction in hypoxia, forms highly reactive oxygen radicals, and binds to intracellular macromolecules	Various cancers, particularly brain and HN	Limited
^{64}Cu-ATSM	Hypoxia	Accumulates in regions with higher CD133+ expression and activates hypoxia inducible factor 1 (possible mechanisms)	Various cancers, particularly brain and HN	Limited
Folate*	Folate receptor α	Binds to folate receptor-α	Various cancers	Limited
^{68}Ga-pentixafor	CXC motif chemokine receptor 4	Binds to CXC motif chemokine receptor 4	Various cancers	Limited
^{11}C-lactate	Lactate metabolism	Undergoes oxidative phosphorylation	Various cancers	Limited
Immuno-PET*	Tumor-associated antigens	Monoclonal antibodies bind to tumor-associated antigens	Various cancers	Limited

*Various radiotracers.

GLUT1 = glucose transporter 1; SSTA = ^{68}Ga-SSTAs (somatostatin analogs); NET = neuroendocrine tumor; FLT = fluorothymidine; NSCLC = non–small cell lung carcinoma; FET = fluoroethyltyrosine; AA = amino acid; LAT1 = L-type amino acid transporter; MET = methionine; FLUC = fluciclovine; ASCT2 = alanine, serine, cysteine transporter 2; ^{18}F-DOPA = 6-^{18}F-fluoro-L-dopa; VMAT = volumetric modulated arc therapy; pheo = pheochromocytoma; PG = paraganglioma; HCC = hepatocellular carcinoma; FAPI = fibroblast-activation-protein inhibitor; FES = fluoroestradiol; FDHT = fluorodihydrotestosterone; MIBG = metaiodobenzylguanidine; FMISO = fluoromisonidazole; ATSM = diacetyl-bis(N^4-methythiosemicarbazone); HN = head and neck.

for selecting patients and for assessing response to PSMA-targeted radionuclide treatments. Somatostatin receptor PET imaging has high sensitivity in detecting various well-differentiated NETs (e.g., carcinoid) expressing high somatostatin receptors (particularly subtypes 2, 3, and 5) and certain types of paragangliomas (*20*). ^{18}F-fluoroestradiol PET helps to determine the estrogen receptor status of breast and ovarian cancers. Radiolabeled amino acid tracers such as ^{11}C-methionine, 6-^{18}F-fluoro-L-dopa, and ^{18}F-fluoroethyltyrosine have high sensitivity in detecting primary and recurrent glioblastoma multiforme. ^{18}F-thymidine has been studied for grading, assessing tumor heterogeneity, and detecting recurrences in gliomas. 6-^{18}F-fluoro-L-dopa is also useful for detecting medullary thyroid carcinomas and succinate dehydrogenase-B–negative paragangliomas (*23*). Various hypoxia-imaging radiotracers help to identify tumor hypoxia, an ability that is important for radiotherapy planning, assessing tumor heterogeneity, and selecting patients for hypoxia-targeted therapeutics. Radiolabeled fibroblast activation protein inhibitors show uptake in various cancers, with promising results (*24*). Immuno-PET imaging with radiolabeled antibodies against tumor-associated or -specific antigens has been studied in detecting cancer and assessing response to treatment.

Targeted radionuclide treatment of cancer using various β- and α-particle emitters is a rapidly evolving area. By showing the presence, extent, and intensity of the target expression in the tumor, theranostic PET imaging helps in selecting patients for targeted radionuclide treatment, determining the treatment dose, and assessing response to treatment.

Precision medicine is selection of the right treatment using various diagnostic tests (molecular, imaging) and analytics for a group of individuals with certain characteristics, whereas personalized medicine is selection of the right treatment for an individual patient. PET offers various radiotracers to image tumor biomarkers such as hypoxia, angiogenesis, apoptosis, metabolism, proliferation, and antigen/receptor expression, which help to determine tumor characteristics and heterogeneity, thus helping in choosing the right treatment and in identifying resistance to therapies with early therapy-response assessment.

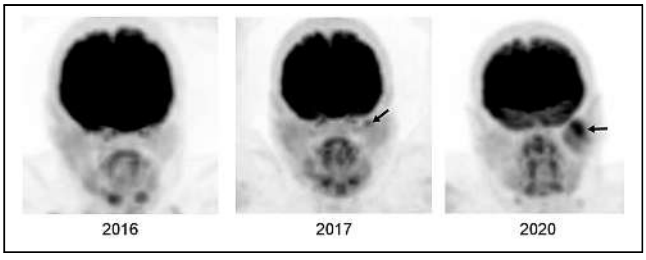

FIGURE 1. Development of parotid cancer in patient with breast cancer. Selected serial ^{18}F-FDG PET maximum-intensity-projection images of head and neck show that mild focal uptake in left parotid gland in 2017 became larger and more hypermetabolic in 2020 (arrows). Histopathologic examination showed mucoepithelial cancer. There was no abnormal uptake in left parotid gland in 2016, possibly because tumor was either absent at that time or was of microscopic or small volume below PET resolution.

^{18}F and ^{68}Ga are the most commonly used PET radionuclides for radiolabeling molecules for cancer imaging. The other PET radionuclides, such as ^{11}C and other radiometals (e.g., ^{89}Zr, ^{64}Cu, ^{86}Y, and radioisotopes of scandium and terbium) have also been studied to label various molecules. Radiometals are used mainly to label peptides, proteins, antibodies, and ligands because of their longer half-lives and longer circulation of such molecules. Longer half-life is also an advantage in shipment.

PET images are supported by various parameters to better assess radiotracer uptake and distribution in the tumor, such as SUV, metabolically active tumor volume, global metabolic tumor volume, total lesion glycolysis, dual- or multiple-time-point PET imaging with retention index, dynamic PET imaging, and parametric PET imaging with kinetic modeling and quantitative analysis (*25*). Various PET response criteria are used to better assess the response to chemotherapy, radiotherapy, and treatment with immune checkpoint inhibitors (*26*).

Figure 1 shows development of a cancer on serial PET images. Supplemental Figure 1 shows PET images of local invasion/infiltration by breast and lung cancers (supplemental materials are available at http://jnmt.snmjournals.org).

PET imaging has a well-established role in cancer management but has certain limitations such as in detecting small tumor foci and in quantifying radiotracer uptake and tumor volume and nonspecificity of radiotracers. The spatial resolution of PET has been increasing (in the range of 5–8 mm for the trunk and 3–5 mm for the brain and extremities), but smaller and microscopic or submillimetric foci cannot be detected. Ultra-high-resolution brain PET scanners are being developed that may detect brain lesions 1.6–1.8 mm in size (*27*). Current PET radiotracers are not purely cancer-specific and may show uptake in benign lesions, normal tissues, and inflammation after treatments (*28*). Low-grade and well-differentiated

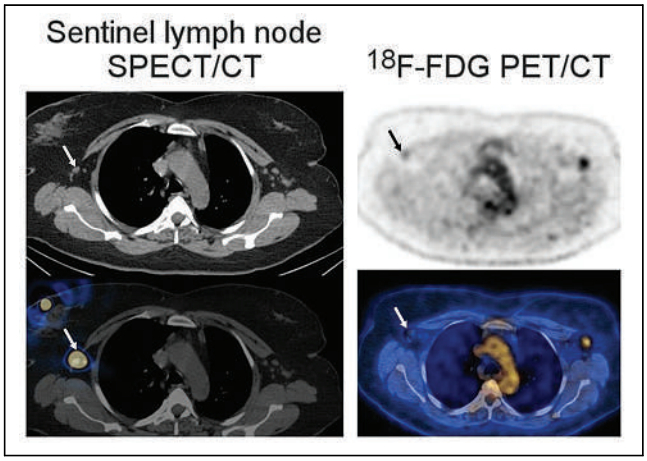

FIGURE 2. Early metastasis in sentinel lymph node as seen on transaxial SPECT/CT and ^{18}F-FDG PET/CT images of patient with newly diagnosed bilateral invasive lobular breast cancer. SPECT/CT shows right sentinel lymph node (arrows). ^{18}F-FDG PET/CT shows mild uptake in right sentinel lymph node (arrows), found on biopsy to be metastasis. ^{18}F-FDG uptake in left axillary lymph node was also due to metastasis. (Adapted from (*38*).)

tumors show low glucose metabolism, or certain tumors may use other fuels for their energy needs; the sensitivity of ^{18}F-FDG PET is reduced in such tumors. Tumor cells may lack or lose antigen or receptor expression, limiting the efficiency of PET radiotracers targeting such expression. Certain PET radiotracers that are relatively more specific for a histologic type of cancer may also show uptake in other cancer types, such as PSMA ligands. PET parameters, particularly SUV, are affected by various factors, most notably blood glucose and body mass index (*25*,*29*). SUV normalized by lean body mass or tumor-to-reference SUV ratios can be used when assessing response to treatments in obese and overweight patients (*30*,*31*). Certain medications can affect the uptake and distribution of radiotracers and should be stopped before PET studies. Calculation of local or global tumor volume with threshold- and algorithm-based methods has certain limitations, with over- or underestimation of the tumor volume (*32*). Artifacts can be seen on PET/CT images because of motion, arm positioning, and dense material or objects (*33*–*35*). Various reconstruction techniques and software are available to overcome some of these artifacts.

MODES OF METASTATIC SPREAD OF CANCER AND PET IMAGES

Metastasis Through Lymphatic System

Cancer cells enter or invade the lymphatic vessels and migrate to the tumor-draining sentinel lymph node. High interstitial fluid pressure in the tumor facilitates the entry of cancer cells into lymphatic vessels (*36*). Tumor cells and cells in the tumor microenvironment produce growth factors that promote peritumoral lymphangiogenesis, which provides tumor cells access to more lymphatic vessels. Cancer cells can also move toward and invade lymphatic vessels by sensing the chemokines produced by lymphatic endothelial cells (chemoattraction) (*36*,*37*).

Although the lymph node is filled with various immune cells, the microenvironment is immunosuppressive. Immunosuppression is believed to occur before metastasis, and the premetastatic niche emerges before cancer cells arrive (*36*). While migrating in the lymphatic vessel, tumor cells continue to grow and survive. Cancer cells can escape the tumor-draining lymph node through the efferent lymphatic vessel or invade the lymph node blood vasculature and further spread to other lymph nodes and distant organs. Figure 2 demonstrates ^{18}F-FDG uptake in a sentinel lymph node, and Supplemental Figure 2 shows uptake in lymphatic channels and lymph nodes (*38*).

Metastasis Through Vascular System

The metastatic cascade of hematogenous metastasis includes development of a metastatic cell, establishment of a premetastatic niche, motility and invasion, intravasation, dissemination and transport, cellular arrest, vascular adhesion, and extravasation and colonization (*39*).

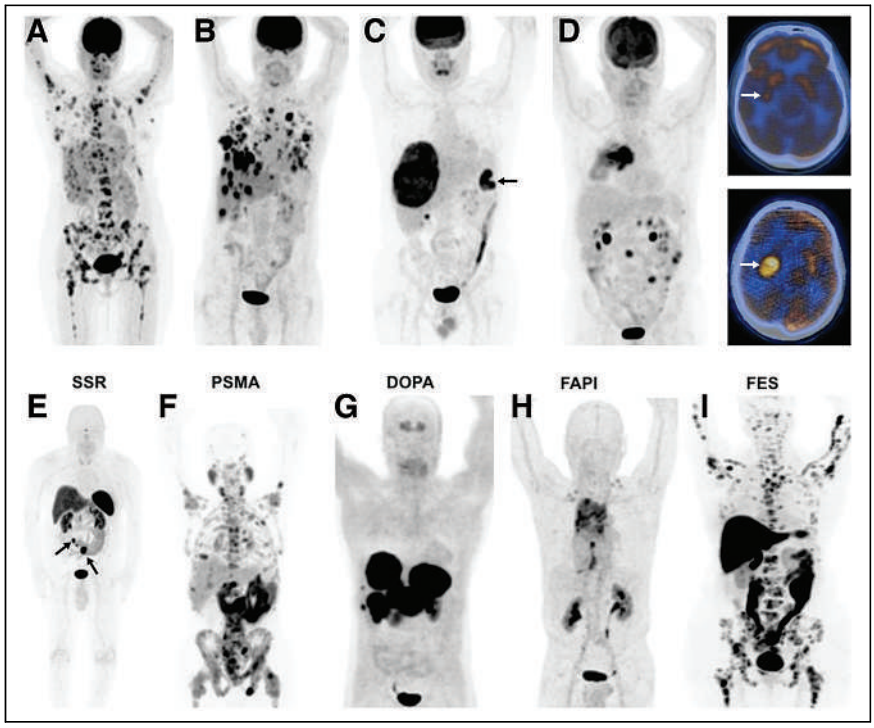

FIGURE 3. ^{18}F-FDG PET images of various cancers and metastases (A–D), and PET images with various other radiotracers (E–I). (A) Right breast cancer (invasive ductal) with multiple metastases in bones, liver, right adrenal, and right axillary lymph nodes. (B) Right breast cancer (poorly differentiated neuroendocrine tumor) with multiple metastases in lungs, liver, and right axillary lymph nodes. (C) Colon cancer in splenic flexure (arrow), with large metastasis in liver. (D) Rapid progression of brain metastasis in patient with cancer in right lung. Whole-body image (left) demonstrated hypermetabolic right lung tumor. On initial PET/CT scan, there was mild focal uptake in tail of right putamen (top right, arrow), but 3 mo later (no treatment), significant increase in size and metabolic activity of metastatic focus in brain was seen (bottom right, arrow). (E) ^{68}Ga-DOTANOC PET image of patient with small-bowel carcinoid, showing primary tumor (left arrow) and multiple mesenteric metastases (right arrow), all with high somatostatin receptor binding. (F) ^{68}Ga-PSMA-11 PET image of patient with prostate cancer, showing diffuse bone and multiple abdominal and pelvic lymph node metastases. (G) 6-^{18}F-fluoro-L-dopa PET image of patient with history of surgically treated well-differentiated ileal neuroendocrine tumor, showing intense uptake in multiple large hepatic metastases. (Adapted from (*43*).) (H) ^{68}Ga-FAPI PET image of patient with non–small cell lung carcinoma, showing intense uptake in primary tumor and metastatic foci in mediastinum and, bilaterally, in supraclavicular regions. (Adapted from (*44*).) (I)^{18}F-fluoroestradiol PET image of patient with invasive lobular breast cancer, showing extensive bone and bone marrow involvement with high estrogen receptor binding. (Adapted from (*45*).)

Before leaving the tumor, cancer cells communicate with the other parts of the body through soluble factors to establish a premetastatic niche (*40*,*41*). Stem cells are mobilized, arrive in the secondary microenvironment, and prepare it before the arrival of cancer cells. Intravasation of detached cancer cells requires partial degradation of the extracellular matrix and basement membrane underlying endothelial cells. During intravascular travel, some tumor cells evade immune attacks, but some are killed by natural killer cells or hemodynamic sheer forces (Supplemental Fig. 3) (*39*). Cancer cells evade the immune attacks by downregulating antigens and secreting substances to trick the immune system into recognizing them as normal cells or to prevent immune cells from directly killing them. By coating the cancer cells, platelets help them gain physical and immune protection. Platelets and cancer cells also secrete substances to act on the monocytes and endothelial cells. Neutrophils can protect cancer cells from natural killer cells. The efficiency of metastasis increases if the tumor cells form emboli. For extravasation, tumor cells develop adhesion to the endothelial cells and penetrate the endothelium and the basement membrane with the help of metastasis-associated macrophages in the target tissue. After extravasation, tumor foci colonize in the new soil. Cancer cells modulate and restructure the new soil. Colonized cancer cells do not always grow as soon as they seed in the new soil. They can stay dormant and become detectable in months to years. Various mechanisms are involved in cancer dormancy and reawakening.

Certain cancers seed in specific organs (organ tropism, seed-and-soil theory), a process that is regulated by multiple factors, such as interaction between tumor cells and the host microenvironment, circulation pattern, tumor-intrinsic factors, and organ-specific niches (*39*–*42*). Liver, lung, bone, and brain are the most frequent sites of distant metastases. Common sites of hematogenous metastases vary among cancer types and subtypes. Figure 3 shows PET images of distant organ metastases from various cancers (*43*–*45*).

Bone is one of the most frequent sites of tumor metastasis or spread from breast and prostate cancers and multiple myeloma. Multiple factors and expression of certain genes contribute to the homing of tumor cells to the bone. In osteolytic metastases and multiple myeloma bone lesions, the bone remodeling process is imbalanced; ephrin B2 and EphB4 expression is downregulated (*46*). There is increased osteoclastic bone resorption driven by osteoclast-activating factors produced by the tumor or cells in the bone microenvironment. Tumor cells also produce osteoblast inhibitor factors. Myeloma cells produce growth factors that stimulate the growth of bone marrow stromal cells, which in turn produce osteoclast-activating factors, such as IL-6, M-CSF, TNFa, and RANKL. In osteoblastic metastases, there is formation of new bone that is immature and of poor quality. Tumor cells secrete factors that induce osteoblastic proliferation and differentiation, such as TGF-β, VEGF, and FGF (*46*). In prostate cancer, prostate-specific antigen and other substances modify the bone microenvironment. Supplemental Figures 4–6 show the histopathology and some PET images of osteolytic and osteoblastic bone metastases (*47*).

Liver is a common site for metastases from breast, lung, and gastrointestinal malignancies. Hepatocytes interact directly with tumor cells to promote liver metastasis and promote the formation of a prometastatic niche via secretion of various substances (*42*). Hepatic stellate and Kupffer cells are also involved in inducing or facilitating liver metastasis. Lung is a common site for metastasis from breast, melanoma, and thyroid malignancies. Tumor-derived factors help tumor cell extravasation to the lung parenchyma. Neutrophils, chemokines, alveolar macrophages, and fibroblasts are involved in facilitating lung metastasis (*42*). Brain is a common metastatic site for lung cancer, breast cancer, and melanoma. Tumor cells produce certain substances to overcome the defense provided by the blood–brain barrier. Astrocytes secrete many factors, such as IL6, TGF-β, and IGF-1, to induce the growth of brain metastases (*48*). Figure 3 shows rapid progression of brain metastasis.

Metastasis Through Celomic Cavities

Peritoneal spread of the tumor can occur because of direct rupture of the tumor into the peritoneal cavity, intraperitoneal seeding from ascites, or hematogenous or lymphatic spread, depending on the type of primary tumor (*49*). Intraperitoneal seeding most commonly occurs from gastrointestinal and ovarian malignancies. During surgery or biopsy, secondary seeding may occur. Tumor cells adhere to the mesothelial lining of the peritoneum and invade the submesothelial connective tissues. Tumor cells initially grow focally in gravity-dependent recesses—in regions of stasis, pouches, paracolic gutters, the umbilicus, and subdiaphragmatic spaces—but eventually diffusely involve both the visceral and the parietal peritoneum. Peritoneal carcinomatosis

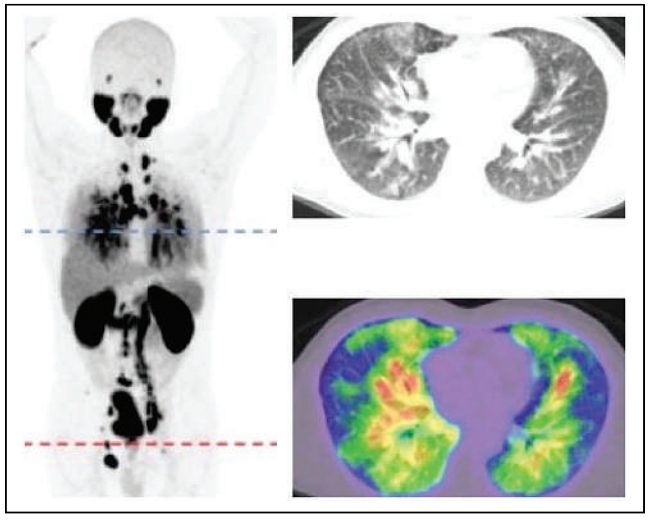

FIGURE 4. Pulmonary LC in patient with prostate cancer. Whole-body PET and transaxial CT and ^{68}Ga-PSMA ligand images show widespread thickening of interlobular septae and diffusely increased radiotracer uptake. (Adapted with permission of (*53*).)

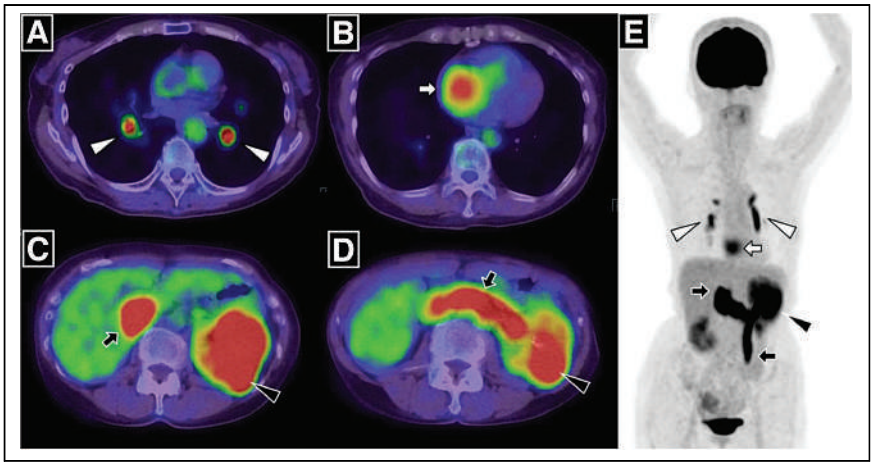

FIGURE 5. Massive pulmonary tumor emboli from intravascular tumor thrombus in patient with renal cell carcinoma. PET/CT and maximum-intensity-projection images demonstrate ^{18}F-FDG accumulation in left renal tumor, which was continuously observed in left renal vein and extended into infradiaphragmatic inferior vena cava and left ovarian vein (C, D, and E, black arrows). ^{18}F-FDG uptake in left distal pulmonary artery and right and left branches (A and E, white arrowheads) and right atrial cavity (B and E, white arrows) is also seen. (Reprinted with permission of (*55*).)

is usually associated with ascites. Supplemental Figure 7 shows ^{18}F-FDG PET/CT images of cases of peritoneal carcinomatosis.

Pleural spread of the tumor (pleural carcinomatosis) can develop as a direct extension of nearby cancer into the pleural space or through hematogenous or lymphangitic spread (*50*). Pleural tumor is usually associated with malignant pleural effusion. Pericardial spread of tumor may occur via lymphatic or hematogenous dissemination, local direct extension, or the transvenous route by various tumors.

The Krukenberg tumor is a rare metastatic signet ring cell tumor of the ovary, with primary tumor in most cases being in the stomach, colon, appendix, or breast (particularly invasive lobular carcinoma). The mechanism could be via lymphogenous, hematogenous, or transcelomic pathways (*51*).

Other Routes of Metastasis

Lymphangitic Carcinomatosis (LC). LC is diffuse infiltration and obstruction of parenchymal lymphatic channels by cancer cells, with associated inflammation. The most common location is the lungs (pulmonary LC), and rarely it can occur in other organs. Pulmonary LC is usually seen in breast, lung, stomach, pancreas, ovary, and cervix cancers. The mechanism of LC is not well understood. It may be due to retrograde tumor spread into the lymphatics through the hilar or thoracic lymph nodes as a result of obstruction in lymphatic drainage. It may also be due to antegrade movement of tumor cells from the pleura to the hilar lymph nodes through lymphatic vessels. Another possibility is hematogenous spread of metastatic disease to the lung interstitium, with subsequent lymphatic involvement. The mechanism may also be via tumor embolism (*52*). Histopathologically, cancer cells are located within or around the lymphatics in the interstitium, with edema and a desmoplastic reaction. Figure 4 shows PET/CT images of a case of pulmonary LC (*53*).

Tumor Embolism and Tumor Thrombus. Tumor embolism can occur when cancer cells from solid tumors enter the circulation as individual or clusters of cells and lodge in various sizes of arteries or due to tumor fragments from an intravascular tumor thrombus. Common sites of tumor embolism are the aortic bifurcation or the femoral, cerebral, pulmonary, renal, or splenic arteries (*54*). Within the artery, a tumor embolus may resolve, remain latent, or progress. Tumor embolism is more common in breast, lung, colon, stomach, kidney, ovary, and liver cancers. A tumor thrombus is an extension of the tumor into a vessel, mainly a vein. A tumor thrombus is most frequently associated with renal cell, adrenal cortical, and hepatocellular carcinomas and with Wilms tumor. Figure 5 shows massive tumor emboli caused by an intravascular tumor thrombus (*55*).

Tumor Spread Through Canaliculi. Tumor can spread through canaliculi such as the bile, mammary, and nasolacrimal ducts; the urinary tract; and the airways. Cancer cells

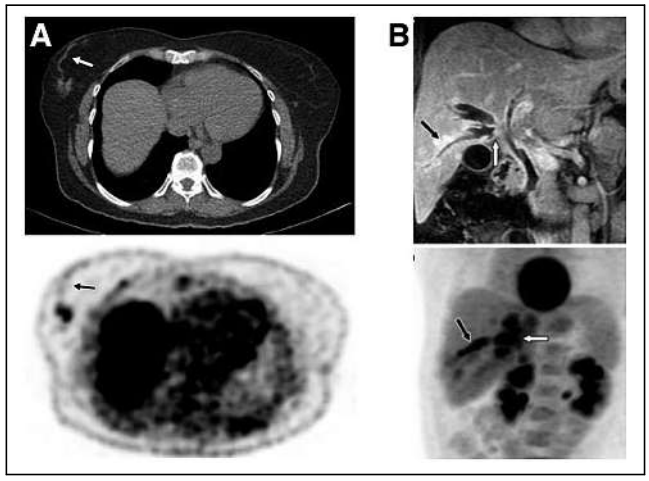

FIGURE 6. (A) Transaxial CT and ^{18}F-FDG PET images of patient with tubular breast cancer show hypermetabolic primary tumor as well as linear mild activity representing intraluminal tumor uptake either in mammary duct extending to nipple or in lymphatic channel extending to Sappey plexus (arrows). (B) Infiltrating perihilar cholangiocarcinoma with peribiliary extension. Coronal T1-weighted contrast-enhanced MR image (top) shows enhancing tumor of confluence of right ducts (white arrow), intrahepatic ductal dilation, and enhancing right peribiliary extension (black arrow), and ^{18}F-FDG PET maximum-intensity-projection image (bottom) shows ^{18}F-FDG–avid perihilar tumor (white arrow) with peribiliary extension (black arrow). (Adapted from (*56*).)

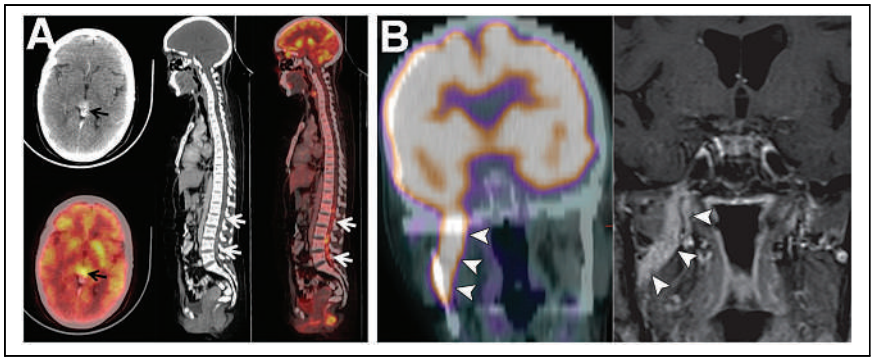

FIGURE 7. (A) Drop metastases in spinal canal from germ cell tumor of pineal gland. Head CT (top left) and ^{18}F-FDG PET (bottom left) show avidly enhancing hypermetabolic nodular lesion in pineal gland (arrows). Sagittal CT (middle) and ^{18}F-FDG PET/CT (right) show increased uptake in ill-defined densities in spinal canal extending from L1 to L5 (arrows). (Adapted from (*58*).) (B) Perineural tumor spread along V3 (mandibular) nerve. Coronal ^{18}F-FDG PET/CT (left) and contrast-enhanced T1-weighted fat-saturated MRI (right) show intense ^{18}F-FDG accumulation and abnormal enhancement along V3 (arrowheads). (Adapted with permission of (*60*).)

can also migrate along the basal side of endothelial cells without entering the lumen. Tumor spread through canaliculi or ducts can be seen as a linear area of increased uptake on PET images. Figure 6 shows PET images of tumor spread via a possible mammary duct in breast cancer and peribiliary extension of tumor in cholangiocarcinoma (*56*).

Leptomeningeal Carcinomatosis. Leptomeningeal carcinomatosis is infiltration of cancer cells in the meningeal space surrounding the brain and spinal cord, which is more commonly seen in breast cancer, lung cancer, and melanomas. Cancer cells can reach the meningeal space by hematogenous spread, direct extension or drop metastases from metastatic or primary brain tumors and then are disseminated by the cerebrospinal fluid flow in the meningeal space (*57*). Leptomeningeal carcinomatosis can also involve cranial nerves. Figure 7A shows drop metastasis into the spinal medullary cavity (*58*). Metastasis to the cerebral ventricles is rare and could be caused by intracranial or extracranial tumors.

Perineural Tumor Invasion and Perineural Tumor Spread. Perineural tumor invasion is a histopathologic (microscopic) finding of local infiltration of the nerves near the tumor, whereas perineural tumor spread is macroscopic extension of the tumor along the nerve sheath. Studies have shown that perineural tumor growth is a molecularly mediated process and that supportive cells within the peripheral nerves interact with the cancer to promote invasion and dissemination of cancer cells along the nerves (*59*). Perineural tumor growth is more commonly seen in head and neck cancers (particularly facial, mandibular, and maxillary nerves) but can also occur with various other cancers such as cancer of the pancreas, prostate, colon, or rectum. MRI is a gold standard in detecting perineural tumor spread. Figure 7B shows PET/MR images of perineural tumor spread (*60*).

CONCLUSION

The biology of the development and spread of cancer and the role of PET imaging in oncology have been summarized in this article, supported by various PET images demonstrating cancer spread patterns.

DISCLOSURE

No potential conflict of interest relevant to this article was reported.

REFERENCES

1. *Global Cancer Facts & Figures.* 4th ed. American Cancer Society; 2018:1–73.
2. Steliarova-Foucher E, Colombet M, Ries LAG, et al. International incidence of childhood cancer, 2001-10: a population-based registry study. *Lancet Oncol.* 2017;18:719–731.
3. Ok CY, Woda B, Kurian E. The pathology of cancer. In: Pieters RS, Liebmann J, eds. *Cancer Concepts: A Guidebook for the Non-Oncologist.* University of Massachusetts Medical School; 2018:1–11.
4. Malarkey DE, Hoenerhoff M, Maronpot RP. Carcinogenesis: mechanisms and manifestations. In: Haschek W, Bolon B, Ochoa R, Rousseaux C, Wallig M, eds. *Haschek and Rousseaux's Handbook of Toxicologic Pathology.* Vol 1. 3rd ed. Academic Press; 2013:107–146.
5. The genetics of cancer. Cancer.Net website. https://www.cancer.net/navigating-cancer-care/cancer-basics/genetics/genetics-cancer. Published March 2018. Accessed April 8, 2022.
6. Welch DR, Hurst DR. Defining the hallmarks of metastasis. *Cancer Res.* 2019;79:3011–3027.
7. Welch DR. Tumor heterogeneity: a 'contemporary concept' founded on historical insights and predictions. *Cancer Res.* 2016;76:4–6.
8. Hanahan D, Weinberg RA. Hallmarks of cancer: the next generation. *Cell.* 2011;144:646–674.
9. Martin TA, Ye L, Sanders AJ, Lane J, Jiang WG. Cancer invasion and metastasis: molecular and cellular perspective. NCBI website. https://www.ncbi.nlm.nih.gov/books/NBK164700/. Published 2013. Accessed April 8, 2022.
10. Tarin D. The fallacy of epithelial mesenchymal transition in neoplasia. *Cancer Res.* 2005;65:5996–6000.
11. Mareel M, Oliveira MJ, Madani I. Cancer invasion and metastasis: interacting ecosystems. *Virchows Arch.* 2009;454:599–622.
12. Wu JS, Jiang J, Chen BJ, Wang K, Tang YL, Liang XH. Plasticity of cancer cell invasion: patterns and mechanisms. *Transl Oncol.* 2021;14:100899.
13. Clark AG, Vignjevic DM. Modes of cancer cell invasion and the role of the microenvironment. *Curr Opin Cell Biol.* 2015;36:13–22.
14. Lugano R, Ramachandran M, Dimberg A. Tumor angiogenesis: causes, consequences, challenges and opportunities. *Cell Mol Life Sci.* 2020;77:1745–1770.
15. Stacker SA, Williams SP, Karnezis T, Shayan R, Fox SB, Achen MG. Lymphangiogenesis and lymphatic vessel remodelling in cancer. *Nat Rev Cancer.* 2014;14:159–172.
16. Badawi RD, Shi H, Hu P, et al. First human imaging studies with the EXPLORER total-body PET scanner. *J Nucl Med.* 2019;60:299–303.
17. NCCN practice guidelines: narrative summary of indications for FDG PET and PET/CT. amazonaws website. http://s3.amazonaws.com/rdcms-snmmi/files/production/public/images/NCCN%20Narrative%20Summary%20Feb%202016.pdf. Accessed April 26, 2022.
18. Sarikaya I. Breast cancer and PET imaging. *Nucl Med Rev Cent East Eur.* 2021;24:16–26.
19. MacMahon H, Naidich DP, Goo JM, et al. Guidelines for management of incidental pulmonary nodules detected on CT Images: from the Fleischner Society 2017. *Radiology.* 2017;284:228–243.
20. Taïeb D, Hicks RJ, Hindié E, et al. European Association of Nuclear Medicine practice guideline/Society of Nuclear Medicine and Molecular Imaging procedure standard 2019 for radionuclide imaging of phaeochromocytoma and paraganglioma. *Eur J Nucl Med Mol Imaging.* 2019;46:2112–2137.

21. Morigi JJ, Stricker PD, Leeuwen PJV, et al. Prospective comparison of ^{18}F-fluoromethylcholine versus ^{68}Ga-PSMA PET/CT in prostate cancer patients who have rising PSA after curative treatment and are being considered for targeted therapy. *J Nucl Med.* 2015;56:1185–1190.
22. Calais J, Ceci F, Eiber M, et al. ^{18}F-fluciclovine PET-CT and ^{68}Ga-PSMA-11 PET-CT in patients with early biochemical recurrence after prostatectomy: a prospective, single-centre, single-arm, comparative imaging trial. *Lancet Oncol.* 2019; 20:1286–1294.
23. Giovanella L, Treglia G, Iakovou I, Mihailovic J, Verburg FA, Luster M. EANM practice guideline for PET/CT imaging in medullary thyroid carcinoma. *Eur J Nucl Med Mol Imaging.* 2020;47:61–77.
24. Hicks RJ, Roselt PJ, Kallur KG, Tothill RW, Mileshkin L. FAPI PET/CT: will it end the hegemony of ^{18}F-FDG in oncology? *J Nucl Med.* 2021;62: 296–302.
25. Sarikaya I, Sarikaya A. Assessing PET parameters in oncologic ^{18}F-FDG studies. *J Nucl Med Technol.* 2020;48:278–282.
26. Wahl RL, Jacene H, Kasamon Y, et al. From RECIST to PERCIST: evolving considerations for PET response criteria in solid tumors. *J Nucl Med.* 2009;50(suppl 1): 122S–150S.
27. Carson R, Berg E, Badawi R, et al. Design of the NeuroEXPLORER, a next-generation ultra-high performance human brain PET imager [abstract]. *J Nucl Med.* 2021; 62(suppl 1):1120.
28. Schierz JH, Sarikaya I, Wollina U, Unger L, Sarikaya A. Immune checkpoint inhibitor related adverse effects and FDG PET/CT findings. *J Nucl Med Technol.* 2021;49:324–329.
29. Sarikaya I, Sarikaya A, Sharma P. Assessing the effect of various blood glucose levels on ^{18}F-FDG activity in the brain, liver, and blood pool. *J Nucl Med Technol.* 2019;47:313–318.
30. Zasadny KR, Wahl RL. Standardized uptake values of normal tissues at PET with 2-[fluorine 18]fluoro-2-deoxy-D-glucose: variations with body weight and a method for correction. *Radiology.* 1993;189:847–850.
31. Sarikaya I, Albatineh AN, Sarikaya A. Revisiting weight-normalized SUV and lean-body-mass-normalized SUV in PET studies. *J Nucl Med Technol.* 2020;48: 163–167.
32. Im HJ, Bradshaw T, Solaiyappan M, Cho SY. Current methods to define metabolic tumor volume in positron emission tomography: which one is better? *Nucl Med Mol Imaging.* 2018;52:5–15.
33. Sarikaya I, Sarikaya A. PET/CT image artifacts caused by the arms. *J Nucl Med Technol.* 2021;49:19–22.
34. Sarikaya I, Elgazzar AH, Sarikaya A, Alfeeli M. Normal bone and soft tissue distribution of fluorine-18-sodium fluoride and artifacts on ^{18}F-NaF PET/CT bone scan: a pictorial review. *Nucl Med Commun.* 2017;38:810–819.
35. Sarikaya I, Yeung HW, Erdi Y, Larson SM. Respiratory artefact causing malpositioning of liver dome lesion in right lower lung. *Clin Nucl Med.* 2003;28: 943–944.
36. Zhou H, Lei PJ, Padera TP. Progression of metastasis through lymphatic system. *Cells.* 2021;10:627.
37. Borsig L, Wolf MJ, Roblek M. Lorentzen, Heikenwalder H. Inflammatory chemokines and metastasis: tracing the accessory. *Oncogene.* 2014;33:3217–3224.
38. Sarikaya I, Sarikaya A. Assessing ^{18}F-FDG uptake in the sentinel lymph node in breast cancer. *J Nucl Med Technol.* 2019;47:149–153.
39. Lambert AW, Pattabiraman DR, Weinberg RA. Emerging biological principles of metastasis. *Cell.* 2017;168:670–691.
40. Psaila B, Lyden D. The metastatic niche: adapting the foreign soil. *Nat Rev Cancer.* 2009;9:285–293.
41. Kaplan RN, Rafii S, Lyden D. Preparing the "soil": the premetastatic niche. *Cancer Res.* 2006;66:11089–11093.
42. Gao Y, Bado I, Wang H, et al. Metastasis organotropism: redefining the congenial soil. *Dev Cell.* 2019;49:375–391.
43. Rust E, Hubele F, Marzano E, et al. Nuclear medicine imaging of gastro-enteropancreatic neuroendocrine tumors: the key role of cellular differentiation and tumor grade—from theory to clinical practice. *Cancer Imaging.* 2012;12:173–184.
44. Giesel FL, Kratochwil C, Lindner T, et al. ^{68}Ga-FAPI PET/CT: biodistribution and preliminary dosimetry estimate of 2 DOTA-containing FAP-targeting agents in patients with various cancers. *J Nucl Med.* 2019;60:386–392.
45. Ulaner GA, Jhaveri K, Chandarlapaty S, et al. Head-to-head evaluation of ^{18}F-FES and ^{18}F-FDG PET/CT in metastatic invasive lobular breast cancer. *J Nucl Med.* 2021;62:326–331.
46. Roodman GD, Silbermann R. Mechanisms of osteolytic and osteoblastic skeletal lesions. *Bonekey Rep.* 2015;4:753.
47. Roudier MP, Morrissey C, True LD, et al. Histopathological assessment of prostate cancer bone osteoblastic metastases. *J Urol.* 2008;180:1154–1160.
48. Valiente M, Ahluwalia MS, Boire A, et al. The evolving landscape of brain metastasis. *Trends Cancer.* 2018;4:176–196.
49. Levy AD, Shaw JC, Sobin LH. Secondary tumors and tumorlike lesions of the peritoneal cavity: imaging features with pathologic correlation. *Radiographics.* 2009; 29:347–373.
50. Agalioti T, Giannou AD, Stathopoulos GT. Pleural involvement in lung cancer. *J Thorac Dis.* 2015;7:1021–1030.
51. Wu F, Zhao X, Mi B, et al. Clinical characteristics and prognostic analysis of Krukenberg tumor. *Mol Clin Oncol.* 2015;3:1323–1328.
52. Biswas A, Sriram PS. Getting the whole picture: lymphangitic carcinomatosis. *Am J Med.* 2015;128:837–840.
53. Tang VD, Campbell P, Pattison DA. Lymphangitic carcinomatosis from prostate cancer identified with gallium-68 prostate-specific membrane antigen positron emission tomography imaging. *Urology.* 2018;114:e1–e2.
54. Azevedo AS, Follain G, Patthabhiraman S, Harlepp S, Goetz JG. Metastasis of circulating tumor cells: favorable soil or suitable biomechanics, or both? *Cell Adh Migr.* 2015;9:345–356.
55. Ogawa Y, Abe K, Hata K, Yamamoto T, Sakai S. A case of pulmonary tumor embolism diagnosed with respiratory distress immediately after FDG-PET/CT scan. *Radiol Case Rep.* 2021;16:718–722.
56. Mar WA, Shon AM, Lu Y, et al. Imaging spectrum of cholangiocarcinoma: role in diagnosis, staging, and posttreatment evaluation. *Abdom Radiol (NY).* 2016;41: 553–567.
57. Kokkoris CP. Leptomeningeal carcinomatosis: how does cancer reach the piaarachnoid? *Cancer.* 1983;51:154–160.
58. Jain TK, Basher RK, Sood A, Mittal BR, Prakash G, Bhatia A. ^{18}F-FDG PET/CT finding of drop metastases from germ cell tumor of pineal gland. *J Nucl Med Technol.* 2017;45:114–115.
59. Bakst RL, Glastonbury CM, Parvathaneni U, Katabi N, Hu KS, Yom SS. Perineural invasion and perineural tumor spread in head and neck cancer. *Int J Radiat Oncol Biol Phys.* 2019;103:1109–1124.
60. Paes FM, Singer AD, Checkver AN, Palmquist RA, De La Vega G, Sidani C. Perineural spread in head and neck malignancies: clinical significance and evaluation with ^{18}F-FDG PET/CT. *Radiographics.* 2013;33:1717–1736.

PET/MRI, Part 4: Clinical Applications

Geoffrey M. Currie[1,2], Jose Leon[3], Elad Nevo[4], and Peter Kamvosoulis[5,6]

[1]School of Dentistry and Health Science, Charles Sturt University, Wagga Wagga, Australia; [2]Department of Radiology, Baylor College of Medicine, Houston, Texas; [3]Core for Translational Research in Imaging, Department of Diagnostic Radiology and Nuclear Medicine, University of Maryland, Baltimore, Maryland; [4]Department of Radiology, Lucille Packard Children's Hospital, Stanford University, Palo Alto, California; [5]Magnetic Resonance Department, New York–Presbyterian/Weill Cornell Medical Center, New York, New York; and [6]Imaging Research, Biomedical Engineering and Imaging Institute, Icahn School of Medicine at Mount Sinai, New York, New York

CE credit: For CE credit, you can access the test for this article, as well as additional *JNMT* CE tests, online at https://www.snmmilearningcenter.org. Complete the test online no later than June 2025. Your online test will be scored immediately. You may make 3 attempts to pass the test and must answer 75% of the questions correctly to receive Continuing Education Hour (CEH) credit. Credit amounts can be found in the SNMMI Learning Center Activity. SNMMI members will have their CEH credit added to their VOICE transcript automatically; nonmembers will be able to print out a CE certificate upon successfully completing the test. The online test is free to SNMMI members; nonmembers must pay $15.00 by credit card when logging onto the website to take the test.

PET/MRI as a hybrid modality provides novel imaging opportunities. Although there is a very broad array of diseases that could benefit from PET/MRI, there is only a narrow range of applications for which the benefit over standard care justifies the higher resource use and, in particular, offers a net positive trade-off over PET/CT. This benefit is generally associated with the omission of CT and the associated radiation dose from the patient workup. This article summarizes the generally accepted clinical applications of PET/MRI in both adult and pediatric populations. Although there are several potential applications and certainly exciting research that may expand applications in the future, the purpose of this paper was to focus on current, mainstream applications. This is the final article in a 4-part integrated series sponsored by the PET/MR and Publication Committees of the Society of Nuclear Medicine and Molecular Imaging–Technologist Section.

Key Words: PET/MRI; PET; MRI; applications

J Nucl Med Technol 2022; 50:90–96
DOI: 10.2967/jnmt.121.263288

Having learned how to establish a PET/MRI facility (*1*), acquired an understanding of the science and technology (*2*), and gained insight into protocols and sequences in PET/MRI (*3*) in the previous articles in this 4-part series, the reader now needs to ascertain how to integrate this knowledge with an understanding of the clinical applications of PET/MRI. For some diseases, MRI offers several advantages over CT, including lack of ionizing radiation, achievement of high soft-tissue contrast, and generation of physiologic images. The promise of multiparametric imaging remains a research rather than clinical tool (*4*). Consequently, when those advantages are important, use of PET/MRI instead of PET/CT could improve detection, localization, staging, and response to therapy surveillance. Indeed, the common clinical applications of PET/MRI encompass those in which improved soft-tissue contrast results in improved diagnostic accuracy (most notably in oncology) and in which radiation dose reduction is a priority (pediatrics). Site-specific pediatric PET/MRI was shown to maintain tumor detection compared with PET/CT but reduce the radiation dose to the patient from 19.6 to 4.7 mSv, with a goal of using digital PET and low-dose protocols to achieve a dose of 1.7 mSv (Ken Herrmann, MD, RAINS Webinar, July 1, 2020). PET/MRI can be undertaken sequentially and coregistered; however, this article (and indeed the series) refers specifically to simultaneous PET/MRI on hybrid systems.

Like the emergence of other technologies, PET/MRI has followed the typical cycle of initial hype, a period of reflection or disillusionment in some cases, and then a more realistic adoption. This cycle is reflected in the journal paper numbers on PubMed, with PET/MRI papers showing exponential growth from 2010, when simultaneous PET/MRI emerged, until 2015 before a flattening of the curve (Fig. 1). The more linear yearly publication rates for PET/CT can be used as a reference, although there is an entire order of magnitude difference from PET/MRI (Fig. 1). The principal clinical applications of PET/MRI appear to relate to oncology and pediatric imaging, although a PubMed search indicates that neurologic applications are of significant interest (Fig. 2). Figure 2 represents all publications in 2020 related to PET/MRI, including research, not just clinical applications. The trend is consistent with previously published survey data (*5*), although the proportion of oncology studies was lower in 2020 (46%) than in the 2016 survey (76%–88%), a finding that may reflect a bias in the literature or an evolution into more nononcology applications. Among oncology applications, the greatest interest in the literature has been attracted by prostate, brain, and neuroendocrine tumor applications (Fig. 3). Outside oncology, neurology, and cardiology, there are several other clinical applications of

Received Sep. 26, 2021; revision accepted Oct. 25, 2021.
For correspondence or reprints, contact Geoffrey M. Currie (gcurrie@csu.edu.au).
Published online Dec. 6, 2021.

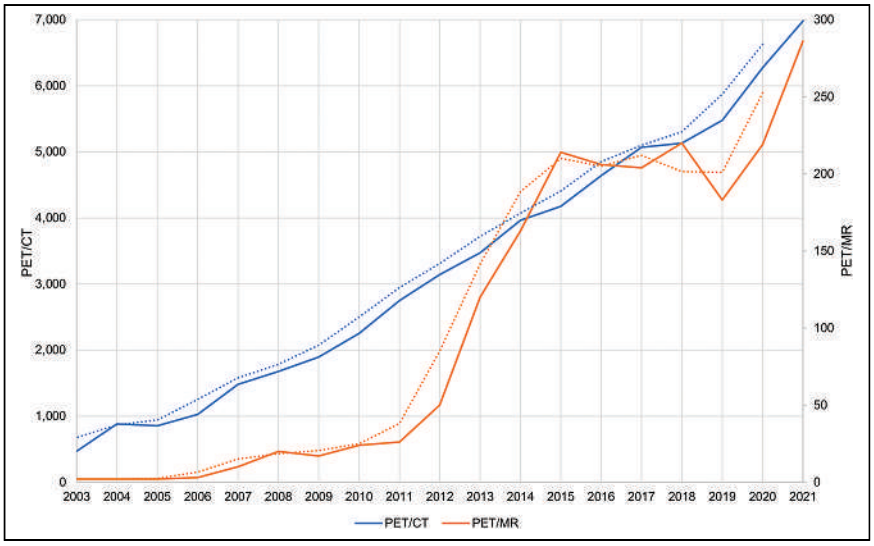

FIGURE 1. Yearly publication numbers from PubMed for PET/MRI (orange) compared with PET/CT (blue). Dashed lines are corresponding moving averages. PET/MRI showed almost exponential growth until 2015 before flattening of curve. Adjustment of 2021 data is based on projection from data collection point 80% through year.

there is a paucity of firm evidence of the clinical utility of simultaneous cardiac PET/MRI (*7*). A key requirement for cardiac PET/MRI is the ability to perform cardiac gating and respiratory gating. Indeed, MRI-based gated motion correction of the cardiac PET scan has been shown to improve image quality over PET-based corrections (*8*). Simultaneous PET/MRI of the heart allows time-efficient imaging of anatomic, functional, and metabolic quantitative information about the heart with reduced coregistration and gated coregistration (*4*). PET/MRI could provide superior sensitivity and specificity associated with differentiating benign from malignant cardiac tumors with the potential to detect metastatic spread (*4*). Both MRI and PET play an important role in cardiac sarcoidosis and, thus, have a proposed benefit in contrast-enhanced ^{18}F-FDG PET/MRI when sarcoidosis is suspected. The inflammatory nature of myocarditis might benefit from the same ^{18}F-FDG PET/MRI approach (*9*). Nonetheless, the principal application of cardiac PET/MRI lies in the evaluation of patients with known or suspected coronary artery disease.

PET/MRI. The most notable is ^{18}F-FDG PET/MRI for the differentiation of fibrotic from inflammatory tissue and for evaluation of systemic Crohn disease and ulcerative colitis (*6*).

CARDIOLOGY APPLICATIONS OF PET/MRI

It is not uncommon for patients to undergo both PET and MRI investigations for cardiac disease, and a role for simultaneous PET/MRI therefore seems logical. Nonetheless,

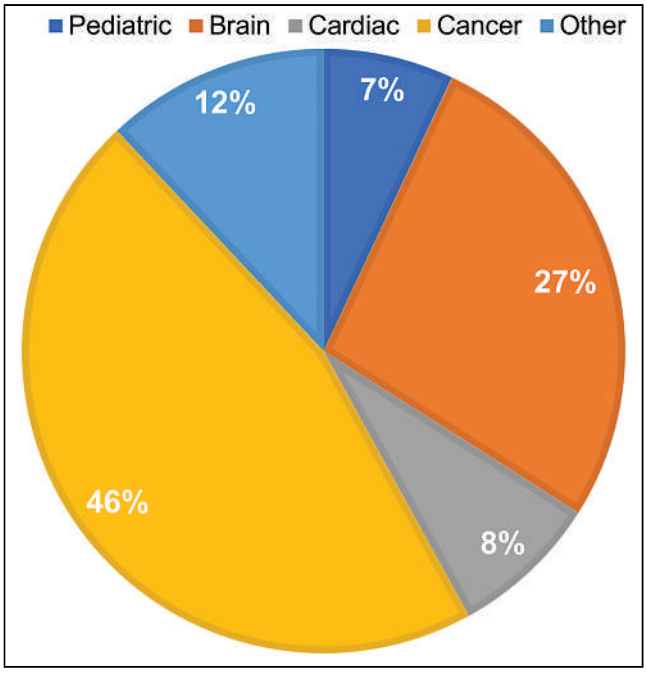

FIGURE 2. Yearly publication numbers for 2020 from PubMed for PET/MRI show that cancer has greatest engagement, followed by brain, other (unlisted applications), cardiac, and pediatric.

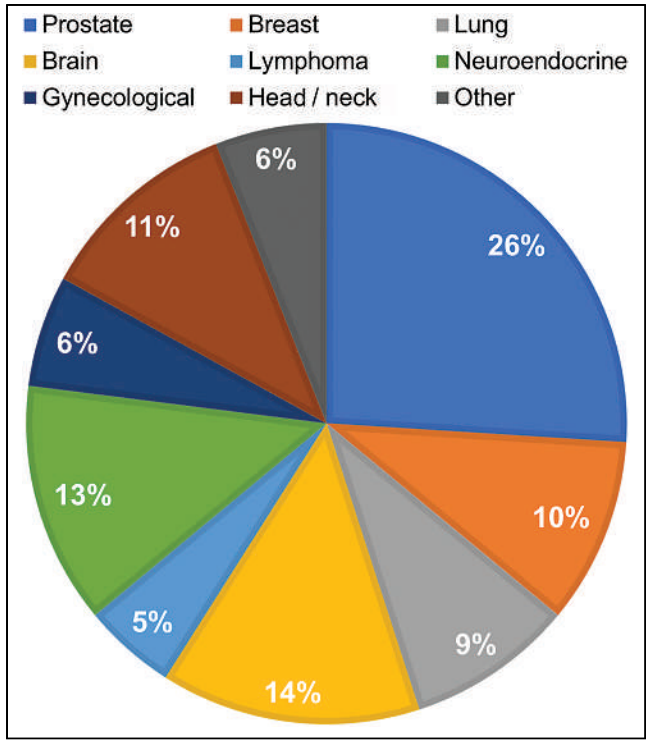

FIGURE 3. Yearly publication numbers for 2020 from PubMed for PET/MRI for various oncology applications suggest that prostate, brain, and neuroendocrine (including pancreatic) are most significant applications.

Atherosclerosis and Coronary Artery Disease

PET myocardial perfusion with ^{13}N-ammonia, ^{82}Rb, or ^{18}F-fluropidez combined with the soft-tissue characterization of MRI provides a valuable application of PET/MRI (*9*). Late gadolinium enhancement is helpful in identifying even small areas of myocardial scarring, whereas T1-weighted sequences identify diffuse myocardial changes (Fig. 4). Furthermore, the MRI sequences can have the addition of MR angiography at both end diastole and end systole. Gated PET and gated MRI data can each provide insights into the functional status of the myocardium. A single 10- to 15-min imaging window provides rich information on the anatomic, morphologic, functional, and molecular status of the myocardium with simultaneous PET/MRI (*9*). ^{18}F-FDG and gadolinium-enhanced PET/MRI can also provide complementary insights in the evaluation of myocardial viability (*9*). Evaluation of myocardial viability and prediction of left ventricular wall motion recovery after revascularization are superior for ^{18}F-FDG PET/MRI over MRI or PET alone (*10*). Although MRI is useful in the assessment of myocardial infarction, combined PET/MRI in heart failure patients with myocardial infarction has some potential using more novel PET tracers such as ^{68}Ga fibroblast activation protein inhibitor (*11*).

Plaque Vulnerability

Imaging plaque vulnerability remains a challenge in this important pathologic condition. PET/MRI potentially combines the inflammatory imaging of macrophages in plaque development using ^{18}F-FDG PET with the high-contrast imaging of luminal stenosis using MRI without the limitation that CT confronts with calcification (*7*). This ability would benefit coronary and carotid plaque vulnerability assessment and could be further developed with novel PET tracers demonstrating increased accumulation associated with plaque vulnerability, such as ^{68}Ga-DOTATATE. Importantly, the MRI coregistration through simultaneous PET/MRI allows clear delineation of plaque morphology from the vascular pool. Both ^{18}F-FDG and ^{18}F-sodium fluoride PET have been used for imaging of inflammation and calcification, respectively, in coronary artery atherosclerosis. PET/MRI in these cases can reduce motion artifacts, add the angiographic phase, and significantly reduce the radiation dose over PET/CT approaches (*12,13*).

Other Cardiac Pathologic Conditions

For cardiac sarcoidosis, MRI provides insight into myocardial structure, function, and the pattern of injury (late gadolinium enhancement)—insight that can be combined with the ^{18}F-FDG PET, which maps myocardial and extracardiac inflammation. In both cases, the changes can be subtle, and combining PET and MRI therefore increases disease detection (*14*). In a direct comparison of PET/CT and PET/MRI using ^{18}F-FDG in cardiac sarcoidosis, PET was considered equivalent whereas MRI provided additional pathologic insights not afforded by CT (*15*).

Myocarditis is another inflammatory condition in which the addition of ^{18}F-FDG PET to MRI may provide additional insight into inflammation or myocyte necrosis not evident on MRI alone, but PET/MRI is not a commonly performed procedure in this condition (*16*). Although MRI is used for the evaluation of cardiac masses, the addition of ^{18}F-FDG for PET/MRI allows differentiation of cardiac masses as malignant or benign with 100% sensitivity and specificity, as reported in 1 study (*17*).

There is an emerging role of PET/MRI with ^{18}F-labeled β-amyloid tracers in assessing cardiac and systemic amyloidosis (*4*). A combination of late gadolinium-enhanced MRI and ^{18}F-sodium fluoride PET can be used to show the characteristic diffuse myocardial enhancement on MRI and differentiation of acquired monoclonal immunoglobulin light-chain and transthyretin-related (familial and wild-type/senile) amyloid subtypes on PET (*18*).

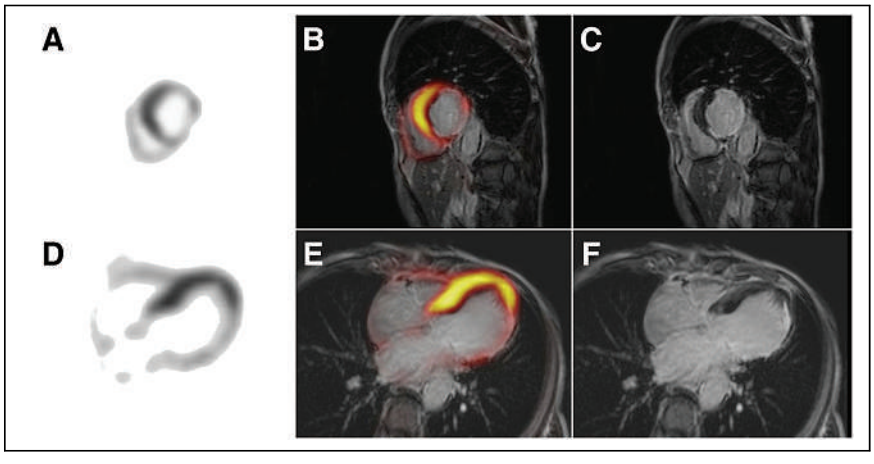

FIGURE 4. Patient with left ventricular ejection fraction of 30% and inferior-to-posterolateral akinesia on echocardiography. ^{18}F-FDG PET/MRI shows decreased metabolic activity of posterolateral wall (A and D), corresponding to late gadolinium enhancement on MR images (C and F) and confirmed on fused images (B and E). (Reprinted from (*31*).)

Protocol Considerations

Attenuation correction on PET/MRI remains a challenge, with a risk of artifacts, especially when imaging smaller structures (e.g., coronary arteries or valves). Given that MRI attenuation correction methods remain confounded by cortical bone and air, the proximity of the heart to both bone and lung means that even recently developed solutions remain imperfect. This limitation is compounded by potential respiratory misalignment and cardiac motion.

ONCOLOGY APPLICATIONS OF PET/MRI

The widest application of simultaneous PET/MRI is in oncology. The

bulk of the literature suggests that PET/MRI is superior to MRI alone for a variety of indications; however, much of the data do not reflect direct comparison of PET/CT and PET/MRI or provide any insight into potential loss from decoupling of PET/CT that would be offset by a PET/MRI gain not seen with an independent PET/CT and MRI scan. Simultaneous PET/MRI combines the enhanced soft-tissue contrast, improved assessment of anatomy, and functional information of diffusion-weighted MRI with the established molecular and metabolic insights of PET to enhance lesion characterization. As discussed previously (*3*), PET/CT is not simultaneous but sequential, and when combined with the rapid acquisition for CT compared with the prolonged PET bed position, this sequential nature can result in inaccuracy associated with small lesions or misregistration associated with physiologic motion (respiratory or cardiac). Indeed, in whole-body PET acquisitions in which the CT is performed before or after the PET acquisition, it is possible for physiologic movement or altered biodistribution to impact registration or attenuation correction (e.g., bladder filling or movement in the gastrointestinal tract). This limitation is largely overcome by simultaneous acquisition at each bed position of the PET and MRI data and the use of motion detection, respiratory gating, and cardiac gating. An important application of PET/MRI in oncology is in the evaluation of the liver, for which MRI is superior to CT (*19*).

Breast Cancer

Since MRI plays an integral role in the diagnosis, staging, and restaging of breast cancer, the role of ^{18}F-FDG PET/MRI in breast cancer is important (*20*). PET can also be performed with tracers that target hypoxia (^{18}F-fluoromisonidazole), estrogen receptors (^{18}F-fluoro-17β-estradiol), and human epidermal growth factor receptor 2 (^{89}Zr trastuzumab, ^{68}Ga-human epidermal growth factor receptor 2-single-domain antibody, or ^{64}Cu-NOTA-trastuzumab). The multiparametric radiomic data associated with PET/MRI are likely to drive improved management. Breast MRI provides excellent contrast and spatial resolution, assessment of vascular permeability, and evaluation of neoangiogenesis, which allow high sensitivity in detection of malignancy (*21*). The combination with ^{18}F-FDG PET produces the metabolic insights that improve specificity, as shown in 1 study that reported an improvement in specificity from 53% to 97% (*22*). Breast-focused PET/MRI is useful in preoperative staging of breast cancer, although there is less value than for ^{18}F-FDG PET/CT in whole-body surveillance. There is significant future potential for whole-body PET/MRI using targeting of estrogen receptors or human epidermal growth factor receptor 2.

Prostate Cancer

PET/MRI can be useful for the initial staging of prostate cancer before therapy and for detecting patients at intermediate or high risk (*14*). PET/MRI can be performed with ^{18}F-choline, ^{18}F-fluciclovine, ^{18}F-DCFPyL, or ^{68}Ga-PSMA. The value of PET/CT in biochemical recurrence will limit the usefulness of PET/MRI (*14*). Diffusion-weighted MRI combined with PET may have value in assessing response to treatment (*14*). The bulk of the literature suggests that ^{68}Ga-PSMA PET/MRI is superior to MRI alone for initial staging of prostate cancer, detection of recurrence, and therapy surveillance (*4*); however, the data do not reflect direct comparison of PET/CT and PET/MRI or provide any insight into potential loss from decoupling of PET/CT that would be offset by a PET/MRI gain not seen with an independent PET/CT and MRI scan.

Lung Cancer

In non–small cell lung cancer, although there was no difference in patient management between PET/MRI and PET/CT, PET/MRI had poorer sensitivity for small lesions in the lung because of respiratory motion (*20*). Furthermore, the limitations of MRI associated with bone and air can cause attenuation correction artifacts. Generally, a free-breathing radial volumetric interpolated breath-hold technique is adopted for assessment of pulmonary nodules.

Neuroendocrine Tumor

Since both MRI and PET are widely used in neuroendocrine tumors, there is some value in simultaneous PET/MRI using ^{68}Ga-DOTATATE for improved delineation and detection of liver metastases (*23*). Diffusion-weighted MRI may combine with the PET imaging to provide richer insights into predicting progression-free survival in advanced disease (*23*). PET/MRI could be particularly useful in assessment of the liver in these patients. ^{68}Ga-DOTATATE PET/MRI with contrast medium was shown to detect more lesions and with improved contrast over PET/CT (*24*), but the addition of a biliary contrast agent will yield more liver lesions (*25*).

Head and Neck Cancer

Recent studies suggest there is no difference between the overall performance of PET/MRI and PET/CT in head and neck cancers; given the complexity and cost, this suggestion could be an argument against PET/MRI (*20*). PET/MRI may improve lymph node metastasis detection (*20*). Compared with PET/CT, PET/MRI in head and neck cancer provides generally similar results, but PET/MRI provides superiority when there is intracranial tumor invasion (*4*). Nonetheless, the role of PET/MRI in head and neck cancer includes TNM staging, radiation therapy planning, and treatment response surveillance, predominantly using ^{18}F-FDG (*26*). In the head and neck, PET/MRI presents challenges associated with bone, air, and soft-tissue interfaces, which undermine the accuracy of attenuation correction and quantitation.

Other Malignancies

PET/MRI is particularly useful in the evaluation of liver metastases, with hybrid techniques providing higher accuracy than PET or MRI individually (*27*). Key protocol requirements include use of a biliary contrast agent for MRI and respiration-gated list-mode PET data (*23*). In 1 study, the management of 22% of colorectal carcinoma patients

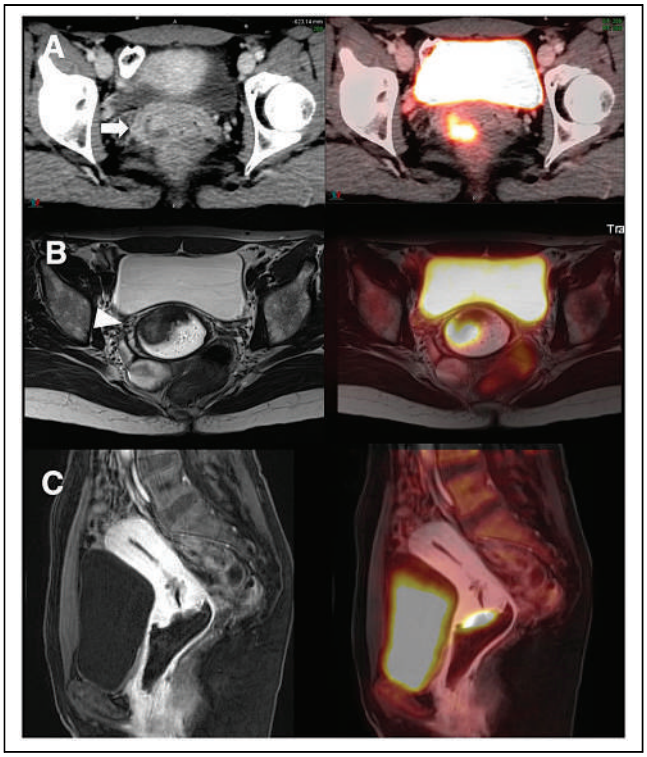

FIGURE 5. Poorly differentiated squamous cell carcinoma of cervix on CT (A, left) and PET/CT (A, right), with corresponding unenhanced T2-weighted turbo spin-echo CT (B, left) and T2-weighted turbo spin-echo PET/MRI (B, right) and contrast-enhanced sagittal MRI T1-weighted MRI (Dixon–visual background extractor sequence) (C, left) and PET/MRI (C, right). (Reprinted from (*32*).)

was changed as a result of PET/MRI, but PET/MRI was noted to be problematic (inferior to PET/CT) in pulmonary lesion detection (*28*). ^{18}F-FDG PET/MRI has also been used in ovarian and cervical malignancies for staging, therapy planning, evaluation of response to therapy, and detection of recurrence (Fig. 5). There has been some discussion of the clinical role of PET/MRI in sarcoma and multiple myeloma. In multiple myeloma, PET/MRI has the advantage of differentiating active from inactive disease and monitoring response to therapy (*6*).

NEUROLOGIC APPLICATIONS OF PET/MRI

There are several potential applications of simultaneous PET/MRI in neurologic conditions, including neurodegenerative and oncologic conditions and epilepsy. Although it is convenient to perform brain PET/MRI as part of a wider whole-body PET/MRI protocol, the ease with which PET, MRI, and CT of the brain are accurately coregistered without hybrid systems is perhaps the biggest barrier to more widespread use of neurologic simultaneous PET/MRI. For clinical sites without hybrid PET/MRI for neurologic use, there is no strong independent justification for investment, despite the advantages of PET/MRI. Nonetheless, the convenience in simultaneous PET/MRI should not be discounted and is especially beneficial when CT is not part of the imaging request. Brain PET can also forgo use of the CT component for attenuation correction, as the calculated methods used before hybrid systems were developed offer an accurate option independent of MRI-based methods. Given that brain imaging is performed at a single bed position, protocols are significantly more convenient than oncology protocols.

Alzheimer Disease and Dementias

Perhaps the greatest challenge in PET/MRI for neurodegenerative disease is the sensitivity and early detection of PET, many years before MRI changes are evident. Nonetheless, MRI offers a valuable anatomic map of physiologic and molecular changes in brain function associated with neurodegenerative disorders and, thus, has potential to improve patient care when simultaneous PET/MRI is performed using ^{18}F-FDG, ^{18}F-labeled β-amyloid (Fig. 6), or ^{18}F-tau radiopharmaceuticals (*29*). MRI could add blood flow information by extending the imaging sequence timings. PET/MRI offers simultaneous imaging of β-amyloid plaque deposition and neuronal injury or degeneration (*6*). Likewise, there is a theoretic benefit for performing simultaneous PET/MRI in Parkinson disease using ^{18}F-6-fluoro-L-dopa or other dopamine radiopharmaceuticals.

Neurologic Malignancy

The independent value of MRI and novel PET radiopharmaceuticals (beyond ^{18}F-FDG) in characterizing brain tumors leaves PET/MRI in a position to have a significant benefit in neurologic malignancy. Clinically, the most important opportunity for PET/MRI in neurologic malignancy is differentiating tumor recurrence from treatment effects (surgery or radiation) (*14*). MRI is the gold standard in brain tumor imaging;

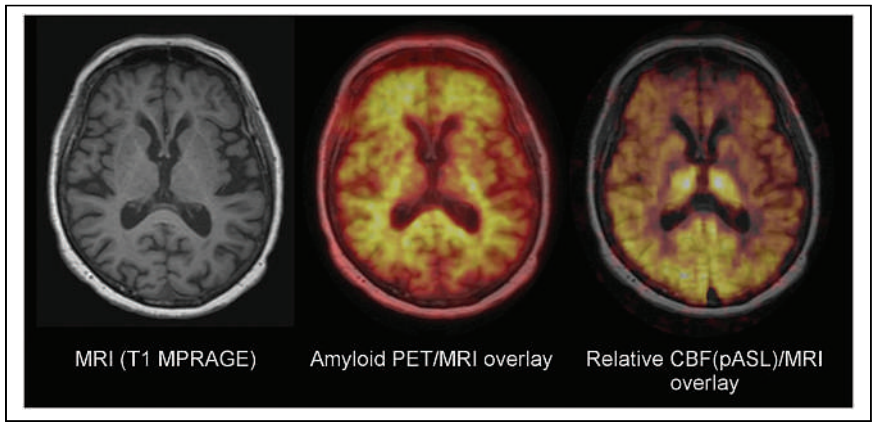

FIGURE 6. Simultaneous PET/MRI in dementia using ^{18}F-florbetaben PET and pulsed arterial spin labeling (pASL) MRI. MPRAGE = magnetization-prepared rapid gradient echo. (Reprinted from (*33*).)

however, molecular imaging provides crucial insights not captured by anatomic imaging. Several PET radiotracers are currently used to evaluate brain tumors, including ^{18}F-FDG, ^{18}F-fluoroethyltyrosine, ^{18}F-6-fluoro-L-dopa, ^{18}F-fluorothymidine, ^{18}F-choline, and ^{18}F-fluoromisonidazole (*30*). PET/MRI using the amino acid metabolism radiopharmaceutical ^{18}F-fluorothymidine enhances MRI evaluation of recurrence in glioma and metastatic brain lesions (*14*). PET/MRI using ^{18}F-fluorothymidine or ^{18}F-FDG may also have a role in differentiating low-grade from high-grade gliomas, especially with respect to aggressiveness and timing of repeat biopsies (*6,14*).

Epilepsy

For patients who have epilepsy with the potential for curable surgery, accurate localization of the seizure foci is essential for surgical planning (*14*). ^{18}F-FDG PET/MRI provides accurate detection to enhance surgical outcomes, and patients have the added benefit of a reduced radiation dose associated with not using CT. Indeed, ^{18}F-FDG PET/MRI provides improved seizure focus detection over either MRI or PET alone (*29*). As with all PET/MRI applications, there is also the convenience to the patient, who may undergo both PET and MRI in a single visit, as opposed to traditionally coming in for 2 separate appointments. This is one of the biggest benefits for patients who experience frequent seizures and may have difficulty making it to 2 appointments, resulting in a delay in receiving care while the patients are waiting to undergo the separate imaging procedures.

PEDIATRIC APPLICATIONS OF PET/MRI

An important application of simultaneous PET/MRI is in the assessment of cancer in pediatric patients. PET/MRI is particularly useful in solid tumors. The advantage of PET/MRI over PET/CT in this population relates to the absence of the radiation dose associated with CT. This advantage could be extended in pediatric patients (and adult patients) by adopting deep-learning approaches for low-dose PET scanning (*14*). The main applications of PET/MRI in pediatric patients include staging, restaging, and response to therapy, predominantly for lymphoma but also leukemia; neuroblastoma, neurofibromatosis type I, and sarcoma; seizure focus localization using ^{18}F-FDG and fused interictal MRI to guide surgical intervention; and infection (e.g., pyrexia of unknown origin) and inflammation (e.g., inflammatory bowel disease).

Although these applications relate to ^{18}F-FDG PET, newer developments may see the emergence of broader applications of PET/MRI in the pediatric population. For example, ^{18}F-*meta*-fluorobenzylguanidine is a PET alternative to ^{123}I-*meta*-iodobenzylguanidine for neuroblastoma, and ^{18}F-fluorothymidine could be a better agent for lymphoma and sarcoma.

CONCLUSION

PET/MRI is a relatively new imaging modality still establishing its place in clinical medicine. Although the potential applications of PET/MRI are broad, the applications in which cost, time, and benefit over standard care, especially when standard care includes PET/CT and MRI, are more limited. Omitting the radiation dose associated with CT remains the primary benefit, although exquisite MRI soft-tissue contrast fused with molecular information from PET provides improved sensitivity and specificity in some diseases. Nonetheless, the time and cost impost, and limitations associated with the interface between bone, air, and soft tissue, continue to plague attenuation correction algorithms. Among the range of clinical applications of PET/MRI discussed, the most significant to clinical practice include neurooncology, neurodegeneration, epilepsy, prostate cancer, neuroendocrine or pancreatic tumors, pediatric malignancy, cardiac inflammation associated with sarcoidosis, myocarditis and plaque vulnerability, and cardiac amyloidosis.

DISCLOSURE

No potential conflict of interest relevant to this article was reported.

REFERENCES

1. Kamvosoulis P, Currie G. PET/MR part 1: establishing a PET/MR facility. *J Nucl Med Technol.* 2021;49:120–125.
2. Currie GM, Kamvosoulis P, Bushong S. PET/MRI part 2: technologic principles. *J Nucl Med Technol.* 2021;49:217–225.
3. Nevo E, Kamvosoulis P, Currie G. PET/MRI, part 3: protocols and procedures. *J Nucl Med Technol.* 2022;50:17–24.
4. Mader CE, Fuchs T, Ferraro DA, Burger IA. Potential clinical applications of PET/MR. *IEEE Trans Radiat Plasma Med Sci.* 2020;4:293–299.
5. Fendler WP, Czernin J, Herrmann K, Beyer T. Variations in PET/MRI operations: results from an international survey among 39 active sites. *J Nucl Med.* 2016;57:2016–2021.
6. Broski SM, Goenka AH, Kemp BJ, Johnson GB. Clinical PET/MRI: 2018 update. *AJR.* 2018;211:295–313.
7. Bergquist PJ, Chung MS, Jones A, Ahlman MA, White CS, Jeudy J. Cardiac applications of PET-MR. *Curr Cardiol Rep.* 2017;19:42.
8. Petibon Y, Sun T, Han PK, Ma C, Fakhri GE, Ouyang J. MR-based cardiac and respiratory motion correction of PET: application to static and dynamic cardiac ^{18}F-FDG imaging. *Phys Med Biol.* 2019;64:195009.
9. Rischpler C, Siebermair J, Kessler L, et al. Cardiac PET/MRI: current clinical status and future perspectives. *Semin Nucl Med.* 2020;50:260–269.
10. Vitadello T, Kunze KP, Nekolla SG, et al. Hybrid PET/MR imaging for the prediction of left ventricular recovery after percutaneous revascularisation of coronary chronic total occlusions. *Eur J Nucl Med Mol Imaging.* 2020;47:3074–3083.
11. Varasteh Z, Mohanta S, Robu S, et al. Molecular imaging of fibroblast activity after myocardial infarction using a ^{68}Ga-labeled fibroblast activation protein inhibitor, FAPI-04. *J Nucl Med.* 2019;60:1743–1749.
12. Robson PM, Dweck MR, Trivieri MG, et al. Coronary artery PET/MR imaging: feasibility, limitations, and solutions. *JACC Cardiovasc Imaging.* 2017;10:1103–1112.
13. Mayer J, Wurster TH, Schaeffter T, et al. Imaging coronary plaques using 3D motion-compensated [^{18}F]NaF PET/MR. *Eur J Nucl Med Mol Imaging.* 2021;48:2455–2465.
14. Hope TA, Fayad ZA, Fowler KJ, et al. Summary of the first ISMRM-SNMMI workshop on PET/MRI: applications and limitation. *J Nucl Med.* 2019;60:1340–1346.
15. Wisenberg G, Thiessen JD, Pavlovsky W, Butler J, Wilk B, Prato FS. Same day comparison of PET/CT and PET/MR in patients with cardiac sarcoidosis. *J Nucl Cardiol.* 2020;27:2118–2129.
16. Nazir MS, Ismail TF, Reyes E, Chiribiri A, Kaufmann PA, Plein S. Hybrid positron emission tomography-magnetic resonance of the heart: current state of the art and future applications. *Eur Heart J Cardiovasc Imaging.* 2018;19:962–974.
17. Nensa F, Tezgah E, Poeppel TD, et al. Integrated ^{18}F-FDG PET/MR imaging in the assessment of cardiac masses: a pilot study. *J Nucl Med.* 2015;56:255–260.
18. Trivieri MG, Dweck MR, Abgral R, et al. ^{18}F-sodium fluoride PET/MR for the assessment of cardiac amyloidosis. *J Am Coll Cardiol.* 2016;68:2712–2714.

19. Catalano OA, Masch WR, Catana C, et al. An overview of PET/MR, focused on clinical applications. *Abdom Radiol (NY).* 2017;42:631–644.
20. Weber W. Clinical PET/MR. In: Schober O, Kiessling F, Debus J, eds. *Molecular Imaging in Oncology.* Springer; 2020:747–764.
21. Plecha DM, Faulhaber P. PET/MRI of the breast. *Eur J Radiol.* 2017;94:A26–A34.
22. Moy L, Noz ME, Maquire GQ, et al. Role of fusion of prone FDG-PET and magnetic resonance imaging of the breasts in the evaluation of breast cancer. *Breast J.* 2010;16:369–376.
23. Hope TA, Pampaloni MH, Nakakura E, et al. Simultaneous ^{68}Ga-DOTA-TOC PET/MRI with gadoxetate disodium in patients with neuroendocrine tumor. *Abdom Imaging.* 2015;40:1432–1440.
24. Sawicki LM, Deuschl C, Beiderwellen K, et al. Evaluation of ^{68}Ga-DOTATOC PET/MRI for whole-body staging of neuroendocrine tumours in comparison with ^{68}Ga-DOTATOC PET/CT. *Eur Radiol.* 2017;27:4091–4099.
25. Kirchner J, Sawicki LM, Deuschl C, et al. ^{18}F-FDG PET/MR imaging in patients with suspected liver lesions: value of liver-specific contrast agent gadobenate dimeglumine. *PLoS One.* 2017;12:e0180349.
26. Huellner MW. PET/MR in head and neck cancer: an update. *Semin Nucl Med.* 2021;51:26–38.
27. Brendle C, Schwenzer NF, Rempp H, et al. Assessment of metastatic colorectal cancer with hybrid imaging: comparison of reading performance using different combinations of anatomical and functional imaging techniques in PET/MRI and PET/CT in a short case series. *Eur J Nucl Med Mol Imaging.* 2016;43:123–132.
28. Kang B, Lee J, Song Y, et al. Added value of integrated whole-body PET/MRI for evaluation of colorectal cancer: comparison with contrast-enhanced MDCT. *AJR.* 2016;206:W10–W20.
29. Sałyga A, Guzikowska-Ruszkowska I, Czepczynski R, Ruchala M. PET/MR: a rapidly growing technique of imaging in oncology and neurology. *Nucl Med Rev Cent East Eur.* 2016;19:37–41.
30. Giovacchini G, Salati V, Garibotto V. Brain tumors. In: Ciarmiello A, Mansi L, eds. *PET-CT and PET-MRI in Neurology.* Springer; 2016:177–194.
31. Ratib O, Nkoulou R. Potential applications of PET/MR imaging in cardiology. *J Nucl Med.* 2014;55(suppl 2):40S–46S.
32. Nguyen NC, Beriwal S, Moon CH, Furlan A, Mountz JM, Rangaswamy B. ^{18}F-FDG PET/MRI primary staging of cervical cancer: a pilot study with PET/CT comparison. *J Nucl Med Technol.* 2020;48:331–335.
33. Drzezga A, Barthel H, Minoshima S, Sabri S. Potential clinical applications of PET/MR imaging in neurodegenerative diseases. *J Nucl Med.* 2014;55(suppl 2):47S–55S.

SNMMI Clinical Trials Network Research Series for Technologists: Clinical Research Primer—Regulatory Process, Part II: The Role of the Institutional Review Board in Food and Drug Administration–Regulated Radiopharmaceutical Research

Charlotte D. Jeffers[1] and John M. Hoffman[2]

[1]*Department of Radiology, University of Alabama at Birmingham, Birmingham, Alabama;* [2]*Department of Radiology and Imaging Sciences, Huntsman Cancer Institute, University of Utah School of Medicine, Salt Lake City, Utah*

CE credit: For CE credit, you can access the test for this article, as well as additional *JNMT* CE tests, online at https://www.snmmilearningcenter.org. Complete the test online no later than June 2025. Your online test will be scored immediately. You may make 3 attempts to pass the test and must answer 75% of the questions correctly to receive Continuing Education Hour (CEH) credit. Credit amounts can be found in the SNMMI Learning Center Activity. SNMMI members will have their CEH credit added to their VOICE transcript automatically; nonmembers will be able to print out a CE certificate upon successfully completing the test. The online test is free to SNMMI members; nonmembers must pay $15.00 by credit card when logging onto the website to take the test.

The goal of clinical research is to advance medical knowledge in hopes of improving patient care. At the core of clinical research is the need to perform research on human volunteers. This is absolutely required for the eventual approval of drugs and certain therapies. Unfortunately, history is replete with stories involving exploitation and abuse of individuals in research. Clinical research using radiopharmaceuticals introduces additional apprehension. Although the past few decades have witnessed significant improvements in safety and ethics, there remain indelible images seared into the psyche of the general population. Those new to clinical research may find themselves asking questions such as, What are the ethical guidelines and regulations for clinical research, How are they enforced and by whom, and How do we ensure the safety of participants? The answer, in large part, is the oversight and actions of the institutional review board. This article will focus on familiarizing the reader with the institutional review board and its role in protecting the rights and welfare of humans participating as subjects in Food and Drug Administration–regulated radiopharmaceutical research.

Key Words: radiopharmaceutical; clinical research; clinical trial; institutional review board

J Nucl Med Technol 2022; 50:97–102
DOI: 10.2967/jnmt.122.264034

This article builds on an earlier publication, "SNMMI Clinical Trials Network Research Series for Technologists: Clinical Research Primer—Regulatory Process, Part I: How and When Radiopharmaceuticals Can Be Used" (*1*). The reader may wish to review the earlier material to fully benefit from this discussion. In addition, institutional review board (IRB) websites are another resource to review an institution's processes, policies, and procedures.

In the United States, the Department of Health and Human Services (HHS) is the principal federal agency for protecting the health of all Americans and providing essential human services. The mission of the HHS is to enhance the health and well-being of all Americans by providing for effective health and human services and by fostering sound, sustained advances in the sciences underlying medicine, public health, and social services. This mandate is fulfilled through several HHS agencies and offices, including the Office of the Assistant Secretary for Health through its Office for Human Research Protections (OHRP), as well as the Food and Drug Administration (FDA) (*2*).

The OHRP provides leadership in the protection of the rights, welfare, and well-being of human subjects involved in research conducted or supported by the HHS. (*3*) The FDA is responsible for protecting public health by ensuring the safety, efficacy, and security of human and veterinary drugs, biologic products, and medical devices and by ensuring the safety of our nation's food supply, cosmetics, and products that emit radiation (*1,4*). To help fulfil their respective mandates, the OHRP and the FDA have established requirements for the oversight and actions of the IRB in clinical research performed under their respective purview. Differences in the rules are due to differences in the statutory scope or requirements (*3*). The OHRP and the FDA have actively worked to enhance human subject protection and reduce regulatory burden by harmonizing the agencies' IRB regulatory requirements and guidance for human subject research (*5–7*). For

Received Feb. 17, 2022; revision accepted Apr. 25, 2022.
For correspondence or reprints, contact Charlotte D. Jeffers (charlottejeffers@uabmc.edu).

the purposes of this discussion, we will focus on IRB requirements only for FDA-regulated radiopharmaceutical research.

IRBs must comply with OHRP and FDA regulations in 45 *Code of Federal Regulations* (CFR) §46 and 21 CFR §50 and §56, respectively, when reviewing research subject to those regulations (*6,7*). The purpose of the IRB is to review research studies to ensure that they comply with applicable regulations, meet commonly accepted ethical standards, follow institutional policies, and adequately protect research participants (*5*).

As evidenced by OHRP and FDA regulatory joint promulgation, the IRB is an integral and requisite component for research involving FDA-regulated clinical studies. But what is the IRB and why is it important? The focus of this article is to acquaint the reader with the IRB and its role in FDA-regulated clinical research involving radiopharmaceuticals.

DEFINITIONS AND TERMS

To facilitate further discussion, the following terms and definitions are provided.

Central (single) IRB is the IRB that conducts reviews on behalf of all study sites that agree to participate in the centralized review process. For sites at institutions that have an IRB that would ordinarily review research conducted at the site, the central IRB should reach agreement with the individual institutions participating in centralized review and those institutions' IRBs about how to apportion the review responsibilities between local IRBs and the central IRB (*8*).

Clinical investigation or *clinical research* means any experiment in which a drug is administered or dispensed to, or used involving, one or more human subjects. The terms *clinical investigation, clinical study, clinical research,* and *clinical trial* are deemed to be synonymous for purposes of this article unless otherwise identified (*9*).

CFR is the codification of the general and permanent rules and regulations FDA-Institutional in the *Federal Register* by the executive departments and agencies of the federal government of the United States. The CFR has 50 titles; each title is dedicated to a particular agency or branch of the federal government. Title 21 is dedicated to food and drugs, and title 45 is dedicated to public welfare (*1,10*).

Contract research organization, as defined in 21 CFR §312, means a person or group that assumes, as an independent contractor with the sponsor, one or more of the obligations of a sponsor, such as design of a protocol, selection or monitoring of investigations, evaluation of reports, and preparation of materials to be submitted to the FDA (*9*).

FDA approval of a drug means that data on the drug's effects have been reviewed and the drug has been determined to provide benefits that outweigh its known or potential risks for the intended population. An FDA-approved drug may be lawfully marketed (*9*).

Good clinical practice is an international ethical and scientific quality standard for designing, conducting, recording, and reporting trials that involve the participation of human subjects. Compliance with this standard provides public assurance that the rights, safety, and well-being of trial subjects are protected (consistent with the principles that have their origin in the Declaration of Helsinki) and that the clinical trial data are credible (*11*).

Institution means any public or private entity or agency (including federal, state, and other agencies). The term *facility* is deemed to be synonymous with the term *institution* for purposes of this article unless otherwise identified (*9*).

IRB, also called an independent ethics committee, means any board, committee, or other group formally designated by an institution to review, to approve the initiation of, and to conduct periodic review of biomedical research involving human subjects. The primary purpose of such a review is to ensure protection of the rights and welfare of the human subjects (*9*).

IRB approval means the determination of the IRB that the clinical investigation has been reviewed and may be conducted at an institution within the constraints set forth by the IRB and by other institutional and federal requirements (*9*).

Investigational new drug means a new drug that is used in a clinical investigation. The term also includes a biologic product that is used in vitro for diagnostic purposes. The terms *investigational drug, investigational new drug,* and *test article* are deemed to be synonymous for purposes of this article unless otherwise identified (*9*).

Investigator means an individual who actually conducts a clinical investigation (i.e., under whose immediate direction the drug is administered or dispensed to a subject). In the event that an investigation is conducted by a team, the investigator is the responsible leader of the team. The lay term used frequently is *primary investigator*. *Subinvestigator* includes any other individual member of that team. The terms *investigator* and *primary investigator* are deemed to be synonymous for purposes of this article unless otherwise identified (*9*).

Multisite clinical trial involves the implementation of the same clinical protocol at 2 or more independent investigational sites where participants are seen for an intervention or an outcome assessment. In a multisite trial, investigational sites are typically administratively or corporately distinct from each other (*8*).

Single-site clinical trial utilizes 1 investigational site to conduct and coordinate the protocol. Although a single-site clinical trial may enroll participants from multiple locations, those participants will receive an intervention or undergo outcome assessments under the direction and oversight of 1 research team located at 1 investigational site (*8*).

Sponsor means the person or organization taking responsibility for and initiating a clinical investigation. The sponsor may be an individual or pharmaceutical company, governmental agency, academic institution, private organization, or other organization. The sponsor does not actually conduct the investigation unless the sponsor is a sponsor–investigator. A person other than an individual that uses one or more of its own employees to conduct an investigation that it has initiated

is a sponsor, not a sponsor–investigator, and the employees are investigators. The terms *sponsor* and *sponsor–investigator* are deemed to be synonymous for purposes of this article unless otherwise identified (*9*).

Sponsor–investigator means an individual who both initiates and conducts an investigation and under whose immediate direction the investigational drug is administered or dispensed. The term does not include any person other than an individual. The requirements applicable to a sponsor–investigator under 21 CFR part 312 include both those applicable to an investigator and those applicable to a sponsor. The terms *sponsor* and *sponsor–investigator* are deemed to be synonymous for purposes of this article unless otherwise identified (*9*).

Subject means a human who participates in an investigation, either as a recipient of the investigational new drug or as a control. A subject may be a healthy human or a patient with a disease (*9*).

IRB PURPOSE, REGISTRATION, AND MEMBERSHIP

Under FDA regulations, as outlined in 21 CFR §50 and §56, an IRB is an appropriately constituted group that has been formally designated or charged to review and monitor biomedical research involving human subjects. The purpose of IRB review is to ensure, both in advance and by periodic review, that appropriate steps are taken to protect the rights and welfare of humans participating as subjects in research. To accomplish this purpose, IRBs use a group process to review research protocols and related materials (e.g., informed-consent documents and investigator brochures). An IRB has the authority to approve, require modifications to (to secure approval), or disapprove research (*12*).

IRB Registration and Approval

In 2009, the FDA, in consultation with the OHRP, enacted a regulation (21 CFR §56.106) requiring IRB registration for IRBs reviewing clinical investigations involving FDA-regulated products. The OHRP issued a companion rule (45 CFR §46) requiring registration for IRBs reviewing federally supported research (*13*).

All IRBs that review human subject research conducted or supported by the HHS, and that are designated under assurances of compliance approved for federal use by the OHRP under 45 CFR §46.103(a), must be registered with the OHRP. The database of registered IRB organizations and IRBs includes information on IRBs that are regulated by the OHRP only, the OHRP and the FDA, or the FDA only (*14*).

The fact that an IRB is registered with the OHRP does not mean that the OHRP has determined that the IRB reviews research in accordance with the requirements of the HHS Protection of Human Subjects regulations, 45 CFR §46, and does not mean that the IRB has the appropriate competence or expertise to review a particular research project (*14,15*).

IRB Membership

As outlined in 21 CFR §56.107, each IRB must have at least 5 members with varying backgrounds to promote complete and adequate review of research activities commonly conducted by the institution. The IRB must be sufficiently qualified through the experience, expertise, and diversity of its members, including consideration of race, sex, cultural backgrounds, and sensitivity to such issues as community attitudes, to promote respect for its advice and counsel in safeguarding the rights and welfare of human subjects. In addition to having the professional competence necessary to review the specific research activities, the IRB must be able to ascertain the acceptability of proposed research in terms of institutional commitments and regulations, applicable law, and standards of professional conduct and practice. The IRB therefore includes persons knowledgeable in these areas. If an IRB regularly reviews research that involves a vulnerable category of subjects, such as children, prisoners, pregnant women, or handicapped or mentally disabled persons, consideration is given to the inclusion of one or more individuals who are knowledgeable about and experienced in working with those subjects (*13*).

Additional criteria for IRB membership include the following. Every nondiscriminatory effort must be made to ensure that no IRB consists entirely of men or entirely of women, including the institution's consideration of qualified persons of both sexes, so long as no selection is made to the IRB on the basis of sex. No IRB may consist entirely of members of a single profession. Each IRB must include at least 1 member whose primary concerns are in the scientific area and at least 1 member whose primary concerns are in nonscientific areas. Each IRB must include at least 1 member who is not otherwise affiliated with the institution and who is not part of the immediate family of a person who is affiliated with the institution. No IRB can have a member participate in the IRB's initial or continuing review of any project in which the member has a conflicting interest, except to provide information requested by the IRB. An IRB may, at its discretion, invite individuals with competence in special areas to assist in the review of complex issues that require expertise beyond or in addition to that available in the IRB. These individuals cannot vote with the IRB. (*13*) The FDA regulations do not preclude a member from being compensated for services rendered. Payment to IRB members should not be related to or dependent on a favorable decision. Expenses, such as travel costs, can also be reimbursed (*12*).

TYPES OF IRBS

Although IRBs may differ from one institution to another, the 2 main types of IRBs are local (institutional) and centralized (single).

Local (Institutional) IRB

Institutions engaged in research involving human subjects usually have their own IRBs to oversee research conducted within the institution or by the staff of the institution. An IRB that is affiliated with an institution may serve only that institution or may serve as a central IRB for multisite

studies. FDA regulations permit an institution without an IRB to arrange for an outside (external) IRB to be responsible for initial and continuing review of studies conducted at the non-IRB institution (*8*). The institution's policies will dictate under what circumstances the institution's IRB can participate in a review process and the role of the institution's IRB in that process, leading to various differences between institutions.

Types of research that may use an institutional or local IRB include single-site or multisite clinical trials (sponsored), radioactive drug research committee studies, investigator-initiated single-site or multisite studies, and single-site clinical trials or other research projects under IND exemption.

Centralized (Single) IRB

The advent of multisite studies introduced complexity and placed significant burdens on IRBs, sponsors, and investigators. In many instances, the IRB at each center of a multisite study would conduct a comprehensive review of the study, resulting in unnecessary duplication of effort, increased time and expense, and confusion. The centralized IRB review process for joint review of cooperative research has become an effective method to address this issue. This type of review process involves an agreement under which multiple study sites in a multicenter trial rely in whole or in part on the review of an IRB other than the IRB affiliated with the research site. Because the goal of the centralized process is to increase efficiency and decrease duplicative efforts that do not contribute to meaningful human subject protection, it may be preferable that a central IRB take responsibility for all aspects of IRB review at each site participating in the centralized review process. Other approaches may be appropriate as well. For example, an institution may permit a central IRB to be entirely responsible for initial and continuing review of a study or may apportion IRB review responsibilities between the central IRB and its own IRB. At clinical sites that are not already affiliated with an IRB, investigators and sponsors typically rely on the review and oversight of a central IRB (*8*).

Although some exemptions are allowed, 45 CFR §46.114(b) requires all institutions located in the United States that are engaged in cooperative research conducted or supported by a federal department or agency to rely on approval by a centralized IRB for the portion of the research that is conducted in the United States (*16*).

Types of research that may use a centralized IRB include multisite commercially funded clinical trials. Types of research that must use a centralized IRB include cooperative research conducted or supported by a federal department or agency.

IRB FUNCTIONS AND OPERATIONS: 21 CFR §56[C]

Each IRB must follow written procedures for the following: conducting initial and continuing review of research at intervals appropriate to the degree of risk, but not less than once a year; determining which projects require review more than annually and which projects need verification (from sources other than the investigator) that no material changes have occurred since previous review; ensuring prompt reporting to the IRB of proposed changes in a research activity; ensuring that changes in approved research, during the period for which IRB approval has already been given, may not be initiated without IRB review and approval except when necessary to eliminate apparent immediate hazards to the human subjects; and ensuring prompt reporting to the IRB, appropriate institutional officials, and the department or agency head for research conducted for FDA-regulated research of any unanticipated problems involving risks to human subjects or others, instances of serious or continuing noncompliance with the applicable FDA regulations or the requirements or determinations of the IRB, and suspension or termination of IRB approval.

Except when an expedited review procedure is allowed, as outlined in §56.110, each IRB must review proposed research at convened meetings at which a majority of the members of the IRB are present, including at least 1 member whose primary concerns are in nonscientific areas. Proposed research cannot be approved unless a majority of the members at the meeting approve it (*17*).

IRBs may decide to make their written procedures available to ensure that others (e.g., investigators or sponsors) are aware of the IRB's requirements and to facilitate compliance. Some IRBs post their written procedures on a website to provide broad access (*17*).

IRB APPROVAL OF CLINICAL RESEARCH, AMENDMENTS, AND DEVIATIONS

To approve research covered by OHRP and FDA regulations, the IRB must determine that all of the following requirements are satisfied:

- Risks to subjects are minimized by using procedures that are consistent with sound research design and do not unnecessarily expose subjects to risk and, whenever appropriate, by using procedures already being performed on the subjects for diagnostic or treatment purposes.
- Risks to subjects are reasonable in relation to anticipated benefits, if any, and the importance of the knowledge that may be expected from the results. In evaluating risks and benefits, the IRB should consider only those risks and benefits that may result from the research (as distinguished from risks and benefits of therapies that subjects would receive even if not participating in the research). The IRB should not consider possible long-range effects of applying knowledge gained in the research (e.g., the possible effects of the research on public policy) as part of those research risks that fall within the purview of its responsibility.
- Selection of subjects is equitable. In making this assessment, the IRB should take into account the purposes of the research and the setting in which the research will be conducted. The IRB should be particularly cognizant of the special problems of research involving vulnerable populations, such as children, prisoners, pregnant women, handicapped or mentally disabled persons, and economically or educationally disadvantaged persons.
- Informed consent is obtained from each prospective subject or the subject's legally authorized representative, in accordance with and to the extent required.

- Informed consent is appropriately documented, in accordance with and to the extent required.
- When appropriate, the research plan adequately provides for monitoring the data collected to ensure the safety of subjects.
- When appropriate, there are adequate provisions to protect the privacy of subjects and to maintain the confidentiality of data. When some or all of the subjects, such as children, prisoners, pregnant women, handicapped or mentally disabled persons, or economically or educationally disadvantaged persons, are likely to be vulnerable to coercion or undue influence, the IRB must ensure that additional safeguards have been included in the study to protect the rights and welfare of these subjects. To approve research in which some or all of the subjects are children, an IRB must determine that all research is in compliance with 21 CFR §50[D] (*18*).

The IRB should receive and review all research activities. The documents reviewed should include the complete documents received from the clinical investigator, such as the protocol, the investigator's brochure, a sample consent document, and any advertising intended to be seen or heard by prospective study subjects. Some IRBs also require the investigator to submit an institutionally developed protocol summary form. A copy of all documentation reviewed must be maintained for at least 3 y after completion of the research at that institution. However, when the IRB makes changes, such as in the wording of the informed-consent document, only the finally approved copy needs to be retained in the IRB records (*18*).

IRB Amendments for Clinical Protocols

Although a clinical investigation is ongoing, IRBs review and consider changes in research as they are received, including protocol amendments. They also review changes to the informed-consent document, reports from investigators or sponsors of unanticipated problems, and other information about the investigation. IRB review of a proposed change in research during the period for which approval is authorized does not constitute continuing review of the research as a whole and thus does not extend the date by which continuing review must occur (e.g., beyond 1 y from the effective date of the initial approval or the most recent continuing review approval). Although an IRB may become familiar with various individual aspects of the study's conduct, such familiarity does not relieve the IRB of the responsibility to conduct continuing review, which provides an opportunity to reassess the totality of the study and ensure that, among other things, risks to subjects are minimized and still reasonable in relation to anticipated benefits, if any, to subjects and the importance of the knowledge that may be expected to result (21 CFR §56.111(a) (1) and (2)) (*18*).

Protocol Deviations

FDA drug regulations do not explicitly address protocol deviations. However, the issue is directly addressed in the *FDA Compliance Program Guidance Manual,* program 7348.811, chapter 48—"Bioresearch Monitoring, Clinical Investigators and Sponsor–Investigators," December 8, 2008. (*19*) The manual states that a protocol deviation or violation is generally an unplanned departure from the protocol procedures or treatment that is not implemented or intended as a systematic change. A protocol deviation could be a limited prospective departure from the protocol (e.g., agreement between the sponsor and the investigator to enroll a single subject who does not meet all inclusion and exclusion criteria). Like protocol amendments, deviations initiated by the clinical investigator must be reviewed and approved by the IRB and the sponsor before implementation, unless the change is necessary to eliminate apparent immediate hazards to the human subjects (21 CFR §312.66) or to protect the life or physical well-being of the subject (21 CFR §812.35(a)(*2*)) and generally communicated to the FDA. The term *protocol deviation* is also used to refer to any other unplanned instances of protocol noncompliance. For example, situations in which the investigator failed to perform tests or examinations as required by the protocol, or failures on the part of study subjects to complete scheduled visits as required by the protocol, would be considered protocol deviations (*19*).

The IRB must determine whether changes to the protocol were documented by an amendment, dated, and maintained with the protocol; reported to the sponsor (when initiated by the clinical investigator); and approved by the IRB and the FDA (if applicable) before implementation (except when necessary to eliminate apparent immediate hazards to human subjects) (*19*).

HOW IS THE IRB MONITORED?

Both the OHRP and the FDA may conduct IRB inspections to determine whether they are operating in compliance with current regulations and statutory requirements and whether the IRBs are following their own written procedures. OHRP regulations for IRBs are FDA-Institutional in 45 CFR §46. The FDA regulations pertinent to IRBs include 21 CFR §50 ("Protection of Human Subjects"), §56 ("IRBs"), §312 ("Investigational New Drug Application"), and §812 ("Investigational Device Exemptions") (*17,20,21*).

FDA inspections of IRBs generally fall into 1 of 2 categories: surveillance inspections (periodic scheduled inspections to review the overall operations and procedures of the IRB) and directed inspections (unscheduled inspections focused on the IRB's review of a specific clinical trial or trials; directed inspections generally result from a complaint, clinical investigator misconduct, or safety issues pertaining to a trial or site) (*20*).

CONCLUSION

Essential to all clinical research is the need to use human volunteers. Although much progress in ethics and safety has been made in the last few decades, past abuses to individuals involved in research are difficult to forget. Protecting the rights and welfare of individuals participating as subjects in clinical research is of paramount importance. To safeguard these fundamental principles, the federal government, through the offices and agencies of the OHRP and the FDA, has

established regulations for the IRB to ensure safety for participants involved in FDA-regulated radiopharmaceutical research.

DISCLOSURE

No potential conflict of interest relevant to this article was reported.

REFERENCES

1. Jeffers CD, Frye SA, Hoffman JM. SNMMI Clinical Trials Network research series for technologists: clinical research primer—regulatory process, part I: how and when radiopharmaceuticals can be used. *J Nucl Med Technol.* 2022;50:2–9.
2. HHS organizational chart. HHS website. https://www.hhs.gov/about/agencies/orgchart/index.html. Modified April 14, 2022. Accessed May 9, 2022.
3. Comparison of FDA and HHS Human Subject Protection Regulations. FDA website. https://www.fda.gov/science-research/good-clinical-practice-educational-materials/comparison-fda-and-hhs-human-subject-protection-regulations. Updated March 13, 2018. Accessed May 10, 2022.
4. What does FDA do? FDA website. https://www.fda.gov/about-fda/fda-basics/what-does-fda-do. Updated June 28, 2021. Accessed May 10, 2022.
5. Lesson 3: what are IRBs? HHS website. https://www.hhs.gov/ohrp/education-and-outreach/online-education/human-research-protection-training/lesson-3-what-are-irbs/index.html. Updated June 28, 2021. Accessed May 10, 2022.
6. Minutes of institutional review board (IRB) meetings guidance for institutions and IRBs. HHS website. https://www.hhs.gov/ohrp/minutes-institutional-review-board-irb-meetings-guidance-institutions-and-irbs.html-0. FDA-Institutional September 22, 2017. Accessed May 10, 2022.
7. OHRP and FDA issue joint guidance on minutes of IRB meetings: HHS website. https://www.hhs.gov/ohrp/ohrp-and-fda-issue-joint-guidance-minutes-irb-meetings.html. Published September 26, 2017. Accessed May 10, 2022.
8. Guidance for industry using a centralized IRB review process in multicenter clinical trials. FDA website. https://www.fda.gov/media/75329/download. Published March 2006. Accessed May 10, 2022.
9. Title 21—food and drugs, chapter I—Food and Drug Administration Department of Health and Human Services, subchapter D—drugs for human use. FDA website. https://www.accessdata.fda.gov/scripts/cdrh/cfdocs/cfCFR/CFRSearch.cfm?fr=312.3#:~:text=Contract%20research%20organization%20means%20a%20person%20that%20assumes%2C,be%20submitted%20to%20the%20Food%20and%20Drug%20Administration. Accessed May 10, 2022.
10. Code of federal regulations. Wikipedia website. https://en.wikipedia.org/wiki/Code_of_Federal_Regulations#:~:text=The%20Code%20of%20Federal%20Regulations%20%28%20CFR%29%20is,that%20represent%20broad%20areas%20subject%20to%20federal%20regulation. Updated April 8, 2022. Accessed May 10, 2022.
11. E6(R2) good clinical practice: integrated addendum to ICH E6(R1). FDA website. https://www.fda.gov/regulatory-information/search-fda-guidance-documents/e6r2-good-clinical-practice-integrated-addendum-ich-e6r1. Published March 2018. Updated August 24, 2018. Accessed May 10, 2022.
12. Institutional review boards frequently asked questions. FDA website. https://www.fda.gov/regulatory-information/search-fda-guidance-documents/institutional-review-boards-frequently-asked-questions . Published January 1998. Updated April 18, 2019. Accessed May 10, 2012.
13. Title 21—food and drugs, chapter I—Food and Drug Administration Department of Health and Human Services, subchapter A—general. FDA website. https://www.accessdata.fda.gov/scripts/cdrh/cfdocs/cfCFR/CFRSearch.cfm?fr=56.107. Updated March 29, 2022. Accessed May 10, 2022.
14. Register IRBs and obtain FWAs. HHS website. https://www.hhs.gov/ohrp/register-irbs-and-obtain-fwas/index.html. Updated December 9, 2021. Accessed May 10, 2022.
15. Institutional review boards; registration requirements. Federal Register website. https://www.federalregister.gov/documents/2009/01/15/E9-682/institutional-review-boards-registration-requirements. Published January 15, 2009. Accessed May 10, 2012.
16. Single IRB exception determinations. HHS website. https://www.hhs.gov/ohrp/regulations-and-policy/single-irb-exception-determinations/index.html. Updated October 8, 2020. Accessed May 10, 2022.
17. Institutional review board written procedures: guidance for institutions and IRBs (2018). HHS website. https://www.hhs.gov/ohrp/regulations-and-policy/guidance/institutional-issues/institutional-review-board-written-procedures/index.html. Updated April 30, 2018. Accessed May 10, 2022.
18. Guidance for IRBs, clinical investigators, and sponsors: IRB continuing review after clinical investigation approval. FDA website. https://www.fda.gov/media/83121/download. Published February 2012. Accessed May 10, 2022.
19. Bioresearch monitoring program (BIMO) compliance programs. FDA website. https://www.fda.gov/inspections-compliance-enforcement-and-criminal-investigations/compliance-program-manual/bioresearch-monitoring-program-bimo-compliance-programs. Updated September 15, 2021. Accessed May 10, 2022.
20. Information sheet guidance for IRBs, clinical investigators, and sponsors: FDA institutional review board inspections. FDA website. https://www.fda.gov/files/about%20fda/published/FDA-Institutional-Review-Board-Inspections—Information-Sheet.pdf. Published January 2006. Accessed May 10, 2022.
21. Guidance for IRBs, clinical investigators, and sponsors: IRB responsibilities for reviewing the qualifications of investigators, adequacy of research sites, and the determination of whether an IND/IDE is needed. FDA website. https://www.fda.gov/files/about%20fda/published/IRB-Responsibilities-for-Reviewing-the-Qualifications-of-Investigators–Adequacy-of-Research-Sites–and-the-Determination-of-Whether-an-IND-IDE-is-Needed-%28Printer-Friendly%29.pdf. Published August 2013. Accessed May 10, 2022.

SNMMI Procedure Standard/EANM Practice Guideline for Molecular Breast Imaging with Dedicated γ-Cameras

Carrie B. Hruska*[1], Christinne Corion*[2,3], Lioe-Fee de Geus-Oei[3,4], Beatriz E. Adrada[5], Amy M. Fowler[6–8], Katie N. Hunt[1], S. Cheenu Kappadath[9], Patrick Pilkington[10], Lenka M. Pereira Arias-Bouda[†3,11], and Gaiane M. Rauch[†5,12]

[1]Department of Radiology, Mayo Clinic, Rochester, Minnesota; [2]Department of Surgery, Haaglanden Medical Center, The Hague, Netherlands; [3]Department of Radiology, Leiden University Medical Center, Leiden, Netherlands; [4]Biomedical Photonic Imaging Group, University of Twente, Enschede, Netherlands; [5]Department of Breast Imaging, The University of Texas MD Anderson Cancer Center, Houston, Texas; [6]Department of Radiology, University of Wisconsin, Madison, Wisconsin; [7]Department of Medical Physics, University of Wisconsin, Madison, Wisconsin; [8]University of Wisconsin Carbone Cancer Center, Madison, Wisconsin; [9]Department of Medical Physics, The University of Texas MD Anderson Cancer Center, Houston, Texas; [10]Department of Nuclear Medicine, University Hospital 12 de Octubre, Madrid, Spain; [11]Department of Nuclear Medicine, Alrijne Hospital, Leiderdorp, Netherlands; and [12]Department of Abdominal Imaging, The University of Texas MD Anderson Cancer Center, Houston, Texas

PREAMBLE

The Society of Nuclear Medicine and Molecular Imaging (SNMMI) is an international scientific and professional organization founded in 1954 to promote the science, technology, and practical application of nuclear medicine. The European Association of Nuclear Medicine (EANM) is a professional nonprofit medical association that facilitates communication worldwide between individuals pursuing clinical and research excellence in nuclear medicine. The EANM was founded in 1985. SNMMI and EANM members are physicians, technologists, and scientists specializing in the research and practice of nuclear medicine.

The SNMMI and EANM will periodically define new guidelines for nuclear medicine practice to help advance the science of nuclear medicine and to improve the quality of service to patients throughout the world. Existing practice guidelines will be reviewed for revision or renewal, as appropriate, on their fifth anniversary or sooner, if indicated.

Each practice guideline, representing a policy statement by the SNMMI/EANM, has undergone a thorough consensus process in which it has been subjected to extensive review. The SNMMI and EANM recognize that the safe and effective use of diagnostic nuclear medicine imaging requires specific training, skills, and techniques, as described in each document. Reproduction or modification of the published practice guideline by those entities not providing these services is not authorized.

These guidelines are an educational tool designed to assist practitioners in providing appropriate care for patients. They are not inflexible rules or requirements of practice and are not intended, nor should they be used, to establish a legal standard of care. For these reasons and those set forth below, both the SNMMI and the EANM caution against the use of these guidelines in litigation in which the clinical decisions of a practitioner are called into question.

The ultimate judgment regarding the propriety of any specific procedure or course of action must be made by the physician or medical physicist in light of all the circumstances presented. Thus, there is no implication that an approach differing from the guidelines, standing alone, is below the standard of care. To the contrary, a conscientious practitioner may responsibly adopt a course of action different from that set forth in the guidelines when, in the reasonable judgment of the practitioner, such course of action is indicated by the condition of the patient, limitations of available resources, or advances in knowledge or technology subsequent to publication of the guidelines.

The practice of medicine includes both the art and the science of the prevention, diagnosis, alleviation, and treatment of disease. The variety and complexity of human conditions make it impossible to always reach the most appropriate diagnosis or to predict with certainty a particular response to treatment.

Therefore, it should be recognized that adherence to these guidelines will not ensure an accurate diagnosis or a successful outcome. All that should be expected is that the practitioner will follow a reasonable course of action based on current knowledge, available resources, and the needs of the patient to deliver effective and safe medical care. The sole purpose of these guidelines is to assist practitioners in achieving this objective.

I. INTRODUCTION

This document provides an update to the previous SNMMI practice guideline for breast scintigraphy for breast-specific γ-systems (*1*).

Received Mar. 29, 2022; accepted Mar. 29, 2022.

For correspondence or reprints, contact Gaiane M. Rauch (gmrauch@mdanderson.org).

* Contributed equally to this work.

† Contributed equally to this work.

DOI: 10.2967/jnmt.122.264204

Nuclear medicine methods for imaging of the breast have been in clinical use since the 1990s, beginning with the technique of breast scintigraphy or "scintimammography," which was performed with ^{99m}Tc-sestamibi and general-purpose γ-cameras with NaI detectors (*2*). Since that time, γ-camera systems dedicated for breast imaging have emerged in the market. These dedicated systems, including some that use semiconductor detectors rather than NaI scintillators, offer improved image quality over conventional scintimammography, leading to new clinical applications and unique guidelines specific to dedicated systems.

The term *molecular breast imaging* (MBI) has been generally used to describe imaging with dedicated γ-camera systems that detect single-photon emitting radiotracers (also previously referred to as breast specific γ-imaging [BSGI]) as well as imaging with dedicated coincidence detection systems that detect positron-emitting radiotracers (referred to as dedicated breast PET [DbPET] or positron emission mammography [PEM]) (*3–5*). In this Joint SNMMI Procedure Standard/EANM Practice Guideline, MBI refers to use of a dedicated γ-camera for planar imaging of the breast, after intravenous injection of ^{99m}Tc-sestamibi.

^{99m}Tc-sestamibi is Food and Drug Administration (FDA)–approved as a second-line diagnostic drug after mammography to assist in evaluation of breast lesions and European Medicines Agency (EMA)–approved for detection of suspected breast cancer when mammography is equivocal, inadequate, or indeterminate. However, in current clinical practice, MBI is frequently used for other indications as well, including screening; due to advances in technology that have improved count sensitivity, MBI is commonly performed at administered activities between 300 and 600 MBq, which is substantially lower than the amount listed in the package inserts (740–1,110 MBq per FDA and 700–1,000 MBq per EMA). ^{99m}Tc-tetrofosmin has also been used for evaluation of breast lesions (*6*).

Results from MBI have been shown useful for detection and monitoring of breast cancer, particularly in settings where conventional modalities of mammography and ultrasound are considered insufficient or where breast MRI is recommended but not feasible. Because MBI provides information on the functional behavior of tumors, it can reveal breast cancers masked by dense fibroglandular tissue on mammography. MBI is well-tolerated by patients, has few contraindications, is associated with low costs, and has a fast interpretation learning curve (*7,8*). MBI also offers the option for MBI-guided biopsy.

II. GOALS

The goals of this guideline are to provide an update on current clinical indications for MBI, to discuss the advantages and disadvantages of MBI, and to describe the MBI examination procedure. The qualifications and responsibilities of personnel involved, the equipment used with MBI, and the image acquisition protocol are also discussed.

III. COMMON CLINICAL INDICATIONS

Common indications for MBI include, but are not limited to, problem solving for indeterminate imaging findings, breast cancer staging, monitoring response to neoadjuvant therapy, breast cancer screening, and surveillance for breast cancer recurrence, as described in more detail below. Guidance on MBI indications has also been provided by American College of Radiology (*9*).

A. Problem Solving

MBI has been proven useful in patients with indeterminate breast abnormalities and remaining diagnostic concerns after physical examination and conventional radiologic workup with mammography and ultrasound. MBI has been studied as a tool for directing management of benign and low suspicion findings. Use of MBI in other problem-solving scenarios is still being studied (*6,10–15*).

B. Local Staging

In patients recently diagnosed with breast cancer, MBI may be used to evaluate the extent of disease and to determine additional sites in the case of multifocal, multicentric as well as contralateral disease (*6,16–22*). MBI may be especially useful in the case of discrepancies between clinical and radiologic findings or indeterminate radiologic findings due to challenging conventional imaging (e.g., mammographically dense breast) and when MRI is contraindicated or unavailable.

C. Treatment Response Monitoring

MBI can be used to evaluate disease extent before and after neoadjuvant chemotherapy (*23,24*). Data have shown MBI to provide evaluation of disease extent similar to that acquired with MRI. Other studies have examined whether the change in tumor size or uptake on MBI could provide prognostic information that predicts tumor response to therapy (*25,26*). Investigations to standardize ^{99m}Tc-sestamibi response criteria, to optimize timing and frequency of imaging, and to examine variability in response with tumor subtypes are ongoing.

D. Screening and Surveillance

As a screening tool, MBI has been useful in detecting mammographically occult breast cancer in women with dense breast tissue (heterogeneously or extremely dense on mammography (*27*)) and in women at elevated risk for breast cancer who are unable to undergo breast MRI screening (*28–33*).

MBI may be used in surveillance for recurrence in women with personal history of breast cancer, especially women whose previous breast cancer was occult on mammography or women who have dense breasts. MBI can help to differentiate between scar tissue and recurrence of disease in patients who underwent surgery, radiotherapy, or biopsy (*34*).

E. Additional Uses

MBI has shown usefulness as a supplement to mammography in patients with difficult conventional imaging, such as patients with mammographically dense breasts, implants and free silicone. MBI has been used as an alternative to MRI when breast MRI is contraindicated or unavailable (*9,34*).

IV. CONTRAINDICATIONS

A. Pregnancy

MBI should be postponed during pregnancy if possible. Because ^{99m}Tc-sestamibi is known to cross the placental barrier, the fetus may be exposed to radiation if a pregnant patient undergoes MBI (see section XI).

B. Allergic Reaction to ^{99m}Tc-Sestamibi

Allergic reaction to ^{99m}Tc-sestamibi is rare and typically mild (see section VI.C). Nevertheless, if a patient presenting for MBI has a known history of hypersensitivity or allergic reaction to ^{99m}Tc-sestamibi, an alternative test to MBI should be considered. If MBI is still pursued, special precautions such as premedication may be warranted to prevent allergic reaction.

V. QUALIFICATIONS AND RESPONSIBILITIES OF PERSONNEL

As this is a joint SNMMI Procedure Standard/EANM Practice Guideline the qualifications and responsibilities of personnel will contain both the American/Canadian and the European rules and expectations.

A. Physician

In the United States and Canada, MBI examinations should be performed under the supervision of and interpreted by a physician certified in nuclear medicine or radiology by the applicable accrediting board, such as the American Board of Nuclear Medicine, the American Board of Radiology, the Royal College of Physicians and Surgeons of Canada, Le College des Medecins du Quebec, or the equivalent.

In Europe, MBI examinations should be performed by or under supervision of a physician specialized in nuclear medicine or nuclear radiology and certified by the accrediting boards. The certified nuclear medicine physician who authorizes the study and signs the report is responsible for the procedure according to national laws and rules.

The physician should participate in maintenance of certification in the field of radiology or nuclear medicine.

B. Technologist

MBI examinations should be performed by a nuclear medicine technologist who is registered/certified in nuclear medicine by the Nuclear Medicine Technology Certification Board (NMTCB), American Registry of Radiologic Technologists (ARRT), or the Canadian Association of Medical Radiation Technologists (CAMRT) or the equivalent. The nuclear medicine technologist works under the supervision of the physician as outlined above. Nuclear medicine technologists who perform MBI should receive additional training in mammographic positioning techniques (*35*). Alternatively, if U.S. state regulations allow, MBI examinations may be performed with radiopharmaceutical administration by a nuclear medicine technologist and image acquisition by a certified mammography technologist.

In Europe, the examination should be executed by qualified registered/certified nuclear medicine technologists (*36*).

C. Medical Physicist

The medical physicist should oversee instrumentation quality control, protocol development, and image processing of MBI examinations. The medical physicist should be able to practice independently in the subfield of nuclear medicine physics. Qualifications are as stated in the *SNMMI Procedure Standard for General Imaging* (*37*).The SNMMI recommends that medical physicists be certified in the appropriate subfield(s) by the American Board of Science in Nuclear Medicine or by the American Board of Radiology, or the equivalent.

The EANM states that a certified medical physics expert (MPE) is responsible for the quality assurance of MBI systems that are in clinical use and also for the identification of possible malfunctions of these systems. The MPE is also responsible for the optimal implementation of procedures considering national and international radiation protection safety standards both for patients and for personnel.

VI. PROCEDURE/SPECIFICATIONS OF THE EXAMINATION

A. Request for MBI

1. Other relevant imaging, such as recent mammogram, should be made available for correlation with the MBI.
2. The interpreting physician should be aware of physical findings, symptoms, and clinical history.
3. The patient's pregnancy and lactation status, date of last menses, and use of hormonal therapies should be determined.
   i. If pregnancy is possible, the study should be delayed until the onset of menses or until a negative pregnancy test is obtained.
   ii. Reporting of the patient's menopausal status, phase of menstrual cycle, and any exogenous hormone therapy use may aid in the radiologist's interpretation with regard to background parenchymal uptake (BPU). Premenopausal women may benefit from scheduling imaging during the follicular phase of their menstrual cycle (typically before day 14) to minimize BPU. In patients currently taking hormone therapy, BPU may be elevated.
4. Ideally, MBI should be performed before interventional procedures, such as biopsy, because ^{99m}Tc-sestamibi may accumulate at sites of inflammation that may confound interpretation. However, MBI may still be performed after intervention as it can effectively evaluate the remainder of the ipsilateral breast tissue and the contralateral breast.
5. Care should be taken in scheduling MBI adjacent to other nuclear medicine studies or therapies that may interfere with imaging (*35*). In particular, MBI should not be scheduled within 24 h before a breast sentinel lymph node localization with a radiotracer.

B. Patient Preparation and Precautions

1. A thorough explanation of the test should be provided by the technologist or physician.

2. Patients should be encouraged to drink water before the MBI examination to stay hydrated for intravenous injection.
3. Although not required, patient fasting (no calorie intake) for approximately 3 h before MBI may increase uptake of ^{99m}Tc-sestamibi in breast tissue by reducing splanchnic and hepatic blood flow (*38*). If fasting is used, special considerations may be needed for diabetic patients.
4. The patient should change into a gown, removing all clothing from the waist up, to better facilitate imaging.
5. Deodorants, lotions, powders, and jewelry (such as necklaces) do not need to be removed for the MBI examination.
6. Although not required, warming the patient's upper torso by wrapping a warm blanket around the patient's shoulders for at least 5 min before injection may increase peripheral blood flow and further increase uptake of ^{99m}Tc-sestamibi in breast tissue (*38*).
7. Confirmation of no current pregnancy should be obtained from female patients of child-bearing capacity, according to local institutional procedures (see sections IV and XI).
8. Confirmation of no previous allergic reaction to ^{99m}Tc-sestamibi should be obtained.
9. For patients who are breastfeeding, no interruption is necessary (see section XI) (*39*).

C. Radiopharmaceutical

1. Two single-photon radiopharmaceuticals, ^{99m}Tc-sestamibi and ^{99m}Tc-tetrofosmin, are EMA-approved for breast imaging indications. ^{99m}Tc-sestamibi is also FDA-approved for breast imaging. In current practice, ^{99m}Tc-sestamibi is most commonly used.
2. ^{99m}Tc-sestamibi should be administered using an indwelling venous catheter or butterfly needle followed by 10 mL of saline to flush the vein.
3. When possible, the tracer should be administered via an upper-extremity vein on the opposite side of the suspected abnormality.
4. Administered activity
   i. MBI has previously been performed with general purpose γ-cameras and administered activities of 740 to 1,100 MBq of ^{99m}Tc-sestamibi per the FDA approval or 700 to 1,100 MBq per the EMA approval. However, the improved count sensitivity of modern MBI systems now facilitate lower administered activity, with many practices now administering 300 MBq or less.
   ii. MBI performed with modern dedicated MBI systems, using approximately 300 MBq (8 mCi) of ^{99m}Tc-sestamibi, will typically attain adequate count density with an acquisition time 7–10 min per view. Administered activity and acquisition time may vary depending on equipment used and practice preference.
   iii. For MBI-guided biopsy procedures, a higher administered activity of 600–800 MBq (16–22 mCi) may be considered to ensure optimal visibility of the target and allow shorter acquisition time (*40*).
5. ^{99m}Tc-sestamibi has been found to adhere to certain types of plastic syringe walls (*41*). Care in selection of a syringe with low ^{99m}Tc-sestamibi adsorption is advised to minimize residual activity. If warranted, residual activity should be measured after injection to obtain an accurate assessment of the net administered activity.
6. Adverse events from ^{99m}Tc-sestamibi are rare (1–6 events per 100,000; $< 0.006\%$) and can include allergic reaction but are typically mild in severity (e.g., flushing, rash, injection site inflammation, or brief metallic taste) (*42,43*).
7. ^{99m}Tc-sestamibi clears from the bloodstream within 2–3 min and is taken up largely by first-pass extraction, with minimal redistribution. ^{99m}Tc-sestamibi uptake in breast tissue has minimal physical decay and minimal washout over a typical examination time (<1 h). Thus, MBI acquisition may begin approximately 5 min after injection, and minor delays between injection and imaging are not problematic (*35*).

D. Protocol/Image Acquisition

1. A detailed guide for MBI technologists has been previously published (*35*).
2. Technologists should verify with the patient the indication for the examination and ask the patient if she has any areas of breast concern. If applicable, the affected side should be imaged first in case the patient cannot tolerate the entire examination. The technologist should confirm that the area of concern will be included in the imaging field of view.
3. Breast positioning
   i. The patient should be seated during the scan time. A specialized chair, such as those designed for seated mammography, is recommended.
   ii. Support the patient's back with pillows as needed to make the scanning time as comfortable as possible.
   iii. The patient's breast should be placed in direct contact with the γ-camera detector and light compression applied to immobilize the breast during image acquisition.
4. Imaging
   i. Imaging may begin within 5 min of injection (see section VI.C.7).
   ii. Planar imaging should be acquired in 2 standard views: cranio-caudal (CC) and mediolateral oblique (MLO), analogous to mammographic views. For single-head systems, CC view is acquired with the detector under the breast, and the MLO view is acquired with the detector at approximately 45° oblique on the lateral side of the breast. If needed, additional views may be acquired.
   iii. Typical image acquisition time is between 7 and 10 min per view. The necessary acquisition time to achieve acceptable image quality will depend on administered activity and specifics of the MBI system, including γ-camera sensitivity and detector pixel size. For MBI detectors with 1.6 or 2.5 mm detector elements, it is suggested to select an acquisition time that will achieve at least 30 counts per pixel or 50 counts per pixel, respectively, in areas of normal breast tissue.
   iv. Images should be labeled with laterality ("left" or "right"). Radioactive ^{57}Co markers may be used.

5. Processing

For the correct interpretation of the images a computer workstation should be available that enables simultaneous display of the MBI and recent mammogram. Adjustment of the image contrast by the interpreting physician may be necessary.

Display parameters, including gray scale linear display and color logarithmic display, can be used in order to optimize interpretation.

E. Interpretation

1. The following relevant information should be considered in the interpretation.
   i. The indication for MBI, clinical problems, history of breast interventions, risk factors, and menopausal state should be listed.
   ii. Any limitations (e.g., suboptimal positioning or artifacts) that are determined to affect image interpretation must be reported.
   iii. Correlation should be made with other available relevant imaging, such as mammography, and clinical findings.
2. A validated molecular breast imaging lexicon for interpretation has previously been published (*8,44*). This lexicon should be used when describing and interpreting imaging findings. The predictive value of MBI lexicon features is being examined (*45–47*).
   i. Background parenchymal uptake (BPU) is defined as the degree of radiotracer uptake within the breast parenchyma in comparison to subcutaneous fat. BPU is assessed visually as photopenic, minimal/mild, moderate, or marked.
   ii. If a lesion is identified, the intensity of uptake within the lesion (photopenic, mild, moderate, or marked), mass or nonmass uptake, and the distribution are described.
   iii. The location and size of any finding are described by the quadrant or clock face position as well as depth or distance from the nipple.
   iv. Lesion size is measured on the image where the finding is best visualized. By definition, x is the longest lesion measurement, y is orthogonal to x on the same image, and z is orthogonal to x and y on the image not used to measure x and y.
   v. Associated findings such as nipple, axillary, or vascular uptake should be described.
3. The final assessment and management recommendations should be provided on every MBI examination.
   i. Assessment categories parallel those of the Breast Imaging Reporting and Database System (BI-RADS) (*27*) and are described as category 0 (incomplete, needs additional imaging); category 1 (negative, routine follow-up); category 2 (benign, routine follow-up); category 3 (very low likelihood of malignancy); category 4 (suspicious, consider biopsy); category 5 (highly suggestive of malignancy, take appropriate action); and category 6 (known malignancy, take appropriate action).
   ii. The assessment is based on the level of suspicion by the interpreting radiologist based on lesion distribution, intensity, and morphology.
   iii. When a final assessment of 1 or 2 is given, no further imaging is necessary.
   iv. Category 0 should be avoided, similar to breast MRI interpretation, and an assessment corresponding to the level of suspicion provided when possible.
      a. All category 0, 3, 4, or 5 lesions undergo diagnostic mammography or ultrasound.
      b. If a correlate is identified on mammography or ultrasound, biopsy can be performed with guidance from one of those modalities.
      c. If no correlate is identified on conventional imaging for a category 3 finding, short-interval follow-up MBI, typically in 6 mo, is recommended. If the lesion decreases in size or intensity on follow-up, it is considered benign. If it increases in size or intensity, MRI- or MBI-guided biopsy is performed. If it remains the same, continued follow-up at 12 and 24 mo after the initial MBI is recommended.
      d. For category 4 or 5 lesions, MBI-guided biopsy or MRI are recommended when conventional imaging does not show a correlate.

F. Interventions

MBI devices with stereotactic biopsy guidance capability are available. Common indications for MBI-guided biopsy include:

1. Suspicious MBI abnormalities that are occult on mammography and (targeted) ultrasound.
2. Mammographic abnormalities, occult on ultrasound but ^{99m}Tc-sestamibi–avid, when stereotactic mammographically guided biopsy is technically challenging.
3. Cases of lesions recommended for MRI-guided biopsy that cannot be performed (e.g., MRI-guided biopsy is not available, is technically challenging, or attempted and unsuccessful).

Various previously published papers provide a detailed description of the MBI-guided biopsy methodology (*40*, *48–50*).

G. Limitations and Pitfalls

1. Motion of the breast relative to the detector may result in image blurring, making small lesions more difficult to detect.
2. Small lesions, especially less than 5 mm, are difficult to detect with current MBI technology.
3. Posterior lesions close to the chest wall may be difficult to include in the MBI field of view. The axilla cannot be reliably imaged with planar MBI acquisitions due to positioning limitations.
4. Due to the smaller field of view of MBI cameras relative to mammography, additional views may be needed for patients with larger breasts.
5. False-positive uptake of ^{99m}Tc-sestamibi is associated with the following etiologies:
   i. Benign lesions (e.g., fibroadenomas, papillomas, fat necrosis, pseudoangiomatous stromal hyperplasia).

ii. Atypical lesions (e.g., atypical ductal hyperplasia, atypical lobular hyperplasia) and lobular carcinoma in situ.
iii. Normal axillary or intramammary lymph nodes.
iv. Inflammation after biopsy, surgery, or external beam radiation therapy.
v. Background parenchymal uptake that may fluctuate with menstrual cycle or exogenous hormone use.

6. Extravasation of the tracer injection may result in areas of abnormal uptake in ipsilateral lymph nodes (*51*).

VII. DOCUMENTATION/REPORTING

The report should provide the referring physician with an answer to the specific clinical questions and must contain the following:

1. The clinical indication for requesting MBI.
2. Relevant clinical information.
3. The administrated dose of the radiopharmaceutical used and injection site.
4. History of previous examinations.
5. Findings.
6. Impression to include assessment category and recommendation for further management.

Additional information specific to the MBI interpretation should be included in the report as described in section VI.E.

VIII. EQUIPMENT SPECIFICATIONS

A. MBI systems have included both single and dual detectors for data acquisition under mammography configurations. A single-detector system comprising pixelated NaI elements coupled to position-sensitive photomultiplier tubes has been previously referred to as BSGI. More recently, MBI systems comprise dual-head cadmium zinc telluride (CZT) detectors with specialized collimation to improve spatial resolution and count sensitivity.

B. MBI systems should be specifically designed for dedicated breast imaging. Compared with conventional γ-cameras, MBI systems have a compact design with minimal dead space at the detector-chest wall edge to allow placement of the breast directly on the surface of the γ-camera in a manner analogous to mammography.

C. MBI systems should have a mechanism to allow breast immobilization.

D. MBI systems should be capable of detecting 140 keV γ-rays of ^{99m}Tc-sestamibi. The energy acceptance window may be symmetric or asymmetric with regard to the 140 keV photopeak, depending on manufacturer recommendations.

E. MBI systems may be equipped with a biopsy attachment (*40,49,50*).

IX. QUALITY CONTROL

A. An MBI quality control program should be established and maintained under the direction of a qualified medical physicist.

B. Acceptance testing of MBI systems should be performed to verify equipment performance specifications from the manufacturer.

C. Annual physics testing should be performed to verify MBI system performance and stability, as required by the sites accrediting body (e.g., The Joint Commission or American College of Radiology) (e.g., AAPM Report no. 177: Acceptance Testing and Annual Physics Survey Recommendations for γ-Camera, SPECT, and SPECT/CT Systems (*52*)). Some of the devices are based on a pixelated design and not a single crystal design. The quality control of these devices may require additional or modified testing to maintain proper operation.

D. Daily uniformity testing of the MBI system should be conducted before imaging patients to assess that system uniformity and bad pixel correction are within manufacturer specifications (typically, integral uniformity should be 5% or less). Uniformity calibrations should be performed when integral uniformity is out of range, per manufacturer recommendations. Daily uniformity flood scans should be repeated after calibrations to ensure that uniformity falls within range. See *SNMMI Procedure Standard for General Imaging* for additional information (*37*).

E. Local and state guidelines may also mandate additional quality control testing.

F. A guide for quality control procedures and recommended routine testing of MBI equipment has been previously published (*53*).

X. PATIENT EDUCATION

A. Patients undergoing MBI should receive a thorough explanation of the examination before radiopharmaceutical administration and commencement of imaging.

TABLE 1
Radiation Dosimetry Estimates in Adults

Radiopharmaceutical	Radiation dose to the breast (mGy/MBq [rad/mCi])	Organ receiving largest radiation dose (mGy/MBq [rad/mCi])	Effective dose (mSv/MBq [rem/mCi])
^{99m}Tc-sestamibi, resting subject	0.0038 (0.014)	Gallbladder: 0.039 (0.14)	0.0071* to 0.0090 (0.026–0.033)
^{99m}Tc-tetrofosmin, resting subject	0.0020 (0.0074)	Gallbladder: 0.036 (0.13)	0.0062* to 0.0080 (0.023–0.030)

Unless otherwise noted, data are from ICRP Publication 128 (*55*).
*An updated estimate of effective dose specific to female subjects was provided in Andersson et al. (*56*).

TABLE 2
Fetal Dose from ^{99m}Tc-Sestamibi (Rest)

Stage of gestation	Fetal dose	
	mGy/MBq	rad/mCi
Early	0.015	0.055
3 mo	0.012	0.044
6 mo	0.0084	0.031
9 mo	0.0054	0.020

^{99m}Tc-sestamibi dose estimates to fetus are from Russell et al. (*57*). No information about possible placental crossover of this compound was available for use in estimating fetal doses.

Patient education materials and preparation instructions, if necessary, may be provided before the MBI appointment.

B. Patient education includes describing the injection of ^{99m}Tc-sestamibi and the rare potential for mild side effects (see section VI.C), explaining the imaging procedure, and informing the patient when examination results will be communicated.

C. When the patient arrives for MBI, the technologist or other staff member should explain the examination to the patient in person, verify that the patient is not pregnant, and give breastfeeding instructions if necessary.

D. Patient-focused information about MBI is provided by SNMMI at DiscoverMI.org (*54*).

XI. RADIATION SAFETY

A. Patient Exposure Considerations

See Section X of the *SNMMI Procedure Standard for General Imaging* (*37*).

^{99m}Tc-sestamibi emits γ-rays with a principal photon energy of 140 keV and has a physical half-life of 6.01 h.

Dose estimates to adult patients and the fetus of pregnant patients are presented in Tables 1 and 2. For a typical administration of 296 MBq (8 mCi) of ^{99m}Tc-sestamibi for MBI, the estimated dose to the breast is 1.1 mGy, the organ receiving the largest estimated dose is the gallbladder (11.5 mGy), and the effective dose is estimated as 2.1–2.7 mSv.

Regarding dose estimates to breastfeeding patients, ICRP Publication 106 (Annex D) suggests that no interruption is needed for breastfeeding patients administered ^{99m}Tc-sestamibi or ^{99m}Tc-tetrofosmin (*39*). However, because of possible free ^{99m}Tc-pertechnetate it is advisable to interrupt the feeding for 4 h.

B. Personnel Exposure Considerations

The technologist total-body radiation exposure depends on the administered activity, the imaging time per patient, and the patient workload. Assuming an administered activity of 296 MBq (8 mCi) of ^{99m}Tc-sestamibi per patient and an approximately 1-h total patient contact time, the total-body radiation dose for an MBI technologist who injects the radiopharmaceutical, performs breast positioning, and remains in the room with the patient during imaging is estimated to be <0.2 mrem per patient (*58*). For example, a modest technologist clinical workload of 1 MBI patient examination per day corresponds to an annual effective dose of approximately 48 mrem (0.48 mSv).

Exposure to radiologists and support staff performing MBI-guided biopsy has been reported as 0.03 mGy/h at a distance of 15 cm from the patient (*40*). Thus, estimated radiation exposure to a radiologist in close contact with the biopsy patient for 20 min is conservatively estimated at 0.01 mGy, which corresponds to an effective dose of 0.01 mSv.

C. MBI Room Shielding Requirements

The standard shielding as used in a mammography examination room is typically sufficient for MBI.

XII. APPROVAL

This Procedure Standard was approved by the Board of Directors (BOD) of the SNMMI on January 28, 2022, and by the BOD of the EANM on November 24, 2021.

XIII. LIABILITY STATEMENT

This guideline summarizes the views of the EANM Oncology & Theranostics Committee and SNMMI. It reflects recommendations for which the EANM and SNMMI cannot be held responsible. The recommendations should be taken into context of good practice of nuclear medicine and do not substitute for national and international legal or regulatory provisions.

XIV. ACKNOWLEDGMENTS

The guidelines were brought to the attention of SNMMI, the relevant EANM Committees, and the National Societies of Nuclear Medicine. The comments and suggestions from SNMMI members and the British, Dutch, and Russian National Society are highly appreciated and have been considered for this guideline.

XV. REFERENCES

1. Goldsmith SJ, Parsons W, Guiberteau MJ, et al. SNM practice guideline for breast scintigraphy with breast-specific gamma-cameras 1.0. *J Nucl Med Technol.* 2010; 38:219–224.
2. Khalkhali I, Diggles LE, Taillefer R, Vandestreek PR, Peller PJ, Abdel-Nabi HH. Procedure guideline for breast scintigraphy. Society of Nuclear Medicine. *J Nucl Med.* 1999;40:1233–1235.
3. Hruska CB, O'Connor MK. Nuclear imaging of the breast: translating achievements in instrumentation into clinical use. *Med Phys.* 2013;40:050901.
4. Fowler AM. A molecular approach to breast imaging. *J Nucl Med.* 2014;55: 177–180.
5. Berg WA. Nuclear breast imaging: clinical results and future directions. *J Nucl Med.* 2016;57(suppl 1):46S–52S.
6. Spanu A, Sanna D, Chessa F, et al. The clinical impact of breast scintigraphy acquired with a breast specific γ-camera (BSGC) in the diagnosis of breast cancer: incremental value versus mammography. *Int J Oncol.* 2012;41:483–489.
7. Hruska CB, Conners AL, Jones KN, et al. Diagnostic workup and costs of a single supplemental molecular breast imaging screen of mammographically dense breasts. *AJR.* 2015;204:1345–1353.
8. Conners AL, Hruska CB, Tortorelli CL, et al. Lexicon for standardized interpretation of gamma camera molecular breast imaging: observer agreement and diagnostic accuracy. *Eur J Nucl Med Mol Imaging.* 2012;39:971–982.
9. American College of Radiology (ACR). ACR practice parameter for the performance of molecular breast imaging (MBI) using a dedicated gamma camera. ACR

website. https://www.acr.org/-/media/ACR/Files/Practice-Parameters/MBI.pdf?la=en; 2017. Accessed April 27, 2022.
10. Wahner-Roedler DL, Hruska CB, O'Connor MK, et al. Molecular breast imaging for women presenting with a history of non-reproducible bloody nipple discharge and negative findings on routine imaging studies: a pilot study. *J Surg Radiol.* 2011;2:92–99.
11. Meissnitzer T, Seymer A, Keinrath P, et al. Added value of semi-quantitative breast-specific gamma imaging in the work-up of suspicious breast lesions compared to mammography, ultrasound and 3-T MRI. *Br J Radiol.* 2015;88:20150147.
12. Chung HW, So Y, Yang JH, et al. Adjunctive breast-specific gamma imaging for detecting cancer in women with calcifications at mammography. *Ann Surg Oncol.* 2017;24:3541–3548.
13. Shermis RB, Redfern RE, Burns J, Kudrolli H. Molecular breast imaging in breast cancer screening and problem solving. *Radiographics.* 2017;37:1309–1606.
14. Hunt KN, Hruska CB, Johnson MP, et al. Molecular breast imaging in patients with suspicious calcifications. *J Breast Imaging.* 2019;1:303–309.
15. Jain R, Katz DR, Kapoor AD. The clinical utility of a negative result at molecular breast imaging: initial proof of concept. *Radio Imaging Cancer.* 2020;2:e190096.
16. Zhou M, Johnson N, Gruner S, et al. Clinical utility of breast-specific gamma imaging for evaluating disease extent in the newly diagnosed breast cancer patient. *Am J Surg.* 2009;197:159–163.
17. Killelea BK, Gillego A, Kirstein LJ, et al. George Peters award: how does breast-specific gamma imaging affect the management of patients with newly diagnosed breast cancer? *Am J Surg.* 2009;198:470–474.
18. Brem RF, Shahan C, Rapleyea JA, et al. Detection of occult foci of breast cancer using breast-specific gamma imaging in women with one mammographic or clinically suspicious breast lesion. *Acad Radiol.* 2010;17:735–743.
19. Kim BB. Usefulness of breast-specific gamma imaging as an adjunct modality in breast cancer patients with dense breast: a comparative study with MRI. *Ann Nucl Med.* 2012;26:131–137.
20. Collarino A, Valdes Olmos RA, van Berkel L, et al. The clinical impact of molecular breast imaging in women with proven invasive breast cancer scheduled for breast-conserving surgery. *Breast Cancer Res Treat.* 2018;169:513–522.
21. Sumkin JH, Berg WA, Carter GJ, et al. Diagnostic performance of MRI, molecular breast imaging, and contrast-enhanced mammography in women with newly diagnosed breast cancer. *Radiology.* 2019;293:531–540.
22. Edwards C, Williams S, McSwain AP, et al. Breast-specific gamma imaging influences surgical management in patients with breast cancer. *Breast J.* 2013;19:512–519.
23. Lee HS, Ko BS, Ahn SH, et al. Diagnostic performance of breast-specific gamma imaging in the assessment of residual tumor after neoadjuvant chemotherapy in breast cancer patients. *Breast Cancer Res Treat.* 2014;145:91–100.
24. Hunt KN, Conners AL, Goetz MP, et al. Comparison of ^{99m}Tc-sestamibi molecular breast imaging and breast MRI in patients with invasive breast cancer receiving neoadjuvant chemotherapy. *AJR.* 2019;213:932–943.
25. Wahner-Roedler DL, Boughey JC, Hruska CB, et al. The use of molecular breast imaging to assess response in women undergoing neoadjuvant therapy for breast cancer: a pilot study. *Clin Nucl Med.* 2012;37:344–350.
26. Mitchell D, Hruska CB, Boughey JC, et al. ^{99m}Tc-sestamibi using a direct conversion molecular breast imaging system to assess tumor response to neoadjuvant chemotherapy in women with locally advanced breast cancer. *Clin Nucl Med.* 2013;38:949–956.
27. D'Orsi CJ, Sickles EA, Mendelson EB, Morris EA. *ACR BI-RADS® Atlas, Breast Imaging Reporting and Data System*. Reston: American College of Radiology; 2013.
28. Brem RF, Rapelyea JA, Zisman G, et al. Occult breast cancer: scintimammography with high-resolution breast-specific gamma camera in women at high risk for breast cancer. *Radiology.* 2005;237:274–280.
29. Rhodes DJ, Hruska CB, Phillips SW, Whaley DH, O'Connor MK. Dedicated dual-head gamma imaging for breast cancer screening in women with mammographically dense breasts. *Radiology.* 2011;258:106–118.
30. Rhodes DJ, Hruska CB, Conners AL, et al. Journal club: molecular breast imaging at reduced radiation dose for supplemental screening in mammographically dense breasts. *AJR.* 2015;204:241–251.
31. Brem RF, Ruda RC, Yang JL, Coffey CM, Rapelyea JA. Breast-specific gamma-imaging for the detection of mammographically occult breast cancer in women at increased risk. *J Nucl Med.* 2016;57:678–684.
32. Shermis RB, Wilson KD, Doyle MT. Supplemental breast cancer screening with molecular breast imaging for women with dense breast tissue. *AJR.* 2016;207:450–457.
33. Rhodes D, Hunt K, Conners A, et al. Abstract PD4-05: Molecular breast imaging and tomosynthesis to eliminate the reservoir of undetected cancer in dense breasts: the Density MATTERS trial. *Cancer Res.* 2019;79(4_suppl):PD4-05.
34. Huppe AI, Mehta AK, Brem RF. Molecular breast imaging: a comprehensive review. *Semin Ultrasound CT MR.* 2018;39:60–69.
35. Swanson T, Tran TD, Ellingson LR, et al. Best practices in molecular breast imaging: a guide for technologists. *J Nucl Med Technol.* 2018;46:3–11.
36. European Association of Nuclear Medicine (EANM). *Advanced Performance and Responsibility Guidelines for the Nuclear Medicine Technologist.* EANM website. https://www.eanm.org/content-eanm/uploads/2017/02/Advanced-Performance-and-Responsibility-Guidelines.pdf. Accessed April 27, 2022.
37. Society of Nuclear Medicine and Molecular Imaging. *SNMMI Procedure Standard for General Imaging*. amazonaws website. http://s3.amazonaws.com/rdcms-snmmi/files/production/public/docs/General_Imaging_Version_6.0.pdf. Accessed April 26, 2022.
38. O'Connor MK, Hruska CB, Tran TD, et al. Factors influencing the uptake of ^{99m}Tc-sestamibi in breast tissue on molecular breast imaging. *J Nucl Med Technol.* 2015;43:13–20.
39. International Commission on Radiological Protection (ICRP). Radiation dose to patients from radiopharmaceuticals: addendum 3 to ICRP publication 53. ICRP publication 106. Approved by the Commission in October 2007. *Ann ICRP.* 2008;38:1–197.
40. Adrada BE, Moseley T, Kappadath SC, Whitman GJ, Rauch GM. Molecular breast imaging-guided percutaneous biopsy of breast lesions: a new frontier on breast intervention. *J Breast Imaging.* 2020;2:484–491.
41. Swanson TN, Troung DT, Paulsen A, Hruska CB, O'Connor MK. Adsorption of ^{99m}Tc-sestamibi onto plastic syringes: evaluation of factors affecting the degree of adsorption and their impact on clinical studies. *J Nucl Med Technol.* 2013;41:247–252.
42. Silberstein EB, Ryan J. Prevalence of adverse reactions in nuclear medicine. Pharmacopeia Committee of the Society of Nuclear Medicine. *J Nucl Med.* 1996;37:185–192.
43. Nyakale N, Lockhat Z, Sathekge MM. Nuclear medicine-induced allergic reactions. *Curr Opin Allergy Clin Immunol.* 2015;28:10–17.
44. Conners AL, Maxwell RW, Tortorelli CL, et al. Gamma camera breast imaging lexicon. *AJR.* 2012;199:W767-74.
45. Choi EK, Im JJ, Park CS, Chung YA, Kim K, Oh JK. Usefulness of feature analysis of breast-specific gamma imaging for predicting malignancy. *Eur Radiol.* 2018;28:5195–5202.
46. Conners AL, Jones KN, Hruska CB, Geske JR, Boughey JC, Rhodes DJ. Direct-conversion molecular breast imaging of invasive breast cancer: imaging features, extent of invasive disease, and comparison between invasive ductal and lobular histology. *AJR.* 2015;205:W374-81.
47. Hruska CB, Geske JR, Conners AL, et al. Background parenchymal uptake on molecular breast imaging and breast cancer risk: a cohort study. *AJR.* 2020.
48. Collarino A, Valdes Olmos RA, van der Hoeven AF, Pereira Arias-Bouda LM. Methodological aspects of ^{99m}Tc-sestamibi guided biopsy in breast cancer. *Clin Transl Imaging.* 2016;4:367–376.
49. Collarino A, Olmos RAV, Neijenhuis PA, et al. First clinical experience using stereotactic breast biopsy guided by ^{99m}Tc-sestamibi. *AJR.* 2017;209:1367–1373.
50. Brem RF, Mehta AK, Rapelyea JA, Akin EA, Bazoberry AM, Velasco CD. Gamma imaging-guided minimally invasive breast biopsy: initial clinical experience. *AJR.* 2018;210:695–699.
51. Werner J, Rapelyea JA, Yost KG, Brem RF. Quantification of radio-tracer uptake in axillary lymph nodes using breast specific gamma imaging (BSGI): benign radio-tracer extravasation versus uptake secondary to breast cancer. *Breast J.* 2009;15:579–582.
52. American Association of Physicists in Medicine (AAPM). *AAPM Report No. 177—Acceptance Testing and Annual Physics Survey Recommendations for Gamma Camera, SPECT, and SPECT/CT Systems.* February 2019. AAPM website. https://www.aapm.org/pubs/reports/RPT_177.pdf?msclkid=f0331b22c64911ec8058af87d0d06e74. Accessed April 27, 2022.
53. Nardinger SM, Tran TD, Swanson TN, et al. Guidelines for quality control testing of molecular breast imaging systems. *J Nucl Med Technol.* 2018;46:349–354.
54. SNMMI DiscoverMI.org: Molecular breast imaging. SNMMI website. http://www.snmmi.org/Patients/Procedures/Content.aspx?ItemNumber=13977&RDtoken=56039&userID=. Accessed April 27, 2022.
55. Mattsson S, Johansson L, Leide Svegborn S, et al. Radiation dose to patients from radiopharmaceuticals: a compendium of current information related to frequently used substances. *Ann ICRP.* 2015;44:7–321.
56. Andersson M, Johansson L, Minarik D, Leide-Svegborn S, Mattsson S. Effective dose to adult patients from 338 radiopharmaceuticals estimated using ICRP biokinetic data, ICRP/ICRU computational reference phantoms and ICRP 2007 tissue weighting factors. *EJNMMI Phys.* 2014;1:9.
57. Russell JR, Stabin MG, Sparks RB, Watson E. Radiation absorbed dose to the embryo/fetus from radiopharmaceuticals. *Health Phys.* 1997;73:756–769.
58. Pletta C, Hruska C, O'Connor M. Molecular breast imaging implications for radiation exposure to the technologist [abstract]. *J Nucl Med.* 2009;50:2023.

Small-Bowel and Colon Transit

Mary Beth Farrell, CNMT

RATIONALE

Intestinal chyme and indigestible solids move through the small and large bowels via complex gastrointestinal contractions. Identifying the location of a motility disorder causing gastrointestinal symptoms can be difficult because the symptoms may be due to upper or lower gastrointestinal tract dysfunction. Thus, it is often helpful to evaluate motility throughout the entire gastrointestinal tract to aid in selection of the appropriate treatment.

Whole-gut transit scintigraphy refers to a combined gastric emptying, small-bowel transit, and colon transit study. This practical protocol tip focuses on small-bowel and colon transit using single-isotope liquid gastric emptying with small-bowel and colon follow-through. An unlabeled standardized meal is an important component of the protocol, affecting the validity of the reference values given. As described in a procedure guideline by the Society of Nuclear Medicine and Molecular Imaging and the European Association of Nuclear Medicine, a dual-isotope study combining a solid meal (^{99m}Tc-labeled egg) and a liquid (^{111}In-diethylenetriaminepentaacetic acid [DTPA] water) may be performed.

CLINICAL INDICATIONS

The study is performed to evaluate gastrointestinal transit abnormalities in symptomatic patients with known or suspected gastroparesis, dyspepsia, irritable bowel syndrome, chronic constipation, chronic diarrhea, chronic idiopathic intestinal pseudoobstruction, scleroderma, celiac disease, or malabsorption syndrome. It may also be performed to demonstrate a motility disorder or slow colon transit or to provide evidence of a defecation disorder or functional rectosigmoid obstruction in patients with constipation.

CONTRAINDICATIONS

- Pregnancy or breastfeeding: pregnancy must be excluded in accordance with local institutional policy. If the patient is breastfeeding, appropriate radiation safety instructions should be provided.
- Allergy to eggs or any component of the meal.
- Hypoglycemia with a blood glucose level of less than 40 mg/dL.
- Hyperglycemia with a blood glucose level of more than 200–250 mg/dL.

DOI: 10.2967/jnmt.121.264294

- A recent nuclear medicine study (radiopharmaceutical-dependent).

PATIENT PREPARATION/EDUCATION

- The patient preparation mirrors the standard gastric-emptying study (*5*). Patients should …
  - Fast overnight or for a minimum of 8 h before the scan.
  - For 48–72 h before the test and on the 4 d of testing, discontinue medications that may affect gastrointestinal motility unless the test is being performed to assess motility while on these medications, which include opiate analgesics, anticholinergic medications, and prokinetic agents (metoclopramide, domperidone, erythromycin).
  - Withhold laxatives.
  - Eat a normal diet for 2 d before the exam and for the 4 d of imaging.
  - Avoid diagnostic studies that require altered eating patterns or ingestion of contrast agents (e.g., bowel contrast) during the 4 d of testing.
- Diabetic patients should …
  - Bring insulin and a glucometer on the day of the procedure.
  - Measure their blood glucose before the exam (if >250 mg/dL, the bowel motility study should be rescheduled because hyperglycemia may delay gastric emptying and impact small-bowel transit accuracy).
  - Administer a scheduled insulin dose just before ingesting the test meal (consult the supervising physician to determine whether the insulin dose should be modified).
- A focused history should be obtained, including …
  - Detailed gastrointestinal symptoms, such as frequency of bowel movements and routine use of laxatives.

TABLE 1
Radiopharmaceutical Identity, Dose, and Route of Administration

Identity	Dose	Route of administration
^{111}In-DTPA	3.7–37 MBq (0.1–1 mCi)	Oral

TABLE 2
Acquisition Parameters

Parameter	Characteristics	Standard/preferred/optional
Camera type	Large field of view, dual head	Preferred
	Large field of view, single head	Standard
Energy peak	172 and 247 keV	Standard
Energy window	20%	Standard
Collimator	Medium energy	Standard
Patient position	Standing or supine	Standard
Camera position	Total abdomen from gastric fundus to pelvis	Standard
Injection-to-imaging time	Immediately on meal completion	Standard
Acquisition type	Planar	Standard
Views	Anterior and posterior	Standard
	Initial (0 h) and 1, 2, 3, 4, 5, and 6 h	
Additional views	Anterior and posterior	Not applicable
	24, 48, and 72 h	
Matrix	128 × 128	Standard
Number of views	2 views at each time point	Standard
Time per view	60 s	Standard
Additional images: time per view	4 min	Standard

- Presence of other systemic illnesses, such as diabetes, celiac sprue, and scleroderma.
- Pertinent test results, such as other radiographic studies and endoscopy.
- Prior surgical procedures.
- Current medications.

RADIOPHARMACEUTICAL IDENTITY, DOSE, AND ROUTE OF ADMINISTRATION

Table 1 presents the radiopharmaceutical identity, dose, and route of administration. ^{99m}Tc-sulfur colloid is the only radiopharmaceutical that has received Food and Drug Administration approval for oral administration. ^{111}In-DTPA is not approved for oral administration. Its use, however, for a study such as this one is typically permitted at sites with a broad license with local approval.

ACQUISITION PARAMETERS

Table 2 presents the acquisition parameters.

ACQUISITION INSTRUCTIONS

- Prepare an unlabeled solid meal using standardized meal ingredients: 4 oz (118 mL) of liquid egg white (e.g., Eggbeaters; Bob Evans Farms, LLC), 2 slices of toasted white bread, 30 g of jam or jelly, and 300 mL of water.
- Prepare the unlabeled meal: cook the egg white in a microwave oven or on a stove, stirring once or twice, until it has the consistency of an omelet. Toast the bread and spread the jelly on it. The egg and toast may be eaten separately or, to decrease the time required for ingestion, as a sandwich.
- Prepare the labeled water: mix the ^{111}In-DTPA in the water. For whole-gut transit, 300 mL of water are used; for a gastric-emptying study, 120 mL are used.
- Instruct the patient to ingest the meal and the liquid within 10 min.
- Acquire the images with the patient either standing or supine.
- Place a ^{57}Co position marker on the iliac crest for every image over the 4-d exam.

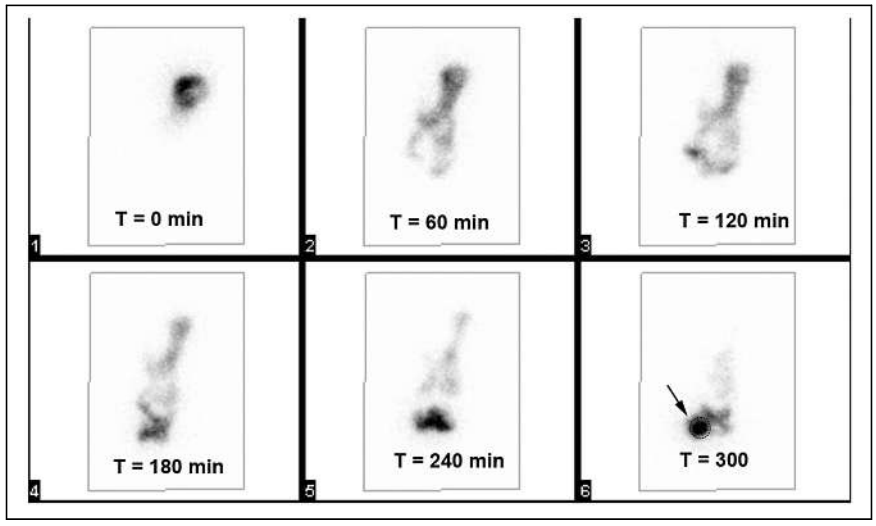

FIGURE 1. Total abdominal and terminal ileum (arrow and circle) regions of interest. (Reprinted from (*4*).)

- Obtain 60-s anterior and posterior images from the gastric fundus to the pelvis immediately after ingestion of the meal.
- Obtain repeat images (same position and views) hourly for 6 h on the same camera.
- Instruct the patient to resume a normal diet and activity.
- Obtain repeat images at 24, 48, and 72 h.
- Correct all images for radioisotope decay and time per image. Thus, the 24-, 48-, and 72-h colon images must be divided by 4 for comparison to the 1-min images on the first day.

COMMON OPTIONS

For certain patients who will not or cannot ingest the standard egg meal, facilities may need to establish an alternative meal. This will need to have similar nutritional content but without eggs or gluten for patients with allergies or intolerance to the standard meal.

PROCESSING INSTRUCTIONS

Small-Bowel Transit (Terminal Ilium Filling Method)

- Draw a large region of interest on the anterior and posterior images to include the entire abdomen for the 2-, 3-, 4-, and 5-h images (Fig. 1).
- Calculate the geometric mean ($\sqrt{}$ [anterior counts × posterior counts]).
- Decay-correct each view.
- Calculate the average total abdominal counts using the 2-, 3-, 4-, and 5-h views. The mean total abdominal counts are used to determine the counts available to fill the terminal ileum at 6 h (small-bowel transit) and to enter the colon (geometric center analysis).
- Draw a region of interest around the terminal ileum at 6 h. Include any activity in the region of interest that has passed through the terminal ileum and into the cecum or colon at 6 h, as this activity has passed through the small bowel.
- Calculate the percentage of activity transited through the small bowel as in the following equation, where counts are the geometric mean and decay-corrected counts for 1 min:

$$\%\ \text{activity transited through the small bowel} = \frac{\text{total counts in the terminal ileum + colon at 6 h}}{\text{mean total abdominal counts (2 to 5 h after meal)}}.$$

- Be aware that normal small-bowel transit is greater than 40% of the total abdominal ^{111}In counts in the terminal ileum or any counts that have passed from the terminal ileum into the colon.

Colon Transit (Geometric Center Method)

Colon transit is determined by calculating the geometric center of the ^{111}In as it moves through the colon. Colon transit is a measure of the progression of radiotracer through the colon. The geometric center is determined from average weighted counts in specific segments of the colon. The 24-, 48-, and 72-h images are used.

- Calculate the geometric center by dividing the colon into 7 anatomic regions. Each region has a numeric value: 1, cecum–ascending colon; 2, hepatic flexure; 3, transverse colon; 4, splenic flexure; 5, descending colon; 6, rectosigmoid colon; and 7, excreted stool (Fig. 2).
- Draw the 6 regions of interest as shown in Figure 2. To calculate the amount of activity that has been defecated and left the body (region 7), subtract the amount retained from the total available counts on day 1, obtained from the average of total abdominal counts between 2 and 5 h (as described for the terminal ileum filling method).

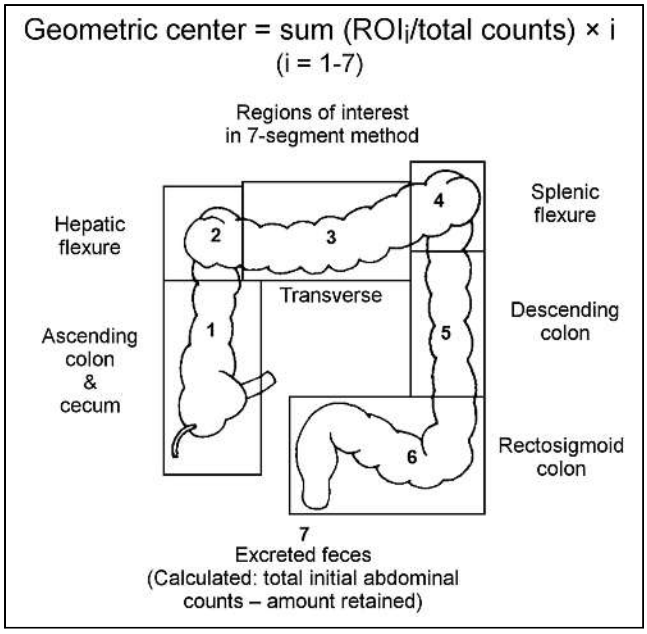

FIGURE 2. Six regions of interest and calculated counts in excreted feces used to calculate geometric center. (Reprinted from (3).)

TABLE 3
Normal Mean Values for Geometric Center

Imaging time from meal ingestion (h)	Mean ± SD
24	4.6 ± 1.5
48	6.1 ± 1.0
72	6.6 ± 0.19

- Calculate the geometric center (the sum of the weighted counts in each region) using the following equation, where $i = 1–7$:

$$\text{Geometric center} = \text{sum (region of interest}_i/\text{total counts)} \times i.$$

In this equation, counts are geometric mean counts corrected for decay and for time per image. For example, the colon images (4 min/frame) need to be divided by 4 for comparison with 1-min images of total abdominal counts on the first day. The reference mean values for the geometric center are shown in Table 3.

SUGGESTED READING

1. Farrell MB. Gastric emptying scintigraphy. *J Nucl Med Technol.* 2019;47:111–119.
2. Maurer AH. Gastrointestinal motility, part 1: esophageal transit and gastric emptying. *J Nucl Med Technol.* 2016;44:1–11.
3. Maurer AH. Gastrointestinal motility, part 2: small-bowel and colon transit. *J Nucl Med Technol.* 2016;44:12–18.
4. Maurer AH, Camilleri M, Donohoe K, et al. The SNMMI and EANM practice guideline for small-bowel and colon transit 1.0. *J Nucl Med.* 2013;54:2004–2013.
5. Thomas KS, Farrell MB. Solid-meal gastric emptying study. *J Nucl Med Technol.* 2019;47:127–128.

A Practical Technique to Improve Visualization of Sentinel Nodes in the Axillary Region on Breast Lymphoscintigraphy: Medial Breast Traction by Patient

Savas Ozdemir[1], Lisa Corner[1], Toby Searcy[1], Swati Sharma[2], and Smita Sharma[3]

[1]*Division of Nuclear Medicine and Molecular Imaging, Department of Radiology, University of Florida, Jacksonville, Florida;* [2]*Department of Radiology, University of Florida, Jacksonville, Florida; and* [3]*Division of Women's Imaging, Department of Radiology, University of Florida, Jacksonville, Florida*

Methods: A standard method of performing breast lymphoscintigraphy is to obtain anterior and lateral views after periareolar intradermal injection of a radiotracer. However, a sentinel lymph node may be obscured by the activity at the injection site, especially on anterior views. Also, breast tissue may cause attenuation to prevent sentinel node visualization. In cases in which a sentinel lymph node is visualized on one view but not the other view or a sentinel lymph node is either not visualized or inadequately visualized, we repeat anterior and lateral views during medial traction of the breast performed by the patient. **Results:** We have found the medial breast traction technique performed by the patient to be especially useful for identification of axillary sentinel nodes. **Conclusion:** Repeat images during medial traction of the breast by the patient is an effective technique to improve visualization of sentinel lymph nodes in the axillary region.

Key Words: breast lymphoscintigraphy; lymphoscintigraphy techniques; sentinel node; medial traction

J Nucl Med Technol 2022; 50:115–118
DOI: 10.2967/jnmt.121.262994

Breast lymphoscintigraphy is an established method in primary staging of patients with invasive breast cancer without a palpable or needle biopsy–proven lymph node. If a sentinel node biopsy is negative, complete axillary dissection is associated with an increased risk of short- and long-term complications such as lymphedema with no benefit in overall survival, disease-free survival, or regional control (*1,2*). Frequently, the procedure needs to be completed in a timely manner to comply with the operating room schedule. Depending on the location of the lymph node and positioning of the breast, activity at the injection site may obscure the sentinel lymph node. Repeat anterior and lateral planar views during medial traction of the breast by the patient is a simple and effective technique to improve visualization of lymph nodes. Demonstration of the sentinel node in 2 planes can help the surgeon determine its location.

Received Aug. 4, 2021; revision accepted Sep. 21, 2021.
For correspondence or reprints, contact Savas Ozdemir (savas.ozdemir@jax.ufl.edu).
Published online Nov. 8, 2021.

MATERIALS AND METHODS

In our routine protocol, we administer approximately 15 MBq (0.5 mCi) of ^{99m}Tc-tilmanocept for same-day surgery, and approximately 35 MBq (1.0 mCi) for next-day surgery, at the 12-o'clock location of the periareolar breast intradermally using aseptic technique, followed by gentle massage to improve drainage of the radiotracer. At our center, we obtain anterior and lateral dynamic images immediately after injection of the tracer, followed by anterior and lateral planar images using a dual-head γ-camera. When the sentinel lymph node is visualized, transmission images are obtained using a ^{57}Co flood source to demonstrate the body contour.

In cases in which, first, a sentinel lymph node is visualized on one view but not the other view (Figs. 1 and 2) or, second, a sentinel lymph node is either not visualized or inadequately visualized by 1 h after injection (Fig. 3), we repeat anterior and lateral views during medial traction of the breast performed by the patient (Fig. 4).

RESULTS

We have found the medial breast traction technique performed by the patient to be especially useful.

DISCUSSION

Since the introduction of breast lymphoscintigraphy, various techniques have been used, including intratumor and peritumor injection, subcutaneous or intradermal injection to the quadrant of the breast where the tumor is located, or combinations of injection techniques (*3,4*). The periareolar injection technique is simple, with a high success rate in sentinel lymph node detection (*5*). The relatively high activity level at the injection site may obscure the sentinel node in the axillary region, especially on the anterior view.

Imaging in the standing (upright) position was demonstrated to improve visualization of the sentinel nodes (*6,7*). Image acquisition when the patient's arm is 90° from the long axis of the patient to simulate the surgical position has been discussed. Because of the impracticality

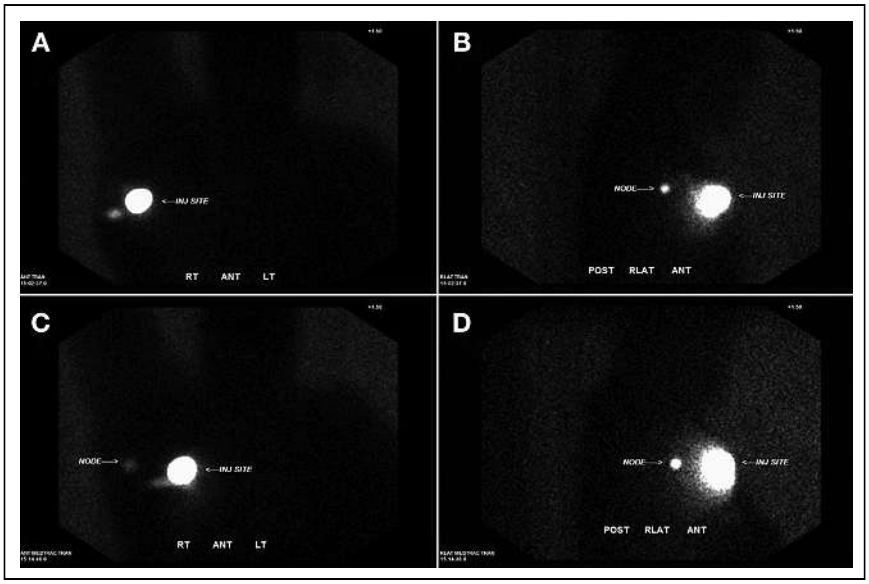

FIGURE 1. (A and B) Anterior (A) and lateral (B) ^{99m}Tc-tilmanocept lymphoscintigraphy transmission images demonstrate focal area of increased uptake superior and posterior to injection site on lateral view. Focus of uptake inferolateral to injection site on anterior view is in lower position than uptake on lateral view in relation to injection site, suggesting it may not correspond to uptake on lateral view. (C and D) Repeat anterior (C) and lateral (D) images during medial breast traction by patient displaces superimposed injection site medially and clearly demonstrate sentinel node in axillary region on anterior view. Focal uptake inferolateral to injection site on anterior view is likely secondary to contamination.

of obtaining lateral views, arm angles of between 135° and 180° have been suggested as a compromise (*8*). However, this is also not the native position of the surgery. Oblique camera views (45° from anterior views) with the arm in a 90° position may be obtained. A modified oblique view of the axilla when the arm was abducted and elevated using a foam wedge elevating the ipsilateral shoulder has been described and demonstrated improved identification of axillary sentinel nodes (*9*). However, this positioning is not practical for image acquisitions in 2

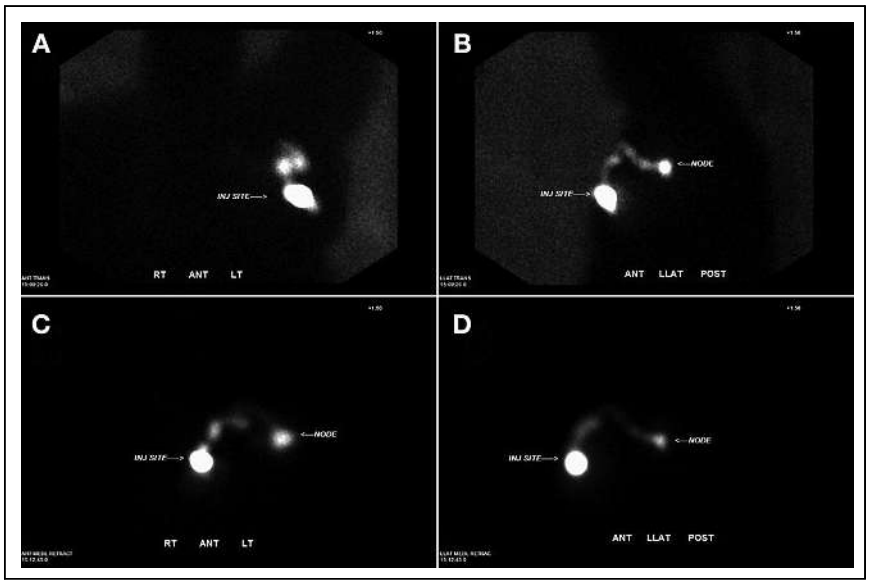

FIGURE 2. (A) Anterior ^{99m}Tc-tilmanocept lymphoscintigraphy image demonstrates focal areas of increased uptake superior to injection site. Sentinel node is not clearly identified. (B) Lateral image demonstrates lymph channels and sentinel node. (C and D) Repeat anterior (C) and lateral (D) images during medial breast traction demonstrate marked improvement of visualization of lymph channels and sentinel node on anterior view.

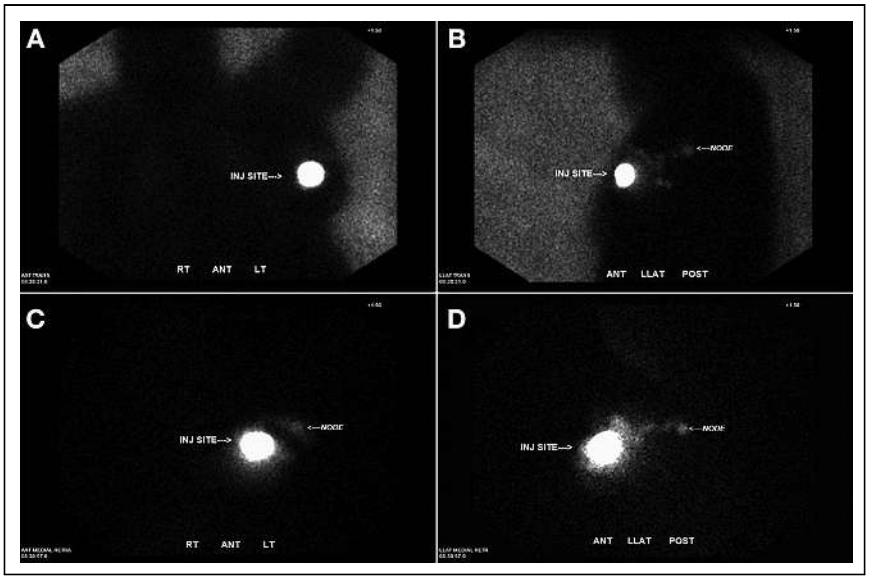

FIGURE 3. (A and B) Anterior (A) and lateral (B) ^{99m}Tc-tilmanocept lymphoscintigraphy images demonstrate focal areas of increased uptake superior and posterior to injection site, which likely represent lymph channels and axillary sentinel node. (C and D) Repeat anterior (C) and lateral (D) images during medial breast traction demonstrate marked improvement of visualization of lymph channels and sentinel node on anterior and lateral views.

different views using a dual-head camera. Also, oblique images may be more difficult to interpret (*8*). Image acquisitions in a prone position with the breast hanging using a special pad with cutouts to move the injection site away from the axilla has been described. This method requires an additional position and maneuvering of the patient and is different from the position during surgery (*10*). Breast displacement maneuvers have been suggested (*8,10,11*). These maneuvers include taping the breast or using a breast holder. In our practice, we have found a medial breast traction technique performed by the patient to be especially useful. SPECT/CT is an excellent modality for evaluation of the sentinel node location. Unfortunately, it has limited use because of its high cost and the additional radiation dose to the patient from the CT portion of the examination. The total effective dose from the low-dose CT portion of SPECT/CT is approximately 3 mSv, as compared with the radiation dose from a ^{57}Co flood source, which is on the order of microsieverts (*12*).

We use a ^{57}Co flood source for transmission images. A ^{153}Gd flood source, which has primary photon emissions significantly below the ^{99m}Tc emission window, has been suggested. This method may improve image quality because of the reduced crosstalk and increase signal-to-noise ratio (*13*). However, the images need to be acquired in a separate window and fused, requiring additional time for postprocessing.

FIGURE 4. Photograph shows medial breast traction during acquisition of anterior and lateral images.

CONCLUSION

Breast lymphoscintigraphy requires coordination with the referring surgeon, the patient preadmission staff, and the operating room staff, especially for same-day procedures. It is important to complete studies in a timely manner. Necessary information needs to be provided to the surgeon. Therefore, patient scheduling, injection technique, and imaging protocol need to be tailored to meet the demand. Repeat imaging during medial breast traction by the patient is a fast, inexpensive, and practical technique to improve visualization of sentinel lymph nodes.

DISCLOSURE

No potential conflict of interest relevant to this article was reported.

KEY POINTS

QUESTION: Can medial breast traction by the patient improve visualization of sentinel lymph nodes in the axillary region?

PERTINENT FINDINGS: Repeat images during medial traction of the breast by the patient is an effective technique to improve visualization of the sentinel lymph nodes.

IMPLICATIONS FOR PATIENT CARE: Improved visualization of the sentinel lymph node can help the surgeon determine its location during surgery.

REFERENCES

1. Krag DN, Anderson SJ, Julian TB, et al. Sentinel-lymph-node resection compared with conventional axillary-lymph-node dissection in clinically node-negative patients with breast cancer: overall survival findings from the NSABP B-32 randomised phase 3 trial. *Lancet Oncol.* 2010;11:927–933.
2. Newman LA. Lymphatic mapping and sentinel lymph node biopsy in breast cancer patients: a comprehensive review of variations in performance and technique. *J Am Coll Surg.* 2004;199:804–816.
3. Young MA. Lymphoscintigraphic mapping in melanoma and breast cancer. *J Nucl Med Technol.* 2020;48:311–314.
4. Thomas KS, Williams J. Lymphoscintigraphy: breast and melanoma. *J Nucl Med Technol.* 2020;48:315–316.
5. Shimazu K, Tamaki Y, Taguchi T, Takamura Y, Noguchi S. Comparison between periareolar and peritumoral injection of radiotracer for sentinel lymph node biopsy in patients with breast cancer. *Surgery.* 2002;131:277–286.
6. Anagnostou C, Baiocco C, Arnulfo A, Liberatore M, Baccheschi AM, Inglese E. The value of imaging in standing position in preoperative breast lymphoscintigraphy. *Clin Nucl Med.* 2011;36:683–688.
7. Pierini A, Dworkin HJ. Is the upright position more sensitive than the supine position in breast cancer sentinel node lymphoscintigraphy? *Clin Nucl Med.* 2001;26:823–825.
8. Krynyckyi BR, Miner M, Ragonese JM, Firestone M, Kim CK, Machac J. Technical aspects of performing lymphoscintigraphy: optimization of methods used to obtain images. *Clin Nucl Med.* 2000;25:978–985.
9. Haigh PI, Hansen NM, Giuliano AE, Edwards GK, Ye W, Glass EC. Factors affecting sentinel node localization during preoperative breast lymphoscintigraphy. *J Nucl Med.* 2000;41:1682–1688.
10. Krynyckyi BR, Kim CK, Goyenechea MR, Chan PT, Zhang ZY, Machac J. Clinical breast lymphoscintigraphy: optimal techniques for performing studies, image atlas, and analysis of images. *Radiographics.* 2004;24:121–145.
11. Giammarile F, Alazraki N, Aarsvold JN, et al. The EANM and SNMMI practice guideline for lymphoscintigraphy and sentinel node localization in breast cancer. *Eur J Nucl Med Mol Imaging.* 2013;40:1932–1947.
12. Law M, Ma WH, Leung R, et al. Evaluation of patient effective dose from sentinel lymph node lymphoscintigraphy in breast cancer: a phantom study with SPECT/CT and ICRP-103 recommendations. *Eur J Radiol.* 2012;81:e717–720.
13. DiFilippo FP, Brunken RC, Neumann DR. Transmission imaging in lymphoscintigraphy with a ^{153}Gd flood source. *J Nucl Med Technol.* 2015;43:253–260.

Whole-Skeleton SUV_{mean} Measured on ^{18}F-NaF PET/CT Studies as a Prognostic Indicator in Patients with Breast Cancer Metastatic to Bone

José Flávio Gomes Marin[1], Paulo Schiavom Duarte[1], Monique Beraldo Ordones[1], Heitor Naoki Sado[1,2], Marcelo Tatit Sapienza[2], and Carlos Alberto Buchpiguel[1,2]

[1]Division of Nuclear Medicine, São Paulo Cancer Institute, São Paulo, Brazil; and [2]Division of Nuclear Medicine, Department of Radiology and Oncology, Medical School of University of São Paulo, São Paulo, Brazil

In this work, we assessed the association between the whole-skeleton SUV_{mean} measured on ^{18}F-NaF PET/CT studies and overall survival (OS) in patients with breast cancer metastatic to bone. **Methods:** We retrospectively analyzed 176 patients with breast cancer and metastatic bone disease who underwent ^{18}F-NaF PET/CT. The outcomes of the patients (dead or alive) were based on the last information available in their files. The SUV_{mean} and SUV_{max} were measured in a whole-skeleton volume of interest (wsVOI). The wsVOI was based on the CT component of the PET/CT study using Hounsfield unit thresholds. The wsVOI was then applied to the ^{18}F-NaF PET image. Univariate analyses were performed to assess the association of SUVs with OS. We also analyzed the association between OS and patient age; presence of visceral metastatic disease; histologic subtype; presence of hormone receptors; human epidermal growth factor receptor 2 expression; and creatinine, cancer antigen (CA) 15-3, and alkaline phosphatase levels. The variables statistically significant in the univariate analyses were included in a multivariate Cox regression OS analysis. **Results:** In the univariate analyses, there were associations between OS and whole-skeleton SUV_{mean} and SUV_{max}, estrogen receptor status, and CA15-3 and alkaline phosphatase levels. In the multivariate analysis, all variables that were statistically significant in the univariate analyses were associated with OS, with the exception of CA15-3. **Conclusion:** In patients with breast cancer metastatic to bone, whole-skeleton SUV_{mean} is an independent predictor of OS.

Key Words: ^{18}F; PET/CT; ^{18}F-NaF; breast cancer; bone metastases

J Nucl Med Technol 2022; 50:119–125
DOI: 10.2967/jnmt.121.262907

The modality ^{18}F-NaF PET/CT has been used for the detection of bone metastases in neoplastic diseases, mainly in those with osteoblastic metastases (*1,2*). It has higher accuracy than ^{99m}Tc-labeled diphosphonate bone scanning even when SPECT or SPECT/CT techniques are used (*3–5*), and this higher accuracy, along with the growing availability of PET/CT equipment (*6,7*), is resulting in the increasing use of ^{18}F-NaF PET/CT in the clinical assessment of metastatic bone disease (*8,9*).

Beside describing the detection of skeletal metastases, some articles have described the capability of ^{18}F-NaF PET/CT to measure the degree of metastatic bone disease (*10,11*) and the utility of this measurement in follow-up (*12*) and in estimation of overall survival (OS) in patients with prostate cancer (*13*) or, less frequently, other neoplastic diseases such as breast cancer (*14*), medullary thyroid cancer (*15*), multiple myeloma (*16*), and urologic malignancies (*17*). Thus, at present, the utility of ^{18}F-NaF PET/CT in cancer patients is not restricted to detection of metastatic bone disease but can also be extended to estimation of the burden of skeletal disease, since this estimation is useful in follow-up of patients and allows prognostic assessment.

However, the methodology used to estimate the burden of metastatic disease is a work in progress, and there is not yet a definitive method for this measurement. Therefore, we developed a methodology to calculate the whole-skeleton SUV_{mean} in ^{18}F-NaF PET/CT studies, and we analyzed this parameter as an indicator of the burden of metastatic bone disease and its independent association with OS in patients with breast cancer.

MATERIALS AND METHODS

Patients

We retrospectively analyzed 176 women with breast cancer metastatic to bone who underwent ^{18}F-NaF PET/CT in our institution between 2011 and 2018 and who underwent creatinine, cancer antigen (CA) 15-3, and alkaline phosphatase analyses within 3 mo of the PET/CT studies. This group represents all such patients found in the electronic medical record files. From these files, we also obtained the patient age; results of ^{18}F-NaF PET/CT; presence of visceral metastases; creatinine, CA15-3, and alkaline phosphatase levels; histologic subtype; hormone receptor status; human epidermal growth factor receptor 2 (HER-2) expression; time from diagnosis to ^{18}F-NaF PET/CT; and OS.

The recorded age of the patients was that at the time of the ^{18}F-NaF PET/CT studies. The outcomes of the patients (dead or alive) were based on the last information available in the electronic files, and the presence of soft-tissue metastases was based on the

Received Aug. 18, 2021; revision accepted Oct. 5, 2021.
For correspondence or reprints, contact Paulo Schiavom Duarte (psduarte@hotmail.com).
Published online Nov. 8, 2021.

results of other imaging studies available at the time of the ^{18}F-NaF PET/CT studies.

Approval by the local Research and Ethics Committee was obtained before this retrospective study began, and the requirement to obtain informed consent was waived.

^{18}F-NaF PET/CT Studies

Around 45–60 min after injection of approximately 185 MBq of the radiopharmaceutical, ^{18}F-NaF PET/CT images were acquired on a Discovery 690 PET/CT scanner with time-of-flight technology (GE Healthcare). All patients underwent whole-body (vertex to toes) 3-dimensional PET/CT. The emission images were obtained at 1 min per bed position (15-cm axial scan field of view with 3 cm of overlap), with 13–15 bed positions per study. The CT transmission images (30 mAs) were obtained for attenuation correction and anatomic correlation of the uptake areas. Other CT acquisition parameters included 120 kVp, a rotation time of 0.5 s, a pitch of 1.375, and an axial slice thickness of 3.75 mm. PET images were reconstructed using iterative technique (ordered-subsets expectation maximization) with 2 iterations and 24 subsets. CT image reconstruction was based on the conventional filtered backprojection method with the GE Healthcare Bone Plus filter.

Determination of Presence of Skeletal Metastases

The presence of metastatic bone disease was based on the ^{18}F-NaF PET/CT findings (metabolic and anatomic patterns), on the results of other imaging studies when available (MRI and high-resolution contrast-enhanced CT), and on follow-up studies performed with either ^{18}F-NaF PET/CT or ^{99m}Tc-methylene diphosphonate (MDP). Patients without bone metastases were excluded from the study.

Calculation of Whole-Skeleton SUVs

The degree of skeletal ^{18}F-NaF uptake was measured in a whole-skeleton volume of interest (wsVOI) using the SUV_{max} and the SUV_{mean} within the wsVOI. wsVOI was based on the CT component of the PET/CT study using a Hounsfield unit threshold (usually 120). wsVOI was then applied to the metabolic image of the PET/CT study (Figs. 1–3) using AMIDE software (*18*).

Statistical Analysis

Statistical analyses were divided into 2 phases. First, univariate analyses were performed to assess the association of OS with whole-skeleton SUV_{mean} and SUV_{max}; age; presence of visceral metastases; histologic subtype (invasive ductal or invasive lobular carcinoma); presence of hormone receptors (estrogen and progesterone); HER-2 expression (positive or negative); and creatinine, CA15-3, and alkaline phosphatase levels. Variables with a statistically significant association with OS in the univariate analyses were selected for multivariate analysis (second phase).

In the univariate analyses, the best cutoffs for the continuous variables (whole-skeleton SUV_{mean} and SUV_{max}, age and creatinine, CA15-3 and alkaline phosphatase levels) to divide the patients into 2 groups with a maximum OS difference between them were defined by maximally selected rank statistics using the Lausen test (*19*). The maximally selected rank statistics also provided the statistical level of significance (*P* value) of the OS difference between the 2 groups. For the binary variables (presence of visceral metastases, histologic subtype, hormone receptor status, and HER-2 expression), the OS analyses between the 2 categories were performed using Kaplan–Meier curves and log rank testing. OS was measured from the date of the ^{18}F-NaF PET/CT, and a *P* value of 0.05 or less was adopted for statistical significance. However, variables with a *P* value of no more than 0.1 in the univariate analyses could be selected for multivariate analysis.

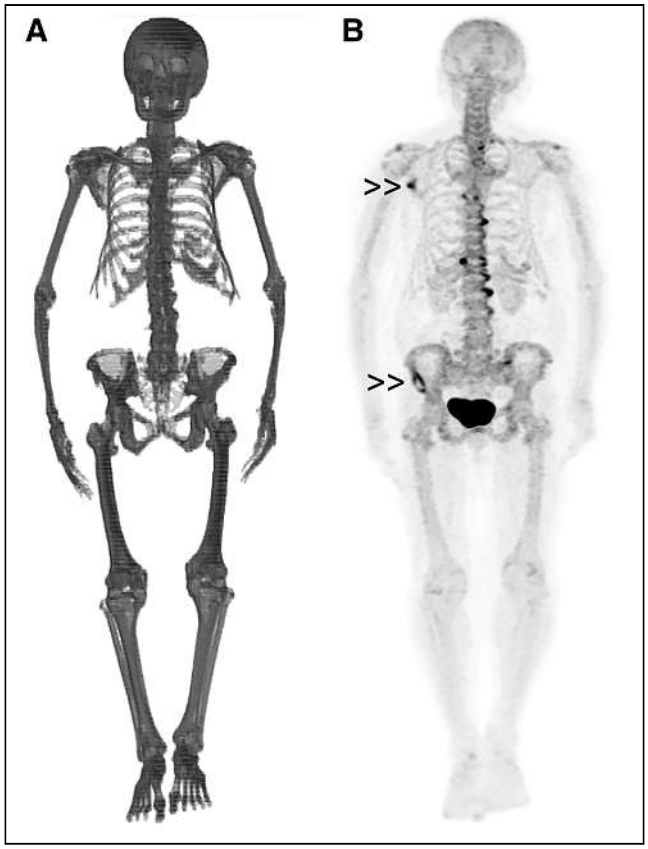

FIGURE 1. wsVOI (A) and coronal maximum-intensity-projection ^{18}F-NaF PET/CT image (B) of patient with a few metastatic sites in skeleton (double arrowheads). Patient presented with whole-skeleton SUV_{mean} of 2.20 and was still alive 1,974 d after study.

Cox proportional-hazards regression was used for multivariate OS analysis. In this analysis, all variables were inserted as binary groups, and the continuous variables were dichotomized using the cut points defined in the Lausen test. A *P* value of 0.05 or less was adopted for statistical significance.

For illustrative purposes, the Kaplan–Meier curves of the variables that were statistically significant in the multivariate analysis are also presented.

We also compared the interval from diagnosis to the ^{18}F-NaF PET/CT studies between groups with a low and a high whole-skeleton SUV_{mean} and SUV_{max}, using unpaired *t* testing.

The Lausen test was performed using R software (version 3.6.1), and the other statistical analyses were done using SPSS (version 20.0; IBM). The descriptive results for the continuous variables are presented as mean, SD, and range.

RESULTS

The patient characteristics and variables analyzed are presented in Tables 1 and 2. The mean follow-up period was 966 d (SD, 606 d; range, 21–2,921 d), and of the 176 patients analyzed, 138 died during the follow-up.

The results of the univariate analyses are presented in Table 3. The following variables had a statistically significant

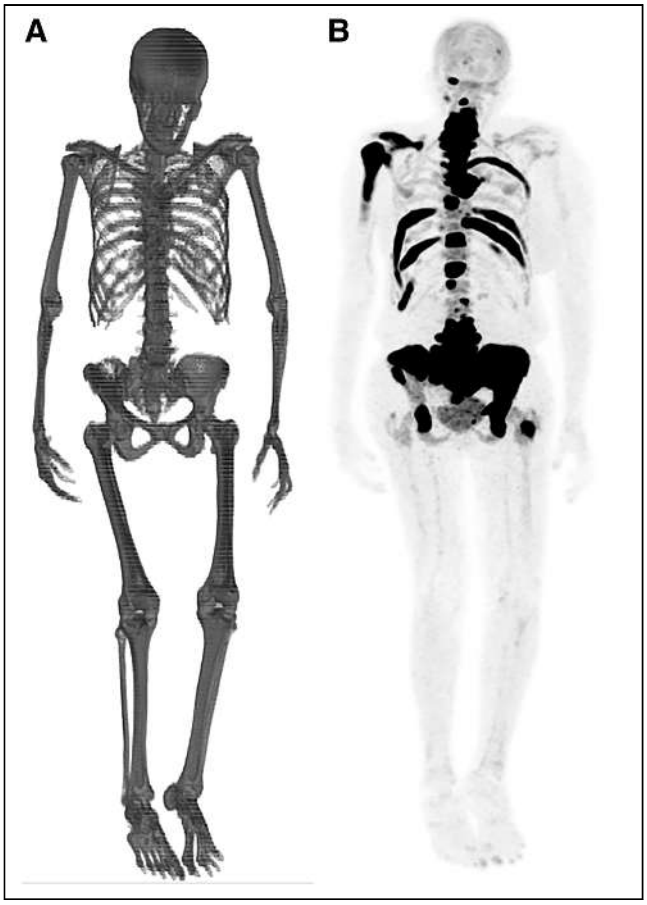

FIGURE 2. wsVOI (A) and coronal maximum-intensity-projection ^{18}F-NaF PET/CT image (B) of patient with multiple metastatic sites in skeleton. Patient presented with whole-skeleton SUV_{mean} of 3.58 and died 153 d after study.

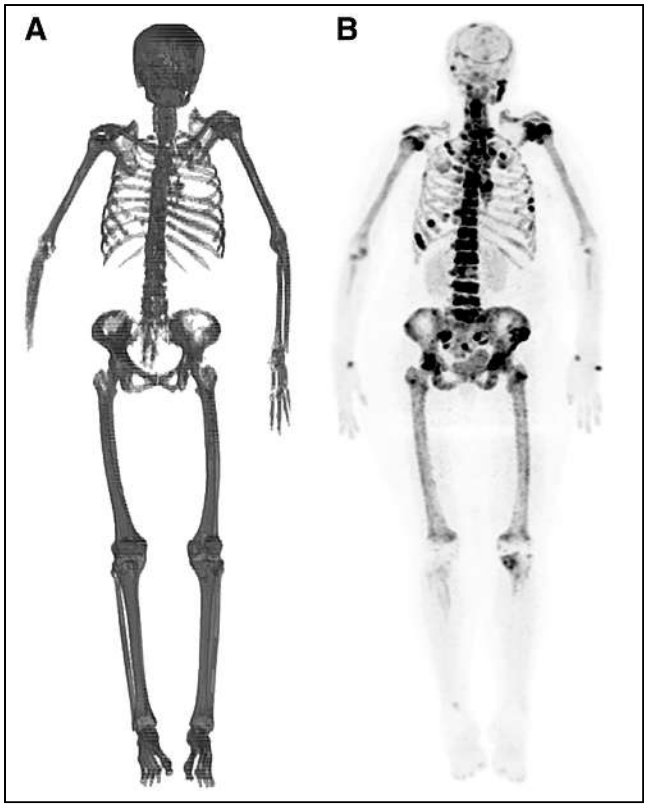

FIGURE 3. wsVOI (A) and coronal maximum-intensity-projection ^{18}F-NaF PET/CT image (B) of patient with widespread metastatic bone disease characterized by diffuse and heterogeneous uptake of radiopharmaceutical in axial and proximal appendicular skeleton. Patient presented with whole-skeleton SUV_{mean} of 4.78 and died 66 d after study. In this case, wsVOI was not able to detect right hand and some fingers of left hand.

association with OS ($P < 0.05$) and were selected for multivariate analysis: CA15-3 and alkaline phosphatase levels, estrogen receptor status, and whole-skeleton SUV_{mean} and SUV_{max}.

In the Cox regression analysis, a high alkaline phosphatase level, the absence of estrogen receptors, and a high whole-skeleton SUV_{mean} and SUV_{max} were related to a poor prognosis (Table 4). The Kaplan–Meier curves of these variables are presented in Figure 4.

There were no statistically significant differences in the time from diagnosis to the ^{18}F-NaF PET/CT studies between groups with a low and a high whole-skeleton SUV_{mean} ($P = 0.82$) and SUV_{max} ($P = 0.79$).

DISCUSSION

Skeletal metastatic disease is common in patients with breast cancer (*20*) and is a cause of morbidity and mortality in these patients (*21*). Moreover, not only the presence of bone metastases but also the number of metastatic sites has been associated with OS, and some studies have shown that patients with multiple sites of metastasis in the skeleton have a shorter OS than do patients with a solitary bone metastasis (*22,23*). In the staging and follow-up of patients with breast cancer, radionuclide bone imaging has a main role due to its high sensitivity in detecting skeletal metastasis, either with ^{99m}Tc-MDP scintigraphy (*24*) or with ^{18}F-NaF

TABLE 1
Patient Characteristics

Characteristic	Mean	SD	Minimum	Maximum
Follow-up time (d)	941.9	578.4	21	2,711
$wsSUV_{max}$	48.5	22.6	6.2	144.2
$wsSUV_{mean}$	3.2	0.9	0.3	6.1
Age (y)	56.9	13.4	27.4	88.2
Creatinine level (mg/dL)	0.7	0.3	0.3	2.7
CA15-3 level (units/mL)	438.1	1,412.4	7.0	12,000.0
ALP level (units/L)	142.1	133.8	21.1	955.0
Diagnosis to PET (d)	1,194.7	1,451.9	−1*	6,794

*^{18}F-NaF PET/CT was performed before result of pathologic study confirmed cancer diagnosis.

$wsSUV_{max}$ = whole-skeleton SUV_{max}; $wsSUV_{mean}$ = whole-skeleton SUV_{mean}; ALP = alkaline phosphatase.

TABLE 2
Visceral Metastasis Status, Hormone Status, and Histologic Subtype

Characteristic	Data
VM	
Absent	131 (74)
Present	45 (26)
Missing	0 (0)
Estrogen receptor	
Absent	18 (10)
Present	156 (89)
Missing	2 (1)
Progesterone receptor	
Absent	41 (23)
Present	130 (74)
Missing	5 (3)
HER-2 expression	
Absent	139 (79)
Present	35 (20)
Missing	2 (1)
Histologic subtype	
IDC	153 (87)
ILC	14 (8)
Other	4 (2.3)
Missing	5 (2.8)

VM = visceral metastases; IDC = invasive ductal carcinoma; ILC = invasive lobular carcinoma.
Data are number followed by percentage in parentheses.

TABLE 3
Results of Univariate Analyses

Variable	Group 1	Group 2	*n* in group 1	*P*
$wsSUV_{max}$	≤32.8	>32.8	42 (24%)	0.02*§
$wsSUV_{mean}$	≤3.13	>3.13	97 (55%)	<0.01*§
Age (y)	≤56	>56	91 (52%)	0.48*
Creatinine (mg/dL)	≤0.83	>0.83	135 (77%)	0.57*
CA15-3 (units/mL)	≤19.0	>19.0	20 (11%)	0.02*§
ALP (units/L)	≤131	>131	118 (67%)	<0.01*§
VM	Absent	Present	131 (74%)	0.15†
Estrogen receptor	Absent	Present	18 (10%)‡	0.01†§
Progesterone receptor	Absent	Present	41 (24%)‡	0.77†
HER-2 expression	Absent	Present	139 (80%)‡	0.24†
Histologic subtype	IDC	ILC	153 (92%)‡	0.40†

wsSUVmax = whole-skeleton SUV_{max}; wsSUVmean = whole-skeleton SUV_{mean}; ALP = alkaline phosphatase; VM = visceral metastases; IDC = invasive ductal carcinoma; ILC = invasive lobular carcinoma.
*Calculated using Lausen test.
†Calculated using log rank test.
‡In relation to 2 groups compared (excluding missing data and other groups).
§Variables selected for multivariate analysis ($P \leq 0.1$).
Variables were divided into 2 groups for OS comparison. Numbers of individuals in group 1, and *P* values of difference in OS between 2 groups, are also presented.

TABLE 4
Results of Cox Regression Evaluating Association of Variables Selected in Univariate Analyses with OS

Variable	Group	HR	95% CI	*P*
$wsSUV_{max}$	>32.8	1.60	1.00–2.57	0.05*
$wsSUV_{mean}$	>3.13	1.57	1.10–2.24	0.01*
CA15-3 level (units/mL)	>19.0	1.26	0.66–2.42	0.48
ALP level (units/L)	>131	2.14	1.47–3.12	<0.01*
Estrogen receptor	Present	0.59	0.35–1.01	0.05*

*Independent variables on Cox regression ($P \leq 0.05$).
$wsSUV_{max}$ = whole-skeleton SUV_{max}; $wsSUV_{mean}$ = whole-skeleton SUV_{mean}; ALP = alkaline phosphatase; HR = hazard ratio.

PET/CT (*25*). However, use of these methods to measure the burden of metastatic bone disease in patients with breast cancer is infrequent, possibly because of the scarcity of studies showing an association between this burden and prognosis and because of technical difficulties with using these measurement methods in clinical practice.

For skeletal scintigraphy with ^{99m}Tc-MDP, there are studies showing an association between prognosis and the bone scan index (BSI), a technique that calculates the percentage of bone metastases either manually (*26*) or, more recently, automatically (*27*). But these studies were mainly on the use of the BSI in prostate cancer patients (*28,29*), and there are only a few articles about the use of the BSI in breast cancer (*30,31*). A possible reason could be the difference in phenotype for bone metastases in these different

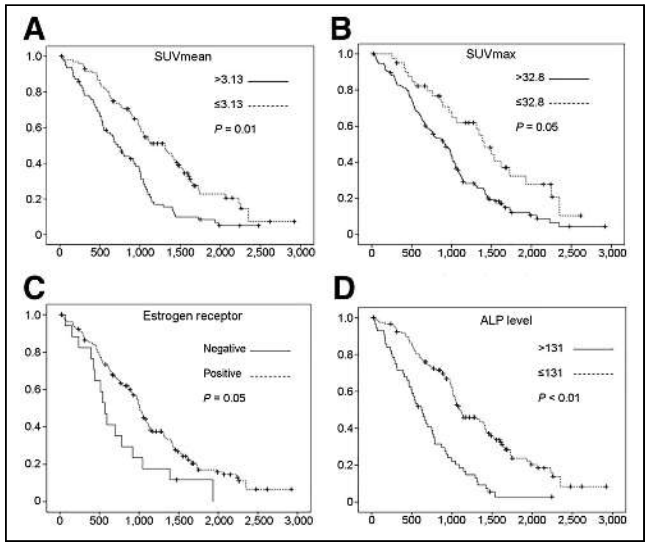

FIGURE 4. Kaplan–Meier curves for whole-skeleton SUV_{mean} (A) and SUV_{max} (B), estrogen receptor status (C), and alkaline phosphatase level (D). *y*-axis displays OS probability, and *x*-axis displays OS time in days. Cutoffs for division of variables into 2 comparison groups are presented in Table 3 and in figure. Statistical significance of OS differences between groups are presented in Table 4 and in figure. + = censored patients; ALP = alkaline phosphatase level.

cancers (sclerotic, lytic, or mixed), with a predominance of the lytic pattern in breast cancer (*32*) and of the sclerotic pattern in prostate cancer (*33*). Since lytic lesions are less well visualized by bone scanning, the BSI tends to underestimate the burden of disease in patients with breast cancer; however, such is not the case for prostate cancer, for which almost all lesions are sclerotic, with an osteoblastic activity that is usually well characterized on radionuclide images.

For ^{18}F-NaF PET/CT studies, some articles have already described methodologies to measure the severity of metastatic bone disease and showed the association of this severity with prognosis. However, as was the case with the BSI, most of the studies were done on patients with prostate cancer (*10,12,13*), and studies on other neoplastic diseases were less frequent (*14–17*). Particularly in breast cancer patients, few studies have investigated the association of the burden of metastatic bone disease measured on ^{18}F-NaF PET/CT with prognosis. Brito et al. (*14*) analyzed a group of 49 patients with breast cancer metastatic to bone and showed that patients with a higher burden of metastatic bone disease had a worse prognosis. Further, these authors published an article validating a method for semiautomatic quantification of ^{18}F-NaF PET/CT studies (*11*). In this sense, our results also support the evidence that the burden of metastatic bone disease measured in ^{18}F-NaF PET/CT studies is associated with OS in patients with breast cancer. However, the methodology of quantification used in our study is different from that used in most of the studies published so far (*10–12*). While the latter is based on the definition of the metabolic boundaries of metastatic lesions using SUV thresholds on PET images, our methodology is based on a wsVOI defined in the CT image using Hounsfield unit thresholds and the further application of this wsVOI on the metabolic images. Nevertheless, this is not the first time this methodology has been used; previous articles described its use to calculate the whole-skeleton SUV_{mean} in a group of patients with normal ^{18}F-NaF PET/CT results (*34*) and to calculate the whole-skeleton SUV_{mean} in ^{18}F-NaF and ^{18}F-FDG PET/CT studies on patients with multiple myeloma (*35*). However, to our knowledge, this is the first time it has been used in a group of patients with breast cancer.

Regarding our results, it is worth highlighting that both SUV metrics (SUV_{mean} and SUV_{max}) were independently associated with OS. This result could be explained by the fact that although whole-skeleton SUV_{max} represents the aggressiveness of the disease, whole-skeleton SUV_{mean} represents the disease burden. This finding is partially in accord with the scarce literature about this issue. Brito et al. (*14*) showed that in patients with breast cancer metastatic to bone, the burden of bone disease measured on ^{18}F-NaF PET/CT was associated with OS in the multivariate analysis whereas SUV_{max} was associated with OS only in univariate analyses. For patients with advanced genitourinary malignancies, Lim et al. (*17*) showed that the burden of metastatic bone disease on baseline ^{18}F-NaF PET/CT was associated with OS whereas SUV_{max} was associated with OS only on posttherapeutic ^{18}F-NaF PET/CT. For prostate cancer patients, Etchebehere et al. (*13*) showed that the burden of metastatic bone disease was associated with OS whereas SUV_{max} was not. Therefore, future analyses are needed to better evaluate the role of SUV metrics in the prognostic assessment of patients with metastatic bone disease, particularly those with breast cancer.

Another interesting result of our study is that besides the whole-skeleton SUV metrics, only estrogen receptor status and alkaline phosphatase level were associated with outcome in the multivariate analysis; CA15-3 level, which was associated with prognosis in the univariate analyses, did not show a statistically significant association with OS in the multivariate analysis. The literature about the association of alkaline phosphatase and CA15-3 level with OS in breast cancer patients is controversial, with some articles corroborating our findings and showing an association between alkaline phosphatase level (*36*) but not CA 15-3 level and prognosis (*37*), whereas others show the opposite finding, with absence of alkaline phosphatase association (*37*) and presence of CA 15-3 association with prognosis (*38*). The literature findings on hormonal receptors and HER-2 status are also heterogeneous, with some articles corroborating our findings that estrogen receptors are more important than progesterone receptors in the prognostic definition (*39*) whereas others show that the relations among these parameters are complex and that the prognosis will depend more on their distinct combination than on the isolated result for a specific parameter (*40*). Regarding the finding that the presence of soft-tissue metastases was not associated with OS, even in the univariate analyses—this finding was in accord with a previous study that showed the burden of metastatic bone disease to be more relevant than the presence of visceral metastases in the prognosis of patients with breast cancer (*14*).

Thus, our results corroborate the importance of measuring the burden of metastatic bone disease as a prognostic indicator in patients with breast cancer, since this burden can be one of the few variables independently associated with OS. Nevertheless, this study presents some limitations. First, it was retrospective, and we did not have complete information on some variables that could potentially have confounded the results, such as the burden and sites of visceral metastases, previous treatments, and disease stage at the time of diagnosis. Therefore, these variables were not part of the analysis, and further studies are needed to learn whether adding them would have changed the results. But we did compare the interval from diagnosis to ^{18}F-NaF PET/CT between groups with a low and a high whole-skeleton SUV_{mean} and SUV_{max}, and no differences in this parameter were found. Consequently, this interval does not appear to be the cause of a higher burden of metastatic bone disease in our patients.

However, the main objective of our study was not to compare the burden of metastatic bone disease with all other potential prognostic variables in patients with breast cancer, especially because these variables are numerous and vary among different studies, but to assess the feasibility of a new methodology to estimate this burden and to analyze the

performance of this methodology as a prognostic indicator. Second, we did not compare the methodology used in our study with those used in previous studies. The methodology we used can have potential advantages, such as not being dependent on SUVs to define the lesions—a particular advantage in breast cancer, for which the presence of lytic lesions with low uptake is common, with limited detectability using SUV thresholds. On the other hand, whole-skeleton SUV_{mean} comprises the degree of uptake in the malignant lesions as well as in benign lesions and normal bone—a particular disadvantage in patients with extensive degenerative bone disease and a low burden of metastatic disease. Nevertheless, the method based on whole-skeleton SUV_{mean} could be further improved by erasing areas with benign uptake from metabolic images before the wsVOI is applied to them. Thus, future analyses on the main advantages, disadvantages, and potential complementarity of these methodologies should be performed.

Last, we should remember that ^{18}F-NaF and ^{99m}Tc-MDP uptake occurs mainly in cortical bone metastases, whereas metastatic lesions initially appear in the bone marrow before invading cortical bone. Therefore, if we wish to properly quantify the burden of metastatic skeletal disease using tracers that are also taken up by bone marrow lesions, such as ^{18}F-FDG and ^{18}F-fluoroestradiol, other segmentation techniques not based strictly on Hounsfield units might be better suited.

CONCLUSION

In our group of patients with breast cancer metastatic to bone, calculation of whole-skeleton SUV_{mean} in ^{18}F-NaF PET/CT studies is feasible, and this measure is an independent predictor of OS.

DISCLOSURE

No potential conflict of interest relevant to this article was reported.

KEY POINTS

QUESTION: Is the whole-skeleton SUV_{mean} in ^{18}F-NaF PET/CT studies associated with OS in patients with breast cancer metastatic to bone?

PERTINENT FINDINGS: It is feasible to create wsVOIs based on the CT component of the PET/CT study using Hounsfield unit thresholds. These wsVOIs can then be applied to the metabolic component of ^{18}F-NaF PET/CT studies to calculate the whole-skeleton SUV_{mean} of the patients. In a retrospective cohort analysis, whole-skeleton SUV_{mean} was found to be an independent predictor of OS in patients with breast cancer metastatic to bone.

IMPLICATIONS FOR PATIENT CARE: The findings of this study can be useful to provide better prognostic information to patients with breast cancer metastatic to bone.

REFERENCES

1. Tateishi U, Morita S, Taguri M, et al. A meta-analysis of ^{18}F-fluoride positron emission tomography for assessment of metastatic bone tumor. *Ann Nucl Med.* 2010;24:523–531.
2. Iagaru A, Young P, Mittra E, Dick DW, Herfkens R, Gambhir SS. Pilot prospective evaluation of ^{99m}Tc-MDP scintigraphy, ^{18}F NaF PET/CT, ^{18}F FDG PET/CT and whole-body MRI for detection of skeletal metastases. *Clin Nucl Med.* 2013;38: e290–e296.
3. Even-Sapir E, Metser U, Mishani E, Lievshitz G, Lerman H, Leibovitch I. The detection of bone metastases in patients with high-risk prostate cancer: ^{99m}Tc-MDP planar bone scintigraphy, single- and multi-field-of-view SPECT, ^{18}F-fluoride PET, and ^{18}F-fluoride PET/CT. *J Nucl Med.* 2006;47:287–297.
4. Jambor I, Kuisma A, Ramadan S, et al. Prospective evaluation of planar bone scintigraphy, SPECT, SPECT/CT, ^{18}F-NaF PET/CT and whole body 1.5T MRI, including DWI, for the detection of bone metastases in high risk breast and prostate cancer patients: SKELETA clinical trial. *Acta Oncol.* 2016;55:59–67.
5. Löfgren J, Mortensen J, Rasmussen SH, et al. A prospective study comparing Tc-hydroxyethylene-diphosphonate planar bone scintigraphy and whole-body SPECT/CT with ^{18}F-fluoride PET/CT and ^{18}F-fluoride PET/MRI for diagnosing bone metastases. *J Nucl Med.* 2017;58:1778–1785.
6. Hellwig D, Marienhagen J, Menhart K, Grosse J. Nuclear medicine in Germany: updated key data and trends from official statistics [in German]. *Nuklearmedizin.* 2017;56:55–68.
7. Páez D, Orellana P, Gutiérrez C, Ramirez R, Mut F, Torres L. Current status of nuclear medicine practice in Latin America and the Caribbean. *J Nucl Med.* 2015; 56:1629–1634.
8. Segall GM. PET/CT with sodium ^{18}F-fluoride for management of patients with prostate cancer. *J Nucl Med.* 2014;55:531–533.
9. Hillner BE, Siegel BA, Hanna L, et al. Impact of ^{18}F-fluoride PET on intended management of patients with cancers other than prostate cancer: results from the national oncologic PET registry. *J Nucl Med.* 2014;55:1054–1061.
10. Rohren EM, Etchebehere EC, Araujo JC, et al. Determination of skeletal tumor burden on ^{18}F-fluoride PET/CT. *J Nucl Med.* 2015;56:1507–1512.
11. Brito AE, Mourato F, Santos A, Mosci C, Ramos C, Etchebehere E. Validation of the semiautomatic quantification of F-fluoride PET/CT whole-body skeletal tumor burden. *J Nucl Med Technol.* 2018;46:378–383.
12. Lapa P, Marques M, Costa G, Iagaru A, Pedroso de Lima J. Assessment of skeletal tumour burden on ^{18}F-NaF PET/CT using a new quantitative method. *Nucl Med Commun.* 2017;38:325–332.
13. Etchebehere EC, Araujo JC, Fox PS, Swanston NM, Macapinlac HA, Rohren EM. Prognostic factors in patients treated with ^{223}Ra: the role of skeletal tumor burden on baseline ^{18}F-fluoride PET/CT in predicting overall survival. *J Nucl Med.* 2015; 56:1177–1184.
14. Brito AE, Santos A, Sasse AD, et al. ^{18}F-fluoride PET/CT tumor burden quantification predicts survival in breast cancer. *Oncotarget.* 2017;8:36001–36011.
15. Ueda CE, Duarte PS, de Castroneves LA, et al. Burden of metastatic bone disease measured on ^{18}F-NaF PET/computed tomography studies as a prognostic indicator in patients with medullary thyroid cancer. *Nucl Med Commun.* 2020; 41:469–476.
16. Zadeh MZ, Seraj SM, Østergaard B, et al. Prognostic significance of ^{18}F-sodium fluoride in newly diagnosed multiple myeloma patients. *Am J Nucl Med Mol Imaging.* 2020;10:151–160.
17. Lim I, Lindenberg ML, Mena E, et al. ^{18}F-sodium fluoride PET/CT predicts overall survival in patients with advanced genitourinary malignancies treated with cabozantinib and nivolumab with or without ipilimumab. *Eur J Nucl Med Mol Imaging.* 2020;47:178–184.
18. Loening AM, Gambhir SS. AMIDE: a free software tool for multimodality medical image analysis. *Mol Imaging.* 2003;2:131–137.
19. Lausen B, Schumacher M. Maximally selected rank statistics. *Biometrics.* 1992;48: 73–85.
20. Lee YT. Breast carcinoma: pattern of metastasis at autopsy. *J Surg Oncol.* 1983; 23:175–180.
21. Coleman RE, Rubens RD. The clinical course of bone metastases from breast cancer. *Br J Cancer.* 1987;55:61–66.
22. Koizumi M, Yoshimoto M, Kasumi F, Ogata E. Comparison between solitary and multiple skeletal metastatic lesions of breast cancer patients. *Ann Oncol.* 2003;14: 1234–1240.
23. Parkes A, Warneke CL, Clifton K, et al. Prognostic factors in patients with metastatic breast cancer with bone-only metastases. *Oncologist.* 2018;23: 1282–1288.
24. Costelloe CM, Rohren EM, Madewell JE, et al. Imaging bone metastases in breast cancer: techniques and recommendations for diagnosis. *Lancet Oncol.* 2009;10: 606–614.

25. Yoon S-H, Kim KS, Kang SY, et al. Usefulness of ^{18}F-fluoride PET/CT in breast cancer patients with osteosclerotic bone metastases. *Nucl Med Mol Imaging.* 2013; 47:27–35.
26. Erdi YE, Humm JL, Imbriaco M, Yeung H, Larson SM. Quantitative bone metastases analysis based on image segmentation. *J Nucl Med.* 1997;38:1401–1406.
27. Nakajima K, Nakajima Y, Horikoshi H, et al. Enhanced diagnostic accuracy for quantitative bone scan using an artificial neural network system: a Japanese multicenter database project. *EJNMMI Res.* 2013;3:83.
28. Ulmert D, Kaboteh R, Fox JJ, et al. A novel automated platform for quantifying the extent of skeletal tumour involvement in prostate cancer patients using the bone scan index. *Eur Urol.* 2012;62:78–84.
29. Nakajima K, Edenbrandt L, Mizokami A. Bone scan index: a new biomarker of bone metastasis in patients with prostate cancer. *Int J Urol.* 2017;24:668–673.
30. Idota A, Sawaki M, Yoshimura A, et al. Bone scan index predicts skeletal-related events in patients with metastatic breast cancer. *Springerplus.* 2016;5:1095.
31. Iwase T, Yamamoto N, Ichihara H, Togawa T, Nagashima T, Miyazaki M. The relationship between skeletal-related events and bone scan index for the treatment of bone metastasis with breast cancer patients. *Medicine (Baltimore).* 2014;93: e269.
32. Glendenning J, Cook G. Imaging breast cancer bone metastases: current status and future directions. *Semin Nucl Med.* 2013;43:317–323.
33. Cook GJR, Azad G, Padhani AR. Bone imaging in prostate cancer: the evolving roles of nuclear medicine and radiology. *Clin Transl Imaging.* 2016;4:439–447.
34. Gomes Marin JF, Duarte PS, Willegaignon de Amorim de Carvalho J, Sado HN, Sapienza MT, Buchpiguel CA. Comparison of the variability of SUV normalized by skeletal volume with the variability of SUV normalized by body weight in ^{18}F-fluoride PET/CT. *J Nucl Med Technol.* 2019;47:60–63.
35. Zadeh MZ, Raynor WY, Seraj SM, et al. Evolving roles of fluorodeoxyglucose and sodium fluoride in assessment of multiple myeloma patients: introducing a novel method of PET quantification to overcome shortcomings of the existing approaches. *PET Clin.* 2019;14:341–352.
36. Chen B, Dai D, Tang H, et al. Pre-treatment serum alkaline phosphatase and lactate dehydrogenase as prognostic factors in triple negative breast cancer. *J Cancer.* 2016;7:2309–2316.
37. Nieder C, Dalhaug A, Haukland E, Mannsaker B, Pawinski A. Prognostic impact of the tumor marker CA 15-3 in patients with breast cancer and bone metastases treated with palliative radiotherapy. *J Clin Med Res.* 2017;9:183–187.
38. Li X, Dai D, Chen B, Tang H, Xie X, Wei W. Clinicopathological and prognostic significance of cancer antigen 15-3 and carcinoembryonic antigen in breast cancer: a meta-analysis including 12,993 patients. *Dis Markers.* 2018;2018:9863092.
39. Lower EE, Glass EL, Bradley DA, Blau R, Heffelfinger S. Impact of metastatic estrogen receptor and progesterone receptor status on survival. *Breast Cancer Res Treat.* 2005;90:65–70.
40. Lv M, Mao Y, Song Y, et al. Clinical features and survival of single hormone receptor-positive breast cancer: a population-based study of 531,605 patients. *Clin Breast Cancer.* 2020;20:e589–e599.

Determining the Minimal Required Ultra-Low-Dose CT Dose Level for Reliable Attenuation Correction of ^{18}F-FDG PET/CT: A Phantom Study

David W. Cheng[1], Monica Ghita[2], David Menard, CNMT[3], and Ming-Kai Chen[4]

[1]*Jacobi Medical Center, Bronx, New York;* [2]*Department of Radiology, School of Medicine, Virginia Commonwealth University, Richmond, Virginia;* [3]*Division of Nuclear Medicine, Department of Diagnostic Radiology, Yale New Haven Hospital, New Haven, Connecticut; and* [4]*Department of Radiology and Biomedical Imaging, Yale University School of Medicine, New Haven, Connecticut*

Our purpose was to investigate the minimal required submillisievert ultra-low-dose CT dose level and the corresponding tube current and voltage for reliable attenuation correction and semiquantitation in ^{18}F-FDG PET/CT in an effort toward radiation dose reduction. **Methods:** We performed a PET/CT investigational study using a National Electrical Manufacturers Association torso phantom containing 6 spheres (10, 13, 17, 22, 28, and 37 mm in diameter) filled with a fixed concentration of 60 kBq/mL and a background of 15 kBq/mL of ^{18}F-FDG. Two sets of PET images, separated by 2 h, were acquired for 3 min at a single bed position using 3-dimensional mode in a Discovery 690 scanner. Several sets of CT images were acquired for attenuation correction with different combinations of tube voltage (80, 100, and 120 kVp) and effective mAs (tube current–time product divided by pitch), using the maximum beam collimation (64 × 0.625 mm). The lowest CT dose acquisition technique available on this scanner is 10 mA, 0.4 s, and 1.375 for the tube current, tube rotation time, and pitch, respectively. The CT radiation dose was estimated on the basis of CT dose index volume measurements performed following the standard methodology and the Imaging Performance Assessment of CT Scanners (ImPACT) calculator. Each of the CT techniques was applied for attenuation correction to the same PET acquisition, using ordered-subset expectation maximization with 24 subsets and 2 iterations. The maximal and average radioactivity (kBq/mL) and SUVs of the spheres were measured. The minimal ultra-low-dose CT dose level for attenuation correction was determined by reproducible SUV measurements (±10%) compared with our reference CT protocol of 100 kVp and 80 mA for a 0.5-s rotation. **Results:** The minimal ultra-low-dose CT dose level for reproducible quantification in all spheres (<10% relative difference) was determined to be 0.3 mSv for a combination of 100 kVp and 10 mA at a 0.5-s rotation and a helical pitch of 0.984 (0.26 mGy measured CT dose index volume). From these results. we could confidently determine the CT parameters for reliable attenuation correction of PET images while significantly reducing the associated radiation dose. **Conclusion:** Our phantom study provided guidance in using ultra-low-dose CT for precise attenuation correction and semiquantification of ^{18}F-FDG PET imaging, which can further reduce the CT dose and radiation exposure to patients in clinical PET/CT studies. On the basis of the data, we can further reduce the radiation dose to the submillisievert level using an ultra-low-dose CT protocol for reliable attenuation correction in clinical ^{18}F-FDG PET/CT studies.

Key Words: research methods; adaptive statistical iterative reconstruction (ASIR); attenuation correction CT; phantom study; reliable SUV quantitation; submillisievert CT

J Nucl Med Technol 2022; 50:126–131
DOI: 10.2967/jnmt.121.262943

Recent evidence from a retrospective large cohort study of over 178,600 United Kingdom residents with radiation exposure from CT scans in childhood assessed a relative risk of 3.18 for leukemia with a cumulative dose of more than 30 mGy, obtainable from as few as 5–10 head CT scans in patients under 15 y of age, and a relative risk of 2.82 for brain cancer with a cumulative dose of 50–74 mGy, obtainable from as few as 2–3 head CT scans, as compared with a low cumulative dose of less than 5 mGy (*1*). In a study of 680,000 Australians exposed to CT scans in childhood and adolescence, Mathews et al. reported an incidence rate ratio of 1.24 for all cancers with an observed dose–response relation of 0.16 per additional CT scan using an estimated average effective radiation dose of 4.5 mSv per scan (*2*). Therefore, the risk of cumulative radiation exposure from medical imaging could be substantial, especially for pediatric patients.

We recently published the results of a phantom study indicating the minimal radioactivity concentration for reproducible SUV_{max} (±10%) quantification to be 1.8 kBq/mL for an acquisition of 10 min, 3.7 kBq/mL for 3–5 min, 7.9 kBq/mL for 2 min, and 17.4 kBq/mL for 1 min with reference standards at a 10-min acquisition (*3*). In light of increased efforts to achieve submillisievert CT studies, iterative reconstruction techniques including adaptive statistical iterative reconstruction (GE Healthcare) and model-based iterative reconstruction (Veo; GE Healthcare) have been used to maintain image quality. Not without controversies (*4,5*), favorable reports have been published for coronary

Received Jul. 30, 2021; revision accepted Sep. 17, 2021.
For correspondence or reprints, contact David Cheng (chengd5@nychhc.org).
Published online Nov. 8, 2021.

CT angiography (*4–7*), chest CT (*8*) for pulmonary embolism (*9*), urinary tract stones (*10*), and CT colonography (*11,12*). Alternatively, dose reduction by sparse-sampled CT (*13*) was achieved in 10 patients by acquiring images at only 25% of the angular projections with subsequent reconstruction of the image data using an iterative algorithm. The authors reported no significant differences in detection of subcentimeter lung lesions between images reconstructed from standard-dose filtered backprojection, submillisievert filtered backprojection, and submillisievert iterative reconstruction, with equal confidence in reporting using the submillisievert iterative reconstruction technique. The scans were reported to be 0.25 mSv, or only one tenth the standard dose.

Although these computer algorithms may restore image quality for qualitative assessment, we are concerned about how ultra-low counts in submillisievert CT studies can affect the SUVs, if they are to be used for attenuation correction. The reproducibility of SUVs, a semiquantitative parameter widely used in clinical PET scans, is essential to assess the aggressiveness of disease and the response of disease to treatments in comparison studies. Since these algorithms are used during image reconstruction, the precision in SUVs is not expected to improve with the paucity of counts, unless quantitation software is modified. Souvatzoglou et al. (*14*) reported only a moderate correlation between the mean values in all segments using low-dose, ultra-low-dose, and slow CT for attenuation correction in 27 cardiac PET/CT scans, with no differences in scoring of qualitative assessment in the 3 groups. Xia et al. (*15*) investigated the feasibility of using ultra-low-dose CT for attenuation correction to reduce the additional radiation burden in respiratory motion compensation. We pursued basic measurements using a phantom over a wide range of CT attenuation scan settings in search of a minimal radiation dose threshold below which SUV determination may not be reliable.

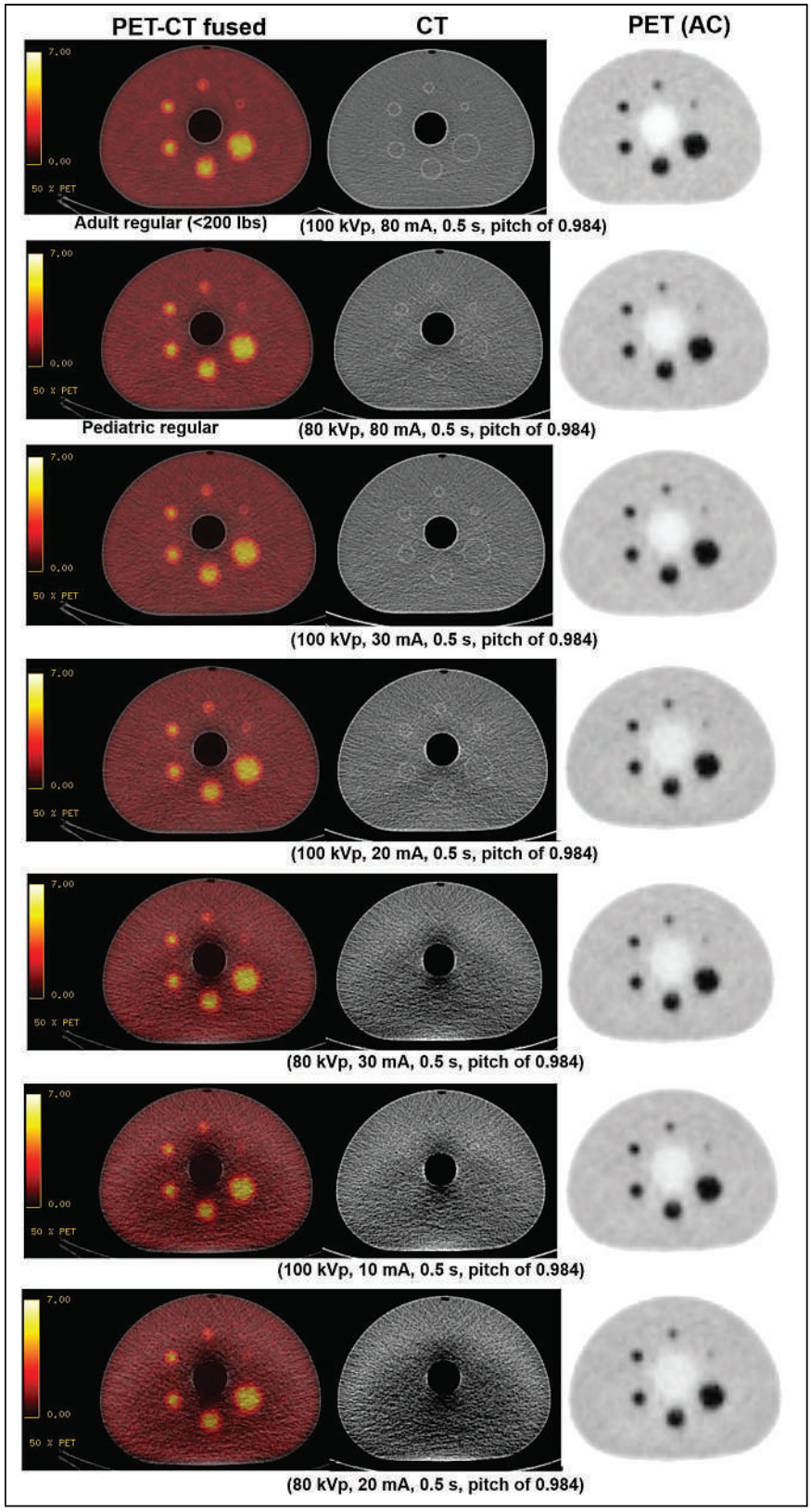

FIGURE 1. Representative images of PET (attenuation-corrected), CT, and PET/CT for phantom and spheres at various CT settings. CT settings of first and second rows are reference regular adult imaging protocol and pediatric imaging protocols, respectively, at Yale New Haven Hospital. In bottom 3 rows, delineation of spheres was not clear on CT images at lower radiation dose settings.

MATERIALS AND METHODS

A Discovery 690 (D-690) PET/CT scanner was used for the experiment (GE Healthcare). The D-690 is equipped with a lutetium-yttrium-orthosilicate detector and a 64-slice CT scanner, has a detection block of 54 (9 × 6) individual lutetium-yttrium-orthosilicate crystals (4.2 × 6.3 × 25 mm) coupled to a single squared photomultiplier tube with 4 anodes, and consists of 24 rings of detectors (total, 13,824 lutetium-yttrium-orthosilicate crystals) for an axial field of view of 157 mm. The transaxial field of view is 700 mm. The D-690 uses a low-energy threshold of 425 keV and a coincidence time window of 4.9 ns and operates in 3-dimensional mode only. The CT portion of the D-690 is a LightSpeed VCT with 912 channels × 64 rows, which allows full 360° rotation scans with variable time ranging from 0.35 to 2 s and reconstructed slice thicknesses of 0.625, 1.25, 2.5, 5, and 10 mm for the maximum fan-beam collimation of 40 mm.

We acquired PET/CT images using a National Electrical Manufacturers Association International Electrotechnical Commission phantom (Body Phantom Set; Data Spectrum Corp.) (Fig. 1), containing 6 hollow spheres (10, 13, 17, 22, 28, and 37 mm in diameter) filled with 60 kBq/mL in a background of 15 kBq/mL (a target-to-background ratio of 4:1) at the beginning and the end of a 2-h interval during the radioactive decay. PET images were acquired for 3 min at a single bed position in list mode using ordered-subset expectation maximization with 24 subsets and 2 iterations and a gaussian 2-mm filter using an Advantage Workstation (GE Healthcare) equipped with version 4.5 software. Multiple CT images were acquired for attenuation correction using different combinations of tube voltage (80, 100, and 120 kVp) and an effective tube current–time product mAs, at maximum beam collimation. The available settings to achieve the lowest effective dose were 10 mA, a 0.4-s rotation, and a pitch of 1.375. The CT images were reconstructed using conventional filtered backprojection. The adaptive statistical iterative reconstruction software for CT dose reduction was not available in our PET/CT scanner at the time of the study.

The radioactivity of the spheres with both SUV_{max} and average SUV (SUV_{ave}) was measured by applying sphere volumes of interest with a threshold of 41% of the maximal value in serial PET images using the Advantage Workstation. We coregistered CT images and adjusted the size of the volume of interest accordingly to make sure all volumes of interest were placed correctly. The SUV computation was derived from the radioactivity concentration (kBq/mL) divided by the total administered radioactivity within the phantom (kBq) and normalized to the total weight of the phantom. The variability of the SUV measurements in each sphere from the attenuation-corrected PET images using CT images with various combinations of tube current and voltage was calculated against the value in each sphere obtained using our standard clinical acquisition setting (100 kVp, 80 mA, 0.5-s rotation, and a helical pitch of 0.984) as the reference. A deviation in SUV (±10%) in comparison with the reference standard is considered acceptable in accordance with the test–retest variability of 20% for ^{18}F-FDG PET studies. Radiation dose estimation for CT scans was based on the CT dose index volume measured using the standard methodology (*16*) and the Imaging Performance Assessment of CT Scanners (ImPACT) CT patient dosimetry calculator, version 1.0.4 (*17*). The ImPACT CT dosimetry calculator is a computer software package that calculates organ and effective doses from CT examinations and makes use of the National Radiological Protection Board Monte Carlo published dose datasets (*18*). The Monte Carlo dose data provide normalized organ dose data for irradiation of a mathematic anthropomorphic phantom with a range of CT scanners, all of which are normalized to an isocenter air dose in the absence of any phantom. Since the particular output of the CT scanner in our PET/CT system is not included in the National Radiological Protection Board database, we selected from the database the model of our scanner (LightSpeed VCT) and manually input (the software provides this option) the measured CT dose index volumes for each individual CT attenuation scan to properly scale the normalized organ doses.

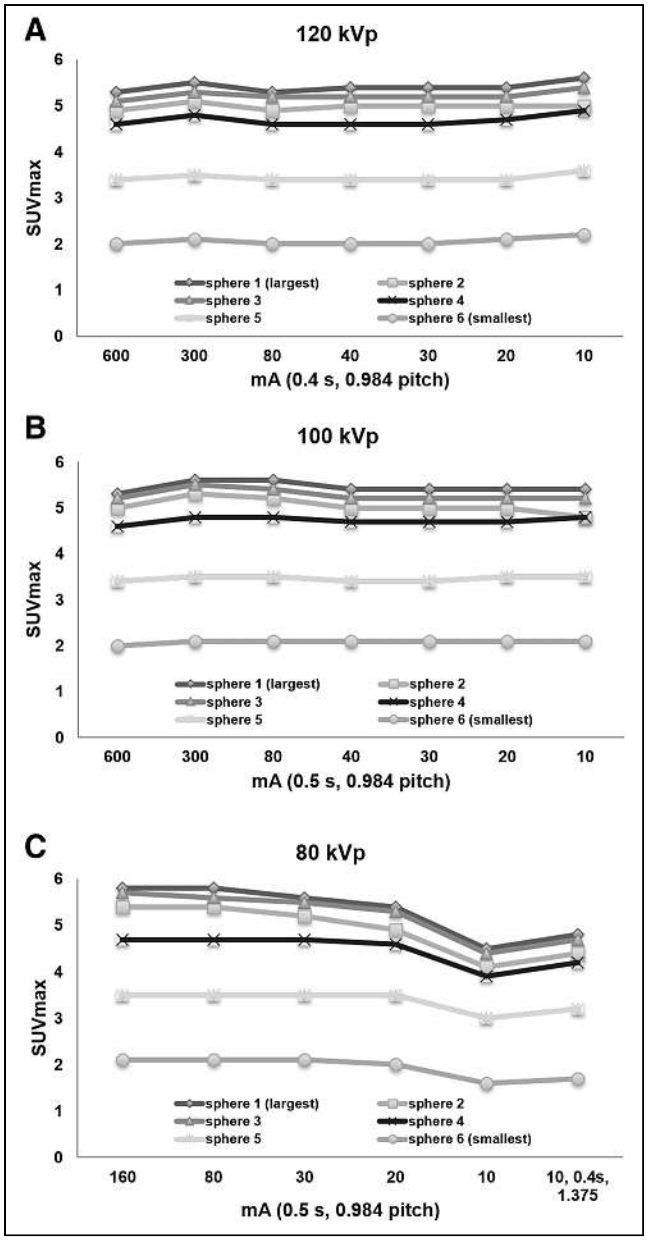

FIGURE 2. Impact on SUV_{max} from attenuation correction with various CT settings: 120 kVp (A), 100 kVp (B), and 80 kVp (C). Attenuation-corrected SUV_{max} measures are overall consistent for all spheres with CT settings of 120 kVp and 10–600 mA (A), 100 kVp and 10–600 mA (B), and 80 kVp and 30–160 mA (C). Attenuation-corrected SUV_{max} measures are slightly decreased (>10%) for some spheres with CT settings of 80 kVp and 10–20 mA (C).

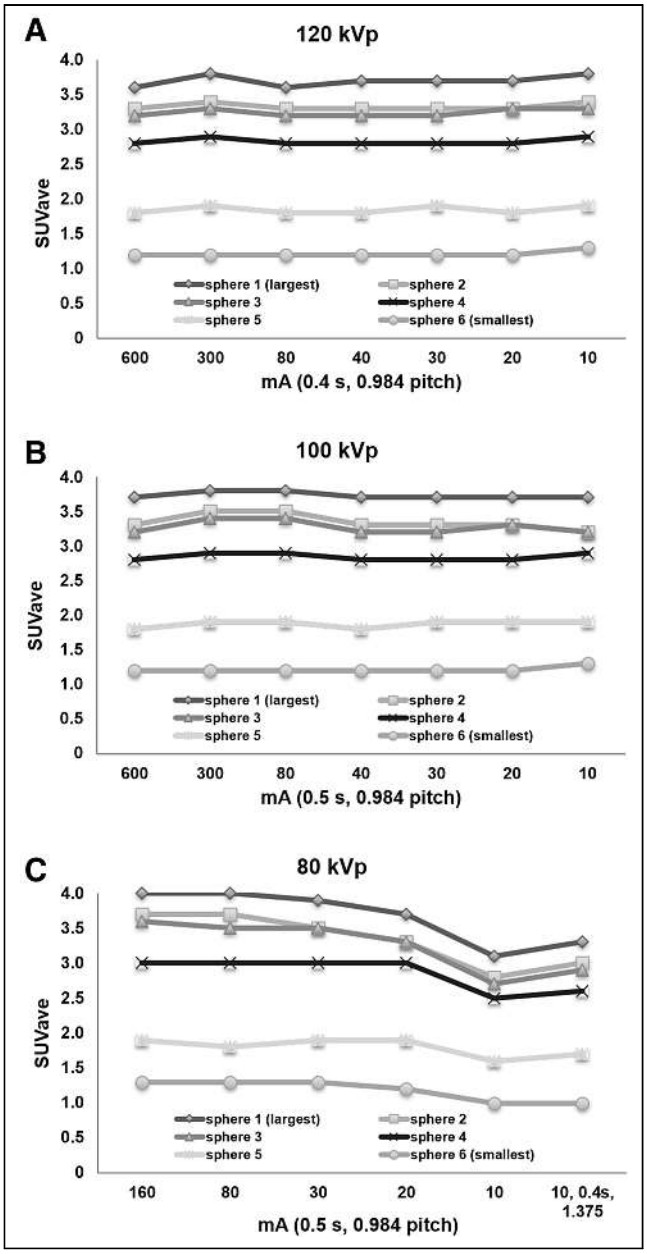

FIGURE 3. Impact on SUV_{ave} from attenuation correction with various CT settings: 120 kVp (A), 100 kVp (B), and 80 kVp (C). Attenuation-corrected SUV_{ave} measures are overall consistent for all spheres with CT settings of 120 kVp and 10–600 mA (A), 100 kVp and 10–600 mA (B), and 80 kVp and 30–160 mA (C). Attenuation-corrected SUV_{ave} measures are slightly decreased (>10%) for some spheres with CT settings of 80 kVp and 10–20 mA (C).

RESULTS

We first performed visual assessments for all PET and CT images of the phantom and spheres (Fig. 1). We were able to identify the spheres clearly, including the smallest at 10 mm, in all the attenuation-corrected PET images with various CT settings, even for the lowest-dose technique after 2 h of radioactive decay. The detectability of PET was not significantly impacted by the low-dose CT setting (Fig. 1) or the low radioactivity of ^{18}F-FDG. However, we could not clearly delineate the spheres in CT images at the lower doses (Fig. 1, bottom 3 rows).

TABLE 1
Estimated CT Doses (mGy) and Effective Doses (mSv) from Various Combinations of kVp and mA

kVp	mA	CT dose index volume (mGy)	mSv
120	600	19.61	32.4
120	300	10.18	16.2
120	80	2.63	4.3
120	40	1.32	2.2
120	30	0.99	1.6
120	20	0.66	1.1
120	10	0.33	0.5
100	600	15.25	20.6
100	300	7.68	10.3
100	80	2.06	2.7
100	40	1.03	1.4
100	30	0.77	1.0
100	20	0.55	0.7
100	10	0.26	0.3
80	160	1.73	2.7
80	80	0.87	1.4
80	30	0.43	0.5
80	20	0.22	0.3
80	10	0.11	0.2
80	10*	0.08	0.1

All 120-kVp CT scans use 0.4-s rotation time and pitch of 0.984. All 100- and 80-kVp CT scans use 0.5-s rotation time and pitch of 0.984, except for 0.4-s rotation time and pitch of 1.375, where noted by asterisk.

We also measured both SUV_{max} and SUV_{ave} within the spheres of the phantom from the attenuation-corrected PET images using the CT images with various combinations of kVp and mAs (Fig. 1). We found overall good consistency in SUV_{max} and SUV_{ave} measurements from attenuation-corrected PET images over a range of effective mAs (10–600 mA, 0.4- to 0.5-s rotation, and pitch of 0.984) at 120 kVp (Figs. 2A and 3A) and 100 kVp (Figs. 2B and 3B). We also found good consistency in SUV_{max} and SUV_{ave} (±10%) measurements over the range of 30–160 mA with a 0.5-s rotation and a pitch of 0.984 at 80 kVp, below which we found a notable reduction (>10%) in SUV_{max} and SUV_{ave} at 10–20 mA, 0.5 s, and a pitch of 0.984 and at 10 mA, 0.4 s, and a pitch of 1.375 at 80 kVp (last 3 sets of measurement points in Figs. 2C and 3C). We repeated the PET and CT acquisition of the phantom after 2 h of radioactive decay and found good reproducibility.

We concluded that the minimum required radiation dose for the helical CT attenuation scan (pitch, 0.984) for precise quantification in all spheres (±10%) was determined by the combination of 100 kVp, 10 mA, 0.5 s, and a pitch of 0.984, with a consequent 0.26-mGy measured CT dose index volume and 0.3-mSv estimated effective dose (Table 1).

DISCUSSION

Our phantom study explored lower limits within the submillisievert realm of ultra-low-dose CT used for attenuation correction required for reproducible semiquantification in ^{18}F-FDG PET imaging. We confirmed that the SUV measurements from the attenuation-corrected PET were consistent, even at very low dose settings of the CT. Therefore, we may confidently further reduce the current CT dose in routine clinical PET/CT studies without compromising the SUV measurements. One important clinical application is to reduce the CT dose in pediatric patients, as they are most susceptible to potential harm from unnecessary radiation exposure, although young adults and even all adults can benefit from a reduction in accumulated radiation dose.

The adequacy of CT-based attenuation correction for pediatric PET was evaluated previously using several phantoms (*19*). That study suggested that adequate attenuation correction can be obtained with very-low-dose CT (80 kVp, 5 mAs, pitch of 1.5:1) for pediatric patients and that such a correction can lead to a 100-fold dose reduction relative to diagnostic CT (*19*). Our current study also demonstrated the adequacy of CT-based attenuation correction with low-dose CT at a setting of 80 kVp, 15 mAs (30 mA with 0.5 s), and a pitch of 0.984, but we did notice more than a 10% reduction in SUV measurements at lower-dose CT settings and noticeable degradation of image quality impacting anatomic localization. The introduction of new iterative reconstruction algorithms in CT might allow a further reduction in the CT radiation dose settings while maintaining the image quality needed for anatomic localization. However, detailed quantitative image quality investigations using appropriate phantoms are needed to validate its feasibility. Weight-based, low-dose pediatric whole-body PET/CT protocols were proposed by the group at Seattle Children's Hospital (*20*). They used a weight-based adjusted ^{18}F-FDG dose for PET and weight-based categories for CT settings. The customized low-dose protocols could potentially reduce the radiation dose by 20%–50% from CT alone while maintaining diagnostic quality (*20*).

At the time this study was conducted, the standard CT settings for the D-690 at Yale New Haven Hospital were 80 mA, a 0.5-s rotation time, a pitch of 0.984, and 100 kVp for a standard adult with a body weight of 70 kg and 80 kVp for the pediatric protocol: 2.7 mSv and 1.4 mSv estimated effective doses, respectively. The CT images were reconstructed with conventional filtered backprojection, providing satisfactory imaging quality for anatomic localization.

On the basis of the results of this study, we could confidently reduce the radiation dose to the submillisievert level using an ultra-low-dose CT protocol for reliable attenuation correction and anatomic localization in clinical ^{18}F-FDG PET/CT studies.

In the current study, we focused only on the impact of PET SUV measures from ultra-low-dose CT. No image quality analysis was performed because this was beyond the purpose of the study. However, the impact of radiation dose reduction on image quality should be assessed if both reliable attenuation correction and accurate extraction of anatomic information are expected from the CT images of a PET/CT study. The new iterative reconstruction algorithms available for CT should be further investigated to improve the quality of ultra-low-dose CT images so as to provide acceptable anatomic information in PET/CT studies.

CONCLUSION

Our phantom study provided guidance in using ultra-low-dose CT for precise attenuation correction and semiquantification of ^{18}F-FDG PET imaging, which can further reduce the CT dose and radiation exposure to patients in clinical PET/CT studies. On the basis of the data, we can further reduce the radiation dose to the submillisievert level using an ultra-low-dose CT protocol for reliable attenuation correction in clinical ^{18}F-FDG PET/CT studies.

DISCLOSURE

No potential conflict of interest relevant to this article was reported.

KEY POINTS

QUESTION: What is the minimal required submillisievert-level dose for ultra-low-dose CT and the corresponding tube current and voltage for reliable attenuation correction and semiquantitation in ^{18}F-FDG PET/CT in an effort to reduce radiation dose?

PERTINENT FINDINGS: The minimal ultra-low-dose CT dose level for reproducible quantification in all spheres (<10% relative difference) was determined to be 0.3 mSv for a combination of 100 kVp and 10 mA at a 0.5-s rotation and a helical pitch of 0.984 (0.26 mGy measured CT dose index volume). Our phantom study provided guidance in using ultra-low-dose CT for precise attenuation correction and semiquantification of ^{18}F-FDG PET imaging.

IMPLICATIONS FOR PATIENT CARE: On the basis of the data, we can further reduce the radiation dose to the submillisievert level using an ultra-low-dose CT protocol for reliable attenuation correction in clinical ^{18}F-FDG PET/CT studies.

REFERENCES

1. Pearce MS, Salotti JA, Little MP, et al. Radiation exposure from CT scans in childhood and subsequent risk of leukaemia and brain tumours: a retrospective cohort study. *Lancet.* 2012;380:499–505.
2. Mathews JD, Forsythe AV, Brady Z, et al. Cancer risk in 680,000 people exposed to computed tomography scans in childhood or adolescence: data linkage study of 11 million Australians. *BMJ.* 2013;346:f2360.
3. Chen MK, Menard DH III, Cheng DW. Determining the minimal required radioactivity of ^{18}F-FDG for reliable semiquantification in PET/CT imaging: a phantom study. *J Nucl Med Technol.* 2016;44:26–30.
4. Heilbron BG, Leipsic J. Submillisievert coronary computed tomography angiography using adaptive statistical iterative reconstruction: a new reality. *Can J Cardiol.* 2010;26:35–36.
5. Behnes M, Haubenreisser H, Huseynov A, et al. Submillisievert ECG-gated whole thoracic CT-angiography for evaluation of a complex congenital heart defect in a young woman. *Int J Cardiol.* 2014;176:e54–e55.

6. Chen MY, Shanbhag SM, Arai AE. Submillisievert median radiation dose for coronary angiography with a second-generation 320-detector row CT scanner in 107 consecutive patients. *Radiology.* 2013;267:76–85.
7. Stehli J, Fuchs TA, Bull S, et al. Accuracy of coronary CT angiography using a submillisievert fraction of radiation exposure: comparison with invasive coronary angiography. *J Am Coll Cardiol.* 2014;64:772–780.
8. Khawaja RD, Singh S, Gilman M, et al. Computed tomography (CT) of the chest at less than 1 mSv: an ongoing prospective clinical trial of chest CT at submillisievert radiation doses with iterative model image reconstruction and iDose4 technique. *J Comput Assist Tomogr.* 2014;38:613–619.
9. Pontana F, Henry S, Duhamel A, et al. Impact of iterative reconstruction on the diagnosis of acute pulmonary embolism (PE) on reduced-dose chest CT angiograms. *Eur Radiol.* 2015;25:1182–1189.
10. Glazer DI, Maturen KE, Cohan RH, et al. Assessment of 1 mSv urinary tract stone CT with model-based iterative reconstruction. *AJR.* 2014;203:1230–1235.
11. Lambert L, Ourednicek P, Jahoda J, Lambertova A, Danes J. Model-based vs hybrid iterative reconstruction technique in ultralow-dose submillisievert CT colonography. *Br J Radiol.* 2015;88:20140667.
12. Gryspeerdt SS, Salazar P, Lefere P. Image quality improvement in submillisievert computed tomographic colonography using a fast 3-dimensional noise reduction method. *J Comput Assist Tomogr.* 2014;38:705–713.
13. Khawaja RD, Singh S, Lira D, et al. Role of compressive sensing technique in dose reduction for chest computed tomography: a prospective blinded clinical study. *J Comput Assist Tomogr.* 2014;38:760–767.
14. Souvatzoglou M, Bengel F, Busch R, et al. Attenuation correction in cardiac PET/CT with three different CT protocols: a comparison with conventional PET. *Eur J Nucl Med Mol Imaging.* 2007;34:1991–2000.
15. Xia T, Alessio AM, De Man B, Manjeshwar R, Asma E, Kinahan PE. Ultra-low dose CT attenuation correction for PET/CT. *Phys Med Biol.* 2012;57:309–328.
16. American Association of Physicists in Medicine Task Group Report 204: Size-Specific Dose Estimates (SSDE) in Pediatric and Adult Body CT Examinations. American Association of Physicists in Medicine; 2011.
17. ImPACT's ct dosimetry tool: CTDosimetry version 1.0.4. impactscan.org website. http://www.impactscan.org/ctdosimetry.htm. Accessed January 24, 2022.
18. Jones DG, Shrimpton PC. *Survey of CT Practice in the UK: Part 3.* National Radiological Protection Board; 1991.
19. Fahey FH, Palmer MR, Strauss KJ, Zimmerman RE, Badawi RD, Treves ST. Dosimetry and adequacy of CT-based attenuation correction for pediatric PET: phantom study. *Radiology.* 2007;243:96–104.
20. Alessio AM, Kinahan PE, Manchanda V, Ghioni V, Aldape L, Parisi MT. Weight-based, low-dose pediatric whole-body PET/CT protocols. *J Nucl Med.* 2009;50:1570–1577.

Comparing the Patient Experience Between a 360° γ-Camera and a Conventional Dual-Head γ-Camera

Hend Komber, David Little, Sarah Cade, Richard Graham, and Stewart Redman

Department of Radiology, Royal United Hospitals NHS Trust, Bath, United Kingdom

Our aim was to explore whether the 360° γ-camera design of the Veriton-CT scanner adversely affects the rate of scan noncompletion due to claustrophobia or other patient experience factors, when compared with a standard dual-head Discovery NM/CT 670 γ-camera. **Methods:** This was a single-center prospective study of all nuclear medicine studies on either of the 2 γ-cameras. It was recorded whether the patient completed the scan as protocoled or, because of claustrophobia, had a shortened scan or no scan. The patients were also offered a patient experience questionnaire, with domains of comfort, scan time, scan noise, and claustrophobia assessed using a 5-point Likert scale. **Results:** Over a 4-mo period, 296 patients were scanned on the Discovery and 274 patients on the Veriton-CT. There was a scan noncompletion rate, due to claustrophobia, of 1.35% for the Discovery and 1.46% for the Veriton-CT. Of the 570 patients involved, 354 (62%) returned their questionnaires. There was no statistical difference between the responses for comfort, scan time, scan noise, or feelings of claustrophobia. **Conclusion:** The study provides evidence that the 360° γ-camera design of the Veriton-CT does not lead to a significantly increased scan failure rate due to claustrophobia and that there is no change in the subjective experience for patients.

Key Words: claustrophobia; Discovery 670; γ-camera; patient experience; Veriton-CT

J Nucl Med Technol 2022; 50:132–136
DOI: 10.2967/jnmt.121.262627

SPECT imaging and hybrid SPECT/CT imaging have undergone multiple developments since the first commercial SPECT/CT scanner became available over 20 years ago (*1*). Identifying the clinical indication of optimized localization and quantification of tracer uptake was essential to the increasing clinical utility (*1*). Moreover, the continued advances in detectors and the emergence of digital cadmium-zinc-telluride cameras have allowed for improved extrinsic resolution (*2*), increased count sensitivity, and reduced scan times (*3*). These advantages allow for superior image quality and presentation using maximum-intensity projections but should be balanced against a patient's ability to tolerate the scan. Although there are limited published data on whether patients experience claustrophobia during γ-camera examinations, claustrophobia is a shared theme with other high-technology medical imaging modalities such as MRI, for which potential negative experiences of discomfort and claustrophobia need to be considered (*4–9*). One study showed that 10% of children undergoing 3-T MRI report feelings of claustrophobia (*4*), and in another study, up to 40% of adults undergoing MRI experience feelings of unpleasantness due to a "confined space" (*8*). A focus on improving patients' experience and using a patient-centered approach is paramount in the development and planning of radiology services (*10*).

In November 2020, a new SPECT/CT scanner with cadmium-zinc-telluride detectors (Veriton-CT; Spectrum Dynamics Medical) was installed in our local nuclear imaging department as a replacement for one of the older cameras. Unlike conventional dual-head Anger cameras, the Veriton-CT comprises a novel setup design, with 12 detectors in a 360° configuration that can be moved closer to the patient during image acquisition. During the scanner procurement process, we wanted to ensure that patients would tolerate this novel design. Acquiring the new scanner presented an opportunity for reflection and exploration of the patient experience of nuclear imaging within the department. The aim of this study was to assess claustrophobia in our patients by comparing the local scan-noncompletion rate, due to claustrophobia, between the new Veriton-CT and a conventional dual-head Discovery NM/CT 670 (GE Healthcare) γ-camera. Secondarily, we wanted to prospectively survey our patients about their subjective perception of several experience factors, including claustrophobia. Together, these investigations could provide both objective and subjective measures of scanner tolerability.

MATERIALS AND METHODS

The institutional review board approved this study, and the requirement to obtain informed consent was waived. This study was registered with the local clinical audit department. The patient experience team of the local hospital was involved from the start of the project and was invited to the nuclear imaging department, where they were able to view the available scanners and patient flow areas. Neither of the 2 scanner manufacturers was involved in the study design or manuscript review. On request, Spectrum Dynamics Medical supplied an image highlighting the different scanner designs.

Scanners and Patients

All patients presenting for nuclear imaging scans between October 28, 2020, and March 12, 2021, were included for analysis.

Received May 25, 2021; revision accepted Sep. 25, 2021.
For correspondence or reprints, contact Stewart Redman (stewart.redman@nhs.net).
Published online Nov. 8, 2021.

Studies were performed on either of the 2 department scanners. The Discovery was installed in November 2012, and the Veriton-CT was installed in November 2020. The characteristics of each scanner are shown in Table 1, and a graphical representation of the difference between a conventional γ-camera and the Veriton-CT is shown in Figure 1. Patient positioning is similar between the 2 scanners. Of note, Veriton-CT protocols are generally shorter than corresponding protocols on the Discovery. For example, an oncology whole-body bone scan takes approximately 18 min on the Veriton-CT (*3*), whereas a bone scan and single-site SPECT take 40 min on the Discovery.

After consideration of the volumes and types of scans going through the department and the process of protocol development, initially it was decided that the Veriton-CT would be used for bone, parathyroid, and lung imaging, with a plan to gradually introduce other indications. During the study period, bone, parathyroid, and lung scans were protocoled for either of the 2 scanners, and the local radiology bookings team allocated the patients on the basis of efficient use of scanning slots. When patients expressed anxiety about the Veriton-CT, they were given the option of undergoing their scan on the Discovery instead.

Questionnaire Development

A review of current literature regarding the patient experience of medical imaging revealed similar studies of patient experience and tolerability of MRI and nuclear imaging (*4*–*8*). Informed by one of these studies (*4*), a cross-sectional patient experience questionnaire was drafted, which contained 4 measures of scan experience (comfort, scan time, scan noise, and claustrophobia). The draft was reviewed by the hospital patient experience team. The final questions are shown in Figure 2. During the prospective data-collection phase, demographic data for all patients undergoing nuclear imaging were recorded in a spreadsheet along with information about whether they completed their scan as protocoled. After the scan, patients were offered a paper questionnaire to fill out before leaving the department. The reception staff then collected the questionnaire from the patient and recorded the responses in the spreadsheet.

Quality Checking and Statistical Analysis

The prospectively collected data were cross-referenced against a retrospectively generated patient list from the radiology information system, to ensure no patients were missed. Whether scans were completed as protocoled was assessed. Variations in the survey responses were assessed using the χ^2 test. Differences in scan noncompletion numbers between the Discovery and the Veriton-CT were assessed using the Mann–Whitney *U* test. Two-tailed tests were used, and a *P* value of less than 0.05 was considered statistically significant. All statistical analysis was performed on GraphPad Prism, version 9, for the Mac operating system (Apple).

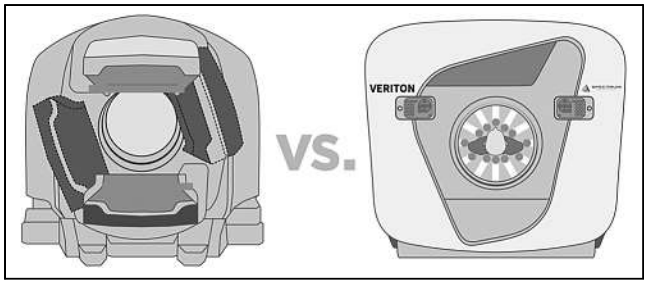

FIGURE 1. Conventional Anger camera (left) vs. Veriton-CT scanner (right), with 360° detector design. (Courtesy of Spectrum Dynamics Medical.)

RESULTS

Study Group

Between October 28, 2020, and March 12, 2021, 296 patients were scanned on the Discovery and 274 were scanned on the Veriton-CT. There was a 62% (354/570) overall questionnaire-response rate. The spread of nuclear imaging scan indications across the 2 scanners is shown in Table 2.

Rate of Scan Noncompletion as Protocoled

All patients presenting for nuclear imaging had some form of imaging during their visit. Overall, 6 of 570 (1.05%) patients failed to complete their scan as initially protocoled, because of claustrophobia (Table 3). Four of these patients were booked on the Veriton-CT; of these, one was able to have a partial scan on the Veriton-CT (patient 1), 2 were able to have a partial scan on the Discovery (patients 2 and 3), and one was able to have a complete scan on the Discovery (patient 4). Two further patients were initially booked on the Discovery (patients 5 and 6) and were able to have only partial scans because of claustrophobia. This gives a composite rate of scan noncompletion as protocoled of 4 of 274 (1.46%) for the Veriton-CT and 4 of 296 (1.35%) for the Discovery ($P = 0.33$, Mann–Whitney *U* test), because of claustrophobia.

Survey Responses

The modal responses in the different experience parameters for each of the scanners was as follows: comfort was "yes very," long scan time was "no not really," loud scan noise was "no not at all," and claustrophobia was "no not at all." There was no statistical significance in the spread of

TABLE 1
Characteristics of Nuclear Imaging Scanners in Our Department

Characteristic	Discovery	Veriton-CT
γ-camera	Anger camera	Digital camera
Detector	Sodium iodide scintillator	12 cadmium-zinc-telluride detectors
Configuration	Dual-head around imaging table	Circular pattern around imaging table
Bore size	70 cm	80 cm
CT	16 slices	16 slices

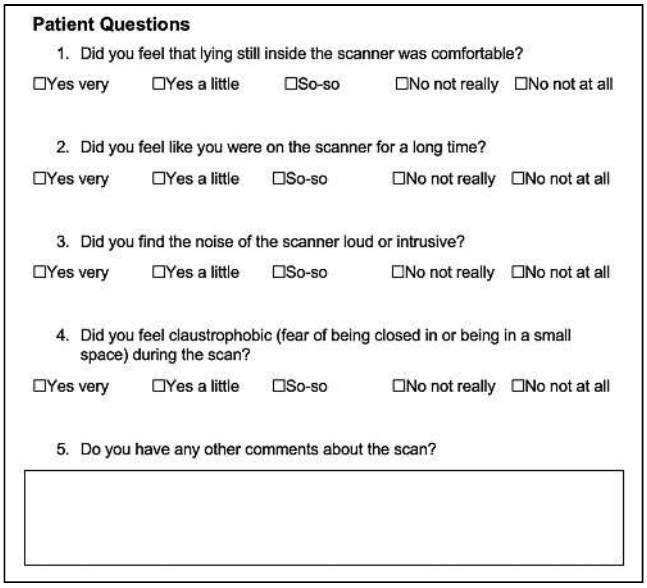
Patient Questions

1. Did you feel that lying still inside the scanner was comfortable?

☐Yes very ☐Yes a little ☐So-so ☐No not really ☐No not at all

2. Did you feel like you were on the scanner for a long time?

☐Yes very ☐Yes a little ☐So-so ☐No not really ☐No not at all

3. Did you find the noise of the scanner loud or intrusive?

☐Yes very ☐Yes a little ☐So-so ☐No not really ☐No not at all

4. Did you feel claustrophobic (fear of being closed in or being in a small space) during the scan?

☐Yes very ☐Yes a little ☐So-so ☐No not really ☐No not at all

5. Do you have any other comments about the scan?

FIGURE 2. Questionnaire on experience of nuclear imaging patient.

the 5-point scale responses across the 2 scanners, when compared using the χ^2 test: comfort ($P = 0.84$), long scan time ($P = 0.39$), loud scan noise ($P = 0.46$), and claustrophobia ($P = 0.44$). In particular, the overall subjective reporting of claustrophobia (patients who answered, "yes very" and "yes a little") was 15 of 138 (10.9%) for the Discovery and 25 of 216 (11.6%) for the Veriton-CT ($P = 0.87$). A graphical representation of the spread of responses from all surveyed patients, comparing the Veriton-CT and the Discovery, is shown in Figure 3.

DISCUSSION

It is recognized that high-technology imaging presents a potential source of patient anxiety, which can limit adequate scan completion (*4–9*). We sought to assess the claustrophobia rate in 2 ways. First, we recorded the rate of scan noncompletion due to claustrophobia and found that few patients were unable to complete their scan fully on the Veriton-CT or Discovery (1.46% and 1.35%, respectively). All patients were able to complete at least part of their scan, which is the most important outcome. Second, a survey of subjective perception of several experience factors was conducted. The modal responses support the finding that overall patient experience is positive across the 2 scanners. Moreover, there was no statistical significance across the responses from the 2 scanners. This shows that the 360° configuration of the Veriton-CT does not significantly affect the subjective patient experience.

There is strong heterogeneity in patient groups for bone imaging, as there was no dynamic bone imaging protocol established for the Veriton-CT. Hence, bone scans for indications

TABLE 2
Spread of Nuclear Imaging Scan Indications Across Discovery and Veriton-CT over 4-Month Period

Indication	Discovery	Veriton-CT
Bone	98	192
Parathyroid	4	27
Lung	16	47
Thyroid	11	0
Renal dimercaptosuccinic acid	17	0
Renogram mercaptoacetyltriglycine	19	0
Cardiac	40	0
Brain ^{123}I-ioflupane scan	31	2
Sentinel node localization and imaging	3	5
Radionuclide selenium homocholic acid taurine bile study	42	0
Gastric emptying study (single)	10	0
Other	5	1
Total	296	274

TABLE 3
Patient Characteristics of Noncompleted Scans Due to Claustrophobia

Patient no.	Indication	Comments regarding claustrophobia
1	Bone	Booked on Veriton-CT but managed only CT, not SPECT
2	Bone	Booked on Veriton-CT but partial scan on Discovery
3	Bone	Booked on Veriton-CT but partial scan (no CT) on Discovery
4	Parathyroid	Booked on Veriton-CT but complete scan on Discovery
5	Bone	Booked on Discovery; head and body done separately
6	Bone	Booked on Discovery but managed only SPECT, not CT

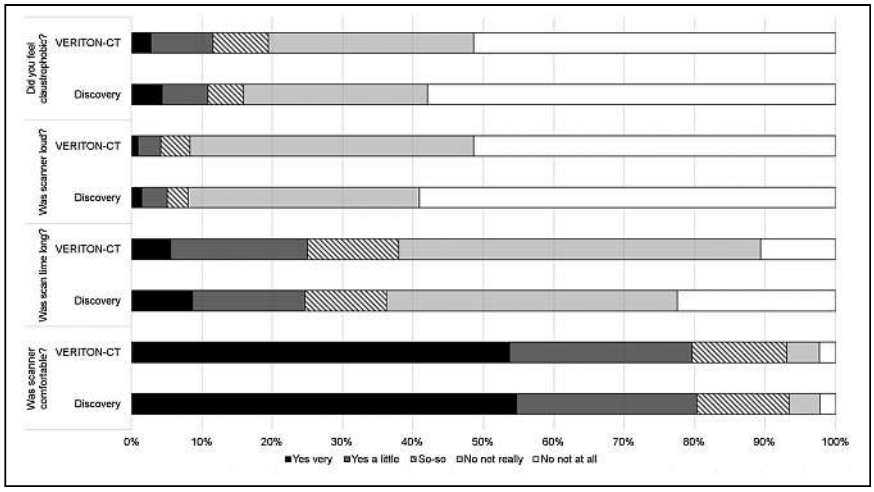

FIGURE 3. Spread of survey responses across 4 experience factors.

such as postarthroplasty imaging, which involved a 3-phase acquisition, were protocoled for the Discovery. This makes subgroup analysis difficult.

Comfort is essential for nuclear imaging as scan times vary greatly but can be up to 1 h long, and it is important for the patient to be able to lie relatively still. The patient tables for the 2 scanners are similar to each other, and it is understandable that there was no difference in perceived comfort. Although this question is likely to be answered mainly from a physical perspective, it seems probable that if patients were feeling psychologic discomfort from claustrophobia, this psychologic discomfort might also have affected the responses to this question. Many of the Veriton-CT scan protocols are shorter than corresponding protocols on the Discovery. For example, an oncology whole-body bone scan takes approximately 18 min on the Veriton-CT (*3*), whereas a bone scan and single-site SPECT take 40 min on the Discovery. However, there is no observed subjective difference in the patient appreciation of scan time. The results from this study give an overview of patient perceptions of scan time, but a separate study including actual time spent on the scanner would be required to draw further conclusions.

The subjective experience of scanner noise also did not reveal any statistical difference between the 2 scanners. Of note, the measured sound level during CT scanning in the Discovery was 74 dB, and that in the Veriton-CT was 72 dB.

For a minority of patients, claustrophobia is a deterring factor in medical imaging (*4–9*). The subjective experience of claustrophobia was relatively low: 10.9% for the Discovery and 11.6% for the Veriton-CT. The nuclear imaging technologists are experts in strategies to reassure patients and guide them comfortably through the scan as much as possible. With this expertise, all patients attending the department were able to complete at least part of their scan. Three patients declined to be scanned at all on the Veriton-CT, whereas all the patients completed at least part of their scan on the Discovery.

There is a potential for subconscious bias among the technologists, who are more familiar with the double-head camera setup of the Discovery. From an ethical standpoint in a 2-scanner department, it is understandable that patients who showed anxiety about the Veriton-CT were given the option to attempt their scan on the Discovery instead. Conversely, patients who were booked for the Discovery were encouraged to complete as much of the scan as they could but were not offered the Veriton-CT scanner as an alternative, because the technologists have years of experience in getting patients through their scans on the Discovery. It is therefore not possible from our study design to say what the rate of scan noncompletion would be for the Veriton-CT if it were the only scanner available. It is possible that some, if not all, of the patients (patients 2–4) would have partially completed their scans on the Veriton-CT.

We have not sought to assess what an individual patient's experience of both scanners would be as a head-to-head comparison, as this would involve scanning the patient twice and potentially on different days. Such an assessment would be both impractical and unethical. However, we believe the relatively large numbers in our study allow us to draw reasonable conclusions without the need to scan patients on both scanners. Going forward, we aim to establish a protocol for brain ^{123}I-ioflupane scans (DaTscans; GE Healthcare) on the Veriton-CT. This type of scanning brings the detector heads very close to the patient's face, and it will be interesting to see whether there is a difference in the rate of scan noncompletion due to claustrophobia or the subjective perception of claustrophobia in this cohort of patients.

CONCLUSION

The 360° SPECT/CT scanner configuration brings the 12 detectors close to the patient, allowing the potential for improved image quality and resolution but raising a question as to whether this proximity can be tolerated by patients. This observational cohort study provides evidence that this scanner configuration does not significantly affect the rate of scan noncompletion due to claustrophobia or the subjective perception of claustrophobia, when compared with the conventional double-head scanner. This finding should reassure nuclear medicine departments regarding this novel design.

DISCLOSURE

No potential conflict of interest relevant to this article was reported.

ACKNOWLEDGMENTS

We thank the nuclear medicine technologists for collecting the data and supporting patients during the study and throughout their careers.

KEY POINTS

QUESTION: Does the novel γ-camera design of the Veriton-CT adversely affect the rate of scan noncompletion due to claustrophobia, when compared with a standard dual-head γ-camera?

PERTINENT FINDINGS: This observational cohort study shows that the 360° SPECT/CT scanner configuration does not significantly affect the rate of scan noncompletion due to claustrophobia (1.46% compared with 1.35% with the conventional γ-camera) or the subjective perception of claustrophobia (10.9% compared with 11.6% with the conventional γ-camera).

IMPLICATIONS FOR PATIENT CARE: The 360° SPECT/CT scanner configuration of the Veriton-CT has the potential to improve image quality and resolution without having a negative impact on the patient experience. This finding should reassure nuclear medicine departments that are considering this novel design.

REFERENCES

1. Van den Wyngaert T, Elvas F, De Schepper S, Kennedy JA, Israel O. SPECT/CT: standing on the shoulders of giants, it is time to reach for the sky! *J Nucl Med.* 2020;61:1284–1291.
2. Liu CJ, Cheng JS, Chen YC, Huang YH, Yen RF. A performance comparison of novel cadmium-zinc-telluride camera and conventional SPECT/CT using anthropomorphic torso phantom and water bags to simulate soft tissue and breast attenuation. *Ann Nucl Med.* 2015;29:342–350.
3. Imbert L, Chevalier E, Claudin M, et al. A one-shot whole-body bone SPECT may be recorded in less than 20 minutes with the high-sensitivity Veriton® CZT-camera [abstract]. *J Nucl Med.* 2019;60(suppl 1):1288.
4. Chou IJ, Tench CR, Gowland P, et al. Subjective discomfort in children receiving 3 T MRI and experienced adults' perspective on children's tolerability of 7 T: a cross-sectional questionnaire survey. *BMJ Open.* 2014;4:e006094.
5. Dyrberg E, Larsen EL, Hendel HW, Thomsen HS. Diagnostic bone imaging in patients with prostate cancer: patient experience and acceptance of NaF-PET/CT, choline-PET/CT, whole-body MRI, and bone SPECT/CT. *Acta Radiol.* 2018;59:1119–1125.
6. Grilo AM, Vieira L, Carolino E, et al. Cancer patient experience in a nuclear medicine department: comparison between bone scintigraphy and ^{18}F-FDG PET/CT. *J Nucl Med Technol.* 2020;48:254–262.
7. Shortman RI, Neriman D, Hoath J, et al. A comparison of the psychological burden of PET/MRI and PET/CT scans and association to initial state anxiety and previous imaging experiences. *Br J Radiol.* 2015;88:20150121.
8. Thorp D, Owens RG, Whitehouse G, Dewey ME. Subjective experiences of magnetic resonance imaging. *Clin Radiol.* 1990;41:276–278.
9. Munn Z, Jordan Z. The patient experience of high technology medical imaging: a systematic review of the qualitative evidence. *JBI Libr Syst Rev.* 2011;9:631–678.
10. Radiology: GIRFT programme national specialty report. Getting It Right First Time website. www.gettingitrightfirsttime.co.uk/wp-content/uploads/2020/11/GIRFT-radiology-report.pdf. Published November 2020. Accessed January 25, 2022.

Amino Acid PET Imaging with ^{18}F-DOPA in the Evaluation of Pediatric Brain Tumors

Mehdi Djekidel[1], Rahaf AlSadi[2], Othmane Bouhali[2,3], and Ata Ur Rehman Maaz[4]

[1]Division of Nuclear Medicine and Molecular Imaging, Department of Diagnostic Imaging, Sidra Medicine, Doha, Qatar; [2]Department of Science, Texas A&M University at Qatar, Doha, Qatar; [3]Qatar Computing Research Institute, Hamad Bin Khalifa University, Doha, Qatar; and [4]Division of Hematology and Oncology, Department of Pediatrics, Sidra Medicine, Doha, Qatar

Although MRI is the workhorse of initial evaluation and follow-up in brain tumors, there are growing data recommending incorporation of amino acid PET imaging at different stages in the management of these patients. Recent recommendations on nuclear medicine and neurooncology clinical practice support the use of amino acid imaging for brain tumors. **Methods:** We present 4 pediatric brain tumor cases imaged with 3,4-dihydroxy-6-^{18}F-fluoro-L-phenylalanine (^{18}F-DOPA), and we review the literature. **Results:** ^{18}F-DOPA showed low level/no uptake in benign conditions and in inflammatory postoperative changes. It showed better definition of viable tumor boundaries than MRI. **Conclusion:** Considering that ^{18}F-DOPA is Food and Drug Administration–approved for the evaluation of parkinsonian syndromes, this tracer could be used clinically for other valuable clinical indications, such as brain tumor evaluations. The value of this use seems to be well established in adults, and evidence of its value in pediatrics has been growing as well.

Key Words: brain tumors; amino acid imaging; PET; nuclear medicine

J Nucl Med Technol 2022; 50:137–142
DOI: 10.2967/jnmt.121.263050

PET has been used in the assessment of brain tumors for 40 y. State-of-the-art MRI has become the gold standard in brain tumor imaging during the various steps of clinical management. ^{18}F-FDG was initially used with some success but faced limitations due to the high background uptake from normal metabolism of glucose by the brain. Amino acid PET has proven superior to ^{18}F-FDG PET and adds incremental value to MRI in imaging of brain tumors. ^{11}C-methyl-L-ethionine (^{11}C-MET), *O*-(2-^{18}F-fluoroethyl)-L-tyrosine (^{18}F-FET), and 3,4-dihydroxy-6-^{18}F-fluoro-L-phenylalanine (^{18}F-DOPA) have shown great clinical value. Considering that ^{18}F-DOPA is Food and Drug Administration–approved for the evaluation of Parkinsonian syndromes, it can be used clinically for other valuable clinical indications as well. ^{18}F-fluciclovine (Axumin; Blue Earth Diagnostics) is also Food and Drug Administration–approved for prostate cancer imaging and is being investigated for brain tumor imaging in adults. Bearing in mind that radiation exposure (albeit minimal) is a matter of concern in pediatrics, amino acid imaging can judiciously be used in the highest-yield case scenarios.

Received Aug. 13, 2021; revision accepted Dec. 28, 2021.
For correspondence or reprints, contact Mehdi Djekidel (mehdjeki@gmail.com).
Published online Apr. 19, 2022.

MATERIALS AND METHODS

We highlight 4 cases of pediatric brain tumor in which ^{18}F-DOPA imaging was used. We discuss its main value, and we review use of amino acid PET imaging in the pediatric population. Scans were acquired on a 3-T MRI scanner and a GE Healthcare Discovery 690 PET/CT scanner at Sidra Medicine. The radiopharmaceutical activities ranged from 99.9 to 118.4 MBq (2.7–3.2 mCi).

RESULTS

Case 1

A 7-y-old boy was referred to our hospital because of visual hallucinations, abdominal pain, headache, and seizures. He was diagnosed with temporal lobe epilepsy and had a further workup including CT and MRI scans of his brain. A well-defined calcified lesion was identified in the right temporal lobe, and surgical excision was recommended. His parents were hesitant to consent to surgery. Amino acid PET imaging using ^{18}F-DOPA was performed to gain additional prognostic information. The lack of ^{18}F-DOPA uptake by the lesion (Fig. 1) was indicative of a more benign or a lower-grade process, and the parents elected for watchful waiting. A few months later, the parents agreed to surgical excision of the lesion, and a right temporal lobe lesionectomy was performed. Histopathologic examination of this lesion revealed meningioangiomatosis, which is a rare, benign disease of the brain. Lack of ^{18}F-DOPA uptake predicted a benign nature for the lesion and provided additional confidence in the management and reassurance to the family.

Case 2

A 3-y-old boy was evaluated for gait issues and lower-extremity weakness. He was then diagnosed with diffuse intrinsic pontine glioma. He received standard focal conformal radiotherapy, with a total dose of 54 Gy. Eight months after finishing treatment, he presented with mild left-sided weakness and limp. He was reevaluated with an MRI scan, which showed that his tumor was overall smaller than on the scan at diagnosis. However, there were areas of signal change, which created concern about disease progression.

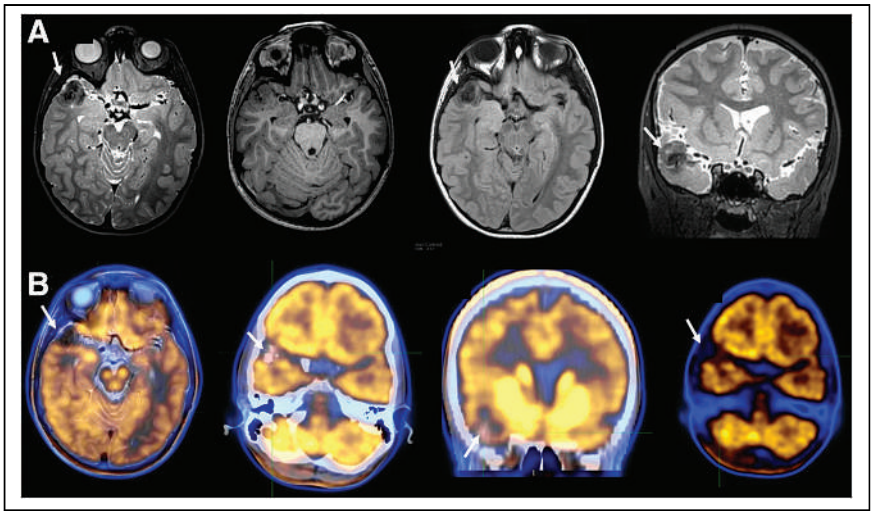

FIGURE 1. No ^{18}F-DOPA uptake in calcified benign right temporal lesion (meningioangiomatosis) (arrows). (A) From left to right: axial T2-weighted, axial T1-weighted, axial fluid-attenuated inversion recovery, and coronal T2-weighted MR images. (B) From left to right: axial ^{18}F-DOPA PET/MR, axial ^{18}F-DOPA PET/CT, coronal ^{18}F-DOPA PET/CT, and axial ^{18}F-DOPA PET images.

An ^{18}F-DOPA scan demonstrated uptake in the area showing contrast enhancement on the MRI scan. The ^{18}F-DOPA scan was also able to delineate the tumor margins with higher accuracy than the MRI scan and provided an additional negative prognostic indicator with regard to the intensity of ^{18}F-DOPA uptake (Fig. 2).

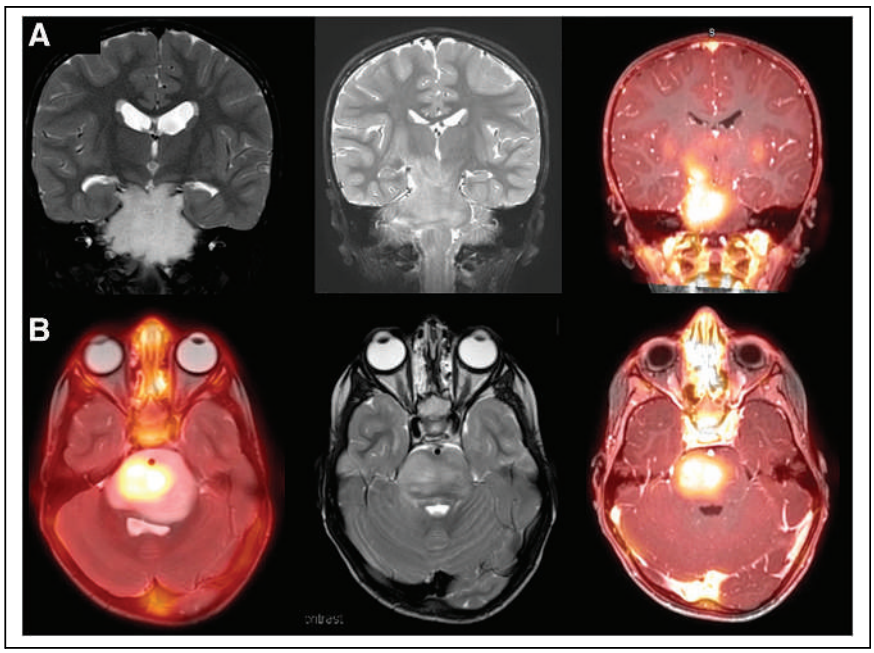

FIGURE 2. Intense ^{18}F-DOPA uptake in recurrent diffuse intrinsic pontine glioma showing better tumor delineation of true tumor boundaries than on the MRI alone and showing that intensity of uptake is likely a prognostic parameter. (A) From left to right: coronal T2-weighted fat-saturated initial, coronal T2-weighted fat-saturated 9-mo follow-up, and coronal ^{18}F-DOPA 9-mo follow-up PET/MR images. (B) From left to right: axial ^{18}F-DOPA PET fused to initial MR, axial T2-weighted fat-saturated 9-mo follow-up MR, and axial ^{18}F-DOPA 9-mo follow-up PET/MR images.

Case 3

A 6-y-old boy presented with an approximately 2-mo history of an abnormally wide gait and leg weakness. He then had increased somnolence at school and an increasing number of falls for 3 wk before the initial diagnosis. He underwent brain MRI. It demonstrated a midline pontine tumor (diffuse intrinsic pontine glioma), which was treated with focal radiotherapy to a total dose of 54 Gy. Six months after completing treatment, he presented to the clinic with recurrent gait abnormalities. An MRI scan showed an alteration in the internal architectural appearance of the brain stem glioma, with marginal dimensional reduction (the glioma was smaller than on the previous scan). There were also changes in diffusion-weighted imaging patterns between scans that could not clearly be characterized. An ^{18}F-DOPA scan was then performed a few days later and demonstrated tumor viability and recurrence (Fig. 3).

Case 4

A 3-y-old girl presented with a 2-mo history of gait disturbance followed by an inability to walk for 3 d before her admission to the hospital. MRI revealed a large tumor in the posterior fossa, prompting neurosurgical intervention and resection. Histopathologic examination of the excised specimen revealed anaplastic ependymoma. Immediate postoperative MRI showed a small, 8-mm, nodule in the resection bed suggestive of residual tumor. Correlative ^{18}F-DOPA PET and MRI performed 3 wk after surgery revealed no uptake in a much smaller nodular density, indicating a favorable postoperative change. This finding obviated second-look surgery (Fig. 4).

DISCUSSION

Amino acid PET imaging has been used successfully for about 15 y and has gained traction in the clinical management of brain tumors as several fluorine-labeled compounds have become more readily available and as data have mounted on a major impact on clinical management (*1–4*). ^{18}F-DOPA and ^{18}F-FET seem to be the agents with the highest accuracy, although only ^{18}F-DOPA

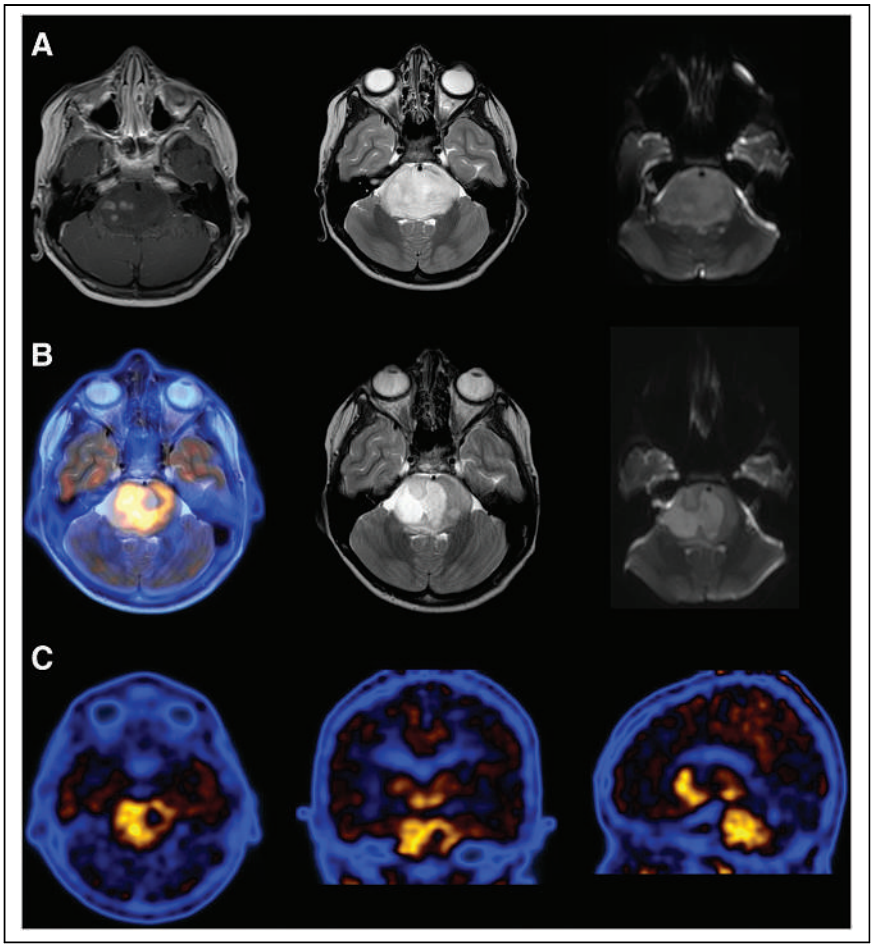

FIGURE 3. No clear change in size of initial diffuse intrinsic pontine glioma tumor 9 mo after initial MRI. Changes in appearance on different sequences showed T2-weighted and diffusion-weighted MRI signal distribution changes. ^{18}F-DOPA scan fused with follow-up MRI clearly delineates tumor viability and recurrence. (A) From left to right: initial axial T1-weighted contrast-enhanced, initial axial T2-weighted, and initial axial diffusion-weighted MR images. (B) From left to right: axial ^{18}F-DOPA T2-weighted 9-mo follow-up PET/MR, axial T2-weighted 9-mo follow-up MR, and axial diffusion-weighted 9-mo follow-up MR images. (C) From left to right: axial ^{18}F-DOPA, coronal ^{18}F-DOPA, and sagittal ^{18}F-DOPA PET images.

is Food and Drug Administration–approved (*1,5,6*). ^{18}F-DOPA can offer complementary and additive valuable information at different stages of brain tumor management (Fig. 5).

Historically, ^{18}F-FDG and ^{11}C-MET have been used in brain tumor evaluation. Higher ^{18}F-FDG uptake has been correlated with higher grade and worse prognosis but is no longer routinely used in the clinic because of its low sensitivity (*2,6*). ^{11}C-MET is limited by its short half-life of 20 min and is used only in centers with an on-site cyclotron. When available, it can provide useful diagnostic and prognostic information (*2,3*). ^{18}F-FET and ^{18}F-DOPA radiotracers are newer and significantly superior and have largely taken over brain tumor imaging with PET (*3,4*). Most recently, the European Association of Nuclear Medicine, Society of Nuclear Medicine and Nuclear Imaging, European Association of Neuro-Oncology, and Response Assessment in Neuro-Oncology Group published practice guidelines and procedure standards for imaging of gliomas using PET with radiolabeled amino acids and ^{18}F-FDG (*6*). These guidelines have consolidated the benefit of PET imaging in the different stages of brain tumor management as described earlier by the Response Assessment in Neuro-Oncology Group (*5*).

Pirotte's group has extensively explored amino acid imaging in pediatrics, described their experience over 10 y with ^{18}F-FDG and ^{11}C-MET, and outlined the value of PET in the presurgical, surgical, and postsurgical management of 126 pediatric cases (*7*). In another study, Pirotte et al. showed in 85 pediatric brain tumors that ^{18}F-FDG PET or ^{11}C-MET PET guided treatment when MRI was unable to assist in selecting accurate biopsy targets (35 patients) or to delineate tumors for maximal resection (50 patients) (*8*). They also showed, in 55 children, that absence of ^{11}C-MET uptake had a high accuracy in excluding high-grade tumors and was able to guide conservative management; increased uptake was also seen in all patients with high-grade tumors (*9*). Pirotte et al. also concluded, in their evaluation of 9 pediatric cases of infiltrative brain tumor, that PET and MR coguidance for accurate stereotactic biopsy of these lesions improved the diagnostic yield, made it possible to reduce the sampling in high-risk or functional areas, and improved the overall quality of therapeutic management (*10*). The latter strategy is clinically relevant because of the histologic heterogeneity of brain tumors (*11–13*). This additional value of PET imaging, when compared with MRI alone, was also highlighted in another series of 103 pediatric cases (*14*).

Furthermore, Morana's group has suggested that ^{18}F-DOPA PET, when added to the MRI work-up in cases of infiltrative gliomas, may offer additional value in diagnosis, prognosis, and therapy assessment (*15–17*). Other groups have also pointed to the impact of a positive ^{18}F-DOPA PET result on overall survival, progression-free survival, and overall management in adults with low-grade primary brain tumors and brain tumor recurrence (*18–21*). On the other hand, Morana's group has also highlighted that although ^{18}F-DOPA can aid in differentiating high- and low-grade brain tumors, one should be cautious because developmental venous anomalies may represent a false-positive finding (*22*). The group recommended that all

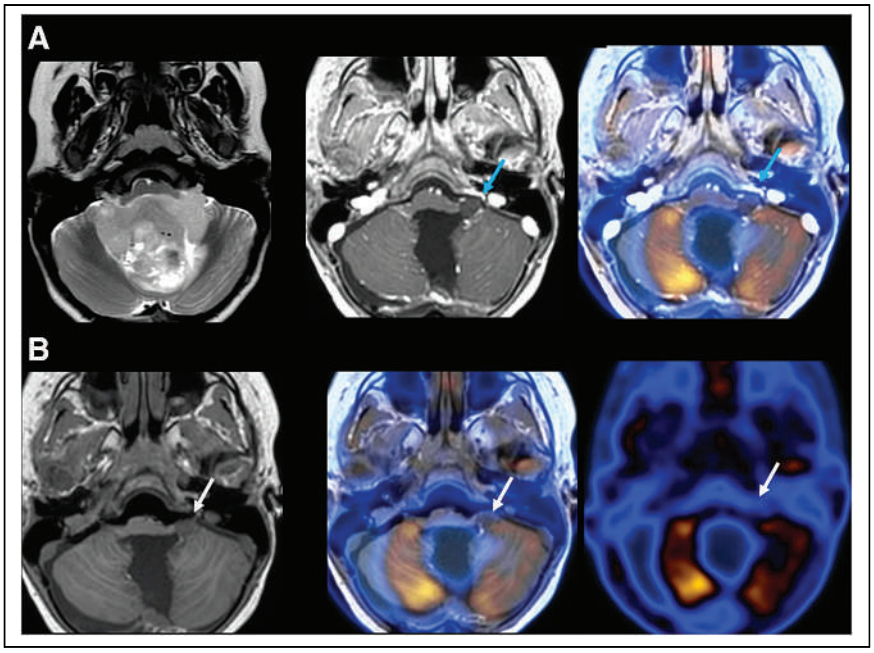

FIGURE 4. A 3-y-old girl after resection of posterior fossa tumor (anaplastic ependymoma: World Health Organization grade III). Three weeks after surgery, 8-mm left-sided nodule (blue arrows) in resection cavity showed no abnormal ^{18}F-DOPA uptake. Follow-up MRI on same day as ^{18}F-DOPA scan showed interval reduction in size and near-complete resolution of this nodule (white arrows), most consistent with initial postoperative changes. (A) From left to right: axial T2-weighted preoperative MR, axial immediately postoperative T1-weighted contrast-enhanced MR, and axial immediately postoperative ^{18}F-DOPA PET/MR images (B) From left to right: axial follow-up postoperative T1-weighted MR (3 wk), axial follow-up ^{18}F-DOPA PET/MR, and axial ^{18}F-DOPA PET images.

^{18}F-DOPA PET interpretations be performed by expert readers and in correlation with the patient's MR images (*22*). This recommendation is of greater importance, considering the increased prevalence of developmental anomalies in children with intracranial neoplasms (*23*). These developmental anomalies were associated with neuronal dysfunction in adjacent brain areas as depicted on ^{18}F-FDG PET (*24*). Morana et al. also reported on the possibility of seeing ^{18}F-DOPA changes in the basal ganglia secondary to network changes due to cortical resection—a possibility that needs to be considered when interpreting these PET scans (*25*). ^{18}F-DOPA PET was also highlighted by Bund et al. to be helpful in the evaluation of 53 nonenhancing brain tumors, although this evaluation was in adults (mean age, 39 y) (*26*). ^{18}F-DOPA PET was able to discriminate between dysembryoplastic neuroepithelial tumor and grade II oligodendroglioma and between low- and high-grade gliomas with no contrast enhancement on MRI (*26*).

In addition, as the management and classification of brain tumors has been shifting from the plain high- or low-grade spectrum and incorporating molecular markers that define distinct biologic subtypes with different clinical courses, it seems natural that metabolic imaging may add a layer of subcategorizing tumors, stratifying management, and altering the course of disease. Suchorska et al. briefly summarized this paradigm in the context of the new, 2016, World Health Organization classification for brain tumors (*27*). At this moment, it may be difficult to differentiate subtypes on the basis of amino acid PET imaging (*27*); however, higher ^{18}F-DOPA uptake has been associated with IDH mutation in diffuse grade II and grade III gliomas (*28*). Although most dynamic data stem from ^{18}F-FET, it seems that current dynamic ^{18}F-DOPA data are a predictor of progression/recurrence and progression-free survival. However, dynamic ^{18}F-DOPA data do not seem to offer any additional value over static parameters such as mean and maximum tumor–to–normal-brain ratios, tumor-to-striatum ratios, and metabolic tumor volume (*29*). Ponisio et al., on the other hand, did not uncover any value to dynamic analysis (*30*). Furthermore, Ginet et al. demonstrated that dynamic ^{18}F-DOPA PET was able to differentiate the molecular features of newly diagnosed gliomas (i.e., presence or absence of isocitrate dehydrogenase mutation), but static uptake parameters were not (*31*). Lastly, Piccardo et al. compared advanced MRI features and metabolic information obtained by ^{18}F-DOPA PET in 22 pediatric midline gliomas. They showed that in comparison to advanced MRI techniques such as ADC maps, arterial spin labeling perfusion maps, and MR spectroscopy, ^{18}F-DOPA PET tumor-to-striatum ratio was the only parameter able to discriminate H3K27 M-mutant from wild-type diffuse midline gliomas independently from histology (*32*).

CONCLUSION

Amino acid imaging with ^{18}F-DOPA is a powerful clinical tool and should be used in agreement with the recent joint guidelines from the European Association of Nuclear Medicine, the European Association of Neuro-Oncology, the Response Assessment in Neuro-Oncology Group (2019), and the Neuro-Oncology Working Group (2016). Wider use and pooling of patient data from multicenter registries would provide even more insight.

DISCLOSURE

Cyclomedical (Hamad Medical Corporation) facilitated provision of ^{18}F-DOPA. No other potential conflict of interest relevant to this article was reported.

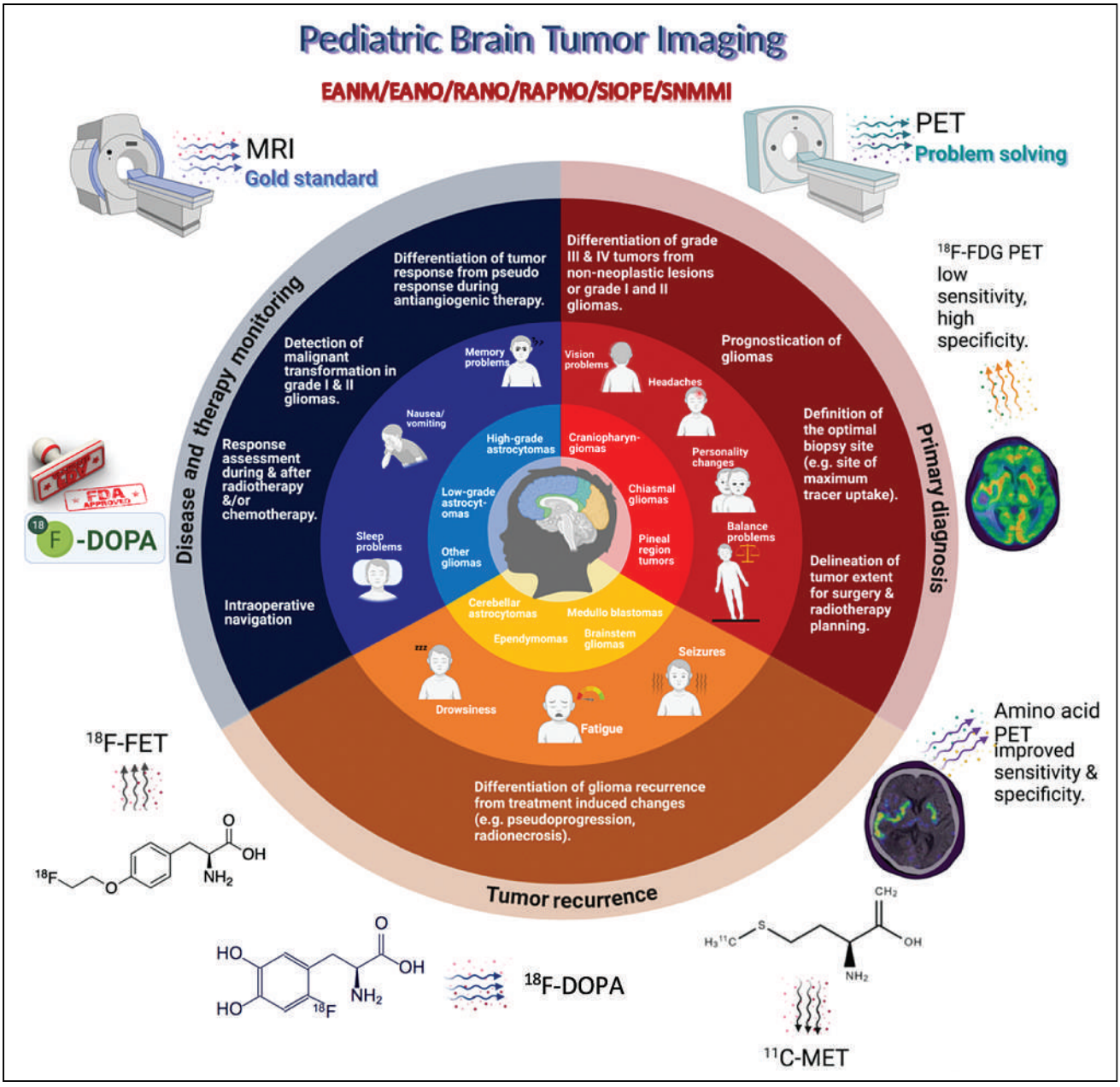

FIGURE 5. Summary diagram. EANM = European Association of Nuclear Medicine; EANO = European Association of Neuro-Oncology; RANO = Response Assessment in Neuro-Oncology; RAPNO = Response Assessment in Pediatric Neuro-Oncology; SIOPE = European Society for Paediatric Oncology; SNMMI = Society of Nuclear Medicine and Molecular Imaging.

KEY POINTS

QUESTION: Is amino acid PET imaging with ^{18}F-DOPA of significant value in pediatric brain tumors?

PERTINENT FINDINGS: Amino acid PET imaging with ^{18}F-DOPA offers valuable clinical information in primary diagnosis, treatment response assessment, pseudoprogression, and recurrence applications in pediatric brain tumors.

IMPLICATIONS FOR PATIENT CARE: Amino acid PET imaging with ^{18}F-DOPA in pediatric brain tumors may change clinical management and improve outcomes.

REFERENCES

1. Galldiks N, Law I, Pope WB, Arbizu J, Langen KJ. The use of amino acid PET and conventional MRI for monitoring of brain tumor therapy. *Neuroimage Clin.* 2016;13:386–394.
2. Lopci E, Riva M, Olivari L, et al. Prognostic value of molecular and imaging biomarkers in patients with supratentorial glioma. *Eur J Nucl Med Mol Imaging.* 2017;44:1155–1164.
3. Katsanos AH, Alexiou GA, Fotopoulos AD, Jabbour P, Kyritsis AP, Sioka C. Performance of ^{18}F-FDG, ^{11}C-methionine, and ^{18}F-FET PET for glioma grading: a meta-analysis. *Clin Nucl Med.* 2019;44:864–869.
4. Misch M, Guggemos A, Driever PH, et al. ^{18}F-FET-PET guided surgical biopsy and resection in children and adolescence with brain tumors. *Childs Nerv Syst.* 2015;31:261–267.
5. Albert NL, Weller M, Suchorska B, et al. Response Assessment in Neuro-Oncology Working Group and European Association for Neuro-Oncology recommendations for the clinical use of PET imaging in gliomas. *Neuro Oncol.* 2016;18:1199–1208.

6. Law I, Albert NL, Arbizu J, et al. Joint EANM/EANO/RANO practice guidelines/SNMMI procedure standards for imaging of gliomas using PET with radiolabelled amino acids and [^{18}F]FDG: version 1.0. *Eur J Nucl Med Mol Imaging.* 2019;46:540–557.
7. Pirotte B, Acerbi F, Lubansu A, Goldman S, Brotchi J, Levivier M. PET imaging in the surgical management of pediatric brain tumors. *Childs Nerv Syst.* 2007;23:739–751.
8. Pirotte BJ, Lubansu A, Massager N, et al. Clinical impact of integrating positron emission tomography during surgery in 85 children with brain tumors. *J Neurosurg Pediatr.* 2010;5:486–499.
9. Pirotte BJ, Lubansu A, Massager N, et al. Clinical interest of integrating positron emission tomography imaging in the workup of 55 children with incidentally diagnosed brain lesions. *J Neurosurg Pediatr.* 2010;5:479–485.
10. Pirotte B, Goldman S, Salzberg S, et al. Combined positron emission tomography and magnetic resonance imaging for the planning of stereotactic brain biopsies in children: experience in 9 cases. *Pediatr Neurosurg.* 2003;38:146–155.
11. Goldman S, Levivier M, Pirotte B, et al. Regional glucose metabolism and histopathology of gliomas: a study based on positron emission tomography-guided stereotactic biopsy. *Cancer.* 1996;78:1098–1106.
12. Goldman S, Levivier M, Pirotte B, et al. Regional methionine and glucose uptake in high-grade gliomas: a comparative study on PET-guided stereotactic biopsy. *J Nucl Med.* 1997;38:1459–1462.
13. Black PM. Brain tumors. Part 1. *N Engl J Med.* 1991;324:1471–1476.
14. Pirotte B, Goldman S, Dewitte O, et al. Integrated positron emission tomography and magnetic resonance imaging-guided resection of brain tumors: a report of 103 consecutive procedures. *J Neurosurg.* 2006;104:238–253.
15. Morana G, Piccardo A, Milanaccio C, et al. Value of ^{18}F-3,4-dihydroxyphenylalanine PET/MR image fusion in pediatric supratentorial infiltrative astrocytomas: a prospective pilot study. *J Nucl Med.* 2014;55:718–723.
16. Morana G, Piccardo A, Puntoni M, et al. Diagnostic and prognostic value of ^{18}F-DOPA PET and ^{1}H-MR spectroscopy in pediatric supratentorial infiltrative gliomas: a comparative study. *Neuro Oncol.* 2015;17:1637–1647.
17. Morana G, Piccardo A, Tortora D, et al. Grading and outcome prediction of pediatric diffuse astrocytic tumors with diffusion and arterial spin labeling perfusion MRI in comparison with ^{18}F-DOPA PET. *Eur J Nucl Med Mol Imaging.* 2017;44:2084–2093.
18. Langen KJ, Galldiks N. Update on amino acid PET of brain tumours. *Curr Opin Neurol.* 2018;31:354–361.
19. Chiaravalloti A, Esposito V, Ursini F, et al. Overall survival and progression-free survival in patients with primary brain tumors after treatment: is the outcome of [^{18}F] FDOPA PET a prognostic factor in these patients? *Ann Nucl Med.* 2019;33:471–480.
20. Herrmann K, Czernin J, Cloughesy T, et al. Comparison of visual and semiquantitative analysis of ^{18}F-FDOPA-PET/CT for recurrence detection in glioblastoma patients. *Neuro Oncol.* 2014;16:603–609.
21. Humbert O, Bourg V, Mondot L, et al. ^{18}F-DOPA PET/CT in brain tumors: impact on multidisciplinary brain tumor board decisions. *Eur J Nucl Med Mol Imaging.* 2019;46:558–568.
22. Morana G, Piccardo A, Garrè ML, Cabria M, Rossi A. ^{18}F-DOPA uptake of developmental venous anomalies in children with brain tumors. *Clin Nucl Med.* 2016;41:e351–e352.
23. Jones BV, Linscott L, Koberlein G, Hummel TR, Leach JL. Increased prevalence of developmental venous anomalies in children with intracranial neoplasms. *AJNR.* 2015;36:1782–1785.
24. Larvie M, Timerman D, Thum JA. Brain metabolic abnormalities associated with developmental venous anomalies. *AJNR.* 2015;36:475–480.
25. Morana G, Piccardo A, Garrè ML, Nobili F, Rossi A. Late persistent increased putaminal ^{18}F-DOPA uptake following ipsilateral frontal resection: evidence for corticostriatal synaptic plasticity? *Clin Nucl Med.* 2015;40:e451–e452.
26. Bund C, Heimburger C, Imperiale A, et al. FDOPA PET-CT of nonenhancing brain tumors. *Clin Nucl Med.* 2017;42:250–257.
27. Suchorska B, Albert NL, Bauer EK, Tonn JC, Galldiks N. The role of amino-acid PET in the light of the new WHO classification 2016 for brain tumors. *Q J Nucl Med Mol Imaging.* 2018;62:267–271.
28. Verger A, Metellus P, Sala Q, et al. IDH mutation is paradoxically associated with higher ^{18}F-FDOPA PET uptake in diffuse grade II and grade III gliomas. *Eur J Nucl Med Mol Imaging.* 2017;44:1306–1311.
29. Zaragori T, Ginet M, Marie PY, et al. Use of static and dynamic [^{18}F]-F-DOPA PET parameters for detecting patients with glioma recurrence or progression. *EJNMMI Res.* 2020;10:56.
30. Ponisio MR, McConathy JE, Dahiya SM, et al. Dynamic ^{18}F-FDOPA-PET/MRI for the preoperative evaluation of gliomas: correlation with stereotactic histopathology. *Neurooncol Pract.* 2020;7:656–667.
31. Ginet M, Zaragori T, Marie PY, et al. Integration of dynamic parameters in the analysis of ^{18}F-FDopa PET imaging improves the prediction of molecular features of gliomas. *Eur J Nucl Med Mol Imaging.* 2020;47:1381–1390.
32. Piccardo A, Tortora D, Mascelli S, et al. Advanced MR imaging and ^{18}F-DOPA PET characteristics of H3K27M-mutant and wild-type pediatric diffuse midline gliomas. *Eur J Nucl Med Mol Imaging.* 2019;46:1685–1694.

Remodeling ^{99m}Tc-Pertechnetate Thyroid Uptake: Statistical, Machine Learning, and Deep Learning Approaches

Geoffrey M. Currie[1] and Basit Iqbal[2]

[1]*Charles Sturt University, Wagga Wagga, Australia, and Baylor College of Medicine, Houston, Texas; and* [2]*Gujranwala Institute of Nuclear Medicine and Radiotherapy, Gujranwala, Pakistan*

Although reference ranges for ^{99m}Tc thyroid percentage uptake vary, the seemingly intuitive evaluation of thyroid function does not reflect the complexity of thyroid pathology and biochemical status. The emergence of artificial intelligence in nuclear medicine has driven problem solving associated with logic and reasoning, warranting reexamination of established benchmarks in thyroid functional assessment. **Methods:** This retrospective study of 123 patients compared scintigraphic findings with grounded truth established through biochemistry status. Conventional statistical approaches were used in conjunction with an artificial neural network to determine predictors of thyroid function from data features. A convolutional neural network was also used to extract features from the input tensor (images). **Results:** Analysis was confounded by subclinical hyperthyroidism, primary hypothyroidism, subclinical hypothyroidism, and triiodothyronine toxicosis. Binary accuracy for identifying hyperthyroidism was highest for thyroid uptake classification using a threshold of 4.5% (82.6%), followed by pooled physician interpretation with the aid of uptake values (82.3%). Visual evaluation without quantitative values reduced accuracy to 61.0% for pooled physician determinations and 61.4% classifying on the basis of thyroid gland intensity relative to salivary glands. The machine learning (ML) algorithm produced 84.6% accuracy; however, this included biochemistry features not available to the semantic analysis. The deep learning (DL) algorithm had an accuracy of 80.5% based on image inputs alone. **Conclusion:** Thyroid scintigraphy is useful in identifying hyperthyroid patients suitable for radioiodine therapy when using an appropriately validated cutoff for the patient population (4.5% in this population). ML artificial neural network algorithms can be developed to improve accuracy as second-reader systems when biochemistry results are available. DL convolutional neural network algorithms can be developed to improve accuracy in the absence of biochemistry results. ML and DL do not displace the role of the physician in thyroid scintigraphy but can be used as second-reader systems to minimize errors and increase confidence.

Key Words: thyroid uptake; hyperthyroidism; machine learning; deep learning; artificial intelligence

J Nucl Med Technol 2022; 50:143–152
DOI: 10.2967/jnmt.121.263081

In 1967, Atkins and Richards (*1*) evaluated the potential role of ^{99m}Tc-pertechnetate in evaluating thyroid function as an alternative to sodium iodide with ^{131}I on the basis that ^{99m}Tc uptake in the thyroid reflects the gland's trapping function. This landmark work used a probe detector rather than γ-camera imaging for the uptake calculation. A small number of hypothyroid patients were included, and all had percentage uptakes below 0.5%. Only 2 of 15 hyperthyroid patients fell below 4%, whereas 4 of 133 euthyroid patients had uptake above 4%. Thus, a cutoff for normality was set at 0.4%–4.0% to provide 87% accuracy in hyperthyroidism, 97% accuracy in euthyroidism, and 100% accuracy in hypothyroidism.

Later work, in 1973, by Maisey et al. (*2*) used a γ-camera, pinhole collimation, and interfaced computer to generate regions of interest for calculation of ^{99m}Tc-pertechnetate uptake in the thyroid. Uptake was 0.2%–3.6% in euthyroid patients, 0.3%–6.2% in the presence of a goiter, 2.8%–8.8% in hyperthyroidism, and 0.1%–0.3% in hypothyroidism, leading to establishment of a reference range of 0.3%–3.4%. More recently, ^{99m}Tc-pertechnetate uptake in euthyroidism was characterized in the range of 0.4%–1.7% in 47 clinically normal patients (*3*). It is widely acknowledged that reference values change with geography and time, particularly in relation to iodine deficiency (*4*). Although widespread use of international standards is common (0.5%–4.5% for example), these values may not reflect either the technique used (probe vs. γ-camera) or population characteristics (e.g., iodine deficiency). In Namibia, investigators found the reference range to be 0.15%–2.14% (*4*) although the study included only 76 patients and all were euthyroid. A U.K. study (*5*) used 60 euthyroid patients to estimate the local reference range as 0.2%–2.0%.

Although reference ranges for percentage uptake vary, the method for calculation of thyroid function on ^{99m}Tc scintigraphy also varies (*6*). A seemingly intuitive evaluation of thyroid function has also been used as a visual evaluation of thyroid activity relative to salivary gland activity (Fig. 1). Such an evaluation does not reflect the complexity of thyroid pathology and biochemical status. When the bulk of patients are euthyroid or hyperthyroid, this simplification is intuitive, but it fails to accommodate subclinical hyperthyroidism, which can produce a low thyroid accumulation of ^{99m}Tc;

Received Aug. 19, 2021; revision accepted Nov. 10, 2021.
For correspondence or reprints, contact Geoffrey M. Currie (gcurrie@csu.edu.au).
Published online Dec. 7, 2021.

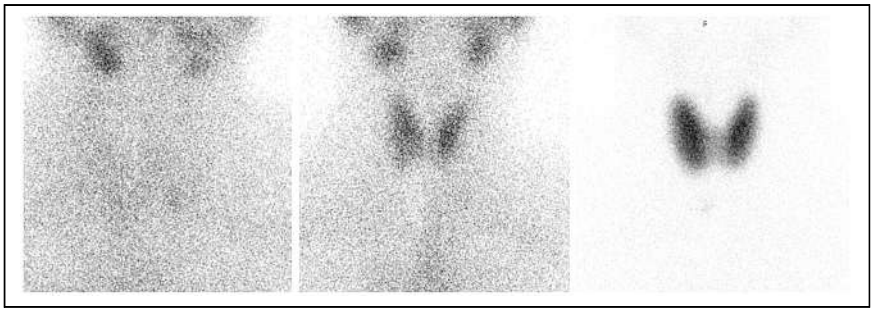

FIGURE 1. Intuitive, but sometimes inaccurate, visual evaluation of thyroid status relative to salivary gland activity. (Left) Salivary gland activity exceeding thyroid gland activity suggests hypothyroidism. (Middle) Salivary gland activity and thyroid gland activity being similar (within same scale) suggests euthyroidism. (Right) Salivary gland activity not being apparent relative to thyroid activity suggests hyperthyroidism. All images were obtained with ^{99m}Tc-pertechnetate using high-resolution, parallel-hole imaging.

triiodothyronine (T3) toxicosis, which can have high or low ^{99m}Tc uptake; subclinical hypothyroidism, which can have elevated or normal ^{99m}Tc accumulation; and primary hypothyroidism, which can have normal or elevated ^{99m}Tc accumulation. Thus, the accuracy of ^{99m}Tc uptake may be more dependent on the pathologic cross section of patients than on the technique itself.

The emergence of artificial intelligence in nuclear medicine has driven problem solving associated with logic and reasoning (*7,8*). Developments in machine learning (ML) and deep learning (DL) provide valuable research tools, particularly for image segmentation and interpretation (*9*). The artificial neural network (ANN) provides the backbone for both ML and DL algorithms. The ANN relies on input of specific data (features) and generally refers to ML. More complex ANNs can produce deep architectures (a high number of layers and nodes) and refers to DL. Deep ANNs are generally associated, in medical imaging, with convolutional neural networks (CNN) that use convolution and pooling layers to extract features from input tensors (images) (*9,10*). Although there have been historical uses of neural networks to classify thyroid-based ophthalmologic conditions and evaluate in vitro laboratory tests, it is only recently that DL approaches have been applied to thyroid scintigraphy. Using SPECT thyroid scintigraphy, 3 DL models based on AlexNet, VGGNet, and ResNet architectures trained on 1,430 clinical studies were modeled and compared with residents in nuclear medicine (*11*). Although the investigators concluded that DL approaches performed well in thyroid scintigraphy, the role of DL might be limited to assisting the physician in training rather than having any specific clinical utility. The algorithms marginally outperformed first-year residents but did not perform as well as second-year residents, let alone experienced physicians. Concurrent use of the DL approaches improved the performance of residents on the order of 5% and reduced reporting time. Nonetheless, there is a need to explore potential clinical and research applications, and the less complex nature of planar thyroid scintigraphy may be better suited to DL approaches. The performance of these algorithms was enhanced by a sanitized dataset with a case population comprising healthy individuals (175), patients with Graves disease (834), and patients with subacute thyroiditis (421). The 3 DL architectures reported a high degree of recall for subacute thyroiditis, poor accuracy for normality, and moderate accuracy for Graves disease (*11*).

The aim of this investigation was to correlate each of the following with biochemical status and compare performance: percentage uptake of ^{99m}Tc, visual correlation of thyroid activity in the thyroid, ML algorithms using an ANN, and DL approaches using a CNN.

MATERIALS AND METHODS

The study retrospectively analyzed 123 patients (90.2% female), with a mean age of 35 y (range, 10–70 y). The mean intravenous dose of ^{99m}Tc was 153.4 MBq. ^{99m}Tc-based thyroid uptake was determined using background-corrected thyroid regions of interest and a measured standard. All calculations were decay-corrected and accounted for residual dose in the syringe after injection. The extracted image features included both background-corrected and non–background-corrected total thyroid, left-side and right-side area (cm^2), counts, and counts per pixel. The ratio of the right lobe to the left lobe for area (cm^2), counts, and counts per pixel was also determined with and without background correction. Additionally, the ratio of thyroid count to background count for total thyroid, right lobe, and left lobe was determined (trapping index). The dose relative to the total count was also calculated, and visual classification of thyroid activity relative to the salivary glands was recorded. Biochemical features included the levels of free thyroxine (T4) (pmol/L), free T3 (pmol/L), and thyroid-stimulating hormone (μIU/mL). The biochemical status of the patient was determined (Table 1) and was further stratified as ternary (hypothyroid, euthyroid, or hyperthyroid) or binary (hyperthyroid or not hyperthyroid) (*1–6,12,13*). Other imaging features were also recorded (e.g., hot or cold nodule and multinodular goiter). Only 96 patients had both imaging features and biochemical status available. The investigation was approved by the institutional ethics committee.

Conventional statistical analysis was undertaken using JMP software (version 15.2.1; SAS Institute). The statistical significance was calculated using χ^2 analysis for nominal data and the Student t test for continuous data. The Pearson χ^2 test was used for categoric data with a normal distribution, and the likelihood ratio χ^2 test was used for categoric data without a normal distribution. F test ANOVA was used to determine statistically significant differences within grouped data. A P value of less than 0.05 was considered significant. Interobserver correlation was evaluated with χ^2 analysis, and interobserver reliability was measured using the Cohen κ-coefficient.

The data were also evaluated using an ANN (Neural Analyser, version 2.9.5; Artificial Intelligence Techniques, Ltd.). There were

TABLE 1
Biochemical Stratification of Patient Studies and Findings (*1–6,12,13*)

Free T3 (2–7 pmol/L*)	Free T4 (12–30 pmol/L*)	Thyroid-stimulating hormone (0.45–4.5 μIU/mL*)	Biochemical status	^{99m}Tc uptake (%)	Comment on uptake reference range
High	High	Low	Hyperthyroidism	>4.5	0% FN rate
Normal	Normal	Low	Subclinical hyperthyroidism	<4.5 including <0.45 or absent	0% TP, comprised FN or FP hypothyroidism
High	Normal	Low	T3 toxicosis	>4.5 or <0.45	FP hypothyroidism
Normal	High	Low	Thyroiditis		No cases
Low	Low	Low	Secondary hypothyroidism		No cases
Normal	Normal	High	Subclinical hypothyroidism	>0.45 but <4.5	100% FN
Low or normal	Low	High	Primary hypothyroidism	>0.45 and in over 50% of cases >4.5	100% FN
Normal	Normal	Normal	Euthyroid	<4.5%	9% FP rate (6% hyperthyroid, 3% hypothyroid)

*Reference range.

42 input variables in 123 patients (instances) using a binary classification of hyperthyroid or euthyroid. A 50:25:25 split of 96 valid instances (excluded missing biochemistry data) was used for training, selection, and testing. The initial network architecture included 16 scaling layer inputs and 3 hidden layers of 6, 4, and 3 nodes, using a logistic activation function (defines the output of each node based on its input) for a single probabilistic layer (binary). The weighted squared error method was used to determine the loss index, and the neural parameter norm was used for the regularization method. A quasi-Newtonian training method was applied using gradient information to estimate the inverse Hessian matrix for each iteration of the algorithm (no second derivatives). The loss function associated with the training phase estimates the error associated with the data that the neural network observes.

A single anterior neck image for the 96 patients was evaluated by 3 independent expert physicians masked to other image and biochemical features. On the basis of the visual appearance, each scan was recorded as euthyroid, hypothyroid, or hyperthyroid. On completion of the stratification, each physician reevaluated the ternary status, with the visual inspection supplemented by the calculated thyroid uptake (%). The physician rating was determined by majority group consensus.

Individual, nonannotated, anterior neck images representative of each patient were evaluated using a CNN classifier (Deep Learning Toolkit Deep Network Designer App in MATLAB, version R2020b; MathWorks). Given the lack of discriminatory power of either visual evaluation or thyroid uptake quantitation using various cutoffs to identify hypothyroidism, the CNN classifier was designed to identify hyperthyroidism or no hyperthyroidism (euthyroid and hypothyroid). Given the lack of complexity in the image data, the architecture used for the CNN was initially modeled on a binary version of AlexNet with 25 layers but optimized using a model that resembled the VGG-19 CNN architecture with a binary output and 30 layers (Table 2; Fig. 2). All patient files were trained and validated 3 times (70:30 random data split) for each of 3 image types; white on black gray scale, black on white gray scale, and the magnitude spectrum of the Fourier transformation of each image (Fig. 3). Specific parameters included an ADAM (adaptive movement estimation) stochastic gradient descent optimizer algorithm, an initial learn rate of 0.001, a maximum of 50 epochs (1 epoch = 1 iteration), and randomization with each epoch.

Situation analysis was undertaken using the confusion matrix for classifier prediction, including true-positives (TPs), false-positives (FPs), true-negatives (TNs), and false-negatives (FNs). Several performance indicators can be gleaned from the confusion matrix, including precision (TPs/[TPs + FPs]), recall (TPs/[TPs + FNs]), accuracy ([TPs + TNs]/[TPs + TNs + FPs + TNs]), and F1 score ($2 \times$ TPs/[$2 \times$ {TPs + FPs + FNs}]).

RESULTS

Statistical Analysis

For the 123 patients, the mean thyroid uptake was 4.4% (95% CI, 3.3%–5.5%), with a median of 2.2% (Table 3). Among the visual findings, 9 patients had increased uptake associated with primary hypothyroidism, 22 had increased uptake because of Graves disease, 9 had multinodular goiters, 2 had nodular thyroids, 28 had a normal morphology, 3 had goiters, 11 had reduced or absent uptake, 7 had autonomous glands with contralateral suppression (6 on the right), 24 had cold nodules (16 on the right), and 8 had hot nodules (4 on the right). Table 4 summarizes other key demographic data.

The mean age of hypothyroid patients (48.0 y) was statistically higher than that for biochemically euthyroid patients (33.7 y) ($P = 0.041$) but not for hyperthyroid patients (36.7 y). There was also a weak positive correlation between age and thyroid size ($P < 0.001$; $R^2 = 0.117$). No other statistically significant relationships were noted for patient age. Men demonstrated a statistically higher mean thyroid area (48.5 cm^2) than women (32.2 cm^2) ($P = 0.003$). There was also a statistically significant difference in the biochemical status ($P = 0.019$), with a disproportionately high

TABLE 2
CNN Architecture, Activations, and Parameters

Layer	Name	Activations	Parameters
1	Tensor input layer	[725,725,3]	
2	2D convolution layer	[239,239,64]	Weights [11,11,3,64], bias [1,1,64]
3	Batch normalization	[239,239,64]	Offset and scale [1,1,64]
4	ReLU layer	[239,239,64]	
5	Max pooling layer	[119,119,64]	Size [3,3], stride [2,2], padding [0,0,0,0]
6	2D convolution layer	[40,40,128]	Weights 5,5,64,128], bias [1,1,128]
7	Batch normalization	[40,40,128]	Offset and scale [1,1,128]
8	ReLU layer	[40,40,128]	
9	Max pooling layer	[19,19,128]	Size [3,3], stride [2,2], padding [0,0,0,0]
10	2D convolution layer	[19,19,256]	Weights [3,3,128,256], bias [1,1,256]
11	Batch normalization	[19,19,256]	Offset and scale [1,1,256]
12	ReLU layer	[19,19,256]	
13	Max pooling layer	[9,9,256]	Size [3,3], stride [2,2], padding [0,0,0,0]
14	2D convolution layer	[9,9,192]	Weights [3,3,256,192], Bias [1,1,192]
15	Batch normalization	[9,9,192]	Offset and scale [1,1,192]
16	ReLU layer	[9,9,192]	
17	Max pooling layer	[4,4,192]	Size [3,3], stride [2,2], padding [0,0,0,0]
18	2D convolution layer	[4,4,192]	Weights [3,3,256,192], bias [1,1,192]
19	Batch normalization	[4,4,192]	Offset and scale [1,1,192]
20	ReLU layer	[4,4,192]	
21	Max pooling layer	[1,1,192]	Size [3,3], stride [2,2], padding [0,0,0,0]
22	Fully connected layer	[1,1,192]	Weights [192,192], bias [192,1]
23	ReLU layer	[1,1,192]	
24	Dropout layer	[1,1,192]	0.5
25	Fully connected layer	[1,1,86]	Weights [86,192], bias [86,1]
26	ReLU layer	[1,1,86]	
27	Dropout layer	[1,1,86]	0.5
28	Fully connected layer	[1,1,2]	Weights [2,86], bias [2,1]
29	Softmax layer	[1,1,2]	
30	Classification layer		Cross entropy loss function

2D = 2-dimensional; ReLU = rectified linear unit.

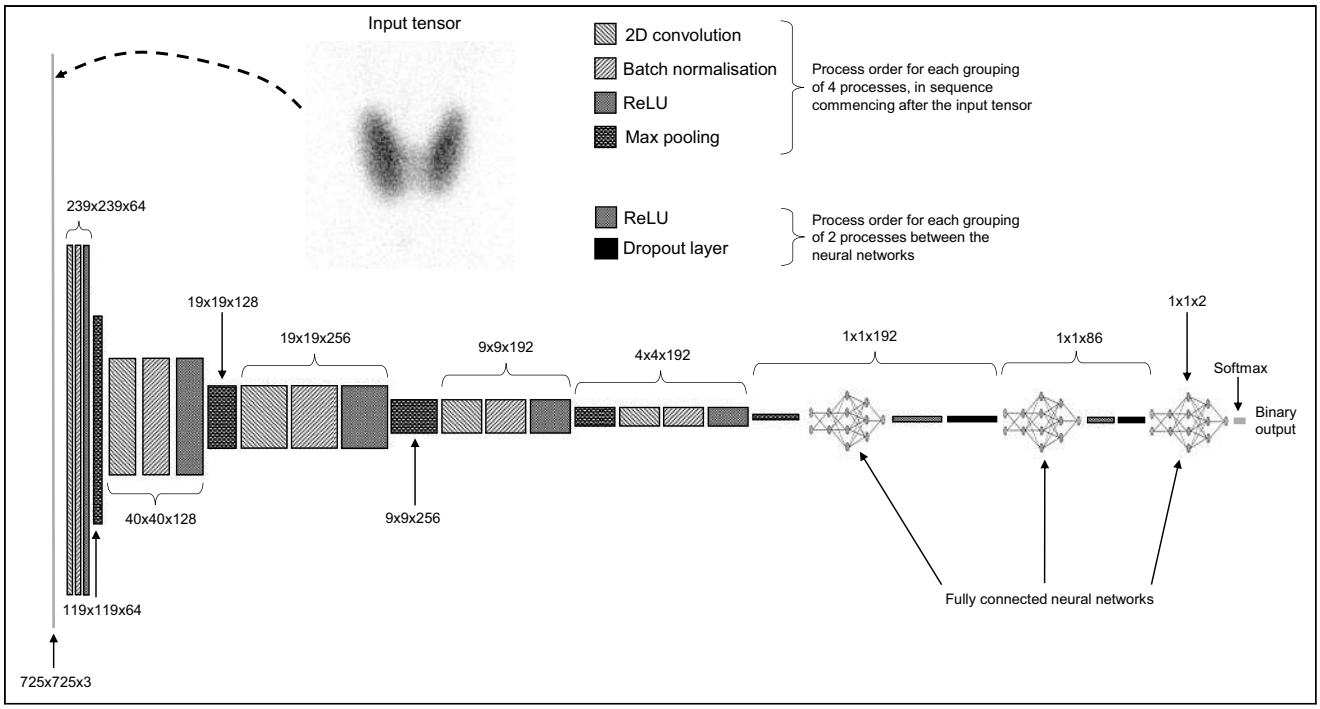

FIGURE 2. CNN architecture. 2D = 2-dimensional; ReLU = rectified linear unit.

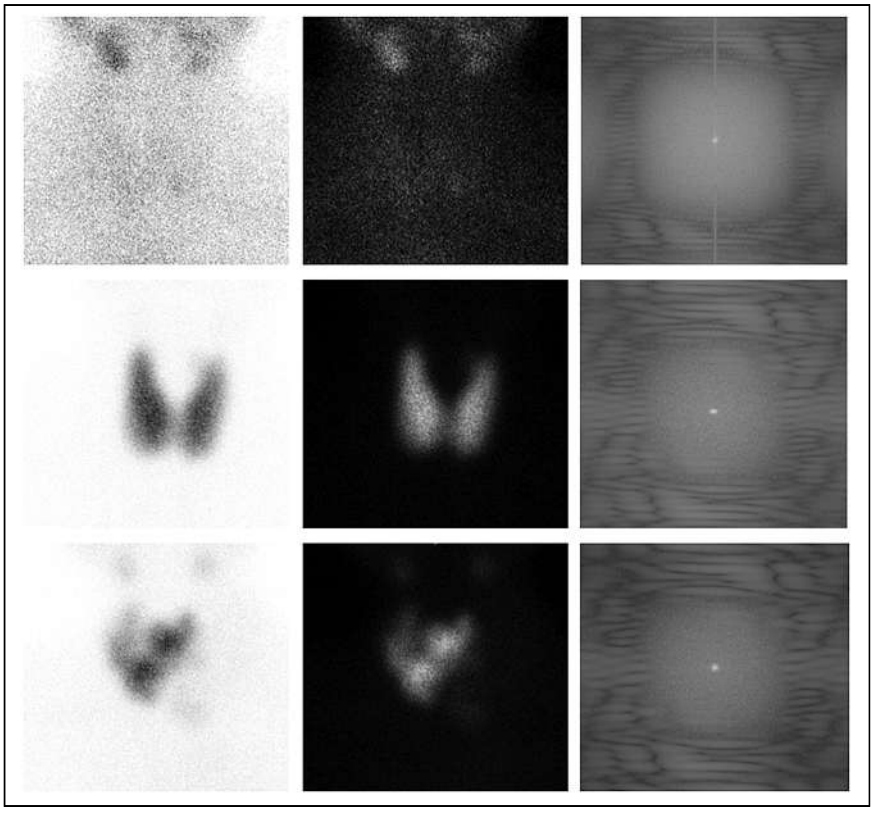

FIGURE 3. Three example patients (top, middle, and bottom) with black on white (left), white on black (center), and magnitude spectrum from Fourier transformation (right) used as inputs for CNN.

representation of hyperthyroidism for men and a lower euthyroid rate. Given the lower representation of men in the thyroid scan population, this observation may reflect lower presentation rates for men in the absence of markedly abnormal thyroid function driving more pressing symptoms. No other statistically significant relationships were noted for patient gender or patient dose (MBq).

There was no statistically significant correlation between thyroid uptake and right-lobe–to–left-lobe ratio ($P = 0.672$), thyroid area ($P = 0.166$), or background counts per pixel (CCP) ($P = 0.416$). The increase in thyroid uptake associated with increasing total counts ($P < 0.001$; $R^2 = 0.458$) and total CPP ($P < 0.001$; $R^2 = 0.356$) was expected. There were also statistically significant relationships between increasing thyroid uptake and increasing thyroid-to-background ratios ($P < 0.001$; $R^2 = 0.376$). The mean thyroid uptake was statistically higher ($P < 0.001$) when the scan showed—relative to appropriately thresholded thyroid activity—no salivary activity (9.1%) than when it showed—relative to faint thyroid activity (2.5%)—salivary activity less than thyroid activity (1.7%), salivary activity equal to thyroid activity (1.1%), or salivary activity greater than thyroid activity (0.4%). A positive correlation between thyroid uptake and both free T4 ($P < 0.001$; $R^2 = 0.351$) and free T3 ($P < 0.001$; $R^2 = 0.365$) was noted; however, no correlation was noted between thyroid uptake and thyroid-stimulating hormone ($P = 0.695$; $R^2 = 0.002$).

Biochemical status demonstrated a statistically significant difference ($P < 0.001$) in mean thyroid uptake stratified as hyperthyroid (9.5%; 95% CI, 7.1%–12.0%), hypothyroid (4.0%; 95% CI, 1.3%–6.7%), and euthyroid (2.5%; 95% CI, 0.9%–4.2%). Hypothyroid studies had a higher mean thyroid uptake than euthyroid studies because of the primary hypothyroidism cases. Excluding primary hypothyroidism, there was no statistically significant difference in thyroid uptake between hypothyroidism and euthyroidism, or between hypothyroidism

TABLE 3
Ternary Classification of Thyroid Function Based on Various Published Reference Ranges

Reference range	Euthyroid	Hyperthyroid	Hypothyroid	Reference
0.45%–4.5%	67.5%	26.8%	7.7%	*6*
0.4%–1.7%	35.0%	61.0%	4.0%	*3*
0.4%–4.0%	65.0%	31.0%	4.0%	*4*
0.3%–3.4%	57.7%	38.2%	4.1%	*2*
0.2%–2.0%	43.1%	52.8%	4.1%	*5*
Biochemical status	53.1%	27.1%	19.8%*	*11*
Salivary classification	44.8%	50.0%	5.2%	—
Physician visual rating	51.0%	43.8%	5.2%	—
Physician rating with uptake value	64.6%	29.2%	6.3%	—

*15.6% were hypothyroid without suppression of uptake (2.1% autonomous, 2.1% secondary hypothyroidism, 11.5% primary hypothyroidism, and 4.2% subclinical hypothyroidism).

TABLE 4
Key Variables

Variable	Mean	95% CI
Total count ratio of right-lobe activity to left-lobe activity	1.5	1.03–2.02
CPP ratio of right-lobe activity to left-lobe activity	1.29	0.98–1.60
Area	33.8 cm^2	31.1–36.5
Size, right	3092 pixels	2,848–3,340
Size, left	2937 pixels	2,662–3,212
Ratio of thyroid to background	4.06	3.43–4.69
Right	4.01 CPP	3.49–4.52
Left	4.08 CPP	3.28–4.89
Ratio of dose to total counts	4.85	3.44–6.26
FT4	21.1 pmol/L	18.1–24.2
FT3	7.1 pmol/L	5.1–9.1
Thyroid-stimulating hormone	4.2 pmol/L	2.3–6.1

and subclinical hyperthyroidism or suppressed hyperthyroidism. Although 4.5% is the cutoff reflecting 100% sensitivity for standard hyperthyroidism, clinical hyperthyroidism with suppression and subclinical hyperthyroidism (both biochemically) are not identified by this reference range.

The optimized cutoff range for thyroid uptake against biochemical status was 0.45%–4.5%, although the lower end of this range is a poor discriminator for hypothyroidism against euthyroidism. For biochemical hyperthyroidism, 70.8% of cases had an uptake greater than 4.5% whereas 29.3% fell below 4.5%. Of those below 4.5%, 100% had biochemically subclinical hyperthyroidism or T3 toxicosis. Of patients with true hyperthyroidism biochemically, 100% had uptake above 4.5%. Conversely, 27.8% of hypothyroidism cases had uptake above 4.5%. There were no hypothyroidism cases that had uptake values below the 0.45% cutoff (all values below this were hyperthyroid or euthyroid biochemically). In the biochemically euthyroid range, only 6% had an uptake above 4.5%, and only 2% had an uptake below 0.45%.

Using the ternary classification, a thyroid uptake above 4.5% had a sensitivity of 70.8% and a specificity of 88.2% for detecting hyperthyroidism. A thyroid uptake below 0.45% had a sensitivity of 0% and specificity of 95.9% for hypothyroidism (Fig. 4, left). A broader biochemical classification of hyperthyroidism saw the sensitivity of the 4.5% cutoff reach 100%, with a specificity of 88.2% (Fig. 4, right).

On the basis of the ternary biochemical status, there was a statistically higher thyroid area for hyperthyroidism (40.7 cm^2) than for hypothyroidism (29.5 cm^2) or euthyroidism (33.0 cm^2) ($P = 0.049$). With reference to Figure 1, the scintigraphic appearance of thyroid activity relative to salivary gland activity correctly identified 70.3% of hyperthyroid studies, 0% of hypothyroid studies, and 62.7% of euthyroid studies (Table 5). Excluding subclinical hyperthyroidism and T3 toxicosis, 94.1% of hyperthyroidism studies were identified using the visual criteria. Table 5 also provides an outline of TP rate (recall) for each set of cutoffs against the biochemical status.

ML

There were 42 input variables in 96 patients (instances) using a binary classification of hyperthyroid or euthyroid. The heat-map correlation matrix identified several redundant

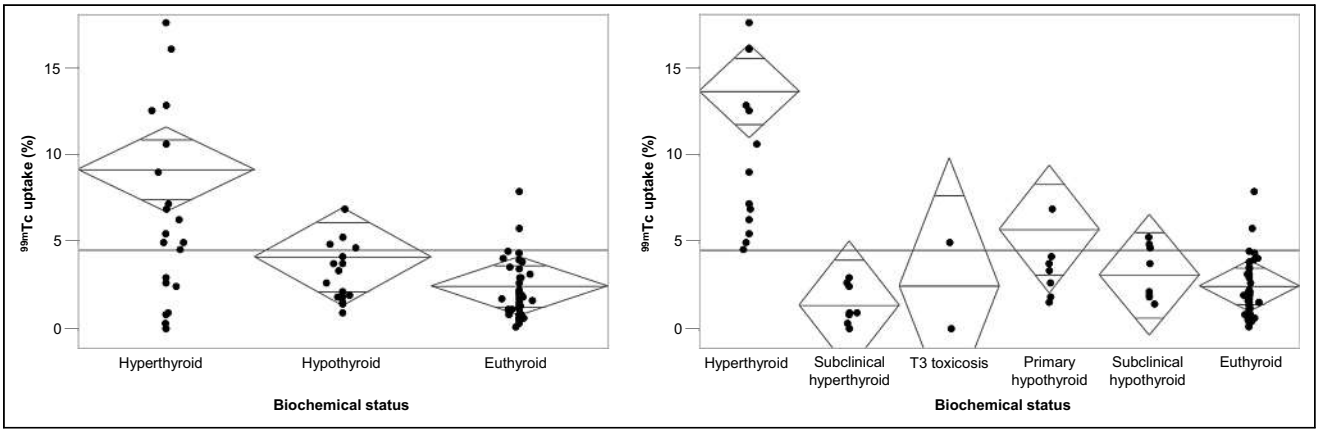

FIGURE 4. (Left) Ternary biochemical status classification against thyroid uptake. (Right) Broader biochemical status classification against thyroid uptake. Horizontal line represents overall mean, and diamonds represent class mean and 95% CIs.

TABLE 5
Ternary Classification of Thyroid Function Based on Recall Against Biochemical Status

Reference range	Euthyroid	Hyperthyroid*	Hypothyroid	Accuracy†
0.45%–4.5%	71.4%	66.6% (100%)	0%	82.6%
0.4%–1.7%	49.0%	74.1% (94.1%)	0%	51.0%
0.4%–4.0%	86.3%	63.0% (94.1%)	0%	77.1%
0.3%–3.4%	74.5%	63.0% (94.1%)	0%	68.8%
0.2%–2.0%	58.8%	74.1% (94.1%)	0%	59.4%
Salivary classification	62.7%	70.3% (94.1%)	0%	61.4%
Physician rating	72.5%	63.0% (89.5%)	0%	61.0%
Physician rating with uptake	88.2%	70.3% (100%)	0%	82.3%

*Data in parentheses exclude subclinical hyperthyroidism and T3 toxicosis.
†Binary accuracy for reference to Table 6.
Accuracy is also provided for binary classification.

variables, and the highest correlation scores were associated with thyroid-stimulating hormone (0.888), appearance of salivary glands on scans (0.627), free T4 (0.575), percentage uptake (0.501), and free T3 (0.491), consistent with the conventional statistical analysis. The network architecture included 16 scaling layer inputs and 3 hidden layers of 6, 4 and 3 nodes. The initial value of the training loss was 1.5473, and the final value after 105 iterations was 0.0172. The initial value of the selection loss was 1.5570, and the final value after 105 iterations was 1.1895.

A growing-inputs method was used to calculate the correlation for every input against each output in the dataset. Beginning with the most highly correlated inputs, progressively decreasing correlated inputs were added to the network until the selection loss increased. The final architecture of the neural network reflected the optimized subset of inputs with the lowest selection loss. In this case, the selection loss and the training loss identified the optimal number of inputs to be 4, with the training loss optimized at 0.0298 and the selection loss being less than 0.0001. The final architecture was 4 scaling-layer inputs; 3 hidden layers of 6, 4, and 1 nodes; an unscaling layer; and a single binary probabilistic layer (Fig. 5).

Several metrics were used to test the final architecture using a subset of the original patient data. Receiver-operator-characteristic analysis demonstrated an area under the curve of 0.933. This correlated with a sensitivity of 100%, a specificity of 80%, and a classification accuracy of 0.846. These results were consistent with scores of 0.60 for precision, 0.75 for F1 score (harmonic mean of sensitivity and precision), 0.693 for the Matthew correlation (correlation between targets and outputs), and 0.8 for the Youden index (probability of a correct decision as opposed to guessing). The cumulative gain analysis demonstrates the benefit of using the developed model over a random guess. On the graph in Figure 6, the positive cumulative gain shows the percentage of positive instances found (y-axis) against the percentage of population (x-axis). Similarly, the negative cumulative gain shows the percentage of negative instances found against the percentage of population. The straight line represents a random classifier. The broader the separation, the better the predictive model. Since the instance ratio provides maximum separation (maximized percentage of positive and negative instances), an instance ratio of 0.40 has a maximum gain score of 0.8. Specifically, but individually, hyperthyroidism is predicted by ^{99m}Tc uptake above 5.7%, free T4 below 20 pmol/L or above 34 pmol/L, free T3 above 9.8 pmol/L, and thyroid-stimulating hormone below 5.5 μIU/mL. In combination, these scaled and weighted input features of the neural network can be expressed mathematically, enhancing the collective predictive capability.

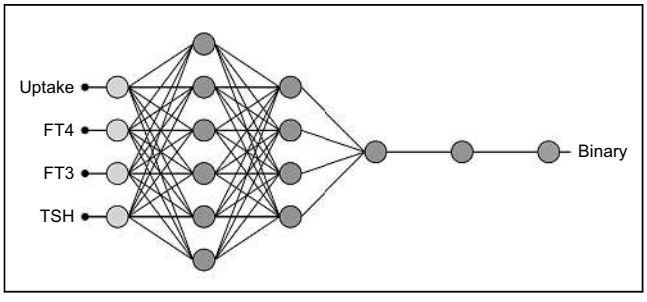

FIGURE 5. Final architecture of trained and validated neural network. TSH = thyroid-stimulating hormone.

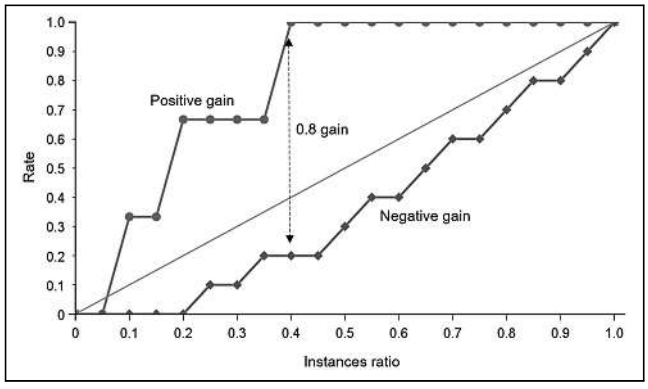

FIGURE 6. Cumulative gain chart demonstrating maximum separation of positive and negative curves to provide cumulative gain score of 0.8 and instances ratio of 0.4 (arrow).

DL

Preliminary network development demonstrated overfitting beyond 30 iterations (epochs); therefore, the maximum epoch number was reset to 30. The results of the triplicated training and validation passes are summarized in Table 6. The variations in validation accuracy reflect the smaller dataset and the random assignment of cases to training and validation. No statistically significant differences (grouped F test) were noted between training and validation accuracy for different types of input tensors ($P = 0.161$ for training accuracy and 0.531 for validation accuracy) despite the higher accuracy for white on black and the lower accuracy for the magnitude spectrum. A direct comparison of white on black against the magnitude spectrum showed P values of 0.068 for training accuracy and 0.280 for validation accuracy.

DISCUSSION

Although thyroid scintigraphy is a well-established technique for the assessment of thyroid function, opinions vary on the role in identifying low versus high thyroid uptake to guide radionuclide therapy. Thyroid scintigraphy is useful in the evaluation of hyperthyroidism to differentiate causes and guide therapy (*14*). Although the specific scintigraphic patterns associated with thyroid pathology do not easily differentiate the biochemical status of the patient (Fig. 7), scintigraphic imaging does provide information useful in identifying patients suitable for radioiodine therapy (*14*). Despite being in widespread use for this purpose internationally, ^{99m}Tc-pertechnetate–based thyroid uptake is not considered suitable in some circles for guiding the therapeutic dosage of radioiodine (*14*). Consistent with the observations of this study, scintigraphy has a limited role in hypothyroidism (*15*).

The challenges and limitations of thyroid scintigraphy are highlighted by poor agreement of physician interpretation. However, with the exclusion of patient history and biochemistry results, the physician interpretation is not done under normal conditions, but for the purpose of this study, the constrained interpretation provides a useful benchmark. Using a thyroid uptake cutoff of 0.45%–4.5%, agreement with physician interpretation was only 63.5%, and using salivary gland appearance, agreement was just 53.1%. Agreement between physicians was not strong, at 59.4%–86.5%, and agreement with biochemistry-grounded truth ranged from 42.7% to 68.8%. This, combined with the poor prediction utility of the salivary gland appearance, contradicts the simplicity of thyroid imaging depicted in Figure 1.

Using the ternary classification of euthyroid, hyperthyroid, and hypothyroid, a thyroid uptake above 4.5% had a sensitivity of 70.8% for detecting hyperthyroidism and a specificity of 88.2%. A thyroid uptake below 0.45% had a sensitivity for hypothyroidism of 0% and a specificity of 95.9%. Specific biochemical classification of hyperthyroidism that excluded T3 toxicosis and subclinical hyperthyroidism improved the sensitivity of the 4.5% cutoff to 100%, with a specificity of 88.2%. This finding highlights the value of thyroid uptake with a cutoff of 4.5% in identifying patients suitable for radioiodine therapy. Given that this goal is the primary one and that scintigraphy has a limited role in hypothyroidism in adults, a binary classification (hyperthyroidism or no hyperthyroidism) provides a more suitable evaluation. The value of an appropriate thyroid uptake cutoff is highlighted in Table 5, which shows that in this

TABLE 6
Triplicate Training and Validation Binary Results (Hyperthyroid or Not Hyperthyroid) for 30-Layer CNN Architecture

Input tensor	Training accuracy	Training loss	Validation accuracy	Validation loss	Mean validation accuracy	Binary accuracy
White on black	82.1%	0.420	75.9%	0.536	80.5%	
	94.0%	0.225	79.3%	0.602		
	91.0%	0.218	86.2%	0.414		
Black on white	83.6%	0.383	82.8%	0.405	78.2%	
	80.6%	0.452	72.4%	0.544		
	91.0%	0.232	79.3%	0.690		
Magnitude spectrum	76.1%	0.459	75.9%	0.530	75.9%	
	74.6%	0.508	72.4%	0.542		
	85.1%	0.306	79.3%	0.380		
Mean	84.2%	0.356	78.2%	0.516		
Initial 25-layer CNN					69.0%	
Conventional metrics						
Normal cutoff, 4.5%						82.6%
Normal cutoff, 4.0%						77.1%
Salivary classification						61.5%
Physician rating						61.0%
Physician rating with uptake						82.3%

Corresponding binary accuracies of best-performing thyroid uptake cutoffs, visual classification against salivary activity relative to thyroid activity, and physician rating are included for comparison.

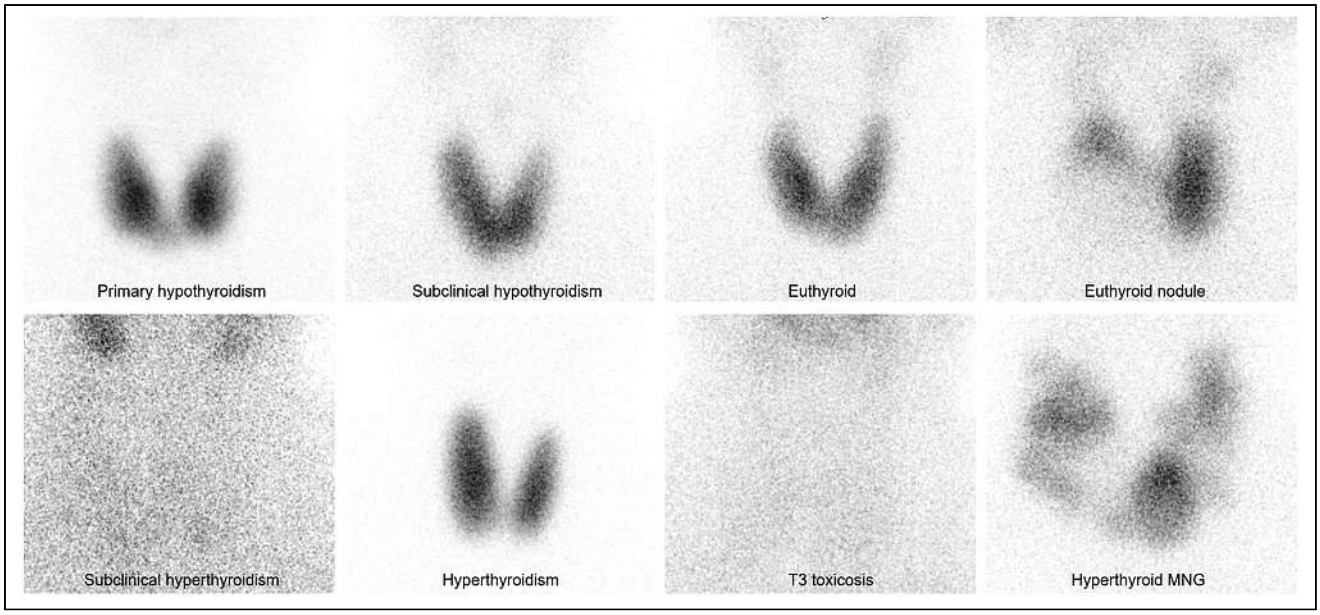

FIGURE 7. Various scintigraphic appearances of thyroid pathology using parallel-hole (high-resolution) collimation and ^{99m}Tc-pertechnetate. MNG = multinodular goiter.

population, binary accuracy was high for a 4.5% cutoff (82.6%) and for physician interpretation augmented by uptake value (82.3%) but was low for salivary gland appearance alone (59.4%) and for masked physician interpretation (61.0%). Indeed, the value and accuracy of 4.5% as the cutoff are reinforced by the similarity in physician interpretation with and without the uptake-augmented information.

Although ML was able to demonstrate improved accuracy to 100%, the algorithm relied on biochemistry not available for physician interpretation. Indeed, the grounded truth relied on the additional value of biochemistry insights to physician insights. In the absence of available biochemistry results, the ML algorithm relies on uptake alone. Conversely, the physician interpretation would improve substantially with the additional insights from biochemistry. In this study, regardless of the apparent performance results, ML augmentation outperformed physician interpretation only because the physician was masked to the biochemistry results available to the ML algorithm. Nonetheless, the role of ML is not and should not be to displace physician reporting but rather to improve accuracy by eliminating error. In this instance, the ML algorithm has been shown to be an accurate second-reader system that can be automated with minimal cost and resources to identify hyperthyroid patients suitable for radioiodine therapy.

In contrast to the success of ML algorithm development, the DL CNN performed more poorly than either the 4.5% cutoff discriminator or the uptake-augmented physician interpretation. The best result was achieved using the white-on-black images (80.5%). Although this result represents only a marginal decrease in performance compared with uptake alone (82.6%) and physician interpretation (82.3%), the CNN was trained on only a single anterior neck image and had no inputs for either the thyroid uptake percentage or the biochemistry results. As a result, the comparative performance should be considered the physician rating without uptake values. In this regard, the 80.5% binary accuracy of the CNN was superior to the physician interpretation (61.0%) and the visual classification against salivary gland appearance (61.5%). Although this result does not suggest displacement of physician interpretation, it does indicate that the accuracy of physician reporting might be improved using the CNN algorithm when biochemistry results are not available.

CONCLUSION

Thyroid scintigraphy is useful in identifying hyperthyroid patients suitable for radioiodine therapy. Physician interpretation relies on an accurate thyroid function assessment (uptake) and an appropriately validated cutoff for the patient population (4.5% in this population). An inappropriate cutoff significantly undermines accuracy. ML ANN algorithms can be developed to improve accuracy as second-reader systems when biochemistry results are available. DL CNN algorithms can be developed to improve accuracy in the absence of biochemistry results. ML and DL do not displace the role of the physician in thyroid scintigraphy but can be used as second-reader systems to minimize errors and increase confidence.

DISCLOSURE

No potential conflict of interest relevant to this article was reported.

ACKNOWLEDGMENT

We thank the 3 physicians who performed the visual analysis of the images. We also thank Hugo Currie from the College of Engineering and Computer Science, Australian

National University, Canberra, Australia, for producing the Fourier magnitude spectrum images for analysis.

KEY POINTS

QUESTION: Can ML and DL approaches improve semantic evaluation of thyroid scintigraphy and uptake in hyperthyroidism?

PERTINENT FINDINGS: ML algorithms can be developed to improve accuracy as second-reader systems when biochemistry results are available. DL CNN algorithms can be developed to improve accuracy in the absence of biochemistry results.

IMPLICATIONS FOR PATIENT CARE: ML and DL do not displace the role of the physician in thyroid scintigraphy but can be used as second-reader systems to minimize errors and increase confidence.

REFERENCES

1. Atkins HL, Richards P. Assessment of thyroid function and anatomy with technetium-99m as pertechnetate. *J Nucl Med.* 1968;9:7–15.
2. Maisey MN, Natarajan TK, Hurley PJ, Wagner HN Jr. Validation of a rapid computerized method of measuring ^{99m}Tc pertechnetate uptake for routine assessment of thyroid structure and function. *J Clin Endocrinol Metab.* 1973;36:317–322.
3. Ramos CD, Wittmann DEZ, de Camargo Etchebehere ECS, Tambascia MA, Silva CAM, Camargo EE. Thyroid uptake and scintigraphy using ^{99m}Tc pertechnetate: standardization in normal individuals. *Sao Paulo Med J.* 2002;120:45–48.
4. Hamunyela RH, Kotze T, Philotheou GM. Normal reference values for thyroid uptake of technetium-99m pertechnetate for the Namibian population. *J Endocrin Metab Diabetes S Afr.* 2013;18:142–147.
5. Macauley M, Shawgi M, Ali T, et al. Assessment of normal reference values for thyroid uptake of technetium-99m pertechnetate in a single centre UK population. *Nucl Med Commun.* 2018;39:834–838.
6. Currie G, Dixon C, Vu T. Validation of a normal range for trapping index in thyroid scintigraphy. *ANZ Nucl Med.* 2004;35:11–16.
7. Currie G, Hawk KE, Rohren E, Vial A, Klein R. Machine learning and deep learning in medical imaging: intelligent imaging. *J Med Imaging Radiat Sci.* 2019;50:477–487.
8. Currie GM. Intelligent imaging: artificial intelligence augmented nuclear medicine. *J Nucl Med Technol.* 2019;47:217–222.
9. Currie G. Intelligent imaging: anatomy of machine learning and deep learning. *J Nucl Med Technol.* 2019;47:273–281.
10. Currie G, Rohren E. Intelligent imaging in nuclear medicine: the principles of artificial intelligence, machine learning and deep learning. *Semin Nucl Med.* 2021;51:102–111.
11. Qiao T, Liu S, Cui Z, et al. Deep learning for intelligent diagnosis in thyroid scintigraphy. *J Int Med Res.* 2021;49:300060520982842.
12. Alswat K, Assiri SA, Althaqafi RMM, et al. Scintigraphy evaluation of hyperthyroidism and its correlation with clinical and biochemical profiles. *BMC Res Notes.* 2020;13:324.
13. Wagieh S, Salman K, Bakhsh A, et al. Retrospective study of Tc-99m thyroid scan in patients with Graves' disease: is there significant difference in lobar activity? *Indian J Nucl Med.* 2020;35:122–129.
14. Mariani G, Tonacchera M, Grosso M, Orsolini F, Vitti P, Strauss HW. The role of nuclear medicine in the clinical management of benign thyroid disorders, part 1: hyperthyroidism. *J Nucl Med.* 2021;62:304–312.
15. Mariani G, Tonacchera M, Grosso M, et al. The role of nuclear medicine in the clinical management of benign thyroid disorders, part 2: nodular goiter, hypothyroidism, and subacute thyroiditis. *J Nucl Med.* 2021;62:886–895.

Thyroid Uptake Exceeding 100%: Causes and Prevention

Dhrumil Naik[1], Sarah Ternan[2], Rene Degagne[2], Wanzhen Zeng[2,3], and Ran Klein[2,3]

[1]*Department of Mechanical Engineering, University of Ottawa, Ottawa, Ontario, Canada;* [2]*Department of Nuclear Medicine, The Ottawa Hospital, Ottawa, Ontario, Canada; and* [3]*Division of Nuclear Medicine, Department of Medicine, University of Ottawa, Ottawa, Ontario, Canada*

Measurements of radionuclide uptake by the thyroid gland reflect its metabolic activity. Thyroid uptake is measured as a percentage of radioactivity retained by the gland at a specified time versus the activity administered to the patient; thus, uptake measurements must fall between 0% and 100%. Here, through a case study, we reviewed sources of error that can lead to uptake of more than 100%, and we describe a novel quality control (QC) indicator to improve the accuracy of uptake measurements in the clinic. **Methods:** Probe efficiency is determined as the ratio between the dose counts of the probe and the independent dose calibrator activity readings. The nominal probe efficiency value (M) was calculated as the mean of readings ($n \geq 20$), and variance was characterized using the SD. Warning levels were set at M $\pm$ (1.96 $\times$ SD), and error levels were set at M $\pm$ (2.58 $\times$ SD). In subsequent routine clinical use, before a capsule is administered, the probe efficiency is calculated and compared with the warning and error limits. We derived M for 3 pairs of probe and dose calibrator devices using several doses and measured independently by several nuclear medicine technologists. **Results:** The recorded data indicated when technologists were made aware of the expected efficiency value, nominal efficiency was statistically different between our old device and the one that replaced it ($P = 0.01$), but coefficient of variation ([SD/M] $\times$ 100%) was not ($P = 0.42$). Using efficiency measurements acquired on the replacement device for the first 20 patients, we derived new QC values (M = 910, SD = 36). In 22 patients measured at our sister site, with the same device models but with the technologists unaware of the QC initiative, the derived QC values were an M of 1,025 and an SD of 116, demonstrating a significant difference between the nominal values of individual devices ($P < 0.001$). Furthermore, variability was significantly lower ($P < 0.001$) when QC was applied than when it was not. **Conclusion:** Adding probe efficiency as a QC indicator during thyroid uptake measurement is simple, can produce more precise clinical measurements, and can help mitigate operator and instrumentation errors.

Key Words: thyroid uptake; radionuclide; quality control

J Nucl Med Technol 2022; 50:153–160
DOI: 10.2967/jnmt.121.262719

Measurements of radionuclide uptake by the thyroid gland reflect its metabolic activity as well as the iodine handling and kinetics in the thyroid tissue. Such measurements show the fraction of radioactivity in the neck relative to that administered to the patient, with a predetermined time between measurement and administration (e.g., 24 h) (*1*). ^{131}I- and ^{123}I-sodium iodide, either in capsule or liquid form, is commonly used as the radiopharmaceutical for thyroid uptake determination. Clinical applications for this procedure include differentiation of hyperthyroidism associated with thyroid dysfunction (e.g., Graves disease or multinodular goiter) from other forms of thyrotoxicosis, such as subacute thyroiditis, and calculation of the activity of radioiodine (^{131}I) to be administered for treatment (*2*). Because thyroid uptake is measured as a percentage of radioactivity retained by the gland at a specified time versus the activity administered to the patient (time = 0), uptake measurements must fall between 0% and 100%.

The basic procedure involves 4 steps (Fig. 1). First, the room background activity and administered activity are measured using a γ-counting probe, with the radioiodine dose positioned in a dedicated neck phantom. Duplicate measurements, including repositioning of the probe, are taken to avoid positioning errors, indicated by discrepant count rates between measurements. Highly discrepant dose counts (e.g., >10%) are investigated and addressed immediately to avoid propagation of errors. Second, the entire activity is administered orally to the patient. Third, at a predetermined time (e.g., at our institution, 24 h after administration), the patient returns for the uptake measurement, and the thyroid and patient background (thigh) counts are measured using the same γ-counting probe. Duplicate measurements, including repositioning of the probe, are taken to avoid positioning errors, indicated by discrepant count rates between measurements. Fourth, if the repeat counts match, the corresponding background measurements are subtracted and radionuclide decay correction is applied. The ratio of net uptake count rate to net administered count rate is the measured thyroid uptake, as shown in the following equation, in which the overbars represent the average of multiple repeat measurements.

$$\text{Percentage uptake} = 100\% \times \frac{\overline{\text{uptake}} - \text{patient background}}{\left(\overline{\text{administered}} - \text{room background}\right) \times \text{radionuclide decay}} \quad \text{Eq. 1}$$

Modern probes are equipped with software to track the measurements and perform the thyroid uptake calculation automatically.

Received Jun. 16, 2021; revision accepted Oct. 8, 2021.
For correspondence or reprints, contact Ran Klein (rklein@toh.ca).
Published online Dec. 6, 2021.

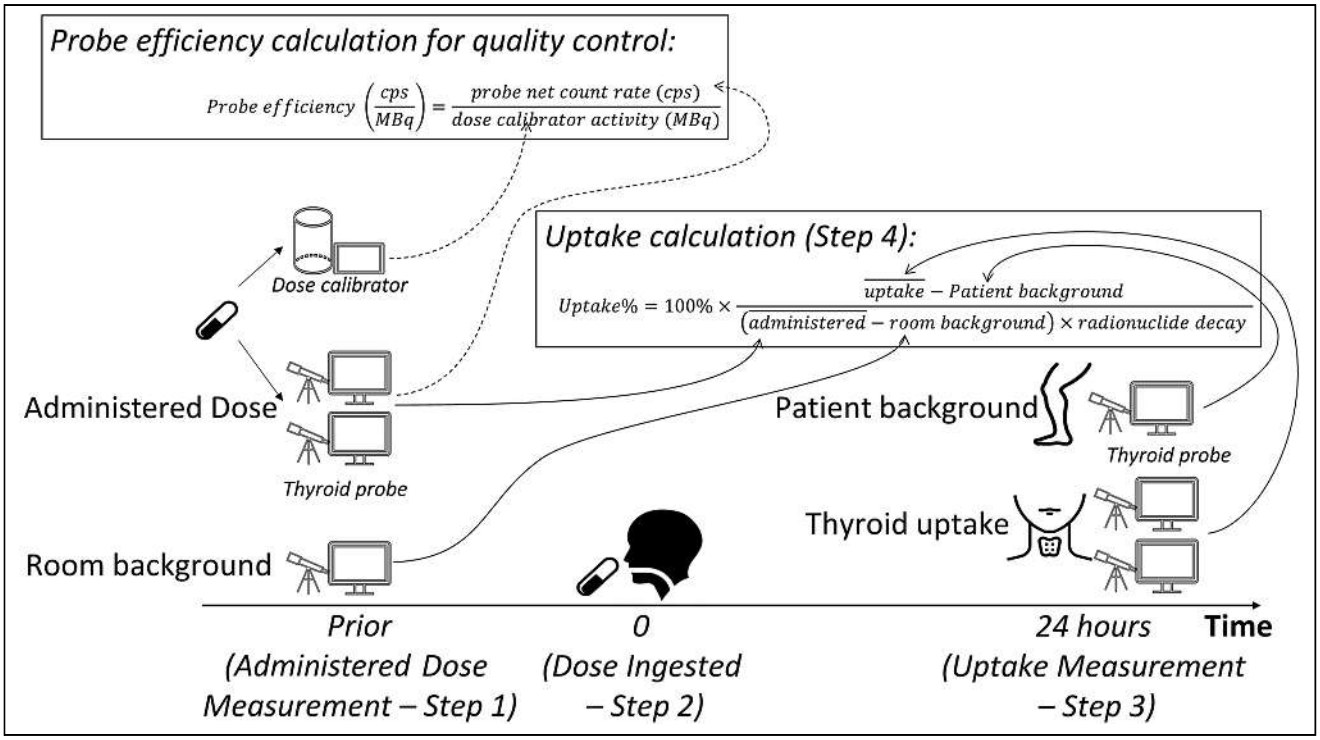

FIGURE 1. Thyroid uptake workflow diagram. At time 0, patient ingests dose of radioiodine that was measured at a prior time using thyroid probe. At 24 h after ingestion, patient returns to department for thyroid uptake measurement using same thyroid probe. Room and patient background measurements are performed with probe at time of dose and thyroid uptake measurements, respectively, for background subtraction before uptake ratio is calculated as percentage. Optional measurement of administered dose with dose calibrator can be used to calculate probe efficiency to be used for QC.

Because thyroid uptake relies on 2 measurements (steps 1 and 3) with few redundancies, quality assurance practices are essential to have confidence in the final reading. The counting technique is an important step, as the technique should include appropriate centering, distance, and positioning of the radiation-counting probe, thyroid phantom, and patient. The technique should be reproducible by technologists to ensure accuracy, and thus all counting should be performed in duplicate. Counting time should be set to a minimum of 60 s to ensure adequate photon-counting statistics (*2*). Finally, before the initial dose or uptake measurements, QC must be performed on the probe, including constancy to ensure that day-to-day counting efficiency is consistent.

Despite these quality initiatives, errors can and do occur. When thyroid uptake values exceed 100%, it is obvious that an error has occurred, but errors may not be detected if uptake values do not significantly deviate from the expected range (by other clinical indicators). Recently, a patient (patient 1) with known hyperthyroidism was referred to our clinic for thyroid uptake measurement and scanning before ^{131}I therapy. The thyroid uptake was measured at 139% at 24 h. This event triggered an investigation by our local quality assurance committee, was discussed at our departmental mortality-and-morbidity rounds, and resulted in corrective actions.

Our clinic consisted of 2 sites, each performing ^{131}I uptake measurements using Captus 3000 γ-probes (Capintec) that had reached the end of support by the manufacturer but were regularly maintained by our local biomedical engineering team. During the time in question, one of the machines was deemed unserviceable (site 1), and while a replacement was being procured, all patients were referred to our other site (site 2), which had a device of the same make and model. QC procedures consisted of routine maintenance and daily constancy tests performed according to manufacturer and professional society guidelines.

On the day that patient 1 was seen, 2 other patients were also referred to the clinic, and all 3 ^{131}I capsules (370 kBq) were measured in a single session in a CRC-55t dose calibrator (Capintec) and using the probe (2 duplicate measurements with room background subtraction). All 3 patients received their assigned capsule and returned for a 24-h uptake measurement, consisting of duplicate thyroid measurements and duplicate thigh measurements as patient background. The results are summarized in Table 1. The original results for patient 1 were clearly erroneous, exceeding 100% uptake, and thus the department physician and technologists immediately started an investigation while the patient was still present. Later that day, the reporting physician flagged the results of patients 2 and 3 as also being suspiciously high, on the basis of other clinical information. Thus, we suspected a technical error and investigated the following possible sources of error (*2*):

TABLE 1
Thyroid Uptake Using ^{131}I Capsules for 3 Patients

	Dose calibrator		Probe							24-h uptake	
Patient no.	Activity (MBq)	Time	Count 1 (cps)	Count 2 (cps)	Room background counts (cps)	Net capsule counts (cps)	Time	Room background time	Probe efficiency (cps/MBq)	Original (%)	Adjusted (%)
1	0.420	9:16	213	210	1	211	8:26	8:23	501	139.6%	71%
2	0.435	10:35	214	216	1	214	8:29	8:23	490	34.8%	18%
3	0.388	9:08	208	206	1	206	13:24	8:23	534	47.0%	24%

Original 24-h thyroid uptake results are shown along with their corresponding adjusted values after compensating for deviations in probe efficiencies from previous patients (Table 2). Time is expressed as time of day (hr:min).

Operator error at thyroid measurement: During the 24-h visit of patient 1, uptake measured was confirmed by 2 independent measurements by 2 other technologists (3 measurements in total, agreeing within 5% of each other), including repeat measurements after removal of clothing. The patient returned for repeat uptake measurements at 48 and 192 h, and the measurements were 138% and 146%, respectively, indicating reproducible high uptake and trapping of the activity (i.e., no washout).

Operator error at radioiodine dose measurement: The process to measure radioiodine capsule counts was simulated with the technologist who had measured the 3 ^{131}I-capsules on the day in question. That technologist has over 20 y of experience and demonstrated proficiency in the procedure. No cognitive errors were identified. Furthermore, as expected, the count rates for all 3 capsules matched, as all 3 capsules were ordered to have the same activity (~370 kBq [10 μCi]) and were from the same batch (Table 1). The 3 capsules were measured sequentially without repositioning of the probe or phantom between capsules.

Background measurements: The room and patient background should be measured near the time that the corresponding administered dose and thyroid measurements are done, respectively. Failure to do so increases the risk of inaccurate background readings that do not reflect changes in the environment in the ensuing time. The results of our case study (Table 1, patient 3) revealed a previously unidentified methodologic error in our clinical practice in which a single background measurement may be used for multiple doses measured hours apart. This practice is unlikely to be a significant source of error in this case, as the probe is housed in an area isolated from the main nuclear medicine department and with low patient traffic. Nevertheless, we have since revised our clinical protocol to state that all doses must be measured within 15 min of the corresponding background reading.

Instrumentation settings: The physicist of the Department of Nuclear Medicine was present for the 48-h assay and verified that the system settings were consistent with the department protocol.

Instrumentation QC: QC logs were reviewed for the probe and indicated consistent and in-range daily QC metrics over the week preceding and the week succeeding the dose administration. In our clinic, QC is performed according to manufacturer recommendations (*3*). Two reference sources (^{137}Cs and ^{152}Eu) are measured daily for energy calibration and precision, linearity, and efficiency constancy. Quarterly, we also perform χ^2 testing of the counting performance of the system and test the minimal detectable dose.

Patient contamination: At 48 h, the physicist reviewed the emission spectrum from the thyroid assay and confirmed that the emission spectrum matched that of ^{131}I, with no indication of contamination from other radioisotopes, and that low counts were present in the patient background reference region. Furthermore, radioactive contamination was ruled out by our radiation safety physicists by biologic assay of the patient and the patient's spouse at 9 d after administration using a separate γ-counting probe. Thus, internal radioactive contamination was ruled out.

Correlation with prior measurement: The patient had a prior thyroid uptake measurement performed 32 mo earlier, measuring 51%.

Correlation with imaging: On the day of, and before, ^{131}I administration, the patient was imaged with ^{99m}Tc-pertechnetate and a pinhole collimator. The images appeared to be visually similar between the 2 studies (Fig. 2); however,

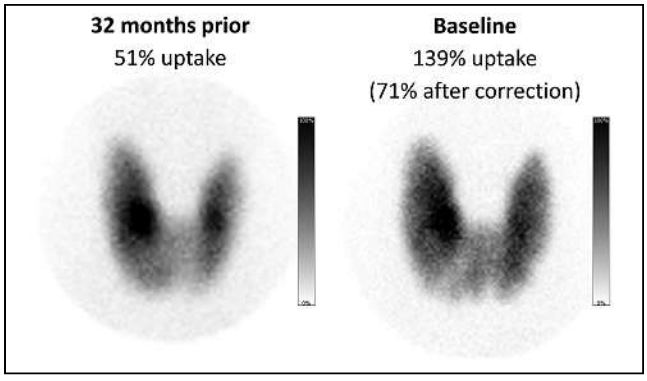

FIGURE 2. ^{99m}Tc-pertechnetate uptake images of patient 1 at time of investigation (baseline) and 32 mo prior to that time. Image intensities were manually normalized to have similar contrast. Biodistribution is similar, contradicting large thyroid uptake change between time points.

a quantitative comparison of ^{99m}Tc-pertechnetate uptake could not be conducted, as these images were acquired using different imaging devices (camera and collimator).

Eventually, we identified a loose contact in the cable between the probe head and the data acquisition card of the device. How long this fault went unnoticed, and its implications on prior measurements, can only be conjectured. This fault was subsequently repaired by biomedical engineering staff and was followed by necessary calibration and QC, including χ^2 testing.

To understand the potential implications regarding the 3 patients, we evaluated probe efficiency as the ratio of probe counts to dose calibrator readings using Equation 2 and as shown in Table 1. We compared these results with those of 14 previous patients in our clinic data (Table 2).

$$\text{Probe efficiency}\left(\frac{\text{cps}}{\text{MBq}}\right)=\frac{\text{probe net count rate (cps)}}{\text{dose calibrator activity (MBq)}} \quad \text{Eq. 2}$$

Although we could not definitively determine the reason (e.g., probe physical configuration or instrumentation failure) for the change in geometric efficiency of the probe during capsule readings on that day, they appeared to be off by a fixed factor. We applied the ratio of efficiencies of the 2 cohorts to adjust the 24-h uptake using Equation 3, which aligned with the clinical histories of all 3 patients.

$$\text{Adjusted 24-h uptake (\%)} = \text{original 24-h uptake (\%)} \times \frac{\text{current average probe efficiency}\left(\frac{\text{cps}}{\text{MBq}}\right)}{\text{previous average probe efficiency}\left(\frac{\text{cps}}{\text{MBq}}\right)} \quad \text{Eq. 3}$$

Nevertheless, we decided to replace this aging machine at site 2 with the same make and model as had been ordered for site 1. Furthermore, we began to implement new QC practices to mitigate similar risks in the future.

The purpose of the current study was to develop a QC method to mitigate errors when measuring radioiodine doses before their administration to the patient. We provide a detailed explanation of the method so that it can be applied by others. These methods include routine measurement of probe efficiency as part of the clinical workflow and comparison to prederived warning levels and error levels to initiate timely action by technologists, physicists, and biomedical engineering staff. We also explain how to derive the warning and error levels, and we provide a spreadsheet for data collection and calculations.

MATERIALS AND METHODS

As a clinical quality assurance study, this retrospective study was approved by the Institutional Research Ethics Board, and the requirement to obtain informed consent was waived.

After our recent upgrade, thyroid uptake measurements were again performed at our 2 sites, using identical thyroid uptake systems (Captus 4000e; Capintec) applying 60-s acquisitions with a 364 keV ± 10% photopeak energy window, and count rates were reported in units of counts per second (cps). To determine these devices' counting efficiencies, the activities of several ^{131}I-NaI capsules were measured in the respective site's dose calibrator. The dose calibrators (Capintec CRC-25 and Capintec CRC-55t) were previously calibrated to a reference standard. Next, the ^{131}I-NaI capsules were measured independently several times by several technologists in duplicate, and with room background count subtraction applied by the probes as would be performed clinically using the neck phantom holder.

TABLE 2
^{131}I Capsule Activity, Probe Net Capsule Count, and Probe Efficiency Results at Clinic for Previous Patients

	Dose calibrator		Probe						
Patient no.	Activity (MBq)	Time	Count 1 (cps)	Count 2 (cps)	Room background counts (cps)	Net capsule counts (cps)	Time	Room background time	Probe efficiency (cps/MBq)
4	0.370	9:22	474	477	1	475	11:33	11:16	1,287
5	0.383	10:35	466	464	1	464	13:26	11:16	1,217
6	0.310	10:45	294	294	3	291	10:43	10:16	939
7	0.290	8:42	286	281	3	281	8:39	8:06	967
8	0.350	9:20	353	349	1	350	15:20	15:18	1,009
9	0.420	13:44	410	408	3	406	10:51	10:16	962
10	0.390	9:40	389	389	4	385	9:31	8:18	987
11	0.410	9:00	362	366	4	360	8:57	8:18	878
12	0.305	10:53	265	269	4	263	10:30	10:24	862
13	0.292	10:10	280	280	3	277	10:07	9:56	949
14	0.302	9:11	271	272	4	268	9:15	8:50	886
15	0.350	11:30	346	346	3	343	10:55	10:52	979
16	0.389	10:30	402	406	3	401	10:05	9:41	1,030
17	0.360	9:02	355	348	3	349	8:59	8:35	968

Time is expressed as time of day (hr:min).

TABLE 3
Example QC Limits for Probe Efficiency with 3 Levels

Level	Lower limit	Upper limit	±range
Pass	808	955	8%
Warning	784–807	956–978	11%
Error	<783	>979	—

Data are cps/MBq for baseline QC (Site2Old).

Probe efficiencies were calculated for each probe measurement as in Equation 2. The nominal probe efficiency value (M) was calculated as the mean of all readings. Because count statistics follow a Poisson distribution and are sufficiently high (~18,000), a gaussian distribution was assumed; therefore, efficiency variance was characterized using the SD of all measurements (*4*). Warning levels were set at M ± (1.96 × SD), and error levels were set at M ± (2.58 × SD) (Table 3), corresponding to an expected false-positive rate of 5% and 1% of capsule measurements, respectively (*5*). The ratio of the SD to the mean is referred to as the coefficient of variation (CV) and expressed as a percentage. Thus, warning and error levels can be expressed as a percentage of the nominal value or in absolute units (cps/MBq).

We determined the nominal probe efficiency, warning levels, and error levels for 3 devices: site 1, new device (Site1New); site 2, old device (Site2Old); and site 2, new device (Site2New). For Site1New, data were acquired from routine clinical worksheets in which no QC was performed on efficiency measurements. These data served as a baseline sample of the variability of the efficiency when QC is not performed. For Site2Old, technologists were explicitly instructed to perform multiple test measurements using multiple capsules on multiple days using the old probe (Captus 3000). In this case, the technologists were aware of the test being performed and paid attention to the expected probe count rates. These data were used to derive a baseline measure of nominal efficiency and its variability. For Site2New, data were collected from routine clinical worksheets in which QC was performed by the technologists on the efficiency measurements using warning and error limits derived from Site2Old (because the nominal values for these machines were similar in preliminary measurements).

In subsequent routine clinical use, before a capsule was administered, the probe efficiency was calculated in the same manner as during calibration and using Equation 2. The calculated efficiency was then compared with the warning and error limits posted at the corresponding site for the probe and dose calibrator used (Table 3). Directives on how to handle pass, warning, and error events were also posted and are detailed in the "Discussion" section.

The difference between nominal values for different devices was tested for statistical significance using a Student unpaired *t* test (*6*). Likewise, differences in percentage CV were evaluated using an *F* test. A *P* value of 0.05 was used as a cutoff for statistical significance.

RESULTS

Mean and percentage CV probe efficiencies are summarized in Table 4 for the 3 devices. Baseline efficiency estimates (Site2Old) consisted of 29 independent samples measured by 7 technologists, using 6 capsules on 6 separate days. The CV was 4%, resulting in the warning and error levels shown in Table 3. These exceeded the variability expected from count statistics alone (~0.5%). Using these baseline QC limits as estimates for the new device at the same site (Site2New), 20 routine clinical patients were worked up. The recorded data indicated that nominal efficiency significantly differed between these 2 devices ($P = 0.01$) but percentage CV did not ($P = 0.42$); new QC limits were derived from these data for subsequent QC testing in the clinic.

The 22 participants who received a thyroid uptake measurement at site 1 (M = 1025, SD = 116), compared with the 20 participants at site 2 (M = 910, SD = 36), demonstrated a significant difference between individual machines ($P < 0.001$) with regard to nominal values, further justifying that specific QC limits were required for each device. Furthermore, in the absence of QC indicators at this site, variability was nearly 3 times greater (CV = 11% vs. 4%).

DISCUSSION

In this work, we set out to enhance the QC of thyroid uptake measurements by ensuring that 2 independent measurements of the dose administered to the patient are consistent: probe count rate and dose calibrator reported activity. We concluded that in our clinical practice, 4% CV was achievable, corresponding to approximately 8% and 10% warning

TABLE 4
Comparison of Probe Efficiencies and Their Variability for 3 Devices (and Practices)

Device	*n*	Nominal efficiency (cps/MBq)	Measured CV	Comment
Site2Old	29	881	4%	QC limits derived with explicit test measurements that served as QC estimates for Site2New
Site2New	20	910*	4%	From clinical data using QC estimate from Site2Old as guideline
Site1New	22	1,025*	11%*	From clinical data without using any efficiency QC

*$P < 0.05$ in comparison to Site2Old.

and error limits, respectively, associated with 95% and 99% CIs, respectively. In other words, using these error and warning limits, we expect to experience false-warning and false-error limits for 1 of every 20 and 100 tests, respectively. These would trigger further investigation, which would be resolved before the dose is administered to the patient and therefore would lead to higher confidence in the final clinical results. It is possible that with further emphasis on QC, the variability (percentage CV) can be further decreased toward more precise thyroid uptake measurements.

We, like others previously (*2*), identified several possible sources of error in high thyroid uptake. We included this detailed description to guide readers in the event that they need to investigate a similar incident in their own clinic. Table 5 highlights a more complete list of potential sources of errors and means to mitigate their occurrence and propagation. However, for our enhanced QC, we focused on the preadministered dose measurement because it is a single point of failure that cannot be conclusively investigated after administration. Erroneous measurements of thyroid activity, on the other hand, can be investigated within several hours, assuming they are caught early enough.

An important finding in this work is that counting efficiencies vary between devices, even of the same make and model, and that nominal values and limits therefore must be determined for each pair of devices (probe and dose calibrator) unless explicit calibration is performed. An additional key finding is that QC testing of efficiency can reduce the variability in clinical practice, as demonstrated by the percentage CV between Site1New and Site2New,

TABLE 5
Potential Sources of Error Leading to Erroneous Thyroid Uptake Measurements

Error source	Means to mitigation of error
Operator	
Probe misalignment during dose assay	Review efficiency against dose calibrator activity measurement; review count rate against typical values for similar dose
Probe misalignment during room background assay	Use phantom and probe ruler, reproducing positioning for dose assay; ensure low count rate consistent with background radiation
Probe misalignment during uptake assay	Palpate for thyroid location; use probe ruler, repositioning between duplicate measures to verify consistency; cross-validate with other time points; cross-validate with imaging
Probe misalignment during patient background assay	Use probe ruler; ensure low count rates; investigate high count rates, including patient or clothing contamination
Wrong uptake time	Preschedule visits according to protocol; use automated time logging by probe software; record all steps in clinical worksheet or software
Wrong dose	Label doses with patient identifiers; verify matching of patient using multiple identifiers; view energy spectrum to confirm correct isotope
Wrong patient	Confirm multiple patient identifiers against software-recorded entry or clinical worksheet; use electronic patient worklist
Instrumentation	
System malfunction	Ensure appropriate QC using quality management system; clearly label and communicate system serviceable status
Clock error	Configure time server synchronization
Acquisition setting error	Use predefined acquisition protocols; password-protect software administrator settings, including protocol settings
Patient	
Motion	Monitor patient during acquisition; repeat acquisition if patient has moved
Incomplete ingestion or vomiting	Monitor patient at dose administration; debrief patient before uptake acquisition
Missed appointment	Time-stamp all patient encounters and counting of administered dose; consider delaying or repeating procedure if there is erroneous uptake time
Internal or external contamination	Inspect energy spectrum for signs of other isotopes; review patient history for exposure to radionuclides (previous medical procedures and occupational or environmental exposures); apply energy windowing
Changes in health	Implement intake questionnaire; review adherence to preparation instructions; correlate with other medical data (*1*)
Diet	Follow societal guidelines for patient preparation, including abstinence from foods high in iodine (e.g., kelp) (*1*)
Medication	Follow guidelines for patient preparation, including extensive list of medications and iodinated contrast agents that interfere with thyroid uptake (*1*); review patient list of medications and medical history
Environmental (background radioactivity)	Remove potential sources of radiation, including from neighboring rooms (e.g., patients, x-ray equipment); use radioiodine-appropriate energy window; ensure that background is measured near time of assay, and QC for low background count rates

which were measured without and with QC, respectively. Obvious sources of variability that should be investigated when QC fails are transcription errors; probe, phantom, or source positioning; and changes in or malfunctioning of the instrumentation.

Radioactive Decay Correction

Probe efficiencies were calculated using Equation 2. This simple calculation ignores radioactive decay, as is acceptable if the dose calibrator and probe measurements are within 1 h of each other and if ^{131}I is used, which has a physical half-life of 8 d (*7*). For shorter-lived isotopes or delays between dose calibrator and probe measurements, a decay correction may be required.

Clinical Application

To apply the proposed QC process in a clinical setting, we propose the following instructions, with tailoring to the clinic's specific workflow and constraints. These instructions comprise 2 sequential steps: determination of QC limits and routine QC.

Determination of QC Limits. For each probe and dose calibrator pair, nominal efficiency values and tolerances must be determined by repeat measurement of sample capsules in a manner that represents the clinical workflow. Considerations include repeat measurements by different technologists on different days and using several doses that span the range of activities used in the clinic for the procedure. The exact methodology will vary depending on the number of technologists in the clinic, but we recommend 30 independent measurements, with 20 as a minimum to ensure adequate statistical power. Using the methods described in the "Materials and Methods" section, the nominal value and tolerances can be determined and posted in the laboratory for routine QC. An example of this QC table can be seen in Table 3. Other, clearly marked, variants—including the use of color, graphics, and accompanying instructions—should be considered in consultation with the technologist team to ensure optimal communication of new QC practices. A sample Microsoft Excel worksheet to derive QC limits from experimental data is provided as supplemental material (available at http://jnmt.snmjournals.org).

Routine QC. During clinical operations, each dose must be measured using a dose calibrator and then using the probe with the neck phantom. The ratio of probe counts to the dose calibrator reading must be calculated as in Equation 2, and the value must be compared with a table as demonstrated in Table 3.

Three possible scenarios arise. In the first, QC passes when the calculated efficiency is between the 2 warning levels. The clinical procedure should proceed as normally. In the second, there is a QC warning when the calculated efficiency is between a warning level and an error level (low or high). The work should be checked or repeated, including by an independent trained clinical staff member. If QC remains at a warning level, the clinical work should proceed if required (e.g., if there are workflow constraints or patient has traveled a great distance), but the physicist, quality manager, or biomedical engineering should be notified of the warning for further investigation. Also, the reporting physician should be notified. In the third scenario, a QC error occurs when calculated efficiency exceeds either lower or upper error levels. If the source of error cannot be identified and corrected, the capsule should not be administered to the patient until the physicist, quality manager, or biomedical engineering has been made aware of the error, has investigated the error, and has resolved the issue.

Liquid Iodine

In our clinic for diagnostic procedures, we currently use radioiodine in capsule form at a single dosage. Nevertheless, the same procedure may be applied to liquid form by preparing representative samples and measuring them both with the dose calibrator and with the probe. However, special accommodations may be necessary, including accounting for changes in the geometric efficiencies of the probe and dose calibrator, depending on the container and liquid volume (*8*).

Furthermore, one should ensure that a consistent efficiency factor is achieved across the entire range of activities used (e.g., if performing uptake measurement using therapeutic doses). This assurance requires that both systems operate in a linear range across the full range of activities and that probe dead times remain below approximately 2%. If greater dead-time factors must be accommodated, a more complicated, activity-dependent efficiency curve may be required.

Strengths and Limitations

These additional QC practices can be implemented in a routine clinical setting with little impact on workflow. This QC provides an extra layer of assurance to boost confidence in the validity of the thyroid uptake results. However, it is important to appreciate a remaining limitation: if the probe efficiency varies between the day of capsule measurement and the day of patient uptake (e.g., 24 h later), erroneous thyroid uptake measurements may still result and go undetected. Therefore, daily QC testing of the probe, including constancy, is still essential to achieve high-quality thyroid uptake measurements.

In this work, we do not report on QC outcomes in our clinic after full implementation of this QC procedure. There have been too few data for meaningful analysis to date (14 at site 1 and 10 at site 2), although none of the data have resulted in warning or error events that triggered investigations by our QC team.

At our institution, thyroid uptake is typically measured at 24 h after oral administration of an ^{131}I capsule. Ideally, the thyroid uptake should be measured at multiple time points to accurately characterize the biologic process, including identification of patients with a rapid turnover time with higher uptake at 4 or 6 h. Acquiring data at these additional

time points may also benefit QC and investigation of anomalous measurements. Likewise, ^{99m}Tc-pertechnetate count rate measurements from the imaging studies may have aided investigation in the case study, but quantitative comparison was hampered by the use of different devices between time points. Use of standardized imaging equipment and protocols within the clinic is therefore advised whenever possible.

CONCLUSION

Thyroid uptake measurements can be prone to operator and instrumentation errors that cannot be detected without QC testing. The ratio between dose counts of the probe relative to independent dose calibrator activity readings is a simple QC indicator that can readily be applied in a clinic to reduce such errors.

KEY POINTS

QUESTION: Can a thyroid probe efficiency test serve as a QC measure toward accurate thyroid uptake measurements?

PERTINENT FINDINGS: Before the radioiodine dose is administered to a patient, the dose can be used to test the thyroid probe–reported count rate against the dose calibrator–reported activity to identify errors exceeding approximately 10%. Many other potential sources of error can facilitate investigation of anomalous thyroid uptake measurements.

IMPLICATIONS FOR PATIENT CARE: This quality assurance measure can easily be implemented in a nuclear medicine clinic to improve quality and confidence in thyroid uptake measurements.

DISCLOSURE

Ran Klein receives revenue shares from the sale of rubidium generators from Jubilant-DraxImage and from the sale of myocardial flow quantification software from Invia Medical Solutions. No other potential conflict of interest relevant to this article was reported.

ACKNOWLEDGMENTS

We thank the staff of the Department of Medicine at The Ottawa Hospital for their collaboration in investigating this case and for their ongoing support in improving quality in our department.

REFERENCES

1. Giovanella L, Avram AM, Iakovou I, et al. EANM practice guideline/SNMMI procedure standard for RAIU and thyroid scintigraphy. *Eur J Nucl Med Mol Imaging.* 2019;46:2514–2525.
2. Thomas KS, Alessi AM, Hall A. Thyroid uptake exceeding 100%: how is that possible? *J Nucl Med Technol.* 2019;47:213–214.
3. *Captus® 4000e Thyroid Uptake System Manual: Revision J*. Mirion Technologies (Capintec); 2020:69–94.
4. Dekking FM, Kraaikamp C, Lopuhaä HP, Meester LE, eds. *A Modern Introduction to Probability and Statistics: Understanding Why and How*. Springer; 2005:404–405.
5. Hazra A. Using the confidence interval confidently. *J Thorac Dis.* 2017;9:4125–4130.
6. Kim TK. T test as a parametric statistic. *Korean J Anesthesiol.* 2015;68:540–546.
7. Amdur RJ, Mazzaferri EL. Half-life and emission products of I-131. In: Amdur RJ, Mazzaferri EL, eds. *Essentials of Thyroid Cancer Management.* Springer; 2005:165–168.
8. Halpern S, Alazraki N, Littenberg R, et al. ^{131}I thyroid uptakes: capsule versus liquid. *J Nucl Med.* 1973;14:507–510.

Monitoring the Occupational Radiation Exposure of an Individual at Multiple Institutions

Sarah Frye[1], Alyssa Reynolds[1], Crystal Botkin[1], Razi Muzaffar[2], and Medhat M. Osman[2]

[1]*Department of Clinical Health Sciences, Doisy College of Health Sciences, Saint Louis University, St. Louis, Missouri; and* [2]*Division of Nuclear Medicine, Department of Radiology, Saint Louis University, St. Louis, Missouri*

Within a few years of its discovery, ionizing radiation demonstrated adverse effects on biologic systems. Since that time, great strides have been made in radiation protection, detection, and personnel monitoring. Monitoring of the occupational radiation dose to individuals is enforced by several regulatory agencies in the United States and is referenced in numerous sections of the *Code of Federal Regulations*. A literature review with an examination of regulatory guidelines and a radiation safety officer survey was conducted to evaluate how often radiation exposure is monitored when an individual receives occupational radiation doses at more than one facility. The length of time a radiation safety officer has overseen the radiation safety program at an institution can impact whether dosimetry reports are requested for individuals who work at multiple places. Despite having safer equipment and occupational radiation exposure standards, there is no universal mechanism to track and record exposure for individuals working at more than one institution.

Key Words: NRC; OSHA; occupational radiation exposure; RSO; radiation safety

J Nucl Med Technol 2022; 50:161–165
DOI: 10.2967/jnmt.120.243154

Occupational radiation exposure must be monitored, regulated, and accurately reported. Individuals exposed to radiation and radioactive materials are routinely monitored with different types of radiation dosimetry badges; these individuals include those working in radiology. Radiology employees may be exposed to radiation from machines, patients, and sealed and unsealed radioactive sources (*1*). When individuals working in radiology are employed by multiple institutions, it is important the individuals' cumulative radiation dose be monitored and accurately recorded at each facility. With the variety of imaging equipment, diagnostic nuclear tracers, therapeutic nuclear tracers, and theranostics being used in different facilities, this is a concern that will grow only more complex.

Occupational exposure can come from 2 different sources: radiation produced by machines and from radionuclides. The type, production, and use of the radioactive material changes which government-sponsored regulatory body in the United States is responsible for controlling and monitoring the radiation. The U.S. Nuclear Regulatory Commission (NRC) regulates commercial nuclear power plants and other uses of nuclear materials—such as in nuclear medicine—through licensing, inspection, and enforcement of its requirements (*2*). The Occupational Safety and Health Administration (OSHA) is part of the U.S. Department of Labor and covers employees who work with radiation-producing machines. The primary goal of the Occupational Safety and Health Act of 1970 was to reduce workplace hazards and implement safety and health programs for both employers and their employees (*3*). The Occupational Safety and Health Act covers most private-sector employers and their workers, as well as some public-sector employers and workers in the 50 states and certain territories and jurisdictions under federal authority (*4*). The Department of Energy (DOE) Office of Environment, Health, Safety, and Security retains a database called the Radiation Exposure Monitoring System. This database includes occupational radiation exposure at DOE facilities that provide an annual report that includes occupational radiation exposure for DOE workers and members of the public in radiation-controlled areas (*5*). The DOE provides available information about the ALARA (as low as reasonably achievable) project descriptions, preparation of the annual data, and the cyber-secure method to transmit these annual submittals (*6*).

The NRC states: "the licensee shall reduce the [radiation] dose that an individual may be allowed to receive in the current year by the amount of occupational dose received while employed by any other person (see § 20.2104(e))" (*2*). This requirement may be a challenge for radiation workers who work at multiple institutions and receive radiation exposure in multiple ways; the individual worker can be exposed to machine-produced radiation, radionuclide-produced radiation, or both simultaneously. Because the personal dosimeters worn by individuals cannot differentiate between radiation produced by machines and radiation from radionuclides, issues arise with determining which governing body takes precedence regarding radiation exposure limits. The rules are not clear as to who should determine which facility or individual is responsible for monitoring the exposure from multiple locations; this lack of clarity brings an added challenge to the individual being monitored and the facilities. This article will examine U.S. government regulations on measuring an individual's occupational

Received Jun. 16, 2021; revision accepted Oct. 4, 2021.
For correspondence or reprints, contact Sarah Frye (sarah.frye@health.slu.edu).
Published online Nov. 8, 2021.

radiation exposure and will present findings from a survey of radiation safety officers (RSOs). The article will explore the challenges in recording an individual's radiation exposure at different facilities with different machines and radioactive tracers.

MATERIALS AND METHODS

The radiation regulations in the United States from OSHA, the NRC, and the DOE were reviewed. A literature review was done to determine whether a study of this type had been completed before, and no study was found. This review included the radiation aspects in the *Code of Federal Regulations,* the published information on the government websites, and the memorandum of agreements between the NRC and OSHA. This review also included individual radiation dose limits, which regulatory agency takes precedence over another when regulations overlap, and wording to determine the party responsible for keeping records of individual radiation exposure when individuals work at multiple institutions. In addition, an electronic survey was sent to RSOs at many types of public and private institutions—including academic, community, and government facilities—regarding radiation safety and each institution's protocol on individual occupational dosimetry reports. The survey was sent and generated using Qualtrics XM software (Qualtrics). The radiation safety survey was sent to 300 RSOs and received 50 responses. The survey questions are listed in Table 1. The e-mail addresses of the RSOs were obtained by an active RSO via a listserv of U.S. Department of Veterans Affairs RSOs and academics across the country.

RESULTS

The literature review provided insight into the complexity of this issue. If radiation is not properly controlled, it can potentially be hazardous to the health of workers (*7*). Ionizing radiation sources may be found in a wide range of occupational settings, including health-care facilities, research institutions, nuclear reactors, nuclear reactor support facilities, nuclear weapon production facilities, and other various manufacturing settings. Biologic effects on a person exposed to ionizing radiation are due to the ionization process, which destroys the capacity for cell reproduction or division or causes cell mutation (*8*). The effects of one type of radiation can be reproduced by any other type. A total given dose will cause more damage if received over a shorter time (*8*). A radiation dosimeter (often referred to as a radiation badge) does not provide protection but detects and measures the amount of radiation to which one has been exposed (*9*). These devices allow wearers to keep track of the radiation they are absorbing, so as to prevent them from falling ill and determine how hazardous a radioactive environment may be (*10*). These badges must be worn when working with x-ray equipment, radioactive patients, and radioactive materials. The dosimeters should not be worn while the wearer is receiving radiation exposure as part of medical or dental care (*11*). The radiation dosimeter worn by an individual must be specific to that individual's occupational environment, as each type of dosimeter will detect different types of radiation (*10*). Many individuals working with radiation in occupational settings are often exposed to both machine-produced radiation and radionuclide-produced radiation.

Radiation produced by machines is overseen by OSHA. Title 10 of the *Code of Federal Regulations,* part 20.1201, subpart C, addresses the occupational radiation dose limits: "the licensee shall control the occupational dose to individual adults" (*2*). Radiation from radionuclides is overseen by the NRC. OSHA and the NRC have the same annual whole-body limits for maximum recommended exposure to individuals but differ in specific radiation doses other than to the whole body. OSHA and the NRC use different periods to collect exposure limits; OSHA has quarterly limits, and the NRC has annual limits. Tables 2 and 3 show the dose limits for OSHA and the NRC, along with a comparison of annual dose for these agencies.

There are several ways that radiation to a worker or the public can be monitored. Title 10 of the *Code of Federal Regulations,* part 20.1502, addresses the conditions requiring individual monitoring of external and internal occupational dose. Workers are required to be monitored if the individual is likely to receive 10% of the maximum permissible radiation dose (Tables 2 and 3) (*12*). Minors, declared pregnant women, and individuals entering an area with high or very high radiation have specific and more restrictive requirements per these

TABLE 1
Radiation Safety Survey

Question	Answer
At what type of institution are you currently employed?	(A) Academic, (B) Community, (C) Government, (D) Other
Is institution you currently work at inside United States?	Yes or no
How long have you worked at this institution?	(A) <1 y, (B) 1–5 y, (C) 5–10 y, (D) >10 y with reference category set as D
Are you currently in charge of radiation safety program at your institution?	Yes or no
Do you request dosimetry reports for employees who work at multiple institutions?	Yes or no
Do you have any other comments or concerns regarding radiation exposure that you would like to share?	(Open for free text)
If you are open to discussing your institution-specific policies, please leave your contact information below.	(Open for free text)

TABLE 2
Dose Limits for OSHA and NRC (*2,8*)

Parameter	Radiation dose limit periods	
	OSHA, quarterly	NRC, annually
Deep dose equivalent	1.25 rem (0.0125 Sv)	5 rem (0.05 Sv)
Shallow dose equivalent	18.75 rem (0.1875 Sv), extremities; 7.5 rem (0.075 Sv), skin	50 rem (0.5 Sv)
Lens dose equivalent	1.25 rem (0.0125 Sv)	15 rem (0.15 Sv)

regulations (*12*). Pocket dosimeters, personal dosimeters, or film badges can be used to monitor radiation exposure (Figs. 1 and 2). Each personal dosimeter must be assigned to and worn by only one individual (*13*). Film badges must be replaced at periods not to exceed 1 mo, and other personal dosimeters evaluated by an accredited National Voluntary Laboratory Accreditation Program processor must be replaced at intervals of no more than 3 mo (*13*).

The radiation regulations in the United States from OSHA, the NRC, and the DOE are not specific on how radiation doses gathered from individuals working at multiple sites should be cumulated, or on the party responsible for cumulating this information. The only statement found in the NRC regulations to mention this issue is, "the licensee shall reduce the [radiation] dose that an individual may be allowed to receive in the current year by the amount of occupational dose received while employed by any other person (see § 20.2104(e))" (*2*). Section 20.2104 states the acceptable amounts and how to reduce limits if an individual is unable to acquire data on the history (1.25 rem per quarter if history not available) (*2*).

The 50 responses to the survey represent a 17% response rate. The survey gathered 36 responses to the question "do you request dosimetry reports for employees who work at multiple institutions?" Of the 36 responses to this question, 26 respondents (72%) answered yes and 10 (28%) answered no (Table 4). χ^2 tests, in the R Environment for Statistical Computing (version 2013; R Core Team), were used to determine whether those with different work experience or different work settings request dosimetry reports for individuals who work at different institutions (Tables 5 and 6). There was a statistically significant difference in dosimetry requests based on work experience ($\chi^2 = 11.041$, $P < 0.05$). Most notably, those with more than 10 y of experience were more likely than not to request the reports. On the other hand, no statistically significant differences in requesting dosimetry reports were found from those working at multiple institutions across different types of institutions ($\chi^2 = 3.3925$, $P > 0.05$).

DISCUSSION

Several regulatory agencies review radiation exposure to the worker. Regarding individuals working at multiple facilities, the regulations state that each dose should be adjusted when a radiation dose is received while the individual is employed at another facility. The regulations do not elaborate on the party responsible for keeping track of the radiation doses for individuals working at multiple institutions. The literature review found that the NRC's annual exposure limit for radiation workers is a 5-rem (0.05 Sv) total dose equivalent. OSHA's occupational dose exposure limits for machine-based radiation doses is also 5 rem (0.05 Sv) per year, but with a limit of 1.25 rem (0.0125 Sv) per quarter. Radiation dosimeters are provided to an individual through that individual's employer. When an individual is employed at more than one facility, the individual usually has a radiation dosimeter for each location.

A total of all radiation exposure a person has encountered is necessary to determine whether the received radiation dose remains within a safe limit. These limits could be lower in states that regulate their radioactive materials, that is, agreement states. The monitoring of radiation exposure across multiple institutions will become more challenging with changes in radiology equipment (e.g., hybrid modalities such as SPECT/CT), new radioactive tracers, and theranostic agents. The monitoring and regulatory issues bring up several questions. Who oversees individual radiation exposure when an employee works at multiple facilities? Is the individual or the RSO or someone else responsible? If it is an RSO, it is the RSO at which institution? Are individuals responsible for requesting and monitoring their own personal radiation limits? Are the individuals required to report that they are employed at more than one institution? If the exposure of a radiation worker is outside the dose limits, to

TABLE 3
Comparison of Annual Dose for OSHA and NRC (*2,8*)

Parameter	OSHA	NRC
Deep dose equivalent	5 rem (0.05 Sv)	5 rem (0.05 Sv)
Shallow dose equivalent	75 rem (0.75 Sv), extremities; 30 rem (0.3 Sv), skin	50 rem (0.5 Sv)
Lens dose equivalent	5 rem (0.05 Sv)	15 rem (0.15 Sv)

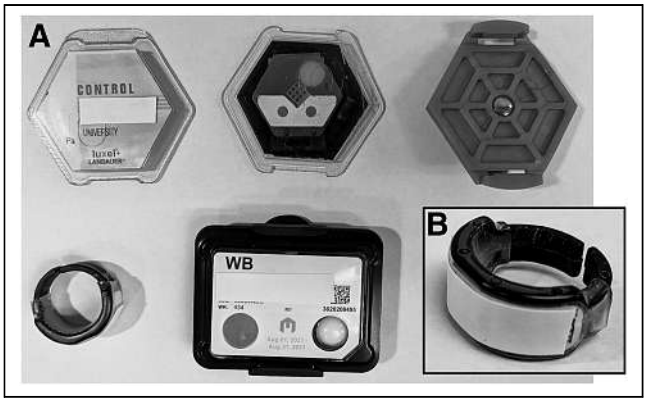

FIGURE 1. Radiation monitoring badges measure over time and do not provide real-time radiation exposure read-out. (A) Clockwise from top left: Luxel+ (Landauer) dosimeter badge that measures radiation exposure due to x-rays, γ-rays, and β-rays with optically stimulated luminescence (OSL) technology (*15*); inside of OSL badge; holder clip for Luxel+ OSL badge; film badge to measure and record radiation exposure due to x-rays, γ-rays, β-rays, and neutron radiation, which incorporates series of filters to determine quality of radiation; and a thermoluminescent extremity badge with a better view in B (*16*). (B) Thermoluminescent dosimetry extremity badge that measures exposure due to x-rays, β-radiation, and γ-radiation (*17*).

whom should this individual report this finding? Would these limits be quarterly or annual? Would ALARA be followed?

The survey sent to RSOs in the United States included basic questions to gather an understanding of the current practice at different institutions across the country. The concerns that RSO respondents listed in the survey included dosimeters not being worn properly, dosimeters not being worn at all, dosimeters left in areas where additional exposure may occur when not being worn, and dosimeters placed under a lead apron versus over a lead apron. The proper positioning of the dosimeter on the body depends on the area in which the radiation worker is employed. The general practice is to wear a body dosimeter at the collar, chest, or waist level and to wear a ring dosimeter on the dominant hand when radionuclides are handled (*11*). Those who wear personal protective

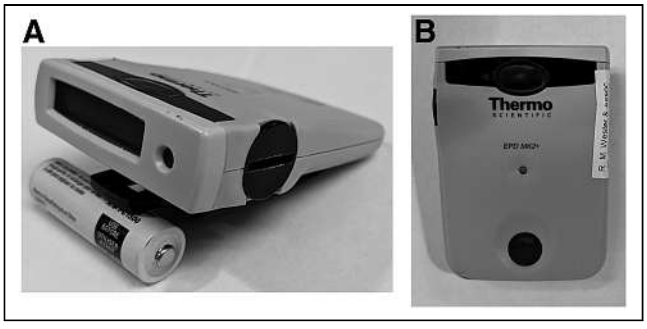

FIGURE 2. Digital electronic pocket dosimeters provide individual with immediate reading of exposure to x-rays and γ-rays (*16*). (A) Front of dosimeter (with AA battery), where real-time exposure can be viewed. (B) Top of dosimeter.

TABLE 4
Descriptive Statistics (Total $n = 36$)

Parameter	*n*	Percentage
RSO experience length		
1 y	3	8.3%
1–5 y	7	19.4%
5–10 y	10	27.8%
10 y	16	44.4%
RSO institution type		
Academic	19	52.8%
Government	5	13.9%
Community	11	30.6%
Other	1	2.8%

equipment, including lead aprons (frequently used in fluoroscopy), should wear their dosimeters at the collar level outside any personal protective equipment (*11*).

The survey found that most, but not all, RSOs at different types of institutions request dosimetry reports when employees work at multiple institutions. Of the respondent RSOs who request such reports, 68% (13/19) are from academic institutions, 82% (9/11) from community hospitals, and 80% (4/5) from government institutions. This study could be expanded to include more RSOs, more facilities, and a deeper knowledge of institutional policies. It would be beneficial to follow up with RSOs to see whether facilities are using policies or procedures for tracking radiation exposure at multiple institutions. The goal would be to expand the survey to more RSOs and receive feedback on their institutions' policies regarding keeping track of badge readings for employees who work at more than one facility and use a different dosimeter at each. A future study could also consider answering some of the questions posed earlier in this "Discussion" section.

If answers cannot be obtained for these questions, a more specific guideline may need to be created. Workers who are exposed to radiation may benefit from having a central repository to which all companies must report. This repository could be like the DOE's Radiation Exposure Monitoring System database. This database could be government-controlled and regulated to follow NRC, OSHA, and DOE requirements. The occupational dose limits would be monitored depending

TABLE 5
Results of χ^2 Test and Descriptive Statistics for Dosimetry Request by Work Experience

Dosimetry request	Work experience (y)			
	<1	1–5	5–10	≥10
Yes	6 (86%)	6 (60%)	0 (0%)	14 (88%)
No	1 (14%)	4 (40%)	3 (100%)	2 (12%)

$\chi^2 = 11.041$ ($P < 0.05$); df = 3. Numbers in parentheses indicate column percentages.

TABLE 6
Results of χ^2 Test and Descriptive Statistics for Dosimetry Request by Institution Type

Dosimetry request	Institution type			
	Academic	Community	Government	Other
Yes	13 (68%)	9 (82%)	4 (80%)	0 (0%)
No	6 (32%)	2 (18%)	1 (20%)	2 (100%)

$\chi^2 = 3.3925$; df = 3. Numbers in parentheses indicate column percentages.

on the type of radiation to which the individual is exposed. If an individual works with machine-produced radiation and radioactive materials, the annual NRC radiation dose limits would take precedence. Agreement states with the NRC would have more stringent limits than the NRC, and the state limits would be followed. If a state wishes to establish programs to assume NRC regulatory authority, the NRC relinquishes to that state its authority to license and regulate byproduct materials (radioisotopes), source materials (uranium and thorium), and certain quantities of special nuclear materials (*14*). If an individual is exposed only to machine-produced radiation, then OSHA's quarterly limits take precedence.

CONCLUSION

The *Code of Federal Regulations* and the radiation regulatory bodies in the United States want monitoring of cumulative radiation doses for an individual exposed to occupational radiation at more than one institution. The literature review of U.S. radiation-governing bodies found no clear guidelines for requiring and recording this cumulative occupational radiation dose when individuals are employed at more than one facility. The survey revealed that there are RSOs—especially those with more than 10 y of experience—requesting dosimetry records for their employees who work at multiple institutions; however, not all institutions are tracking these records. It is in the facility's and the individual's best interest to draw attention to an individual's combined exposure rate when employed at multiple facilities. The development of policies and regulations by institutions or regulatory bodies may need to be explored. These policies may need to address the different types of radiation and how it is produced, as well as capture the accumulation of radiation exposure at multiple institutions.

DISCLOSURE

No potential conflict of interest relevant to this article was reported.

REFERENCES

1. Imaging and radiology. MedlinePlus website. https://medlineplus.gov/ency/article/007451.htm. Updated March 21, 2022. Accessed March 30, 2022.
2. Subpart C—occupational dose limits. § 20.1201 Occupational dose limits for adults. U.S. NRC website. https://www.nrc.gov/reading-rm/doc-collections/cfr/part020/part020-1201.html. Published May 21, 1991. Updated March 24, 2021. Accessed March 30, 2022.
3. Workplace safety: OSHA and OSH act overview. FindLaw website. https://www.findlaw.com/employment/workplace-safety/workplace-safety-osha-and-osh-act-overview.html. Updated December 5, 2018. Accessed March 30, 2022.
4. About OSHA. U.S. Department of Labor website. https://www.osha.gov/aboutosha. Accessed March 30, 2022.
5. Rao N, Hagemeyer DA, McCormick YU. DOE 2016 occupational radiation exposure. Osti.gov website. http://www.osti.gov/servlets/purl/1425887. Published January 1, 2017. Accessed March 30, 2022.
6. Occupational radiation exposure. Energy.gov. http://www.energy.gov/ehss/corporate-reporting-analysis/databases/occupational-radiation-exposure. Accessed March 30, 2022.
7. Radiation. U.S. Department of Labor website. http://www.osha.gov/SLTC/radiation/index.html. Accessed March 30, 2022.
8. Ionizing radiation. U.S. Department of Labor website. http://www.osha.gov/SLTC/radiationionizing/introtoionizing/ionizinghandout.html. Accessed March 30, 2022.
9. Personal radiation dosimeter. University of Texas Health Science Center at Houston website. http://www.uth.edu/safety/radiation-safety/personal-radiation-dosimeter.htm. Accessed March 30, 2022.
10. Flournoy B. How do dosimeters work? Sciencing website. https://sciencing.com/do-dosimeters-work-5167635.html. Updated November 30, 2018. Accessed March 30, 2022.
11. Your radiation dosimeter: a tutorial. Duke University website. https://www.safety.duke.edu/sites/default/files/badge_tutorial.pdf. Accessed March 30, 2022.
12. § 20.1502 Conditions requiring individual monitoring of external and internal occupational dose. U.S. NRC website. https://www.nrc.gov/reading-rm/doc-collections/cfr/part020/part020-1502.html. Updated March 24, 2021. Accessed March 30, 2022
13. § 34.47 Personnel monitoring. U.S. NRC website. https://www.nrc.gov/reading-rm/doc-collections/cfr/part034/part034-0047.html. Updated August 26, 2020. Accessed March 30, 2022.
14. Agreement state program. U.S. NRC website. https://www.nrc.gov/about-nrc/state-tribal/agreement-states.html. Updated January 13, 2021. Accessed March 30, 2022.
15. Luxel®+ PA. Landauer website. https://www.landauer.com/luxel-radiation-dosimeter-badges-pa. Accessed March 30, 2022.
16. Film badges. Iowa State University website. https://www.nde-ed.org/NDEEngineering/RadiationSafety/radiation_safety_equipment/film_badges.xhtml. Accessed March 30, 2022.
17. Saturn® TLD Ring. Landauer website. https://www.landauer.com/sites/default/files/product-specification-file/Saturn_Ring_2.pdf. Published 2017. Accessed March 30, 2022.

The Impact of COVID-19 on First-Year Undergraduate Nuclear Medicine Students' Practical Skills Training

Melissa Shields and Helen M. Warren-Forward

School of Health Sciences, College of Health, Medicine, and Wellbeing, University of Newcastle, Australia, Callaghan, New South Wales, Australia

Clinical placement is an important component of any undergraduate nuclear medicine program. For first-year students, it is an introduction to clinical nuclear medicine, which helps them better understand the profession as well as consolidate their learning to date. Clinical placements for first-year students usually take the form of 2 wk of full-time attendance at a nuclear medicine site. At the University of Newcastle, in Australia, part of the clinical placement course includes radiopharmacy laboratory sessions in a simulated environment to develop necessary skills and confidence. Because of the coronavirus disease 2019 (COVID-19) pandemic, restrictions were put in place that meant cancelling clinical placements for first-year students and reducing time in the radiopharmacy laboratory from 2 h to 1 h per session. The aim of this study was to evaluate whether a clinical alternative portfolio in lieu of clinical placement was effective in increasing the students' knowledge and skills in nuclear medicine practice and whether specifically developed instructional videos for preparation of the radiopharmacy laboratory sessions compensated for the reduced time. **Methods:** A paper-based survey was given to the 50 students enrolled in the first-year professional practice course. This survey, containing 56 questions, consisted of both open questions and closed Likert-scale questions about the changes to the radiopharmacy laboratory sessions and the clinical alternative portfolio in 2 separate sections. Quantitative and qualitative analysis was performed on the resulting data. **Results:** There was a 94% response rate to the survey. Most students watched the preparatory radiopharmacy videos at least once and strongly agreed that each video adequately prepared them for the associated laboratory session. Just over half (51%) the students thought the reduced time in the laboratory was sufficient to complete the required tasks. Most students agreed that the modules included in the clinical alternative portfolio increased their knowledge of nuclear medicine practice. **Conclusion:** Despite the restrictions put in place because of COVID-19, the learning outcomes of the first-year nuclear medicine professional practice course were met. The preparatory videos for the radiopharmacy laboratory sessions and the clinical alternative portfolio were positively received and gave the students a good introduction to clinical nuclear medicine.

Key Words: nuclear medicine practice; students; COVID-19; clinical placement

J Nucl Med Technol 2022; 50:166–173
DOI: 10.2967/jnmt.121.262814

Received Jun. 28, 2021; revision accepted Sep. 29, 2021.
For correspondence or reprints, contact Melissa Shields (melissa.shields@newcastle.edu.au).
Published online Nov. 8, 2021.

Clinical education for any health-care student has long been used to develop the student's practical skills and knowledge and reinforce the theoretic knowledge taught at the university (*1*). Experiencing actual patients in a real clinical situation gives the student a unique learning experience not achieved in the classroom (*2*). For first-year nuclear medicine students, their first clinical placement is their initial foray into clinical nuclear medicine. As well as consolidating their learning, it gives the students a better understanding of the profession as a whole, helping them realize whether this is the correct career choice for them (*1*).

As part of the Bachelor of Medical Radiation Science (Nuclear Medicine) (honors) program at the University of Newcastle, Australia, students complete 43 wk of clinical placement over 4 y. Clinical placements for first-year students usually take the form of 2 wk of full-time attendance at a nuclear medicine site. The emphasis of this clinical placement is to develop communication skills among themselves and patients and staff, develop technical skills (e.g., using the γ-camera), and put into practice any theory learned. They are assessed on their clinical competence by a clinical supervisor who is a practicing nuclear medicine technologist working at the clinical site. There are also written assessments for the student to complete, including a case study and reflective report.

To develop the crucial technical skills needed for their first placement, students are educated in radiopharmacy techniques in a specifically designed radiopharmacy within the University of Newcastle. The radiopharmacy laboratory has 10 student benches and an instructor's bench, each fitted with a commercial L-block and all the necessary equipment to maintain radiation safety in the workplace (e.g., lead pots and syringe shields). For first-year students, time in the radiopharmacy involves learning about radiation safety, needle skills, ^{99}Mo/^{99m}Tc generator elution, and quality control testing of the eluate. Students also learn how to draw up doses and basic methods for reconstituting a kit. In the simulated environment, there is no radioactivity involved, the generator systems are preused and over 6 mo old, and saline is used to practice drawing up doses. In this way, the student can develop the necessary skills and confidence without contaminating themselves and their environment. The advantages of using this simulation-based education includes protecting the

TABLE 1
Description of Preradiopharmacy Laboratory Videos

Video no.	Description	Length (min)
1	Laboratory introduction	5
2	Needle skills and dose calibrator	11
3	Generator elution and quality control	10
4	Point source and dose dispensing	7
5	Technegas	8
6	Radiopharmaceutical kit	4

student, the clinical supervisor, and ultimately the patient from unnecessary risks (in this instance, unnecessary ionizing radiation exposure) and offering the opportunity to practice high-risk events while receiving feedback in a safe environment (*3,4*).

The radiopharmacy laboratory sessions and the 2-wk clinical attendance are combined into the course "MRSC1330: Nuclear Medicine Professional Practice IB," which takes place during semester 2, year 1, of the program for a Bachelor of Medical Radiation Science (honors) (nuclear medicine).

The COVID-19 pandemic imposed several restrictions on the delivery of MRSC1330. This necessitated a change in the course to adapt to the restrictions while still providing a quality learning experience for students. Radiopharmacy laboratory sessions, which were conducted on campus face-to-face, were allowed to continue during 2020; however, strict social distancing rules applied, and the amount of time students and staff were in the same room was regulated. All persons not living together were instructed to stay 1.5 m away from each other, and there was a limit of 1 person per 4 m^2 allowed within a room; this meant that a maximum of 6 students and the instructor were allowed in the radiopharmacy laboratory for each session, instead of the usual 10. Each session was repeated 9 times to accommodate the 50 students enrolled in the course. Each session also needed to be limited to 1 h instead of the usual 2 h, reducing the time available to demonstrate the learning task each week. To combat this time constraint, a set of 6 instructional videos was made by the course coordinator for each learning task (Table 1).

The 2 wk of clinical placement were also cancelled. In their place, a clinical alternative portfolio consisting of 4 modules was created to offer another learning experience for the student. Details of the clinical alternative portfolio are provided in Table 2. The portfolio was designed to be closely aligned to existing clinical placement learning outcomes. The portfolio constituted 80% of the total marks for the course, with the other 20% coming from a radiopharmacy skills assessment task.

The students were instructed to watch the prerecorded videos and read the laboratory notes before attending their radiopharmacy session each week. These were designed to familiarize the students, in advance, with the material to be covered each week because of the reduced time frame of the laboratory sessions. The prerecorded videos and the laboratory notes for the course were available on Blackboard Learn, a learning management system, making them suitable for viewing online from home.

The "Communication" module consisted of a set of prereadings and a workshop. The prereadings contained information on communication techniques and the importance of effective communication. To accommodate COVID-19 restrictions, 4 communication workshops were held on campus, with 3 workshops having 12 students in attendance and the fourth having 14. Each workshop was broken into two 2-h blocks over 2 d. In the first block, students had interactive discussions about why introductions are important, whom they might need to communicate with while on placement as a student technologist, what some of the issues facing their patients might be, and how to become more aware of nonverbal communication and cultural sensitivities. The students were also shown videos of nuclear medicine technologists interacting with patients. In the second block, students were divided into groups of 2 and were required to perform scenario-based exercises to develop their communication skills. The activities included students role-playing being either a technologist or a patient for various medical conditions, including being a patient with vision impairment, cancer, dementia, or pain. For assessment, students were required to write a reflective report. The report was designed to help students increase their understanding of effective

TABLE 2
Clinical Alternative Portfolio

Module	Description/summary of learning	Assessment
"Communication"	Effective communication techniques; types of people technologists need to communicate with; hands-on communication workshop	Reflective report (20%)
"Work, Health, and Safety"	Health and safety in workplace; risk assessment	"Hazard Identification Risk Assessment and Control" worksheet (20%)
"Case Study"	Methods for writing a case study	Bone scan case study (20%)
"Introduction to Nuclear Medicine Practice"	Patient identification, consent, and privacy; typical procedure for 3-phase bone scan; γ-camera operations	Audio recording of bone scan explanation (20%)

communication and to help inform their future experiences when communicating with patients and clinical staff (*2*).

The "Work, Health, and Safety" module was developed to inform students of the protocol and processes in place to maximize safety in the workplace. As well as being a key capability for nuclear medicine technologists (workplace safety forms part of the Medical Radiation Board of Australia's professional capabilities document) (*5*), young workers may be less aware of work, health, and safety risks and responsibilities and therefore at more risk of workplace injury (*6*). As an assessment, students were required to complete a "Hazard Identification Risk Assessment and Control" worksheet on an area of their choice (e.g., workplace or shopping center). The worksheet was developed by a work, health, and safety academic from the university, with input from the course coordinator.

The "Case Study" module was developed because the writing of case studies is an integral part of the assessment of clinical placements within the nuclear medicine program at the University of Newcastle. In this module, students were required to choose a pathologic condition commonly imaged using bone scans and then write it up in the style of a case study.

As part of the "Introduction to Nuclear Medicine Practice" module, the students were given short videos on the operation of γ-cameras (supplied by GE Healthcare and Siemens) and a video of a bone scan. For the assessment, students were required to make a short audio recording explaining a bone scan to a patient. This task simulated what they would have been doing while on clinical placement but also tied together the knowledge learned in the "Communication" module. They needed to be able to correctly identify the patient as well as communicate information about a bone scan at a level a typical patient would understand.

The aim of this study was to evaluate whether the radiopharmacy instructional videos provided sufficient information to allow the student to confidently complete the laboratory sessions in the reduced time and whether the clinical alternative portfolio was effective in increasing the students' knowledge and skills in nuclear medicine practice.

MATERIALS AND METHODS

Study Participants

The participants were all 50 students enrolled in the first-year "Nuclear Medicine Professional Practice 1B" course in 2020. Ethics approval was granted by the University of Newcastle's Human Research Ethics Committee under its quality assurance scheme (QA242). Written consent was not obtained because this was an anonymous survey and consent was implied through completion and submission of the survey.

Survey

A paper-based survey was given to the students, as well as a participant information statement explaining the details of the study. The survey was administered after the final course assessment. The students were informed that participation was entirely their choice and nonparticipation would have no bearing on their marks or progression in the course. The survey consisted of 2 main sections. Section A contained 33 questions relating to the radiopharmacy laboratory sessions and the 6 instructional videos; section B contained 23 questions about the clinical alternative portfolio. The questions were a combination of closed questions using 5-point Likert scales and open-ended questions for written comments.

Analysis of Results

Quantitative data from the survey were analyzed using weighted sum averages (WSA) of the Likert scale scores. The WSA analysis allowed comparison of the usefulness of each preradiopharmacy video and the clinical alternative tasks.

To determine whether the restructured radiopharmacy laboratory sessions had any effect on student learning, the results from the 2020 (COVID-19–restricted) radiopharmacy skills assessment were compared with the results from students who took the assessment in 2019. The 2020 cohort completed its first clinical placement in April 2021, and the effect of the clinical alternative portfolio was assessed by comparing the results from the 2021 clinical placement with the results from the 2019 cohort after completion of the same (though their second) clinical placement block. A 1-tailed *t* test was used to assess the statistical difference in the results of students between corresponding years.

The written comments from the survey were independently analyzed using thematic analysis by the authors. A range of themes and subthemes was derived and reviewed for agreement. Any disagreement was resolved through discussion.

RESULTS

In total, 47 of 50 students (94% response rate) completed the evaluation survey. Although 3 papers were incomplete, the completed parts of the survey have been included in the analysis.

Quantitative Analysis

Radiopharmacy Laboratory Sessions. Most students (98% [45/46]) watched each video at least once, with students watching most videos at least twice (Table 3). The exception was the "Radiopharmaceutical" video, with 34% (16/46) of students watching it more than 3 times. Students strongly agreed that each video was easy to understand, with the WSA ranging from 4.61/5 for the "Point Source and Dose Dispensing" video to 4.79/5 for the "Laboratory Introduction" video (Fig. 1).

When asked if each video adequately prepared them to participate in the associated radiopharmacy laboratory session, again most students strongly agreed (Table 4). The lowest ranked was the "Technegas" (Cyclomedica) video, and the highest ranked video was the "Radiopharmaceutical" video.

In response to questions about whether the laboratory sessions were long enough, 19% (9/47) of students strongly agreed ("plenty of time") and 32% (15/47) agreed ("just enough time") (Fig. 2). Thirty-six percent of students (17/47) disagreed ("some sessions could have been longer") or strongly disagreed ("all sessions could have been longer"). Overall, the WSA was just over neutral, at 3.19.

Clinical Alternative Portfolio. Students were asked if they believed that the clinical alternative portfolio increased

TABLE 3
Number of Times That Students Watched Each Radiopharmacy Preparation Video (n = 46)

Video no.	Description	0 times	1 time	2 times	3 times	>3 times
1	Laboratory introduction	0%	43%	51%	4%	2%
2	Needle skills and dose calibrator	0%	27%	47%	16%	11%
3	Generator elution and quality control	0%	40%	33%	14%	14%
4	Point source and dose dispensing	2%	24%	46%	13%	15%
5	Technegas	0%	55%	30%	11%	4%
6	Radiopharmaceutical kit	2%	17%	28%	19%	34%

their knowledge of nuclear medicine practice (Fig. 3). Most students either strongly agreed or agreed with this, with the WSA ranging from 4.11 for the "Risk Assessment" module to 4.37 for the "Introduction to Nuclear Medicine Practice" module. Although a couple of students disagreed that some parts of the portfolio increased their knowledge ("Case Study" and "Communication" modules), no student strongly disagreed.

Most students agreed that the communication workshop was effective in increasing their awareness of communicating with both patients and people in general (Table 5). Only 1 student disagreed. That student thought that the workshop was "helpful in parts."

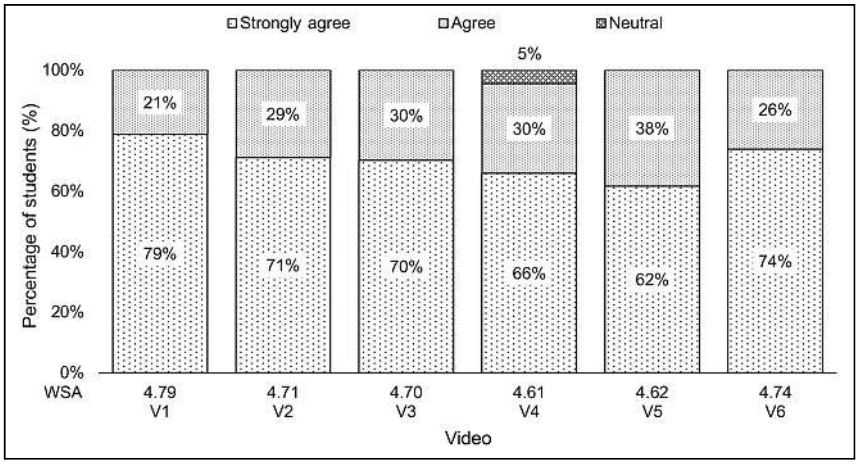

FIGURE 1. Percentage of students indicating that video was easy to understand. Video descriptions are provided in Table 1.

Of the 3 videos that students were instructed to watch as part of the "Introduction to Nuclear Medicine Practice" module, most students watched them at least once (Table 6). Although all 3 videos ranked well, the GE Healthcare video on the operation of the γ-camera scored slightly higher than the Siemens video both in ease of understanding (WSA, 4.53 vs. 4.42) (Fig. 4) and in supporting student learning (WSA, 4.65 vs. 4.45) (Fig. 5).

Comparison of Results with Previous Cohorts. Marks were compared between this COVID-19–affected 2020 cohort and the 2019 cohort (not affected by COVID-19 restrictions). There was no statistical difference ($t = 1.23$, $P = 0.11$) between the 2019 and 2020 radiopharmacy results, despite the fact that students in 2020 obtained slightly higher results (average, 94.5%; SD, 5.84) than students in 2019 (average, 92.5%; SD, 8.09).

Similarly, there was no statistical difference ($t = 1.89$, $P = 0.12$) between the 2019 and 2021 (COVID-19–affected) clinical placement results, despite the fact that students in 2021 obtained higher results (average, 78.6%; SD, 13.82) than students in 2019 (average, 74.64%; SD, 14.06).

Qualitative Analysis

Radiopharmacy Laboratory Sessions. The written comments from the open-ended questions concerning the radiopharmacy laboratory sessions uncovered

TABLE 4
Percentage of Students Indicating That Videos Adequately Prepared Them to Participate in Associated Radiopharmacy Laboratory

	Adequately prepared					
Parameter	Strongly agree	Agree	Neutral	Disagree	Strongly disagree	WSA
Laboratory introduction	68%	28%	4%	0%	0%	4.64
Needle skills and dose calibrator	67%	29%	2%	2%	0%	4.60
Generator elution and quality control	64%	32%	4%	0%	0%	4.60
Point source and dose dispensing	70%	26%	4%	0%	0%	4.65
Technegas	64%	30%	6%	0%	0%	4.57
Radiopharmaceutical kit	72%	26%	2%	0%	0%	4.70

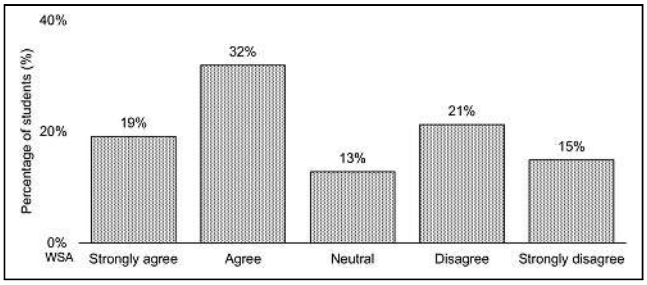

FIGURE 2. Percentage of students indicating that laboratory sessions were long enough to complete each task.

4 major themes: timing of the laboratory sessions; delivery of the laboratory sessions; content of the videos; and student learning, understanding, and confidence.

Regarding timing of the sessions, just over 50% of the students indicated that there was enough time in the laboratory each week to finish their specific tasks and that "any longer than 1 h and I feel it would drag on for too long" (participant [P] 44) or "we always had enough time and also to ask questions if we needed to" (P 10). However, some students felt that the laboratory time was too short, and they felt rushed: "by the time you get organized and put gloves/gowns on its not enough time to have multiple goes at eluting the generator and practicing getting doses" (P 25) and "I would have liked more time, a lot of our labs were cut short and rushed" (P 15). One student who indicated that there was sufficient time in the laboratory commented that "more practice to help understand the method" (P 5) was needed. Students also commented that it "would have been better if we had more individual time with the lab instructor" (P 13) and that there was "not enough time to check everyone individually" (P 27).

Regarding delivery of the sessions, some students felt that the sessions needed to be delivered more than once a week: "the labs were good, however it would have been more efficient if we did them twice a week" (P 23) and "it is also hard to solidify skills 1 h a wk, as after a week has passed I felt I had forgotten everything" (P 33). It was also felt that another review laboratory session was needed: "maybe 2 labs before the test would have been more beneficial than one" (P 20). The smaller group size was felt to be a positive consequence of the COVID-19 restrictions, as "smaller groups allow for a better group dynamic" (P 47).

Regarding the content of the videos, the preparatory radiopharmacy videos were well received by all students: "They were very clear and extremely helpful" (P 1). Students felt that the content within the videos was extremely helpful for their preparation each week: "the intro video alongside the in-class video helped me understand the lab thoroughly" (P 9); "all the videos were great as a hands-on learner watching them made it easier to grasp before heading in" (P 45); and "they matched what we were expected to do" (P 27). However, some students were looking for some more specific content to be added to the videos: "however a top down… camera angle could have helped with organizing [and] arranging the materials" (P 28); "a little more detailed" (P 34); "high camera view on generator" (P 40); and "adding some 'tips and tricks' would be great for example, how to remove a tricky needle cap" (P 16).

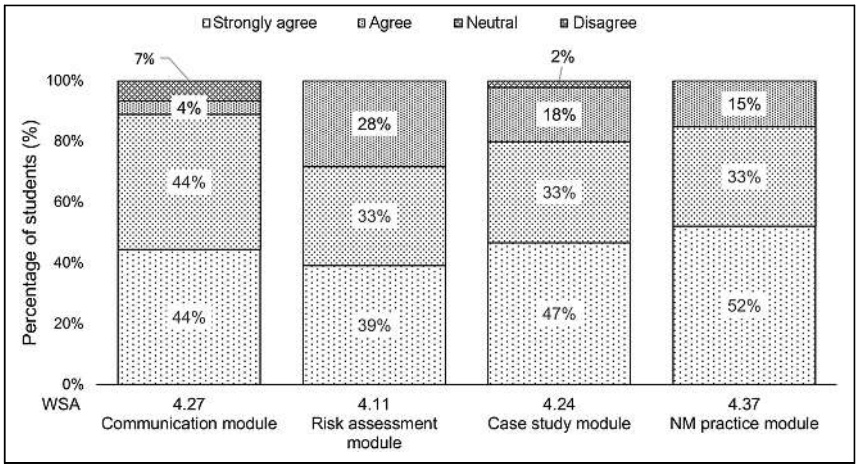

FIGURE 3. Percentage of students indicating that module increased their knowledge of nuclear medicine practice. NM = nuclear medicine.

TABLE 6
Number of Times That Students Watched Each "Introduction to Nuclear Medicine Practice" Video (n = 46)

Parameter	0 times	1 time	2 times	3 times	>3 times
Bone scan video	11%	46%	33%	9%	2%
GE Healthcare video	24%	50%	20%	7%	0%
Siemens video	28%	54%	13%	4%	0%

TABLE 5
Percentage of Students Indicating That Communication Workshop Increased Their Awareness of How to Better Communicate with Patients and with People in General

Parameter	Strongly agree	Agree	Neutral	Disagree	Strongly disagree	WSA
With patients	66%	30%	2%	2%	0%	4.6
Generally with people	52%	35%	11%	2%	0%	4.4

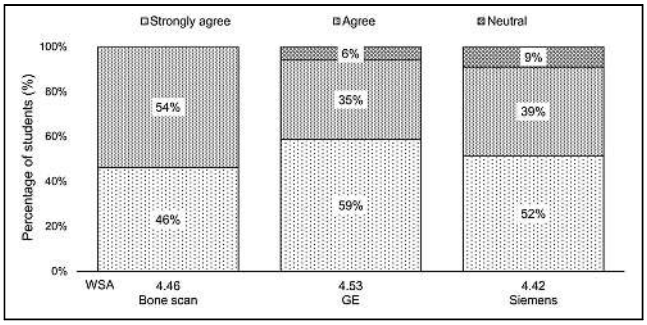

FIGURE 4. Percentage of students indicating that "Introduction to Nuclear Medicine Practice" video was easy to understand.

Regarding student learning, understanding, and confidence, the students felt that, overall, the videos added to their learning experience: "really great for reviewing what we have learnt. I watched them multiple times." (P 27); "I believe that every subsequent year after this should have them as they provide a great source of study and reassurance" (P 28); and "I think every year they should be done. I know they were only done for COVID-19 but I think they are very beneficial." (P 33). Specific videos also helped students understand health and safety aspects of the laboratory: "this video helped me avoid a needle stick injury" (P 42). Students were able to watch the videos at any time during the semester, which also made them useful for their assessment: "good tool to revise for practical exam" (P 16) and "I loved having them there to look back on" (P 10). However, other students felt that the videos helped with their understanding: "they were really good for my understanding" (P 17) and "the … .video helped me understand the lab thoroughly" (P 9). The videos also helped with students' confidence: "they really helped reduce some of the anxiety and stress of the labs because you know what you're in for before you get there" (P 16).

Clinical Alternative Portfolio. The written answers to the clinical alternative portfolio open-ended questions revealed 4 major themes: preparation for future clinical placement, communication skills, increased understanding and skills, and content of modules.

Regarding preparation for future clinical placement, students felt that the clinical alternative portfolio prepared them for future clinical placements, especially the "Communication," "Introduction to Nuclear Medicine Practice," and "Case Study" modules. The modules "gave us a real insight into clinical situations. How to prepare for placement, what to expect, how to talk to patients" (P 21); "case studies will be done throughout my career—this gives me experience" (P 42); and "good to organize thoughts on how things work in a practice" (P 16).

Regarding communication skills, learning how to communicate in a nuclear medicine setting was helpful for students: "communication in a clinical setting is very different from everyday settings, and this is not something you realize without exposure. It made me aware of what I did not know and provided skills that will make adjusting to clinical practice less of a shock" (P 16). Having different scenarios meant that the students could experience a diverse range of clinical situations: "the workshop helped me understand how to communicate with all different patients with different needs. I gained a better understanding about communication toward patients, and how important it is" (P 24) and "it made me more aware of how to communicate effectively with a wide range of professionals and patients" (P 46).

Regarding achieving a better understanding and an increase in skills, for some students the clinical alternative portfolio gave them a better understanding of nuclear medicine because it "helped me to better understand what scans are for, what other images need to be done and how they are done" (P 37). Because of the extra reading required to complete some assessment tasks, "I noticeably gained knowledge of [nuclear medicine] in general due to extensively researching" (P 1). The clinical alternative portfolio also built on the basic skills and knowledge the students had acquired from courses delivered in semester 1: "refreshed my memory and helped" (P 43) and "allowed us to put into practice what we learnt in previous modules" (P 36).

Regarding the content of the modules, some students felt that simulating the clinical setting in the communication workshops made the learning easier: "I didn't understand how daunting communication could be and I'm glad I learnt before placement" (P 15) and "able to interact without the pressure of a patient" (P 44). The γ-camera operation videos were also well received, as "in some ways it could possibly be even more helpful than work placements. Such as the videos of the cameras that we can revisit and pause—allowing us to learn at our own pace" (P 47). The risk assessment module, although helpful to some students—"made me aware as to just how many risks there could be in a workplace" (P 25) and "it was able to bring my attention to things I may not have thought about"(P 26)—lost some importance to others as it was not specifically focused on a health-care setting: "it did not add to my knowledge about the workplace" (P 28) and "didn't necessarily provide insight into safety hazards within a hospital setting" (P 32).

Overall, the clinical alternative portfolio was seen to be an excellent alternative to attending clinical placement for some students: "I believe this was the best possible alternative to a clinical practice" (P 14); "it was helpful and an

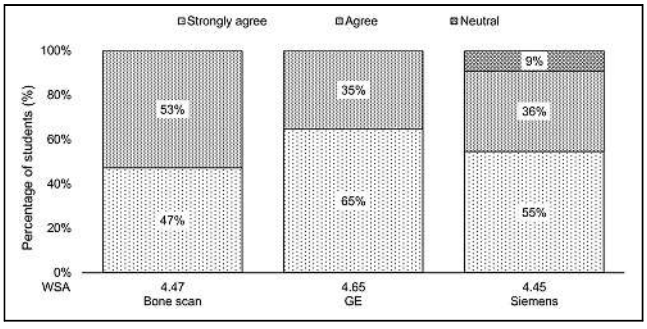

FIGURE 5. Percentage of students indicating that "Introduction to Nuclear Medicine Practice" video supported their learning.

impressive solution to missing work placement" (P 47); "I thought it provided us with the knowledge needed to take us into placement next year" (P 3); and "the portfolio was a great assessment that helped due to the cancellation of placement" (P 8). However, some students did not feel there was much benefit in completing the alternative tasks: "As we weren't able to use the machines or deal with patients it was hard to understand the normal practice" (P 36). When asked what they would change about the clinical alternative portfolio, some students simply answered, "go on placement."

DISCUSSION

Both the radiopharmacy instructional videos and the clinical alternative portfolio, put in place because of COVID-19 restrictions, were successful in terms of student learning. The radiopharmacy instructional videos provided sufficient information for the student to confidently complete the laboratory sessions, given the reduced time spent in the laboratory each week. Similarly, the clinical alternative portfolio increased the first-year students' knowledge and skills in nuclear medicine practice despite cancellation of their clinical placement.

Radiopharmacy Laboratory Sessions

Most students strongly agreed that the instructional videos adequately prepared them for the weekly radiopharmacy laboratory session, with most students watching each video at least twice and finding them easy to understand. However, only half the students thought that the amount of time spent in the laboratory each week was sufficient for their learning. At the time, the videos were made in response to a reduced amount of time spent in the laboratory each week, allowing for a briefing on the learning objective to be done before entering the laboratory. However, this study has shown that the videos were much more than that. The videos helped students with various learning styles prepare for the laboratory session each week. It is the role of the health science educator to accommodate the different learning styles of students (*7*), which include concrete experience (feeling), reflective observation (watching), abstract conceptualization (thinking), and active experimentation (doing) (*7*). In this instance, the students are provided videos and written instructions (watching and thinking) and then given the opportunity to practice what they have learned (doing). The videos added to the learning experience provided by the simulation-based radiopharmacy laboratory sessions, providing essential knowledge and the chance to rewatch for review purposes. The laboratory sessions provided first-year nuclear medicine students with a realistic and relevant learning experience, an essential element of simulation-based education (*4,8*). Although their time in the laboratory was reduced, each student received the same level of training, which is sometimes not afforded in clinical practice because of the inconsistent teaching styles of supervisors (*1,4,9*).

Clinical Alternative Portfolio

The decision to cancel the clinical placement was not taken lightly, as there are many known advantages to exposing the student to the profession at such an early stage in their studies (*1*). Most students either agreed or strongly agreed that all 4 modules of the portfolio increased their knowledge of nuclear medicine practice and safety in the workplace and prepared them for future clinical placements. This agreement was backed up by similar clinical placement results when comparing this cohort with the previous cohort.

Preparation for Future Clinical Placement

As with the radiopharmacy laboratory sessions, all students received the same educational experience, therefore eliminating the inequality in learning due to varying clinical placement encounters (*1,4,9*). A recent study by Ketterer et al. (*9*) stated that participation in simulated placement activities did not disadvantage the therapeutic radiography (radiation therapy) student and that simulated placement activities "should play a major role" in the training of students. However, the lack of patient interaction and the inability of students to immerse themselves in the profession will ensure that this portfolio is used as a preparation tool and not a replacement for clinical placement.

Communication Skills

Effective communication within any medical setting is imperative; it reduces patient anxiety, addresses any concerns the patient may have, and educates the patient about the procedure (*10*). The first-year nuclear medicine cohort had varying levels of experience with communication, ranging from having no experience to having communication experience through retail work to already being a health professional (some students in this cohort were trained dental hygienists and nursing assistants); however, most students agreed or strongly agreed that the module increased their awareness of how to communicate with patients or people in general. The inclusion of communication skills training in the clinical alternative portfolio provided examples of effective communication within the workplace, as well as patient–technologist interactions, within a safe learning environment. This environment allowed students to practice their evolving communication skills and make errors without the fear of reprisal (*4,10*).

Content of Modules

The modules in the clinical alternative portfolio were designed to be equivalent to the learning outcomes of clinical placement. Although, on placement, previous first-year students were assessed on their communication skills with both staff and patients and were required to complete a risk assessment task and a bone scan case study, they also needed to write a reflection based on a personal interaction with a person from a culturally diverse or indigenous background. By aligning the set tasks in the clinical alterative portfolio with the traditional placement learning outcomes, the students in this study were provided with the same

learning opportunities as previous students in an attempt to increase their understanding of nuclear medicine practice. A mixture of teaching methods was used in the portfolio, including face-to-face teaching, prerecorded lectures, self-directed learning, and industry-recorded videos. As well as catering to different learning styles, this mix gave students the flexibility of blended learning (*11,12*).

Limitations

A limitation of this study was the relatively small sample size ($n = 47$), though this represented 94% of the eligible participants. Another limitation was the lack of generalizability due to the research's being conducted for a single course at a single Australian university.

CONCLUSION

During 2020, in the midst of a worldwide pandemic, first-year nuclear medicine students at the University of Newcastle were provided with a safe environment to develop their radiopharmacy skills and be introduced to clinical nuclear medicine practice. The learning outcomes of the radiopharmacy laboratory sessions were still met, despite the time restrictions put in place, and the student learning experience was enhanced by the preparatory videos. With the loosening of COVID-19 restrictions—and because of the student feedback—the students will return to 2-h radiopharmacy laboratory sessions in 2021. The videos will also be used as part of the prelab preparation. The clinical alternative portfolio enabled students to acquire a basic understanding of clinical nuclear medicine without the need to attend nuclear medicine practice sessions. Although the clinical alternative portfolio was positively received, it should not replace clinical placement for first-year students. Instead, it should be used as a method of preparation for students about to embark on their first clinical placement in a nuclear medicine department.

DISCLOSURE

No potential conflict of interest relevant to this article was reported.

REFERENCES

1. Currie G, Wheat J. The first year clinical placement for undergraduate medical radiation science students: tool or toil? *J Med Radiat Sci.* 2005;52:18–22.
2. Stagnetti K, Schoo A, Welch D, eds. *Clinical and Fieldwork Placement in the Health Professions.* 2nd ed. Oxford University Press; 2013:3, 34.
3. *The Sim Guide: Allied Health Scenarios, Templates and Tips for Simulation Based Education.* Health Education and Training Institute; 2015:13.
4. Hazell L, Lawrence H, Friedrich-Nel H. Simulation based learning to facilitate clinical readiness in diagnostic radiography: a meta-synthesis. *Radiography.* 2020; 26:e238–e245.
5. Professional capabilities for medical radiation practice. Medical Radiation Practice Board of Australia website. https://www.medicalradiationpracticeboard.gov.au/Registration-Standards/Professional-Capabilities.aspx. Published March 1, 2020. Accessed January 13, 2022.
6. Young workers. Worksafe ACT website. https://www.worksafe.act.gov.au/initiatives/young-workers. Accessed January 13, 2022.
7. Zoghi M, Brown T, Williams B, et al. Learning style preferences of Australian health science students. *J Allied Health.* 2010;39:95–103.
8. Shiner N. Is there a role for simulation based education within conventional diagnostic radiography? A literature review. *Radiography.* 2018;24:262–271.
9. Ketterer SJ, Callender J, Warren M, et al. Simulated versus traditional therapeutic radiography placements: a randomised controlled trial. *Radiography.* 2020; 26:140–146.
10. Kelly T, Surjan Y, Rinks M, Beech J, Warren-Forward HM. Communication: preparing undergraduate radiation therapy students for initial clinical patient interactions. *Radiography.* 2019;25:320–326.
11. Bleiker J, Knapp KM, Frampton I. Teaching patient care to students: a blended learning approach in radiography education. *Radiography.* 2011;17:235–240.
12. Hyde E. A critical evaluation of student radiographers' experience of the transition from the classroom to their first clinical placement. *Radiography.* 2015; 21:242–247.

Interview with Nuclear Medicine Technology Educators on the Impact of COVID-19 on Programs, Outcomes, and Employers

Sarah Frye[1] and Jennifer Prekeges[2]

[1]*Saint Louis University, St. Louis, Missouri; and* [2]*Bellevue Community College, Bellevue, Washington*

Coronavirus disease 2019 (COVID-19) has influenced changes at health-care facilities. The editors of *Journal of Nuclear Medicine Technology* were interested in learning how the pandemic has affected nuclear medicine technologists (NMTs) and NMT programs. We (two of the associate editors and NMT educators) invited NMT educators to participate in a qualitative interview study to get perspective on the effects of the pandemic on their programs, institutions, and communities. The interview questions were shared with participants ahead of their scheduled interviews. Four educators were interviewed, and selections from their comments are included in this article. The comments revealed that students seem anxious but inquisitive and ready for the changing health landscape. Most programs have seen changes in student retention, with most programs seeing an increase in enrollment. COVID-19 has made educators and students think about flexibility and how to benefit from hybrid learning. Programs have seen challenges regarding personal protective equipment and vaccine requirements. All interviewed educators noted the excellent job market for students, particularly that many job offers include incentives or sign-on bonuses. The conclusion was that COVID-19 forced programs to adapt to many of these changes, enhancing student learning. NMT educators are excited about the future of molecular imaging and NMTs.

Key Words: COVID-19; educator; NMT program; employer; students

J Nucl Med Technol 2022; 50:174–178
DOI: 10.2967/jnmt.121.264136

Without a doubt, coronavirus disease 2019 (COVID-19) has had a worldwide impact. COVID-19 has put a major strain on health-care facilities and health-care workers. Since February 2020, health-care employees have been on the front lines of the pandemic, which has led to many challenges, including increased physical demand, scheduling changes, personal health risks, burnout, and staffing shortages. Health-care systems are seeing increases in employee turnover due to job changes, early retirement, and exits to other professions (*1*). The molecular imaging world has experienced this impact firsthand, with changes to studies, protocols, staffing, and education. The editors of *Journal of Nuclear Medicine Technology* were interested in learning how this impact has affected nuclear medicine technologists (NMTs) and NMT programs. We (two of the associate editors and NMT educators) invited NMT educators to participate in an interview study to get firsthand information on how this impact has been seen in their communities. The purpose of this article is to educate readers on the trends and changes that NMT educators have seen because of the pandemic.

MATERIALS AND METHODS

The goal of this semiqualitative interview study was to get a first-person perspective from current NMT educators on the effect of the pandemic on their NMT programs, institutions, and communities. The interview format was an informal question-and-answer session. Convenience sampling was used to invite U.S. NMT educators to participate, with a goal of including individuals from different geographic areas and different types of programs (associate's degree and bachelor's degree; in-person and remote learning). Six educators were invited, and 4 accepted. Two interview dates were needed to accommodate the interviewees' schedules, the first being January 25, 2022 (with 3 of the NMT educators) and the second being February 3, 2022 (with the fourth NMT educator). The participants agreed to be identified and for their comments to be recorded.

The participants were Jay Smith, University of Iowa, Iowa City, IA; Julie Bolin, GateWay Community College, Phoenix, AZ; Grace Tursi-Wenzler, Bronx Community College, New York, NY; and Leesa Ross, Chattanooga Community College, Chattanooga, TN. Before the interviews, we sent the questions to the participants; these questions appear as subheads in the Results section of this article and were based on previous discussions between ourselves. We conducted the recorded interviews via Zoom and then transcribed them. Many of the answers are included here. We chose to use actual quotations from the interviews so that our perceptions of the answers would not be a factor.

RESULTS

How Have Your NMT Students and Your Applicants Been Changed, or Been Affected, by COVID-19? In What Ways Are They Approaching Their Future in the NMT Field Differently?

Overall, the group felt that incoming students seem inquisitive and ready to work in the health-care setting. NMT programs have seen the effects of anxiety but also a willingness of students to adapt to the changing health landscape. Most

Received Mar. 18, 2022; revision accepted Apr. 18, 2022.
For correspondence or reprints, contact Sarah Frye (sarah.frye@health.slu.edu).

programs have seen changes in student retention, with many programs having an increase in NMT enrollment even if overall institution enrollment has dropped.

Ross: "The group that began the year with COVID in full effect [had] very high anxiety. They seemed to stress about everything in life and in school. In our opinion, it was because they were on edge living through a pandemic, and that spilled over into everything that they did. Everything seemed urgent. They were, however, the most social class we have had in a long time through online outlets. The second year of COVID, when people became more relaxed over the pandemic, the group seemed a little less anxious."

Tursi-Wenzler: "Program retention [in] the last 2 years with COVID … I feel like it's been a little bit challenging. The pandemic has made [it] way more challenging for students to commit to clinical [rotations] and stay in the program."

Prekeges: "It seemed like COVID hit a lot of people really hard in terms of making major life changes [in] that they were planning to go in one direction and [now] they're going in a completely different direction. But the interest that I've had for my upcoming application cycle has been much higher, and much higher quality. It almost seems like there's a group of people out there [who] have decided that this COVID thing is here, they're going to take it by the horns, and they're going out there to work in health care."

Ross: "I think that they seem to be more inquisitive; maybe they've had to do more research online. And they are … getting used to doing research by being online for things instead of just being in the classroom. But they seem to be more inquisitive about everything. They want the details, [the] step by step of everything."

How Has Your Program Enrollment Been Affected?

Bolin: "We've actually had an increase in admissions, and I think that part of it [is that] we were just approved for a bachelor's degree program. And our goal for the bachelor's degree is to offer dual certification."

Smith: "We're seeing our numbers stay pretty steady. We have an "Introduction to the Radiation Sciences" course. It's a 1-credit course offered every semester that's really open to anybody. So, it does a great job of bringing people in, and we get a lot of prospective nursing students and pharmacy students and everything else, all the allied health-care staff. Our numbers are trending up across all the modalities."

Bolin: "The students anticipate, going into a health-care field, that [they are] going to be around people who are sick. They've just accepted that as this is [the] working environment, and it is what it is, it's not going away."

How Have Overall University/College Applications Been Affected?

Smith: "[The] university as a whole [was] down in 2020, by 10%. It's bounced back a little bit, a point or two. The total applicants in the radiation sciences are up, but most of that increase is due to ultrasound."

Tursi-Wenzler: "The university as a whole is definitely down. But knock on wood, the nuclear medicine program [is] not. We're, if anything, getting more applicants in."

Bolin: "We were down like 14% approximately across all of Maricopa [Community College District]. In terms of allied health, our numbers have never dropped. All of the allied health programs have wait lists; I think nuclear medicine has the smallest wait list currently. And it's 2 years minimum."

Ross: "I have a feeling my applicant pool is actually going to be higher, which is odd because enrollment is really low at the college. We're [down significantly from] what we used to be, from 3 or 4 years ago."

What Changes Have You Made to Your NMT Program to Address COVID? Are These Driven by Your Institution, Your Clinical Sites, or Your Employers?

The general thoughts of the group for this question included how much COVID-19 has made educators and students think about flexibility. The initial impact of changing courses because of COVID-19 had a major effect on pedagogic growth. Many programs used this opportunity to have remote and hybrid learning, which has continued to benefit programs.

Bolin: "We went through a terrible transition process when COVID first hit, of trying to transition all of our classes to online. And there was a huge learning curve to that. But I think that we've primarily gotten that figured out. And we've all adapted and figured out ways that we can provide quality education to our students, even if we have to transition out of the in-person setting into more of a virtual setting. And I think all the allied health-care folks have really stepped up to the plate and made their courses very user-friendly. We're also flexible with our students … ; if they have to miss a clinical day, we have built in extra hours. So, they typically don't suffer, or they don't have to be delayed. We, in fact, never delayed any of our graduations for our students."

Tursi-Wenzler: "With the original online transition, the hardest part was ensuring exam integrity. And [after] our students … were hit with the pandemic in 2020, we definitely had a drop in board exam [scores]. Since [then] we've been able to at least get the midterms and final in person."

Smith: "I think we're just going to be hybrid from now [on]. Because as soon as we think, you know, everybody's back, somebody is out again. So, we just roll with it; we just assume we're going to have to [use] Zoom. The students seem to have no problem adjusting to that."

Ross: "[My program was already mostly online, so normally] we do our radiation badge exchange on-site, and while they're there, we usually do some kind of lab with them. [When COVID hit], we canceled the lab. And then, when we did start labs back, we had to split them up because we had 15 students, and we limited it to 10 [people], including instructors, in the classroom at a time.

And so, we split them into 2 groups. [Now] it's opened back up, and now we don't have any limits."

Bolin: "I record all of my lectures ahead of time. And they're always posted and available to the students. So, anyone who has to miss a class, they are not missing content in any way. And then we offer a lot of office hours. I'm not sure why, [but] I haven't been able to figure out what I can do to promote them wanting to reach out to me a little bit more; it's just that some students will and some won't. What I have found is that if I offer … an image review session, or a virtual check-in, or … 'if you have questions, drop in during this time,' a lot of students will show up. Not all of them have questions, but at least they are present. So, I can check in with them."

Tursi-Wenzler: "Transitioning online was definitely challenging in a lot of ways; we've pretty much been online or hybrid since the pandemic hit. The Remind app has been a huge help. If something happened, I could just text the students quickly; I know that they're receiving the information."

Ross: "I meet with students on WebEx, [as well as with] applicants, potential students, and my advisees. We conduct our interviews through WebEx, [and] we were going to convert that back. But we liked doing that because we could get clinic supervisors from other areas to log on and help with the interviews. Because they didn't have to drive, they could log in from work to do the interviews."

Bolin: "[When we first transitioned back to in-person learning, the students] didn't like it. They felt like it was a waste of time to have to be present [traffic, getting alternate childcare]. My students who started virtually kind of want to stay that way. My students who started in person are terrified that they may have to transition into a virtual environment."

Prekeges: "There were always those people who, when I said, "Well, I can get you in the program, but it's going to be [at a distant location] and not here in your area," they'd say, "Oh, no, no, no! I need to be in the class[room] with you." But once they experience not having to actually get in their car and drive, everybody becomes a convert to the virtual environment."

Frye: "I have anxiety going back and forth [between in-person and virtual learning], [and] I know this stuff [because I teach it], right? So, I imagine the stress and the anxiety for these poor students [is even greater]."

Ross: "Even though everybody has gone back to the campus, [the college is] still not pushing you to be on site. With [our program] being online, we've pretty much been working remotely, most of the time, as well. But it was interesting to see this [shift in the college's stance], because [my colleague] and I had been asking for years to be able to work out of our house. Now they're like, "you can stay home as much as you want if you don't have any meetings or anything on campus." They're just not pushing you to be on campus unless you have set times that you might be with students."

Tursi-Wenzler: "I think our 5-year plan is mainly to really use what we've learned during the pandemic, and try to use that in ways that are going to benefit us and the students, [such as] test administration or organizing grade assessment, which is such a huge part of [Joint Review Committee on Educational Programs in Nuclear Medicine Technology] standards and requirements now. And I think the pandemic has really made me realize how much the students have on their plates. The college on my end has excellent counseling services. [If I sense a student is struggling,] I can direct them to somebody who is trained to talk to that."

Bolin: "What I've learned is that we need to be a little bit more flexible, and we have the tools that we can remain flexible but [still] provide quality education. And I think that moving forward, I would like to see us implement some of the changes that we've made. I'd like to see us keep some of those."

What Are Some of the Changes You've Experienced Particularly Related to COVID-19 Requirements in the Clinical Setting?

In the clinical setting, COVID-19 created challenges regarding personal protective equipment and vaccine requirements.

Bolin: "We pay for the students to do the N95 fit testing. And at one point, we were having to send all of our students with their own [personal protective equipment]."

Ross: "Most of the sites are requiring that [students] have an N95 mask … . Before, they just could wear any type of mask, but now it's an N95. And the sites are supplying them. And then, of course, all of them are starting to require the [COVID-19] vaccine."

Tursi-Wenzler: "In New York State, they're requiring that all health-care employees [including students] [be] vaccinated. There's been very, very few medical exemptions, so all the students pretty much have to be vaccinated. So, that's something we're trying to make very clear in information sessions … . And the college has definitely amped up the testing. So, they have on-site testing that they're doing at the college, which has been helpful."

Frye: "[The University required] that we be fully vaccinated as of the fall semester—students, faculty, and staff—and now they require boosters too. Adding that navigation is difficult."

Ross: "[The students] got back in the clinic really quick. The sites are seeing some revolving of employees, some transitioning; people are switching hospitals and relocating and moving. So there is some adjustment there. But I think that the really big difference is [that] they're not allowed to work with COVID patients."

What Trends Are You Seeing on the Employer Side?

All educators expressed how great the job market is for students, particularly in that many of these jobs include incentives or sign-on bonuses. These educators indicated a need to fill positions from which people had retired, and some stated that new positions are being created in their areas.

Smith: "I've just been dying to say how good the job market is for students. [Our seniors] graduate May 15, and 2 or 3 of them have accepted job offers already. Earliest ever! And a couple of them are fending off multiple job

offers because pretty much everywhere they send a resume to, even blindly, they'll just get a job offer."

Tursi-Wenzler: "[In] the last 2 years, students have not only received multiple job offers but [also] changed jobs already. I had a couple of students [who] got hired right after they graduated in May and then [took] a better job or one that they were really hoping for within that short time period."

Bolin: "There's lateral and upward mobility even for technologists who don't seem to have years … of experience. And here, a lot of our clinical sites are wanting and preferring technologists [who] are dual-certified. And I think that that's more prominent in our clinic setting, as opposed to our hospital setting."

Ross: "We're regional, so we try to keep our students separated so that we don't flood the market in one area. But we did take 6 in Chattanooga last year, and I thought, oh my goodness, they are not going to be able to find a job or anything. And then they all were able to find jobs that [they] wanted … . One just decided to be a stay-at-home wife after she went to school. She never even looked. But 5 of them found jobs, and one of them even got a $15,000 sign-on bonus here, local, where there's a school."

Are Employers Worried About Too Many or Too Few Technologists?

Smith: "In the Midwest, it seems they're just filling retirement positions."

Bolin: "So in our area, in my immediate area, we're actually seeing quite a bit of expansion in terms of some positions being added to existing hospitals, some hospitals choosing to have smaller satellites, and then a huge explosion in outpatient, particularly, PET/CT, as well as cardiac. We're doing a lot of cardiac PET now, and some of our clinical partners are expanding their outpatient cardiac sites."

Tursi-Wenzler: "I think that there's been more filling [of] retirement [positions] in comparison to saying, 'Let's create another technologist position in our department.' But I do think that PET/CT is definitely increasing. So, that has been adding some … jobs in the department."

Bolin: "We've seen some transition into the industry setting as well. For some of our technologists who were either in education or in the clinical setting, and [have] opted to transition into industry, there's just more positions available that are in the industry setting."

Ross: "It seems to be regional. Some areas are sending technologists home early due to a lack of patients, and others are struggling to find technologists to handle the workload or fill department needs."

If Too Few, Are There Changes for Pay or Other Incentives Being Offered?

Smith: "I think this year, we're going to see significant increases because everybody knows everybody's hiring. We're seeing, with existing technologists, our department … trying to get a recruitment and retention process or program in line, and they know that pay is going to be a big part of that."

Bolin: "The initial starting salary is higher. And then, in addition to that, especially if you're in an outlying area, they're really increasing the wages in some way, whether it's retention bonuses, relocation assistance, or hiring bonuses. It's a good time to be a clinical technologist."

Ross: "The wages seemed to be about staying the same. I think if people try to negotiate, they might be able to get a little bit. But what we found with the sign-on bonus [for] our student is they wouldn't [negotiate] the hourly wage, but they were offering a $10,000 sign-on bonus. She asked for more hourly wage, and when they didn't do that, her counteroffer was a bigger sign-on bonus. And they were, like—'Sure, you can have more money on the sign-on bonus.' They didn't even flinch."

What Are Your Thoughts/Hopes for the NMT and Radiology Field over the Next 5 Years?

The consensus for this question was that the requirements for entry-level NMTs keep increasing, and many of these requirements address multimodality training. Diversity, equity, and inclusion will be increasingly demanded, and radiopharmaceutical and theranostic studies may expand the profession.

Bolin: "The education standards for NMTs continue to just go up … . We always want to say that we teach for competent entry-level technologists, but that entry level is not just clinical anymore; it's kind of expanding into other areas."

Smith: "How do we work that into the curriculum as educators? How do we fit this stuff in our programs when they're jam-packed already? But you know, we've got to draw the line somewhere. And we need to keep our eye on the ball, which is producing good entry-level technologists. [We need to make] sure it's market-driven. We don't want to be requiring [students] to learn stuff that they don't need to know as entry-level nuclear medicine technologists. I think we need to include theranostics."

Bolin: "I think that we're going to see an explosion of radiopharmaceutical development, with all of the advancements in radiochemistry and radiopharmacy. I think that the pharmaceutical development and potential theranostics applications are going to continue to increase. And I feel like we need to own that as nuclear medicine technologists, because otherwise, somebody is going to steal it."

Ross: "I'm hoping that theranostics continues to take off and that we see even more radiopharmaceuticals approved. We've seen an increase in PET; I'd like to see something new in basic nuclear medicine. And then who knows where PET/MRI is going to go. It seems to be slowly increasing the number of units over the United States."

Bolin: "Each state has … unique working conditions for our technologists. So, it can be difficult to create a program where you're trying to train your students to be able to work in nuclear medicine, in general, but then state-to-state specifics make that very difficult. And [it is also difficult] to incorporate additional curriculum whenever you are confined to only being able to have a program that is a certain length."

Bolin: There's a huge drive, at least in certain areas, for multimodality technologists. So, they're wanting us to have technologists that … I almost want to say, [are] like radiology technologists or medical imaging technologists, not just nuclear medicine [and] not only CT."

Tursi-Wenzler: Then, for employers, I really just think the best advice is to give incentives for additional certifications; it's going to benefit them in the long run if they can have a technologist [who] can do multiple different studies."

Bolin: "I think that some of our students are now asking for, or our clinical partners are expecting, more about diversity, equity, and inclusion and [new] courses or established courses specifically relating to that. And I find that I'm kind of challenged in figuring out where to incorporate it because I just don't have any more space."

DISCUSSION

The passion and dedication of the interviewees to their profession were evident. They are excited for their students, the future of molecular imaging, and the growth of the nuclear medicine field, including more employment opportunities, more tracers, and the expansion of theranostics.

Overall, the group was impressed by the adaptability and intelligence of their current and incoming students. Educators were forced to adapt programs when the COVID-19 pandemic started, and many of these changes have enhanced the NMT programs with flexibility for student learning.

Most programs have seen an increase in NMT enrollment even if overall institution enrollment has dropped. It was also clear that the NMT students are coming into a great employment market that includes incentives or sign-on bonuses.

As we continue to adapt to the new nuclear medicine environment in a post–COVID-19 health setting over the next few years, it would be beneficial to conduct additional research on this topic, using informal polling with qualitative questions and interviewing more educators in nuclear medicine technology and in radiology in general.

CONCLUSION

The interviews showed that NMT educational programs have been significantly affected by the COVID-19 pandemic, with a considerable increase in the flexibility needed to address educational issues. At the same time, approvals of new diagnostic and therapeutic radiopharmaceuticals have increased the content needed for entry-level practice. Programs have looked toward the future with revised curriculum requirements and increased use of virtual formats. The interviewees made particular note of the hot job market for NMTs. Graduates are getting multiple job offers nationwide, with incentive pay often included. Employers are facing labor shortages in some geographic areas just as the business of nuclear medicine is expanding. The Bureau of Labor Statistics predicts 1,500 job openings a year for NMTs (*2*). Industry leaders have predicted as much as a 30% expansion of our business in the next decade, based on new radiopharmaceuticals and new theranostic techniques. At the same time, many long-time technologists are approaching retirement. These trends point to a continuing need for new graduates in the field. Telehealth is not an option for NMTs; we are front-line health-care professionals. Both educational programs and employers are important to the future of our field.

DISCLOSURE

No potential conflict of interest relevant to this article was reported.

REFERENCES

1. Michelson D. Covid-19 is no longer the biggest issue facing hospitals. Staffing is. STAT website. https://www.statnews.com/2022/01/19/covid-19-no-longer-biggest-issue-facing-hospitals-staffing-is/. Published January 19, 2022. Accessed May 3, 2022.
2. Occupational outlook handbook: nuclear medicine technologists. U.S. Bureau of Labor Statistics website. https://www.bls.gov/ooh/healthcare/nuclear-medicine-technologists.htm. Updated April 18, 2022. Accessed May 3, 2022.

Hybrid Imaging with SPECT/CT and SPECT/MRI in Hepatic Splenosis

Mehdi Djekidel[1] and Mark Michalski[2]

[1]*Division of Nuclear Medicine, Department of Radiology, Sidra Medicine, Doha, Qatar; and* [2]*MGH and BWH Center for Clinical Data Science, Boston, Massachusetts*

Hepatic splenosis is a rare entity, for which indeterminate liver lesions can pose a clinical dilemma. In difficult cases, scintigraphy can be of great value, especially with novel SPECT/CT and SPECT/MRI techniques.

Key Words: oncology; hepatic splenosis; RBC scan; SPECT/CT; SPECT/MRI; sulfur colloid

J Nucl Med Technol 2022; 50:179–181
DOI: 10.2967/jnmt.121.263013

Splenosis commonly occurs incidentally and locates to bowel surfaces, the parietal peritoneum, the mesentery, and the diaphragm but can potentially occur anywhere in the peritoneal cavity. Patients frequently have a history of splenectomy or trauma. On the other hand, hepatic splenosis is a rare entity and may present clinically. Indeterminate liver lesions can pose a clinical dilemma and may lead to additional investigations, anxiety, follow-up imaging, and even invasive procedures. MRI usually performs extremely well. In difficult cases, scintigraphy can be of great value, especially with novel SPECT/CT and SPECT/MRI techniques. We describe the impact of hybrid imaging in the case of a 29-y-old woman with hepatic splenosis.

CASE REPORT

Our patient presented with epigastric, right-upper-quadrant abdominal pain. She had undergone splenectomy and cholecystectomy 10 y previously because of hereditary spherocytosis. A year earlier, for workup of nephrolithiasis, she had undergone abdominal CT, which demonstrated an incidental hepatic hypodensity that could not be characterized (Fig. 1A). After symptomatic management, the patient was discharged but returned twice in the subsequent weeks because of continued abdominal pain and showed mildly elevated results on liver function tests. Consequently, the patient underwent abdominal ultrasound, which demonstrated a small, hyperechoic lesion within the right lobe of the liver (Fig. 1B). The findings were confirmed by MRI, which demonstrated an indeterminate exophytic mass within segment VI of the liver (Fig. 2).

After developing fevers and malaise and experiencing continued pain, the patient was admitted to the hospital, and her blood work showed atypical lymphocytes, elevated levels of lactate dehydrogenase and uric acid, and Epstein–Barr virus serologies consistent with acute mononucleosis. A biopsy of the liver lesion yielded islands of mature red blood cells and hematopoietic tissue but no hepatic tissue. Pathologic examination could not yield a definitive diagnosis.

^{18}F-FDG PET/CT was then performed to evaluate for a possible malignancy. The scan revealed extensive metabolically active lymphadenopathy throughout the body. A pertinent finding is that the hepatic mass was not metabolically active, as seen in Figure 3. However, this finding was not sufficient, as some cancers may not be ^{18}F-FDG–avid.

Biopsy of the left axillary lymph node biopsy was performed and found reactive lymphoid hyperplasia positive for Epstein–Barr virus. Infectious mononucleosis was established; however, the nature of the hepatic lesion remained unclear even after a biopsy. Further investigations were sought.

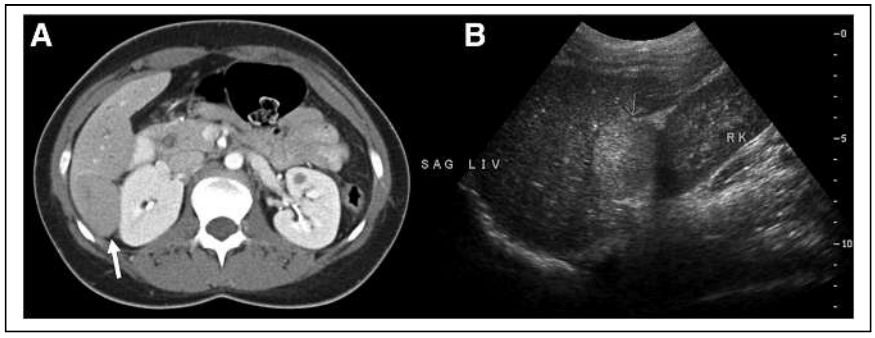

FIGURE 1. (A) Single-phase CT scan obtained at different hospital does not demonstrate typical arterial enhancement (arrow). (B) Ultrasound image shows hyperechoic mass (arrow). Mass would typically be hypoechoic.

Received Aug. 6, 2021; revision accepted Oct. 25, 2021.
For correspondence or reprints, contact Mehdi Djekidel (mdjekidel@sidra.org).
Published online Dec. 6, 2021.

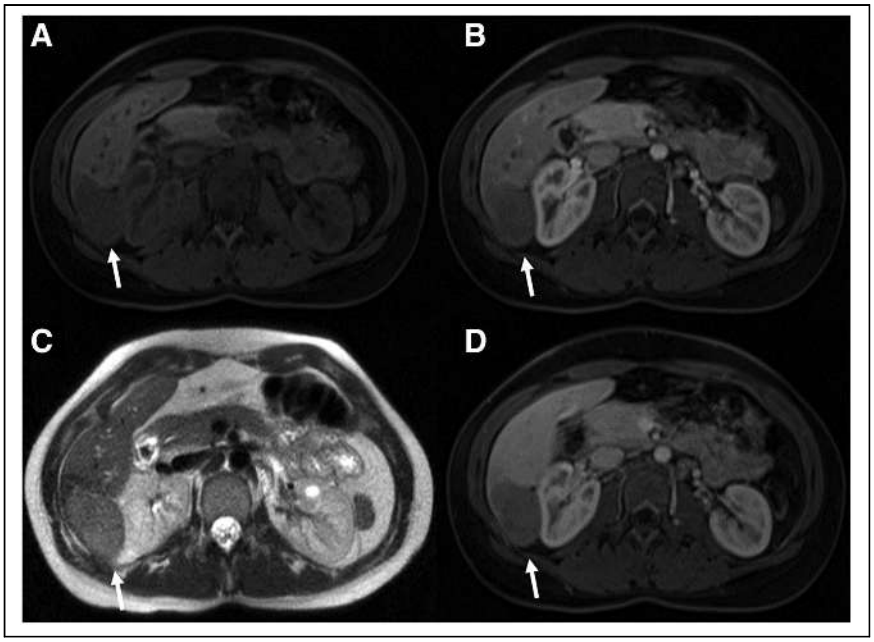

FIGURE 2. Axial MR images of area of lesion (arrows). (A) T1-weighted fat-saturated volumetric interpolated breath-hold examination (VIBE) sequence shows typical hypointensity. (B) Arterial-phase T1-weighted VIBE sequence shows no uptake of gadoxetate disodium (Eovist; Bayer). (C) T2-weighted sequence shows typical hyperintensity. (D) Portal venous–phase T1-weighted VIBE sequence shows no gadoxetate disodium uptake.

Because hematopoietic tissue was found in the hepatic lesion biopsy sample, a ^{99m}Tc-radiolabeled heat-damaged red blood cell SPECT/CT scan was obtained to evaluate for hepatic splenosis. This scan showed focal uptake correlating with the mass seen on the MRI (confirming hepatic splenosis) and a smaller focus of uptake in the left upper quadrant of the abdomen (splenule), shown in Figure 4. The patient was advised that her abdominal pain was likely related to inflammation of the ectopic splenic tissue and would improve with resolution of her infectious mononucleosis. She has done well.

DISCUSSION

Even with a relevant clinical history (splenectomy, trauma), hepatic splenosis can be challenging to diagnose and can be confused with focal nodular hyperplasia, adenoma, hepatocellular carcinoma, or metastases (*1–4*). MRI is the modality of choice for evaluating liver lesions. However, in clinical practice, the findings may not always be straightforward.

A review of the literature showed that about 75% of reported cases of hepatic splenosis were in men and that 95% of reported cases had a history of splenectomy. Only about 37% had no risk factors, and about 60% either had risk factors for hepatocellular carcinoma or had a preexisting malignancy.

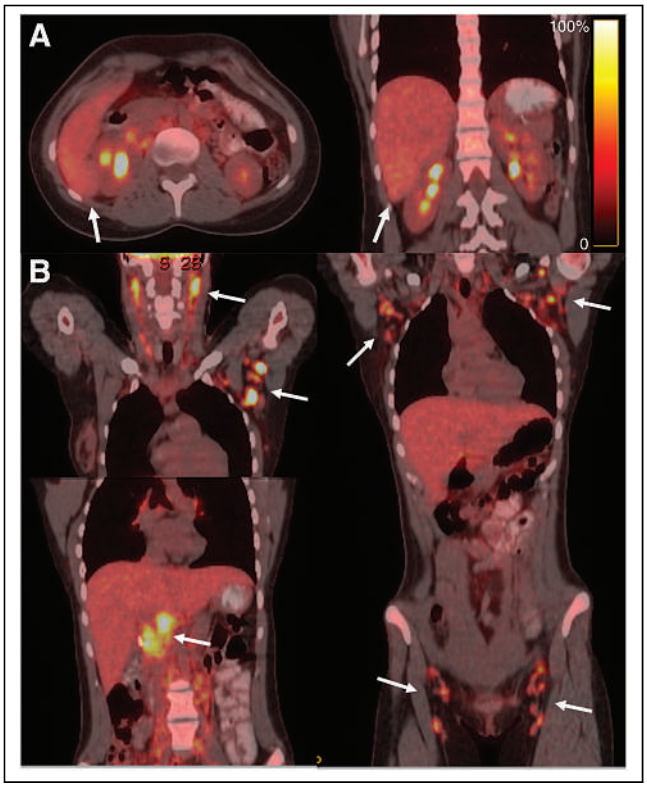

FIGURE 3. ^{18}F-FDG PET/CT images of lesion and lymphadenopathy (arrows). (A) Axial (left) and coronal (right) images show liver lesion exhibiting glucose metabolic activity similar to that of surrounding normal parenchyma. (B) Coronal (bottom left and right) images show widespread ^{18}F-FDG–avid lymphadenopathy.

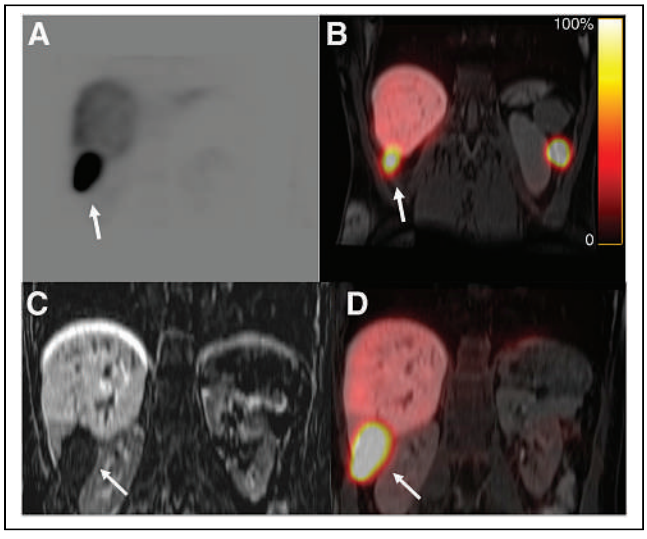

FIGURE 4. (A and B) ^{99m}Tc-labeled heat-damaged red blood cell images show increased uptake in hepatic (A) and left flank (B) splenule. (C and D) Coronal T1-weighted MR (C) and SPECT/MR (D) images show intrahepatic splenosis in unusual location (arrows).

The blood supply of splenules is derived from local arteries at implantation sites (*1*). Even though ^{99m}Tc-sulfur colloid or ^{99m}Tc-labeled heat-damaged red blood cells efficiently target ectopic splenic tissue (*5,6*) and clinch the diagnosis, invasive diagnostic measures are still performed in more than 50% of cases. About 79% of reported cases used a biopsy, fine-needle aspiration, or surgery to fully diagnose the hepatic lesion. It is surprising that only 21% underwent scintigraphy.

Coregistration of datasets from SPECT/CT or SPECT/MRI and ^{99m}Tc-labeled heat-damaged red blood cells is the best test to evaluate for splenosis or accessory spleens. Sulfur colloid, because of its normal liver biodistribution, would be a second choice. The sensitivity, specificity, and accuracy of these studies have improved. Prior reported concerns about the detectability of small lesions, or proximity to major vascular structures and the remaining spleen, are no longer applicable. As in our case, several tests were performed, whereas scintigraphy would have completed the work-up early. These techniques should be used more frequently to decrease complications, the financial burden, and anxiety related to costly follow-up imaging and invasive procedures.

CONCLUSION

In difficult cases of hepatic splenosis, scintigraphy can be of great value, especially with novel SPECT/CT and SPECT/MRI techniques.

DISCLOSURE

No potential conflict of interest relevant to this article was reported.

REFERENCES

1. Lee JB, Ryu KW, Song TJ, et al. Hepatic splenosis diagnosed as hepatocellular carcinoma: report of a case. *Surg Today.* 2002;32:180–182.
2. Choi GH, Ju MK, Kim JY, et al. Hepatic splenosis preoperatively diagnosed as hepatocellular carcinoma in a patient with chronic hepatitis B: a case report. *J Korean Med Sci.* 2008;23:336–341.
3. Yoshimitsu K, Aibe H, Nobe T, et al. Intrahepatic splenosis mimicking a liver tumor. *Abdom Imaging.* 1993;18:156–158.
4. Gruen DR, Gollub MJ. Intrahepatic splenosis mimicking hepatic adenoma. *AJR.* 1997;168:725–726.
5. Foroudi F, Ahern V, Peduto A. Splenosis mimicking metastases from breast carcinoma. *Clin Oncol (R Coll Radiol).* 1999;11:190–192.
6. Lu HC, Su CW, Lu CL, Chang CP, Lin HC. Hepatic splenosis diagnosed by spleen scintigraphy. *Am J Gastroenterol.* 2008;103:1842–1844.

Ancillary Finding on Myocardial Perfusion Imaging Due to Urinary Bladder Displacement

Sarah Frye[1], Ejda Bajric[2], and Avril Slavin[2]

[1]*Clinical Health Sciences, Saint Louis University, St. Louis, Missouri; and* [2]*John Cochran Division, VA St. Louis Healthcare System, St. Louis, Missouri*

When patients are referred for SPECT myocardial perfusion imaging with ^{99m}Tc agents, attention focuses on the tracer activity in the myocardium. Apart from myocardial activity, normal biodistribution of ^{99m}Tc-sestamibi and ^{99m}Tc-tetrofosmin is seen in the thyroid, liver, gastrointestinal tract, kidneys, and urinary bladder. These structures may be visualized when a γ-camera with a large field of view is used for SPECT imaging. This case report presents a serendipitous finding of a pelvic mass, which was identified because of the extended field of view afforded by the conventional γ-camera used for SPECT myocardial perfusion imaging and detected because of a review of the raw images by the nuclear medicine technologist. This case emphasizes the importance of training the nuclear medicine technologist to review the raw data in the entire field of view before study completion.

Key Words: myocardial; MPI; pelvis; SPECT; bladder

J Nucl Med Technol 2022; 50:182–183
DOI: 10.2967/jnmt.121.263344

Incidental extracardiac findings in patients who undergo PET/CT and SPECT/CT have been documented, with the fraction of incidental findings being as high as 60% (*1*). The number of incidental findings that led to potentially treatment-altering diagnoses of previously unknown and treatable malignancies was low, at no greater than 0.5% (*1*). It is important to review incidental findings, as these will occasionally be found when the CT datasets of hybrid SPECT/CT and PET/CT myocardial perfusion imaging (MPI) studies are carefully reviewed in different imaging windows (*1*). Another published study showed that 60% of the major findings and 48% of the minor findings in SPECT/CT MPI studies were unknown at the time of nuclear imaging (*2*). This study stated that potentially significant abnormal findings on the nondiagnostic-CT portion of the cardiac SPECT/CT examination were detected in 10.5% of reported patients (*2*). These data suggest that, in addition to the emission image findings, the CT findings should routinely be assessed for major diagnostic abnormalities (*2*). The requirement for institutional review board approval was waived, as this retrospective descriptive report of observations does not attempt to answer research questions; every attempt has been made to protect the patient's privacy.

CASE REPORT

A 73-y-old man with a past medical history of tobacco use, non–insulin-dependent diabetes, hypertension, and hyperlipidemia was referred for an MPI pharmacologic stress test because of increasing dyspnea symptoms at rest and with exercise. He was unable to undergo a treadmill exercise test because of symptomatic claudication of the right leg after walking more than a short distance. The findings of a chest radiograph were

FIGURE 1. (A) Photograph showing typical patient positioning (supine with arms raised) during MPI and relative size of field of view. (B) Photograph of Siemens Symbia dual-head γ-camera in John Cochran Division of VA St. Louis Healthcare System.

Received Oct. 7, 2021; revision accepted Dec. 28, 2021.
For correspondence or reprints, contact Sarah Frye (sarah.frye@health.slu.edu).
Published online Feb. 23, 2022.

FIGURE 2. (A) SPECT image of abdomen and pelvis showing deviation of urinary bladder (maximum-intensity projection). Arrow shows deviation of urinary bladder. (B) SPECT/CT image of abdomen and pelvis showing deviation of urinary bladder by large mass (coronal view). Arrow shows deviation of urinary bladder in CT portion of image.

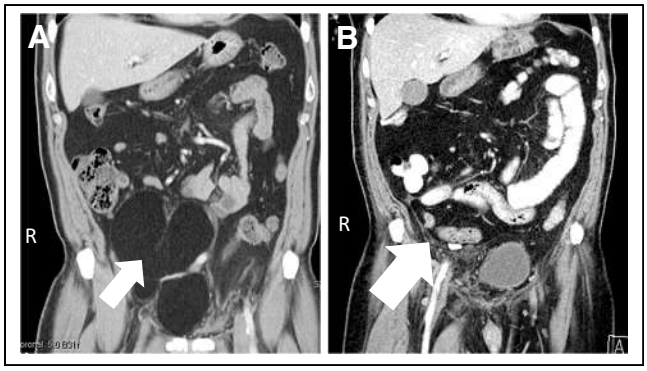

FIGURE 3. (A) Coronal view of abdomen and pelvis from dedicated diagnostic CT scan showing large lipoma in pelvis. This scan was obtained immediately after MPI study. Arrow shows deviation of urinary bladder before resection. (B) Coronal view from dedicated CT scan after resection of lipoma. Arrow shows where lipoma was before resection.

unremarkable. A transthoracic echocardiogram showed normal left ventricular systolic function and mild diastolic dysfunction. Both pulmonary function tests and the ankle brachial index test had normal results.

The patient was given an intravenous injection of 307.1 MBq (8.3 mCi) of ^{99m}Tc-sestamibi on arrival in the nuclear medicine department and underwent ungated rest SPECT MPI 30 min later. The imaging was acquired on a Siemens Symbia with dual large-field-of-view detectors (53.3 × 38.7 cm detector dimensions) and parallel-hole low-energy, high-resolution collimation (Fig. 1). Subsequently, in the stress laboratory, 0.4 mg of regadenoson followed by 1,172.9 MBq (31.7 mCi) of ^{99m}Tc-sestamibi was administered intravenously, and gated SPECT MPI was performed 60 min later.

When reviewing the rotating raw SPECT images before reconstruction of the rest and stress MPI images, the nuclear medicine technologist (NMT) noticed unusual displacement of the urinary bladder to the left, which was visible because of urinary excretion of the radiotracer (Fig. 2A). Before releasing the patient, the NMT brought this finding to the attention of the attending nuclear medicine physician. The patient denied knowledge of a pelvic abnormality, and no prior cross-sectional images of the abdomen or pelvis were found in the electronic medical record. It was decided that SPECT imaging with CT of the abdomen and pelvis was warranted to further characterize the finding.

The MPI scan showed normal myocardial perfusion and normal left ventricular function. The SPECT/CT scan of the abdomen and pelvis showed deviation of the urinary bladder anteriorly, superiorly, and to the left by a large lipoma in the pelvis (Fig. 2B). The lipoma, which appeared to be multilocular and to have a thin capsule, measured approximately 10 × 15 × 9 cm, and caused a leftward deviation of the bowel loops, the inferior vena cava, and the infrarenal aorta. The right iliac arteries and veins were draped over the lipoma and were stretched anteriorly and to the left of midline. These findings were confirmed on diagnostic contrast-enhanced CT of the abdomen and pelvis (Fig. 3A), and CT angiography showed displacement and stretching of the right common iliac, external iliac, and internal iliac arteries without stenosis. The patient underwent surgical excision, with no untoward surgical complications. Dedicated CT of the abdomen and pelvis was completed after resection (Fig. 3B). Pathologic examination confirmed a benign lipoma, and the patient reported resolution of claudication after excision.

DISCUSSION

This case highlights the unique role of the NMT, who, in many clinical units, is the one individual reviewing raw rotating images in the entire field of view before image reconstruction. By virtue of such a dedicated review, unexpected findings can be further explored before the patient leaves the department. As we describe in this report, following such a protocol may reveal clinically important findings leading to appropriate investigation and diagnosis, thereby expediting patient management.

CONCLUSION

This case emphasizes the importance of training the NMT to review raw data in the entire field of view before study completion.

DISCLOSURE

No potential conflict of interest relevant to this article was reported.

REFERENCES

1. Port S. Incidental findings on hybrid SPECT-CT and PET-CT scanners: is it time for new training and reporting guidelines? *J Nucl Cardiol.* 2019;26:1694–1696.
2. Goetze S, Pannu HK, Wahl RL. Clinically significant abnormal findings on the "nondiagnostic" CT portion of low-amperage-CT attenuation-corrected myocardial perfusion SPECT/CT studies. *J Nucl Med.* 2006;47:1312–1318.

Explore SNMMI's Online Career Center!

Explore the benefits of the SNMMI Career Center by logging in or creating a new account today.

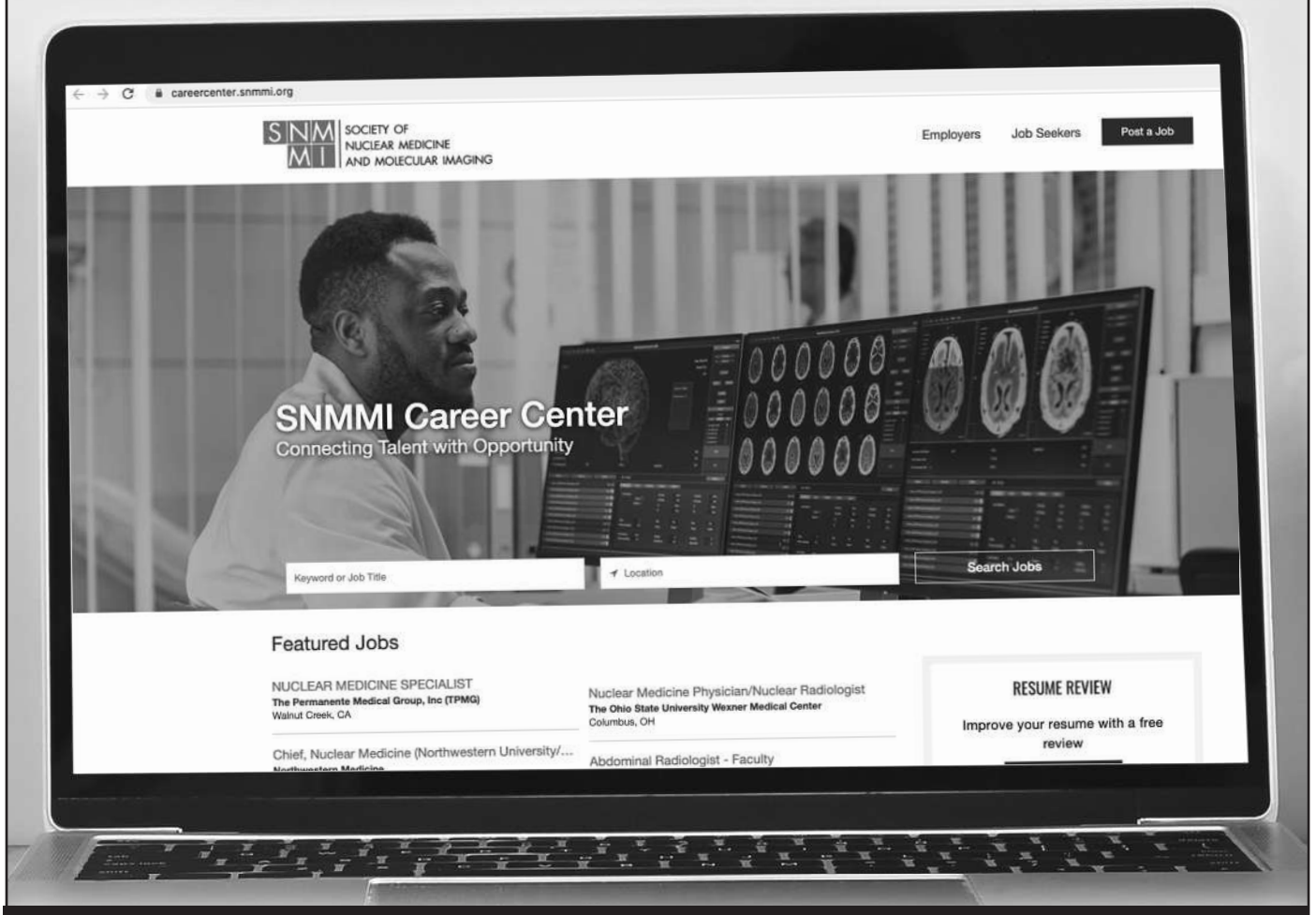

careercenter.snmmi.org

**Note: Single sign-on has been enabled for this platform and you can use your member login credentials to access the Career Center. If you are unsure of your password, to go to the SNMMI password reset link to create a new password.*

SNMMI Value Initiative

SOCIETY OF NUCLEAR MEDICINE & MOLECULAR IMAGING

ARRT Celebrates Nuclear Medicine Technology

Certifying Nuclear Medicine Technologists since 1963

Follow us on social media

Ensuring Gold Standard
Patient Care Since 1922

We Are Here for Him
So He Is There for Her

Come see us in Vancouver at SNMMI Booth #1226

At **Jubilant Radiopharma**, our pharmacies are advancing the prostate cancer imaging field by partnering with the most innovative biotech companies and healthcare experts around the world in support of our mission.

Distribution
Our pharmacy network delivers the right dose, at the right time

Quality
Our legacy of dependability and trust is built on years of quality assurance

Commercialization
Your partner for product development and access to the global market

Development
Our expansive R&D network is focused on a pipeline of innovation

SNMMI Value Initiative
SOCIETY OF NUCLEAR MEDICINE & MOLECULAR IMAGING

Proud Leadership Circle Members of the SNMMI Value Initiative

Jubilant Radiopharma
790 Township Line Road, Yardley, PA 19067
Phone: 215.550.2810

JUBILANT RADIOPHARMA